

University of Groningen

Weighing stars from birth to death

Serenelli, Aldo; Weiss, Achim; Aerts, Conny; Angelou, George C.; Baroch, David; Bastian, Nate; Beck, Paul G.; Bergemann, Maria; Bestenlehner, Joachim M.; Czekala, Ian

Published in:
Astronomy and Astrophysics Review

DOI:
[10.1007/s00159-021-00132-9](https://doi.org/10.1007/s00159-021-00132-9)

IMPORTANT NOTE: You are advised to consult the publisher's version (publisher's PDF) if you wish to cite from it. Please check the document version below.

Document Version
Publisher's PDF, also known as Version of record

Publication date:
2021

[Link to publication in University of Groningen/UMCG research database](#)

Citation for published version (APA):

Serenelli, A., Weiss, A., Aerts, C., Angelou, G. C., Baroch, D., Bastian, N., Beck, P. G., Bergemann, M., Bestenlehner, J. M., Czekala, I., Elias-Rosa, N., Escorza, A., Van Eylen, V., Feuillet, D. K., Gandolfi, D., Gieles, M., Girardi, L., Lebreton, Y., Lodieu, N., ... Zwintz, K. (2021). Weighing stars from birth to death: mass determination methods across the HRD. *Astronomy and Astrophysics Review*, 29(1), [4]. <https://doi.org/10.1007/s00159-021-00132-9>

Copyright

Other than for strictly personal use, it is not permitted to download or to forward/distribute the text or part of it without the consent of the author(s) and/or copyright holder(s), unless the work is under an open content license (like Creative Commons).

The publication may also be distributed here under the terms of Article 25fa of the Dutch Copyright Act, indicated by the "Taverne" license. More information can be found on the University of Groningen website: <https://www.rug.nl/library/open-access/self-archiving-pure/taverne-amendment>.

Take-down policy

If you believe that this document breaches copyright please contact us providing details, and we will remove access to the work immediately and investigate your claim.

Downloaded from the University of Groningen/UMCG research database (Pure): <http://www.rug.nl/research/portal>. For technical reasons the number of authors shown on this cover page is limited to 10 maximum.



Weighing stars from birth to death: mass determination methods across the HRD

Aldo Serenelli · Achim Weiss · Conny Aerts · George C. Angelou · David Baroch · Nate Bastian et al. [*full author details at the end of the article*]

Received: 15 June 2020 / Accepted: 5 April 2021 / Published online: 26 May 2021

© The Author(s), under exclusive licence to Springer-Verlag GmbH Germany, part of Springer Nature 2021

Abstract

The mass of a star is the most fundamental parameter for its structure, evolution, and final fate. It is particularly important for any kind of stellar archaeology and characterization of exoplanets. There exist a variety of methods in astronomy to estimate or determine it. In this review we present a significant number of such methods, beginning with the most direct and model-independent approach using detached eclipsing binaries. We then move to more indirect and model-dependent methods, such as the quite commonly used isochrone or stellar track fitting. The arrival of quantitative asteroseismology has opened a completely new approach to determine stellar masses and to complement and improve the accuracy of other methods. We include methods for different evolutionary stages, from the pre-main sequence to evolved (super)giants and final remnants. For all methods uncertainties and restrictions will be discussed. We provide lists of altogether more than 200 benchmark stars with relative mass accuracies between $[0.3, 2]\%$ for the covered mass range of $M \in [0.1, 16] M_{\odot}$, 75% of which are stars burning hydrogen in their core and the other 25% covering all other evolved stages. We close with a recommendation how to combine various methods to arrive at a “mass-ladder” for stars.

Keywords Stars: fundamental parameters · Stars: evolution · Stars: binaries: eclipsing · Stars: planetary systems · Galaxy: stellar content · Methods: numerical · Asteroseismology

I. Czekala: NASA Hubble Fellowship Program Sagan Fellow.

Extended author information available on the last page of the article

Contents

1	Introduction and motivation: the need for stellar masses.....	3
1.1	Masses for stellar physics.....	4
1.2	Masses for exoplanetary science.....	5
1.3	Evolution of stellar systems.....	7
1.4	Evolution of (dwarf) galaxies.....	8
2	Direct method: dynamical masses.....	9
2.1	Principles.....	10
2.1.1	Radial-velocity measurements.....	10
2.1.2	Spectral disentangling.....	11
2.1.3	Propagation of the systematic and random errors: accuracy vs. precision.....	13
2.2	Benchmark binary systems.....	15
2.3	Dynamical masses from visual binaries.....	18
2.4	Fundamental masses at the lower end of the stellar mass range.....	20
2.5	Mass estimation of non-eclipsing spectroscopic binaries.....	27
2.6	Evolved stars.....	27
2.6.1	Intermediate-mass giants.....	28
2.6.2	Red giant branch stars with oscillations.....	29
2.6.3	Interacting binaries.....	30
2.6.4	CSPNe and hot subdwarfs.....	31
2.7	Pre-main sequence stellar masses from protoplanetary disk rotation.....	33
3	Direct method: gravitational lensing.....	34
4	Semi-empirical and analytic relations.....	35
4.1	Stellar granulation-based method.....	35
4.2	Spectroscopic mass estimates for low- and intermediate-mass stars.....	38
4.2.1	H α fitting.....	38
4.2.2	C/N fitting.....	40
4.2.3	Li abundances.....	41
4.2.4	Sphericity.....	42
4.2.5	Summary.....	42
4.3	Spectroscopic surface abundance method for low- and intermediate-mass stars.....	43
4.3.1	Data-driven methods.....	43
4.3.2	Performance and limitations.....	44
4.4	Analytical/empirical relations for estimating stellar masses.....	45
4.5	Spectroscopic masses of high-mass stars.....	48
4.6	Pulsational mass of Cepheids.....	51
5	(Strongly) model-dependent methods.....	52
5.1	Isochrone fitting.....	52
5.2	HRD fitting of low- and intermediate-mass evolved stars.....	54
5.3	Evolutionary masses for high-mass stars.....	57
5.3.1	Mass estimates for early stages.....	57
5.3.2	Mass estimates for core-collapse supernovae progenitors.....	61
6	Asteroseismic masses.....	63
6.1	Global asteroseismology of low-mass stars.....	64
6.1.1	Scaling relations.....	64
6.1.2	Grid-based modelling.....	65
6.1.3	Accuracy tests.....	67
6.2	Detailed frequency modelling of solar-type stars.....	69
6.2.1	Solar-type dwarfs.....	69
6.2.2	Subgiant stars.....	70
6.2.3	Accuracy of the obtained masses.....	71
6.2.4	Uncertainties in seismic modelling due to atomic diffusion and initial helium abundance.....	72

6.3	Asteroseismic masses from gravity-mode pulsators.....	74
6.4	Asteroseismic mass determination with inverse methods.....	79
6.5	Onward to pre-main sequence asteroseismic masses.....	82
7	Remnants	83
7.1	White dwarfs.....	83
7.2	Neutron stars.....	86
7.3	Black holes.....	87
7.4	Remnant populations	88
8	Summary and conclusions: the mass ladder	89
	Glossary	97
	References.....	100

1 Introduction and motivation: the need for stellar masses

The mass of a star is one of the two fundamental properties that determine its structure and evolution, including the nuclear element production and the final fate—as a White Dwarf, a Neutron Star, or a Black Hole. Compared to the initial chemical composition, mass is the much more influential parameter, also because the variation from star to star in the dominating elements, hydrogen and helium, is rather low, while stellar masses range from below 0.1 to more than 100 solar masses (M_{\odot}).

Without an accurate knowledge of the masses of stars, theoretical models of their interior cannot deliver reliable ages, chemical yields, or observable properties like brightness, electromagnetic spectrum, or oscillation frequencies. Although the theory of stellar evolution and the theoretical models have problems of their own, stellar mass is definitely a *necessary* requirement as input for the computation of accurate models.

Unfortunately, while being so basic, this quantity is at the same time extremely difficult to determine, as there exists no direct observable that would yield it. Therefore, one usually has to resort to indirect methods, most of which in themselves are model-dependent. A notable exception are dynamical masses derived from multiple-star systems.

In this review, we summarize a variety of methods to estimate—if not determine—stellar masses. These methods are often applicable to specific stars or stellar aggregates only. They may depend on specific available observables, but may also be suited for cross-calibration of methods. Apart from introducing methods and problems in stellar mass determinations, the review also contains a suggested list of benchmark stars that may serve as cross-calibration objects. At all moments, the reader should be aware that this paper deals with determination of present-day mass of stars. Relating this to the initial mass of the star requires accurate understanding of stellar winds or past history of star, e.g., mass exchange in binary or multiple systems. Such topics go beyond the scope of this review article.

The paper contains a lot of information. Before going any further, most readers might find it convenient to first turn to Sect. 8 in which we present a summary of the methods, including a comprehensive table. It also includes the idea of a mass ladder, represented with a summary plot showing the accuracy/precision of methods and

range of applicability. Section 8 may also help the reader to decide on which sections to focus her/his attention.

In the next subsections, a number of astrophysical topics will be highlighted, illustrating why knowledge of stellar masses is indispensable. Subsequently, the main part of the paper treats various methods of mass determination, covering the entire Hertzsprung–Russell Diagram (HRD hereafter). For the sake of clarity and consistency, we adopt the following definition and terminology in terms of the ranges covered for the mass: low-mass stars have $M \lesssim 1.3 M_{\odot}$, intermediate-mass stars have $1.3 \lesssim M \lesssim 8 M_{\odot}$, and high-mass stars cover $M \gtrsim 8 M_{\odot}$. A glossary for acronyms used in the paper is included in the last section.

1.1 Masses for stellar physics

As was mentioned above, mass is the most basic parameter that determines the structure and evolution of a star. The physical processes in stars range from particle physics to hydrodynamical flows, including nuclear, atomic, and gravitational physics. Many of the physical processes and effects appear or work differently in stars of different mass. Examples are the occurrence of convective cores on the main sequence or the ignition of helium-burning under degenerate or non-degenerate conditions. The latter separates stars with masses below or above $\sim 2.3 M_{\odot}$ and depends also on the cooling of the helium core by neutrinos. While stellar models predict the separating mass for any given chemical composition, a determination of the stellar mass of stars at the tip of the Red Giant Branch allows one to test the implemented neutrino cooling functions (Raffelt and Weiss 1995). As the brightness of the Red Giant Branch (RGB hereafter) tip is a powerful distance indicator (Serenelli et al. 2017b), this has far-reaching consequences also for extragalactic physics and cosmology.

Other examples are the evolution of intermediate- and high-mass main-sequence stars, which depend strongly on the size and mass of the—convectively or otherwise—mixed core (e.g., Kippenhahn et al. 2012, chap. 32). Accurate masses, which are tightly connected to the convective core masses (m_{cc} hereafter) for intermediate- and high-mass stars, allow us to determine the presence and effectiveness of mixing processes throughout the star. Such processes occur in the radiatively stratified layers, from the bottom of the envelope all the way through the outer layers, enabling the transport of matter processed in the stellar core to the stellar surface and vice versa. A major unknown connected with the uncalibrated mixing processes is the mass of the helium core reached by the end of the core-hydrogen burning phase. The future life of the star, and its ultimate chemical yields, is largely determined by this unknown amount of helium buried in the deep interior. Stellar evolution models beyond core-hydrogen burning differ by orders of magnitude in their physical quantities, because the treatment of the interior physics for mixing in various stellar evolution codes relies on different theoretical concepts and implementations (e.g., Martins and Palacios 2013). High-precision masses for blue supergiants could largely help alleviate the differences in the theoretical post main-sequence model tracks of high-mass stars.

Intermediate-mass stars are known to lose significant fractions of their initial mass during the Asymptotic Giant Branch (AGB) phase by dust-driven winds. A determination of the mass of White Dwarfs (WD) in relation to their initial mass (initial-final mass relation; IFMR) is accessible, for example, in stellar clusters or binary systems. This facilitates the determination of at least the integrated mass loss across the evolution (Salaris et al. 2009). This is also the case for the high-precision masses derived from asteroseismology of pulsating white dwarfs (Hermes et al. 2017). Unravelling the relation between the birth mass, the remnant WD mass, and the stellar wind of AGB stars is crucial for the understanding of the chemical evolution of galaxies.

Similarly, the mass of observed high-mass stars in relation to their brightness and, therefore, to their initial mass yields valuable information about the effectiveness of radiation-driven stellar winds and of the chemical yields that such winds deliver to the surroundings. For birth masses above $\sim 15 M_{\odot}$, radiation-driven winds are effective throughout the entire lifetime of the star, leading yet again to a natural distinction in terms of mass as far as efficiency in metal provision to the interstellar medium is concerned.

The temperature, respectively, the radius, of cool giants depend on the extent of convective envelopes and on the structure of the stellar atmosphere (Tayar et al. 2017). The correlation with stellar mass is that the higher the mass the hotter (smaller) the giant. With accurate mass determinations the correct structure of a giant's outermost layers can be inferred and, therefore, our knowledge about convection be enhanced.

These few examples illustrate why accurate stellar masses are necessary to improve stellar models, which are ultimately used for many important aspects of astronomy and astrophysics, from distance determinations in the Universe to age predictions and chemical enrichment laws of galaxies.

1.2 Masses for exoplanetary science

The past decade has witnessed both a dramatic growth in the number of known exoplanets,¹ and a tremendous advance in our knowledge of the properties of planets orbiting stars other than the Sun. Space-based transit surveys such as CoRoT (Baglin et al. 2006), *Kepler* (Borucki et al. 2010), and K2 (Howell et al. 2014) have revolutionized the field of exoplanetary science. Their high-precision and nearly uninterrupted photometry have opened up the doors to planet parameter spaces that are not easily accessible from ground, most notably, the Earth-radius planet domain. High-precision spectrographs, such as HIRES (Vogt et al. 1994), HARPS (Mayor et al. 2003), and ESPRESSO (Pepe et al. 2014) have enabled the detection and mass determinations of planets down to a few Earth masses. Focusing on bright stars ($5 < V < 11$), space missions such as the TESS (Ricker et al. 2015) and PLATO (Rauer et al. 2014) satellites will allow us to take a leap forward in the study of Neptunes, super-Earths, and Earth-like planets, providing golden targets for atmospheric characterization with the James Webb Space Telescope (JWST), the

¹ More than 4360, as of October 9, 2020. Source: exoplanet.eu.

European Extremely Large Telescope (E-ELT), the Thirty-Meter Telescope (TMT), and the ARIEL space telescope (Tinetti et al. 2018).

We can rightfully argue that the passage of a planet in front of its host star provides us with a wealth of precious information that allows us to investigate the nature of planetary systems other than ours. Radial velocity (RV) measurements of the host star enable us to detect the Doppler reflex motion induced by the orbiting planet and, combined with transit photometry, give us access to the geometry of the orbit (inclination, semi-major axis, eccentricity), enabling the measurement of the planetary mass, radius, and mean density (Seager and Mallén-Ornelas 2003). This allows us to study the internal structure and composition of planets—by comparing their positions on a mass-radius diagram with theoretical models (Gandolfi et al. 2017; Van Eylen et al. 2018)—and distinguish between gas giants, ice giants, and terrestrial worlds with or without atmospheric envelopes.

The knowledge of the planetary properties intimately relies on the knowledge of the parameters of the host star. Most notably, the planetary radius and mass can be derived from combining Doppler spectroscopy with transit photometry *only* if the stellar mass M and radius R are known. The uncertainty on M and R directly influences the uncertainty on the mass and radius of exoplanets. When stellar masses and radii are determined in a variety of inhomogeneous ways, the resulting exoplanet masses and radii will also be inhomogeneous, potentially limiting our understanding of exoplanet compositions (Southworth et al. 2007; Southworth 2010, 2012; Torres et al. 2012b; Mortier et al. 2013). With planet-to-star radius ratio and radial velocity semi-amplitudes determined to better than 2 and 10% in several cases (Pepe et al. 2013; Gandolfi et al. 2017; Prieto-Arranz et al. 2018; Gandolfi et al. 2018; Van Eylen et al. 2016, 2018), the uncertainty on stellar mass and radius can become important sources of uncertainty in the determination of the planetary mass, radius, and composition.

Model-independent and accurate stellar radii for low-mass stars can be determined by combining broadband photometry with the *Gaia* parallax (Gaia Collaboration et al. 2018), following, e.g., the procedure described in Stassun et al. (2018). Model-independent stellar masses can be accurately measured only in double-lined or visual eclipsing binary systems (Sect. 2). It then should not come as a surprise if the most precise masses of host stars have been obtained for circum-binary planets (see, e.g., Doyle et al. 2011). For planets discovered using the transit method, precise mass determinations can be obtained by using the spectroscopically derived effective temperature T_{eff} and iron abundance $[\text{Fe}/\text{H}]$, along with the mean stellar density ρ_{\star} obtained from the modeling of the transit light curve (Sozzetti et al. 2007; Winn 2010). The stellar mass can then be inferred by comparing the position of the star on a T_{eff} vs. ρ_{\star} diagram with a grid of evolutionary tracks computed for the spectroscopic iron abundance $[\text{Fe}/\text{H}]$ (see, e.g., Gandolfi et al. 2013, and Sect. 5.1). While this is valid for planets in circular orbits, it reinforces the need for independent stellar mass determinations because, in this case, the mean stellar density, combined with a precise measurement of the duration and of the shape of a planetary transit, can be used to infer exoplanet orbital eccentricities (e.g., Van Eylen and Albrecht 2015; Xie et al. 2016; Van Eylen et al. 2019) or

predict orbital periods of planets that transit only once (e.g., Osborn et al. 2016; Foreman-Mackey et al. 2016).

The need for accurate stellar masses is also important both at the beginning and the end of the lifetime of planets. Accurate measurements of the masses and ages of pre-main sequence (pre-MS hereafter) stars, and evolutionary models mapping these quantities to readily observable attributes, are vitally important for addressing many questions in the field of planet formation. For example, these quantities are needed to determine the ages of young star forming regions (e.g., Pecaut and Mamajek 2016), assess the dynamics and lifetimes of protoplanetary disks (and thus constrain the duration of the planet formation epoch; e.g., Andrews et al. 2018), and convert the luminosity and orbital parameters of directly imaged exoplanets into constraints on planet mass (e.g., Marois et al. 2008; Macintosh et al. 2015).

Finally, accurate stellar masses are required for the study of planets orbiting evolved stars. Subgiant and giant stars are observed to have fewer close-in giant planets (see, e.g., Johnson et al. 2010; Ortiz et al. 2015; Reffert et al. 2015). The origin of this is subject to debate, and may be caused by tidal evolution (Rasio et al. 1996; Schlaufman and Winn 2013) or be the result of the higher mass of observed evolved stars compared to observed main-sequence stars (Burkert and Ida 2007; Kretke et al. 2009). Precisely determining the mass and evolutionary stage of these evolved planet-host stars is difficult but may help understand and distinguish between these mechanisms (e.g., Campante et al. 2017; North et al. 2017; Stello et al. 2017; Ghezzi et al. 2018; Malla et al. 2020), in particular for evolved stars around which short-period planets have been detected (see, e.g., Van Eylen et al. 2016; Chontos et al. 2019).

1.3 Evolution of stellar systems

Stellar systems such as open and globular clusters are believed to be free of non-baryonic dark matter and consist of stars with different masses and various types of stellar remnants (white dwarfs, neutron stars and black holes). Because of their relatively low number of stars and small sizes (compared to galaxies), the dynamical evolution of these systems is governed by gravitational N -body interactions (e.g., Meylan and Heggie 1997). To estimate the relevant dynamical timescales, such as the crossing time and the relaxation time, the total number of stars and remnants and their masses are needed, combined with their phase space distribution (Spitzer and Hart 1971). Insight into the dynamical state and evolution of star clusters can thus be obtained from the masses of their member stars combined with their positions and velocities and (model-informed) assumptions on the properties of the dark remnants.

The stars in stellar clusters have the same age and iron abundance,² making them important tools in studies of the stellar initial mass function (IMF, see, e.g., Bastian et al. 2010a). For old globular clusters ($\gtrsim 10$ Gyr) the mass function is affected by stellar evolution at masses $\gtrsim 1M_{\odot}$, making it impossible to infer the IMF at these

² Noticeable exceptions are the most massive globular clusters ($> 10^6 M_{\odot}$), such as ω Centauri, which display spreads in age and [Fe/H] (e.g., Villanova et al. 2007).

masses with star counts. Because the remnant population depends on the IMF, it is possible to gain some insight into the IMF of stars that have evolved off the main sequence. For example, Hénault-Brunet et al. (2020) presented a method to infer the IMF slope at masses $\gtrsim 1M_{\odot}$ in globular clusters by probing the contribution of dark remnants to the total cluster mass profile with dynamical multimass models and then relate a parameterized IMF above the main-sequence turn-off (MSTO) mass to a remnant mass function with an IFMR. An additional challenge in using old clusters for IMF studies is that they are dynamically evolved, which results in the preferential ejection of low-mass stars ($\lesssim 0.5M_{\odot}$, e.g., Paust et al. 2010; Sollima and Baumgardt 2017). Despite these complications, stellar masses in star clusters provide valuable constraints on the IMF at high redshift, in extreme star formation environments and covering a large range of metallicities ($-2 \lesssim [\text{Fe}/\text{H}] \lesssim 0$).

Finally, all old globular clusters ($\gtrsim 10\text{Gyr}$) and many young(er) massive star clusters ($\gtrsim 2\text{Gyr}$; $\gtrsim 10^5 M_{\odot}$) contain multiple populations, in the form of star-by-star abundance variations, and different inferred helium abundance as well, that have been identified both spectroscopically (e.g., Carretta et al. 2009, 2010) and photometrically (e.g., Niederhofer et al. 2017; Milone et al. 2017). The radial distributions of stars with different abundances are different, with the polluted stars typically being more centrally concentrated (Nardiello et al. 2018; Larsen et al. 2019). This finding may hold important clues about how the multiple populations form, but because helium enriched stars are less massive (at the same luminosity), dynamical mass segregation can affect the primordial distribution during the evolution (Larsen et al. 2015). The stellar mass function of the various populations may also provide insight into whether the population formed in multiple bursts or not (Milone et al. 2012). Having accurate masses ($\lesssim 10\%$) of large samples of stars with different (He) abundances in globular clusters would provide valuable additional constraints on the origin of multiple populations in star clusters.

1.4 Evolution of (dwarf) galaxies

Galactic Archaeology (or perhaps better Palaeontology) uses what we understand of the resolved stellar populations of all ages in a galaxy to reconstruct the history of the entire system going back to the earliest times. It is possible to determine a galactic scale star formation history, as well as the chemical evolution history from careful measurements of large samples of individual stars (e.g., Tolstoy et al. 2009). The ability to accurately carry out this reconstruction of past events heavily relies upon having good age estimates for the stellar population in the system. Age determinations always depend on stellar models, and, as we mentioned before, an indispensable prerequisite for accurate stellar models are precise stellar masses. In the following, we discuss the particular consequences of uncertainties in stellar masses for the galactic archaeology of dwarf galaxies. The more accurate the age determinations are, the more precise will be the conclusions about the galactic history. If the ages are inaccurate, then the true timescale for fundamental events in the history of a galaxy remains uncertain because it is not possible to disentangle a unique evolutionary path for the system. We are almost certain that absolute age

determinations are inaccurate, but in a dwarf galaxy having correct relative ages is all that is needed to follow most of the evolution we see in the system.

The most accurate ages of resolved stellar populations come from the MSTO region in a colour–magnitude diagram (CMD). Yet these still tend to have errors of ± 1 Gyr at ages > 5 Gyr old, corresponding to errors in stellar mass of order $0.1 M_{\odot}$, even for relative ages, due to the narrow range of luminosity of these MSTO stars at these ages (e.g., de Boer et al. 2011). This method is related to mass determinations by isochrone methods, which will be presented in Sect. 5.1.

Distinguishing age effects from metallicity effects can be complicated; this is the so-called age-metallicity degeneracy. The only chemical abundance measurements of resolved dwarf galaxies come from spectroscopy of individual RGB stars in these relatively distant systems. This represents a mismatch in age and metallicity/abundance determinations, because they might come from different stellar populations and directly determining masses and thus ages of RGB stars is particularly uncertain at present. Knowledge of the masses of main-sequence and MSTO stars can be used to limit the range of isochrones used to determine the mass of RGB stars and their ages (e.g., de Boer et al. 2012). This helps to improve the age determinations that are then used to link chemical enrichment processes over the history of star formation to the star formation rates.

If the intrinsic accuracy of age determinations of RGB stars could be improved, it would lead to a more direct link between the star formation and chemical evolution processes, and on much shorter timescales, than is presently possible. At present the limits in age accuracy remain a major uncertainty for understanding rapid evolutionary processes that must have occurred at early times in all galaxies. The majority of stars in any galaxy have $[\text{Fe}/\text{H}] > -2$. So far no zero metallicity stars have been found (Frebel and Norris 2015). Hence there was a universal early and rapid chemical enrichment process. However, understanding the nature of this event requires better ages, i.e., masses of low-mass stars than are currently available. We can monitor the build up of chemical elements, but as we are not able to associate an accurate age to the stars as they enrich in various chemical elements we cannot be sure how stochastic this process has been, and over what timescale. Answering the questions whether the stars that first formed in a galaxy have peculiar properties (e.g., an unusual initial mass function) and if this why we do not observe primordial stars today requires accurate present-day mass functions and ages, and thus mass determinations of individual RGB stars in dwarf galaxies.

2 Direct method: dynamical masses

Binary stellar systems offer a unique opportunity to measure the masses of stars in a fundamental way, independently of models and calibrations. Particularly interesting are double-lined eclipsing binary systems, because the combination of their radial-velocity analysis, which provides the minimum masses of the binary components, and the light-curve analysis, from which the inclination and the radius relative to the semi-major axis can be measured, yields the absolute individual masses and radii of the stars. These can potentially be derived with accuracies to the 1% level or better

(see Torres et al. 2010, for a review). Since the method is so fundamental, we discuss the principles, different methods, and achievable accuracy in greater detail in the following section, along with some highlighted examples.

2.1 Principles

Binary stars are the primary source for fundamental stellar quantities: masses, radii, and effective temperatures, hence luminosities. The masses of binary system components follow from the orbital dynamics of the stars. Due to the orbital motion, line-of-sight velocities are changing, and spectral lines are shifted according to the Doppler effect. The measurement of radial velocities (RVs) solves a set of the orbital elements, which in the general case of an eccentric orbit are period P , time of periastron passage T_{per} , eccentricity e , longitude of periastron ω , and the semi-amplitudes K_A and K_B of the velocity curves for the components A and B, respectively. Once the orbital elements are determined, the masses can be computed from the equations (for a full derivation see Hilditch 2001, pp. 29–46):

$$M_{A,B} \sin^3 i = P(1 - e^2)^{(3/2)} (K_A + K_B)^2 K_{B,A} / 2\pi G. \quad (1)$$

A factor $\sin^3 i$ enters this equation as a projection factor, since the orbital plane of a binary system is in general inclined by an angle i to the line-of-sight. This purely geometrical effect has an important consequence for the mass determination. Since the inclination i of a binary star orbit cannot be determined from the RVs, complementary observations besides the spectroscopic determination of the RVs are needed. If the binary system is also an eclipsing system, the inclination i can be determined from the light curve analysis. Should the binary system be non-eclipsing, i could still be derived from astrometric-interferometric observations, which, moreover, allows one to determine the orientation of the system.

2.1.1 Radial-velocity measurements

It is obvious from Eq. 1 that the masses are very sensitive to the radial velocity (RV) semi-amplitudes, since $M \sim K^3$. To get an empirical stellar mass with an accuracy of about 3%, the velocity semi-amplitudes should be determined with uncertainties of less than 1%. Thus the quality of the measurements of the radial velocities along the orbital cycle is of critical importance. The most widely used are cross-correlation methods in which essentially a position of a cross-correlation profile is measured either by fitting a certain function to it (Gaussian or whatever), or by computing its first-order moment (center of gravity). Cross-correlation methods differ in the templates used. In ‘classical’ cross-correlation (Simkin 1974; Tonry and Davis 1979) a rotationally broadened spectrum is used as a template. The broadening function (Rucinski 1992) uses a rotationally unbroadened template where only thermal and pressure line broadening sources are considered. The least-squares deconvolution (Donati and Collier Cameron 1997) is a discrete cross-correlation where the template is a set of delta-functions. We refer to these methods as cross-correlation function (CCF) methods. A new concept of measuring the RVs which

significantly increased the precision was pioneered by Campbell and Walker (1979). They put a hydrogen fluoride (HF) absorption cell into the light path to the spectrograph, which enables the recording of a rich spectrum superimposed on a stellar spectrum. This provided a stable wavelength scale. The subsequent development of high-precision RV measurements was due to Marcy and Butler (1992) who used an iodine absorption cell instead of the life endangering HF cell. Konacki (2005) combined the power of the iodine cell with disentangling techniques and eventually reached a record breaking precision in the determination of stellar masses with an extra bonus of separating the components' spectra.

The spectrum of a binary system consists of the individual components' spectra. Due to the orbital motion, the composite spectrum usually is quite complex due to various inevitable blends of the components' spectral lines. Determination of the RVs from the CCF between the composite binary spectrum and an appropriate template spectrum improves the quality of the solutions for the orbital elements (cf. Hilditch 2001, pp. 71–85). The problem of template mismatches can be partially solved by using a 2D CCF method, which is achieved with the widely used *todcor* code (Zucker and Mazeh 1994). The Least-squares deconvolution (LSD) technique enables the determination of a mean line profile from a single exposure, which enhances the signal-to-noise ratio (S/N hereafter) considerably, allowing for precise measurements of the RVs for complex and high contrast systems as shown by Tkachenko et al. (2013).

2.1.2 Spectral disentangling

In the spectral disentangling (SPD) method (Simon and Sturm 1994) the orbital elements of a binary system are determined directly from the time-series analysis of the observed composite spectra. The intrinsic spectra of the individual components are reconstructed simultaneously (see Fig. 1 for the illustrative case of V453 Cyg). This improves and generalises the Doppler tomography technique introduced by Bagnuolo et al. (1991) since no prior knowledge of the RVs is needed. In principle, the composite spectrum of a binary system is the linear combination of the intrinsic spectra of the components shifted according to the orbital motion in the course of the orbital cycle. In the composite spectra the components' spectra are diluted but otherwise the line profiles are preserved.

In principle, the system of linear equations representing the time series of observations must be solved. Obviously, there are more equations than unknowns, and the problem should be solved by some regularisation conditions while solving the equations via least squares methods. Simon and Sturm (1994) used the singular-value decomposition technique, whilst Hadrava (1995) transformed the problem to Fourier space making the calculations less demanding in CPU time and memory. Further improvements in Fourier-space disentangling were implemented in *fdbinary* (Ilijić et al. 2004). Another promising approach in SPD has been realised by Czekala et al. (2017b) using Gaussian processes. An overview of different disentangling and separation techniques is given in Pavlovski and Hensberge (2010).

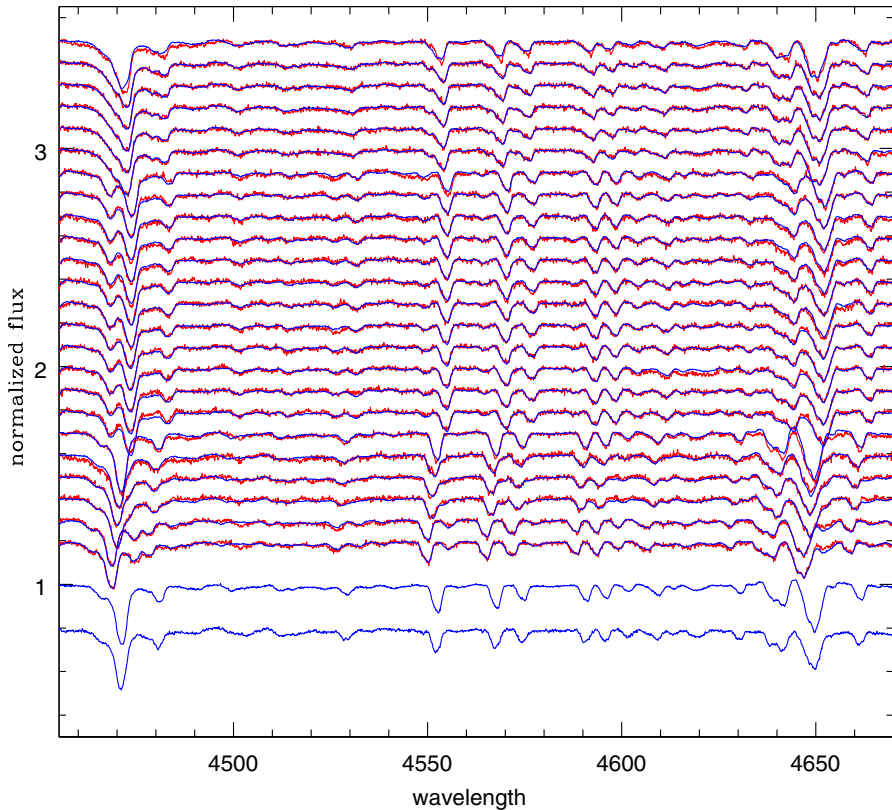


Fig. 1 Spectral disentangling of a time-series of observed high-resolution échelle spectra of the binary system V453 Cyg (shown in red). The spectra at the bottom (in blue) are the disentangled spectra of the primary (upper) and secondary component (lower). Fits to the observed spectra are overplotted (in blue). Image reproduced with permission from Pavlovski and Southworth (2009), copyright by the authors

As is illustrated in Fig. 1, the individual spectra of the components are revealed from SPD. This is an important outcome since these spectra can then be analysed with all spectroscopic analytical methods as used for single stars. In turn, the atmospheric parameters, such as effective temperatures, gravities, abundances, etc., for each of the components can be determined with important feedback for the light curve analysis. A procedure for a complementary iterative analysis of the spectroscopic and photometric observations for eclipsing binaries is elaborated upon in Hensberge et al. (2000) and Pavlovski and Hensberge (2005). The methodology has been improved and updated in Pavlovski et al. (2018). SPD is at the core of the procedure to determine a whole set of fundamental stellar quantities for each of the components, such as their luminosity, metallicity, chemical composition, age, and distance.

Most SPD applications so far do not take into account any intrinsic variability of the individual components. As an example, it was found from high-precision μ -mag level TESS space photometry that the primary of V453 Cyg is a β Cep pulsator

(Southworth et al. 2020). The pulsational nature of this binary cannot be deduced from mmag-level ground-based photometry but is readily visible from the asymmetric nature of the line profiles shown in Fig. 1. A similar situation occurs for the massive binary β Cep pulsator β Centauri, for which iterative SPD analysis taking into account its nonradial oscillations was performed by Ausselees et al. (2006). The pulsational nature of this rapidly rotating β Cep star was readily detected from time-series spectroscopic line-profile variations while it remained elusive in mmag-level ground-based photometry (Aerts and De Cat 2003). The pulsational characters of this multiple system is nowadays obvious from BRITe space photometry (Pigulski et al. 2016). Ignoring the intrinsic pulsations causing line-profile variability in iterative SPD analyses to derive component masses is not a severe limitation when the rotational line broadening is dominant over the pulsational line broadening, as is the case for β Centauri. However, whenever these two phenomena cause line broadening of similar order, the SPD should be improved by inclusion of line-profile variability modelling from a proper time-dependent pulsational velocity field at the stellar surface in addition to time-independent rotational broadening while performing the SPD, as in the application of the β Cep stars σ Scorpii (Tkachenko et al. 2014a) and α Virginis (Tkachenko et al. 2016).

2.1.3 Propagation of the systematic and random errors: accuracy vs. precision

The availability of échelle spectra with high spectral resolution, spanning wide spectral ranges in a single exposure has had a big impact on the quality of the RV measurements. The increased precision in the determination of stellar masses from detached eclipsing binaries is evident and is now at a level considerably below 1%. This is true in particularly for solar- or late-type stars, with spectra rich in spectral lines. For high-mass stars with an intrinsically much smaller choice of spectral lines, the current precision is still above 1%, but was significantly improved over the past decade (cf. Table 2). Inadequacies in the template spectra needed in the CCF, BF, or TODCOR methods are the main source of systematic errors and eventually in the determination of the components' masses. The best approach to trace the systematic errors due to the templates in the RV measurements is through numerical simulations. This approach was first applied by Popper and Hill (1991), Latham et al. (1996), and Torres et al. (1997) to derive corrections to be applied to measured RVs. This revealed that such corrections depend sensitively on the characteristics of the binary system. Therefore, they suggest that this effect should always be verified on a case-by-case basis.

An important exercise has been undertaken by Southworth and Clausen (2007) on real observations and the presence of strong line-blending. They measured RVs, using double-Gaussian fitting, one- and two-dimensional cross-correlation, and spectral disentangling. They analysed the performance of these methods in the determination of the orbital parameters. Whilst the methods of Gaussian fitting and CCFs required substantial corrections to account for severe line blending, they confirmed that spectral disentangling is not seriously affected and is superior to

other methods in this respect. This result is not unexpected, since in principle there is no need for a template spectrum in SPD.

An example of the variety of solutions coming from these different techniques of RV measurements is given in Table 1 for the binary system V453 Cyg. Only the results for the RV semi-amplitudes, in terms of the measured quantity $M \sin^3 i$, are listed. Without a detailed examination of the quality of the observational data (number of acquired spectra, spectral resolution and S/N, systematic errors) it is not possible to judge which of the solution is the most accurate one. The precision claimed for different solutions is higher than the differences between them but none of these solutions took into account the pulsational nature of the β Cep-type primary as discovered from TESS space photometry by Southworth et al. (2020).

A sensitive test for the accuracy of spectral disentangling discussed in Sect. 2.1.2 was performed from binaries with total eclipses. Disentangled spectra were matched to the components' spectra taken during the total eclipses. The observations for a few totally eclipsing binaries have shown the robustness of spectral disentangling in revealing accurately extracted individual spectra (Simon and Sturm 1994; Pavlovski and Southworth 2009; Hełminiak et al. 2015; Graczyk et al. 2016). Such test also proved the accuracy in the RV zero-point.

The concept of calibrating the spectrograph's wavelength scale with an absorption cell introduced by Campbell and Walker (1979), nowadays being regularly used in Doppler-shift searches of exoplanets, was also applied for measuring the RVs of the spectroscopic binary systems by Konacki (2005) and Konacki et al. (2009). This novel technique enabled to accurately determine RVs down to precisions of about 20–30 m s⁻¹ in the case of F-type binaries, and about 10 m s⁻¹ for late-type binaries. Further upgrading this method, Konacki et al. (2010) combined it with tomographically disentangled spectra, and reached a precision and accuracy of the RVs of the order of 1–10 m s⁻¹. These RV measurements made possible the determination of the most accurate masses of binary stars. The fractional accuracy in $M \sin i$ ranges from 0.02% to 0.42%, which

Table 1 Comparison of the spectroscopic solutions derived by different methods for the double-lined system V453 Cyg, ignoring the pulsations of the primary discovered in TESS data by (Southworth et al. 2020)

Method	K_A (km s ⁻¹)	K_B (km s ⁻¹)	$M_A \sin^3 i$ (M_\odot)	$M_B \sin^3 i$ (M_\odot)	Ref.
CCF	171.0 ± 1.5	222.0 ± 2.5	13.81 ± 0.35	10.64 ± 0.22	Pop91
SPD	171.7 ± 2.9	223.1 ± 2.9	14.01 ± 0.44	10.78 ± 0.38	Sim94
Gaussian	173.2 ± 1.3	213.6 ± 3.0	12.87 ± 0.39	10.44 ± 0.22	Bur97
TODCOR	173.7 ± 0.8	224.6 ± 2.0	14.35 ± 0.28	11.10 ± 0.14	Sou04
SPD	172.5 ± 0.2	221.5 ± 0.5	13.85 ± 0.07	10.79 ± 0.04	Pav09
SPD	175.2 ± 1.3	220.2 ± 1.6	13.87 ± 0.23	11.03 ± 0.18	Pav18

References: Pop91: Popper and Hill (1991), Sim94: Simon and Sturm (1994), Bur97: Burkholder et al. (1997), Sou04: Southworth et al. (2004), Pav09: Pavlovski and Southworth (2009), Pav18: Pavlovski et al. (2018)

rivals the precision in mass of the relativistic double pulsar system PSR J0737-3039 components (Weisberg and Huang 2016).

Controlling systematic and random errors in the spectroscopic RV measurements is only part of the error budget in the final determination of stellar masses. For an absolute determination of the dynamical masses, the inclination of the orbital plane has to be known. Usually i is deduced from the light-curve analysis, which is hampered by the many degeneracies and correlations in a multi-dimensional parameter space. Among the most pronounced ones are the degeneracies between the inclination and possible third light in a system and between the ratio of the radii and the light ratio for partially eclipsing systems. Hence extensive Bayesian calculations are a prerequisite to map confidence levels and the strength of correlations for the parameters involved in the light curve analysis. Maxted et al. (2020) address this important issue by performing an experiment in which the light curve solution was derived by several experts using different codes, optimisation routines, and strategies for the calculations of the uncertainties. A similar investigation in the determination of spectroscopic orbital elements would be worthwhile.

2.2 Benchmark binary systems

Torres et al. (2010) compiled a list of 94 detached eclipsing binary (DEB) systems along with the α Cen system, all of which satisfy the criterion that the mass and radius of both components are known within an uncertainty of $\pm 3\%$ or better. Their sample more than doubles the earlier one assembled by Andersen (1991), who had set a more stringent threshold for the uncertainty of only $\pm 2\%$. This same strict threshold was used by Southworth (2015), whose online catalogue DEBCat³ is constantly upgraded with new and precise published solutions for detached eclipsing binaries. At the time of writing, DEBCat contains 244 systems, including the important extension to extragalactic binary stars based on devoted work by the Warsaw–Torun group (e.g., Pietrzyński et al. 2013; Graczyk et al. 2014, 2018).

In Table 2 we collected all the DEBs matching two criteria: (i) the masses and radii should be determined with a precision better than 2% for high-mass, and gradually down to 1% for low-mass stars, and (ii) the metallicity for the components were determined by spectroscopic analysis, either from disentangled spectra or from double-lined composite spectra. Moreover, for the majority of stars in Table 2 a detailed abundance determination is available. Altogether, 40 binary systems satisfy all these prerequisites and constitute an optimal sample of benchmark stars for probing theoretical evolutionary models. The parameters of these 80 stars are collected in Table 2. The mass–radius and mass–temperature relationships of these benchmark stars are shown in Fig. 2, where those indicated in red are evolved objects. The two insets in the separate panels of this figure represent the stars with a mass below $1 M_{\odot}$. The evolved binary components clearly deviate from the tight correlations.

³ <https://www.astro.keele.ac.uk/jkt/debcats/>.

Table 2 List of benchmark DEBs suitable for comparison to theoretical evolutionary models

Star	$M (M_{\odot})$	$R (R_{\odot})$	$\log g$ (cgs)	$\log T$ (K)	Ref.
AH Cep	16.14 ± 0.26	6.51 ± 0.10	4.019 ± 0.012	4.487 ± 0.008	Pav18
	13.69 ± 0.21	5.64 ± 0.11	4.073 ± 0.018	4.459 ± 0.008	
V478 Cyg	15.40 ± 0.38	7.26 ± 0.09	3.904 ± 0.009	4.507 ± 0.007	Pav18
	15.02 ± 0.35	7.15 ± 0.09	3.907 ± 0.010	4.502 ± 0.008	
V578 Mon	14.54 ± 0.08	5.41 ± 0.04	4.133 ± 0.018	4.477 ± 0.007	Gar14
	10.29 ± 0.06	4.29 ± 0.05	4.185 ± 0.021	4.411 ± 0.007	
V453 Cyg	13.90 ± 0.23	8.62 ± 0.09	3.710 ± 0.009	4.459 ± 0.008	Pav18
	11.06 ± 0.18	5.45 ± 0.08	4.010 ± 0.012	4.442 ± 0.009	
CW Cep	13.00 ± 0.07	5.45 ± 0.05	4.079 ± 0.008	4.452 ± 0.007	Joh19
	11.94 ± 0.08	5.10 ± 0.05	4.102 ± 0.008	4.440 ± 0.007	
V380 Cyg	11.43 ± 0.19	15.71 ± 0.13	3.104 ± 0.006	4.336 ± 0.006	Tka14
	7.0 ± 0.14	3.82 ± 0.05	4.120 ± 0.011	4.356 ± 0.023	
DW Car	11.34 ± 0.12	4.56 ± 0.05	4.175 ± 0.008	4.446 ± 0.016	SCI07
	10.63 ± 0.14	4.30 ± 0.06	4.198 ± 0.011	4.423 ± 0.016	
CV Vel	6.067 ± 0.011	4.08 ± 0.03	4.000 ± 0.008	4.255 ± 0.012	Alb14
	5.952 ± 0.011	3.94 ± 0.03	4.021 ± 0.008	4.250 ± 0.012	
U Oph	5.09 ± 0.06	3.44 ± 0.01	4.073 ± 0.004	4.220 ± 0.004	Joh19
	4.58 ± 0.05	3.05 ± 0.01	4.131 ± 0.004	4.182 ± 0.004	
β Aur	2.376 ± 0.027	2.762 ± 0.017	3.932 ± 0.005	3.971 ± 0.009	Sou07
	2.291 ± 0.027	2.568 ± 0.017	3.979 ± 0.005	3.964 ± 0.009	
YZ Cas	2.263 ± 0.012	2.525 ± 0.011	3.988 ± 0.004	3.979 ± 0.005	Pav14
	1.325 ± 0.007	1.331 ± 0.006	4.311 ± 0.004	3.838 ± 0.015	
SW Cma	2.239 ± 0.014	3.014 ± 0.020	3.830 ± 0.007	3.914 ± 0.008	Tor12
	2.104 ± 0.018	2.495 ± 0.042	3.967 ± 0.015	3.908 ± 0.008	
V1229 Tau	2.221 ± 0.027	1.843 ± 0.037	4.253 ± 0.019	4.001 ± 0.026	Gro07
	1.586 ± 0.042	1.565 ± 0.015	4.231 ± 0.024	3.861 ± 0.022	
TZ For	2.057 ± 0.001	8.34 ± 0.11	2.915 ± 0.023	3.693 ± 0.003	Gal16
	1.958 ± 0.001	3.97 ± 0.08	3.539 ± 0.037	3.803 ± 0.005	
WW Aur	1.964 ± 0.007	1.927 ± 0.011	4.162 ± 0.007	3.901 ± 0.024	Sou05
	1.814 ± 0.007	1.841 ± 0.011	4.167 ± 0.007	3.885 ± 0.024	
RR Lyn	1.927 ± 0.008	2.57 ± 0.02	3.900 ± 0.005	3.901 ± 0.024	Tom06
	1.507 ± 0.004	1.59 ± 0.03	4.214 ± 0.018	3.885 ± 0.024	
XY Cet	1.773 ± 0.016	1.873 ± 0.035	4.142 ± 0.016	3.896 ± 0.006	Sou11
	1.615 ± 0.014	1.773 ± 0.029	4.149 ± 0.014	3.882 ± 0.007	
HW CMa	1.721 ± 0.011	1.643 ± 0.018	4.242 ± 0.010	3.879 ± 0.009	Tor12
	1.781 ± 0.012	1.662 ± 0.021	4.247 ± 0.011	3.886 ± 0.008	
V501 Mon	1.645 ± 0.004	1.888 ± 0.029	4.103 ± 0.013	3.876 ± 0.006	Tor15
	1.459 ± 0.003	1.592 ± 0.028	4.199 ± 0.016	3.845 ± 0.006	
HD 187669	1.504 ± 0.003	11.33 ± 0.28	2.507 ± 0.020	3.667 ± 0.007	Hel15
	1.505 ± 0.004	22.62 ± 0.50	1.907 ± 0.019	3.636 ± 0.007	
BK Peg	1.414 ± 0.007	1.988 ± 0.008	3.992 ± 0.004	3.797 ± 0.006	Cla10a
	1.257 ± 0.005	1.474 ± 0.017	4.201 ± 0.010	3.801 ± 0.006	

Table 2 continued

Star	$M (M_{\odot})$	$R (R_{\odot})$	$\log g$ (cgs)	$\log T$ (K)	Ref.
AD Boo	1.414 ± 0.009	1.612 ± 0.014	4.173 ± 0.008	3.818 ± 0.008	Cla08
	1.209 ± 0.006	1.216 ± 0.010	4.351 ± 0.007	3.789 ± 0.008	
NP Per	1.321 ± 0.009	1.372 ± 0.013	4.284 ± 0.008	3.808 ± 0.006	Lac16
	1.046 ± 0.005	1.229 ± 0.013	4.278 ± 0.009	3.657 ± 0.015	
V1130 Tau	1.306 ± 0.008	1.489 ± 0.010	4.208 ± 0.006	3.822 ± 0.005	Cla10b
	1.392 ± 0.008	1.782 ± 0.011	4.080 ± 0.006	3.821 ± 0.005	
VZ Hya	1.271 ± 0.006	1.314 ± 0.005	4.305 ± 0.005	3.809 ± 0.010	Cla08
	1.146 ± 0.007	1.112 ± 0.007	4.405 ± 0.006	3.799 ± 0.010	
AI Phe	1.247 ± 0.004	2.912 ± 0.014	3.606 ± 0.004	3.791 ± 0.011	Kir16
	1.197 ± 0.004	1.835 ± 0.014	3.989 ± 0.007	3.711 ± 0.010	
EF Aqr	1.244 ± 0.008	1.338 ± 0.012	4.280 ± 0.007	3.789 ± 0.006	Vos12
	0.946 ± 0.006	0.956 ± 0.012	4.453 ± 0.011	3.715 ± 0.009	
WZ Oph	1.227 ± 0.007	1.401 ± 0.012	4.234 ± 0.008	3.790 ± 0.007	Cla08
	1.220 ± 0.006	1.419 ± 0.012	4.221 ± 0.008	3.786 ± 0.007	
KIC 3439031	1.226 ± 0.002	1.407 ± 0.002	4.230 ± 0.001	3.815 ± 0.015	Hel19
	1.227 ± 0.003	1.403 ± 0.003	4.233 ± 0.002	3.815 ± 0.015	
FL Lyr	1.210 ± 0.008	1.244 ± 0.023	4.331 ± 0.016	3.796 ± 0.008	Hel19
	0.951 ± 0.004	0.900 ± 0.024	4.508 ± 0.023	3.740 ± 0.019	
LL Aqr	1.196 ± 0.001	1.321 ± 0.006	4.274 ± 0.004	3.784 ± 0.003	Gra16
	1.034 ± 0.001	1.002 ± 0.005	4.451 ± 0.004	3.756 ± 0.004	
WASP 0639-32	1.154 ± 0.004	1.834 ± 0.023	3.974 ± 0.011	3.801 ± 0.003	Kir18
	0.783 ± 0.003	0.729 ± 0.008	4.607 ± 0.010	3.732 ± 0.006	
AL Dor	1.103 ± 0.001	1.121 ± 0.010	4.381 ± 0.008	3.779 ± 0.008	Gal19
	1.102 ± 0.001	1.118 ± 0.010	4.383 ± 0.008	3.776 ± 0.008	
V568 Lyr	1.087 ± 0.004	1.397 ± 0.013	4.184 ± 0.078	3.752 ± 0.007	Bro11
	0.828 ± 0.002	0.781 ± 0.005	4.570 ± 0.059	3.683 ± 0.013	
V636 Cen	1.052 ± 0.005	1.018 ± 0.004	4.444 ± 0.004	3.771 ± 0.006	Cla09
	0.854 ± 0.003	0.830 ± 0.004	4.532 ± 0.005	3.699 ± 0.009	
V530 Ori	1.004 ± 0.007	0.980 ± 0.013	4.457 ± 0.023	3.777 ± 0.007	Cla09
	0.596 ± 0.002	0.587 ± 0.007	2.915 ± 0.023	3.589 ± 0.013	
V565 Lyr	0.996 ± 0.003	1.101 ± 0.007	4.352 ± 0.005	3.748 ± 0.007	Bro11
	0.929 ± 0.003	0.971 ± 0.005	4.432 ± 0.008	3.735 ± 0.010	
47 Tuc V69	0.876 ± 0.005	1.315 ± 0.005	4.143 ± 0.003	3.803 ± 0.014	Bro17
	0.859 ± 0.006	1.162 ± 0.006	4.242 ± 0.003	3.773 ± 0.016	
YY Gem	0.598 ± 0.005	0.620 ± 0.006	4.630 ± 0.008	3.582 ± 0.011	Tor02
	0.601 ± 0.005	0.604 ± 0.006	4.655 ± 0.051	3.582 ± 0.011	

Table 2 continued

Star	$M (M_{\odot})$	$R (R_{\odot})$	$\log g$ (cgs)	$\log T$ (K)	Ref.
HAT-TR-	0.448 ± 0.001	0.455 ± 0.004	4.774 ± 0.006	3.504 ± 0.015	Har18
I 318-007	0.272 ± 0.004	0.291 ± 0.002	4.944 ± 0.004	3.491 ± 0.015	

The following criteria were used for this selection: (i) the masses of the components are determined with a precision better than 2% for high-mass stars, 1% for intermediate mass stars, and less than 0.5% for low-mass stars; (ii) metallicities are determined from a spectroscopic analysis, either from disentangled spectra or from a global fitting of the double-line composite spectra with synthetic spectra. The table is sorted by decreasing mass of the primary component

References: Pav18: Pavlovski et al. (2018), Gar14: Garcia et al. (2014), Joh19: Johnston et al. (2019b), Tka14: Tkachenko et al. (2014b), SCI07: Southworth and Clausen (2007), Alb14: Albrecht et al. (2014), Sou07: Southworth et al. (2007), Pav14: Pavlovski et al. (2014), Tor12: Torres et al. (2012a), Gro07: Groenewegen et al. (2007), Gal16: Gallenne et al. (2016), Sou05: Southworth et al. (2005), Tom06: Tomkin and Fekel (2006), Sou11: Southworth et al. (2011), Tor15: Torres et al. (2015b), Hel15: Helminiak et al. (2015), Cla10a: Clausen et al. (2010a), Cla08: Clausen et al. (2008), Lac16: Lacy et al. (2016), Cla10b Clausen et al. (2010b), Kir16: Kirkby-Kent et al. (2016), Vos12: Vos et al. (2012), Hel19: Helminiak et al. (2019), Gra16: Graczyk et al. (2016), Kir18: Kirkby-Kent et al. (2018), Gal19: Gallenne et al. (2019), Bro11: Brogaard et al. (2011), Cla09: Clausen et al. (2009), Tor14: Torres et al. (2014), Bro17: Brogaard et al. (2017), Tor02: Torres and Ribas (2002), Har18: Hartman et al. (2018)

Many of the stars in Table 2 have been or are currently being observed with space photometry assembled with TESS or BRITe, delivering levels of precision ten- to hundred times better than ground-based multi-colour photometry. In several cases, these space data reveal intrinsic variability of the components that was not detectable in photometry from the ground, but was already hinted at from spectroscopic time series for the case of V453 Cygni as illustrated in Fig. 1 and in Southworth et al. (2020). With that kind of new observational information, we have reached the stage where the methodological binary modelling framework needs to be upgraded, as the data are nowadays so precise that the current ingredients upon which the methods rely are no longer able to explain the measurements up to their level of precision. It is, therefore, to be anticipated that the results for the masses as listed in Table 2 will be improved and will lead to even more accurate masses in the not too distant future. Moreover, new eclipsing binaries with pulsating components are being discovered efficiently from space photometry (Bowman et al. 2019b; Handler et al. 2020; Kurtz et al. 2020; Southworth et al. 2021), opening up the opportunity of tidal asteroseismology from combined dynamical and asteroseismic (cf. Sect. 6) mass estimation.

2.3 Dynamical masses from visual binaries

The inclination i of the orbit to the tangent plane of the sky is given by the angle i . Its importance for determining the masses of the components in double-lined spectroscopic binaries was emphasized in Sect. 2.1. Eclipsing binaries are not the only type of binary systems which provide the inclination. Visual binaries, which

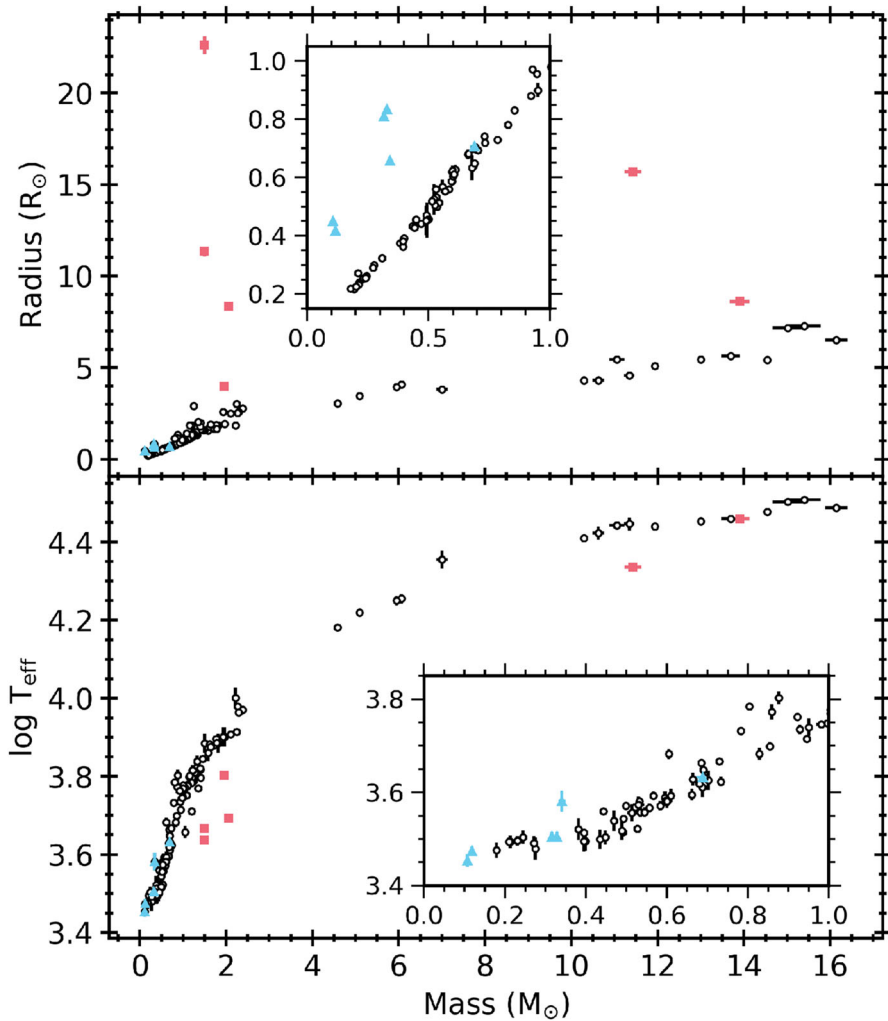


Fig. 2 Mass-radius and mass-temperature relations of the benchmark stars listed in Tables 2 and 4. The insets show the stars with masses below the solar mass. Cyan triangles are pre-MS stars while red squares represent evolved stars

are spatially resolved, allow the determination of the inclination angle from the orbital solution as well. Astrometric or interferometric measurements of visual binaries provide the orbital elements from a projection of the orbit on the plane of sky. Complementary spectroscopic measurements measure the radial velocities along the line of sight. The result are four orbital components: the period P , the time of periastron passage T_{per} , the eccentricity of the orbit, and the longitude of periastron ω . Torres (2004), Cunha et al. (2007), and Torres (2014) demonstrated that the spatial orientation of the orbit, the “3D orbit”, can be determined as well.

Thanks to the development of interferometric instrumentation (Hummel 2013), astrometric measurements eventually match the precision of the spectroscopic RV measurements, such that high-precision orbital elements can be determined from complementary observations, giving stellar masses on a level competitive to that of detached eclipsing binaries. In Table 3 a list of visual binaries with component masses more precise than 3% is given. The complementary approach allows the determination of the orbital parallax ϖ_{orb} , which, in turn, makes possible that of luminosities in an independent way.

The angular dimension, and thus the radii of the components of visual binaries can hardly be resolved even by modern interferometers. A successful measurement for stars in the α Cen system was achieved by Kervella et al. (2017) using the VLTI/PIONIER interferometer. Using the Mark III optical interferometer at Mount Wilson Observatory, Hummel et al. (1994) measured the radii of the giant and subgiant stars in the α Aur system, a non-eclipsing spatially resolved binary system (Torres et al. 2015a). In case the components are spatially resolved, the spectral energy distribution (SED) can be measured, allowing the determination of atmospheric parameters (effective temperatures and surface gravities, hence radii), and the calibration of the fundamental stellar quantities (Lester et al. 2019a, b, 2020; Bond et al. 2020).

The most complete way for the extraction of the stellar fundamental quantities is to spatially resolve eclipsing SB2 system. The first successful interferometrically resolved eclipsing system was β Aur by Hummel et al. (1995) by using the Mark III optical interferometer. Recently, Lester et al. (2019a) spatially resolved the double-lined eclipsing binary system HD 224121 from long baseline interferometry with the CHARA Array at Mount Wilson. In their comprehensive study Lester et al. (2019a) combined interferometric measurements, high-resolution spectroscopy and light-curve photometry. In addition, the authors determined the atmospheric parameters from tomographically separated spectra of the components and the radii from the spectral energy distribution. This kind of analysis allows the intercomparison of physical parameters of stars derived by different astrophysical methods. Further progress in spatially resolving double-lined eclipsing binaries was recently achieved by Gallenne et al. (2019), who resolved 6 DEBs with the VLTI/PIONIER in the infrared. They were able to derive masses and orbital parallaxes with a precision below 1%.

2.4 Fundamental masses at the lower end of the stellar mass range

Low-mass eclipsing binaries (EBs) with late-K and/or M dwarf components represent an excellent specific test-bed to improve models in the lowest mass regime, study the mass-radius relation at different ages and spectral types, and to better understand low-mass star-formation. This is because both masses and radii can be measured with precisions better than a few per cent. The advent of transit surveys from the ground (e.g., HAT-Net, SuperWASP, KELT, MEarth) and space (CoRoT, *Kepler*, *K2*) revealed a significant number of low-mass stars and brown dwarfs eclipsing solar-type stars (Irwin et al. 2010; Deleuil et al. 2008; Steffen et al. 2012; Siverd et al. 2012), and giants (e.g., Bouchy et al. 2011).

Table 3 List of visual binaries for which the masses of the components are determined with a precision better than 3%

Binary	a (mas)	M_1 (M_\odot)	M_2 (M_\odot)	π_{orb} (mas)	Ref.
μ Cas	998.5 ± 1.3	0.7440 ± 0.0122	0.1728 ± 0.0035	132.66 ± 0.69	Bon20
HD 28363 A	374.9 ± 1.0	1.341 ± 0.026	–	21.75 ± 0.11	Tor19
μ Ori B	266.9 ± 1.4	1.401 ± 0.028	1.369 ± 0.028	21.07 ± 0.18	Fek02
δ Equ	231.965 ± 0.008	1.192 ± 0.012	1.187 ± 0.012	54.41 ± 0.14	Mut08
1 Gem A	201.0 ± 0.4	1.94 ± 0.01	–	21.39 ± 0.03	Lan14
HIP 96656	189.38 ± 0.63	0.8216 ± 0.0037	0.7491 ± 0.0022	31.26 ± 0.011	Hal20
HIP 61100	102.9	0.834 ± 0.017	0.640 ± 0.011	38.82 ± 0.23	Kie18
HIP 87895	80.64	1.132 ± 0.014	0.7421 ± 0.0073	36.35 ± 0.20	Kie16
α Aur	56.442 ± 0.023	2.5687 ± 0.0074	2.4828 ± 0.0067	75.994 ± 0.089	Tor15
α Cen	17.592 ± 0.013	1.1055 ± 0.0039	0.9373 ± 0.0033	747.17 ± 0.61	Ker17
δ Vel A	16.51 ± 0.16	2.43 ± 0.02	2.27 ± 0.02	39.8 ± 0.4	Mer11
HIP 101382	15.378 ± 0.027	0.8420 ± 0.0014	0.66201 ± 0.00076	46.121 ± 0.084	Kie18
HIP 20601	11.338 ± 0.022	0.8798 ± 0.0019	0.72697 ± 0.00094	16.703 ± 0.034	Hal20
ι Peg	10.33 ± 0.10	1.326 ± 0.016	0.819 ± 0.009	86.91 ± 1.0	Bod99
ζ^1 UMa	9.83 ± 0.03	2.43 ± 0.07	2.50 ± 0.07	39.4 ± 0.3	Hum98
α CMa	7.4957 ± 0.0025	2.063 ± 0.023	1.018 ± 0.011	378.9 ± 1.4	Bon17
HD 24546	6.99 ± 0.06	1.434 ± 0.014	1.409 ± 0.014	26.04 ± 0.13	Les20
HIP 14157	5.810 ± 0.034	0.982 ± 0.010	0.8819 ± 0.0089	19.557 ± 0.07	Hal16
δ Del	5.4676 ± 0.0037	1.78 ± 0.07	1.62 ± 0.07	15.72 ± 0.22	Gar18
Ψ Cen*	5.055 ± 0.020	3.187 ± 0.031	1.961 ± 0.015	13.049 ± 0.063	Gal19
HD 8374	5.05 ± 0.02	1.636 ± 0.050	1.587 ± 0.049	16.00 ± 0.15	Les20
HIP 117186	4.677 ± 0.034	1.647 ± 0.022	1.316 ± 0.034	8.551 ± 0.080	Hal20
o Leo	4.46 ± 0.01	2.12 ± 0.01	1.87 ± 0.01	24.16 ± 0.19	Hum01
σ Ori A	4.2860 ± 0.0031	16.99 ± 0.20	12.81 ± 0.18	2.581 ± 0.017	Sch16
HD 28363 B	4.108 ± 0.015	1.210 ± 0.021	0.781 ± 0.014	21.75 ± 0.11	Tor19
NN Del*	3.508 ± 0.013	1.4445 ± 0.0020	1.3266 ± 0.0021	5.953 ± 0.023	Gal19
12 Boo	3.451 ± 0.018	1.4160 ± 0.0049	1.3740 ± 0.0045	27.72 ± 0.15	Bod05
β Aur	3.3 ± 0.1	2.41 ± 0.03	2.32 ± 0.03	40.16 ± 0.81	Hum95
1 Gem B	2.638 ± 0.005	1.707 ± 0.005	1.012 ± 0.003	21.39 ± 0.03	Lan14
HD 185912*	2.57 ± 0.03	1.361 ± 0.004	1.332 ± 0.004	24.540 ± 0.179	Les19b
HD 224355	2.392 ± 0.009	1.626 ± 0.005	1.608 ± 0.005	15.630 ± 0.064	Les19a
HR 8257	2.028 ± 0.013	1.561 ± 0.021	1.385 ± 0.019	13.632 ± 0.095	Fek09
V4090 Sgr*	1.596 ± 0.011	2.15 ± 0.07	1.11 ± 0.02	10.845 ± 0.083	Gal19
KW Hya*	1.329 ± 0.007	1.975 ± 0.029	1.487 ± 0.013	11.462 ± 0.074	Gal19
σ^2 CrB	1.225 ± 0.013	1.137 ± 0.037	1.090 ± 0.036	43.93 ± 0.10	Rag09

Table 3 continued

Binary	a (mas)	M_1 (M_\odot)	M_2 (M_\odot)	π_{orb} (mas)	Ref.
63 Gem A	0.5973 ± 0.0089	1.402 ± 0.032	1.181 ± 0.027	30.22 ± 0.26	Mut10

The table is sorted by decreasing angular separation between the components, expressed in milliarcsec (mas). Also, the orbital parallaxes are given. Eclipsing binaries resolved by interferometry are marked with an asterisk

References: Bon20: Bond et al. (2020), Tor19: Torres et al. (2019), Fek02: Fekel et al. (2002), Mut08: Muterspaugh et al. (2008), Lan14: Lane et al. (2014), Hal20: Halbwachs et al. (2020), Kie18: Kiefer et al. (2018), Kie16: Kiefer et al. (2016), Tor15: Torres et al. (2015a), Ker17: Kervella et al. (2017), Mer11: Mérand et al. (2011), Bod99: Boden et al. (1999), Hum98: Hummel et al. (1998), Bon17: Bond et al. (2017b), Les20: Lester et al. (2020), Hal16: Halbwachs et al. (2016), Gar18: Gardner et al. (2018), Gal19: Gallenne et al. (2019), Hum01: Hummel et al. (2001), Sch16: Schaefer et al. (2016), Bod05: Boden et al. (2005), Hum95: Hummel et al. (1995), Les19a: Lester et al. (2019b), Les19b: Lester et al. (2019a), Fek09: Fekel et al. (2009), Rag09: Raghavan et al. (2009), Mut10: Muterspaugh et al. (2010)

New discoveries arising from exoplanet surveys have provided useful information for the investigation of stellar fundamental properties, including masses in particular, mainly for the low-mass regime. Examples are the case of triple eclipsing systems or transiting planets orbiting binary eclipsing systems (Carter et al. 2011; Doyle et al. 2011; Welsh et al. 2012). Three-body effects cause transit and/or eclipse time variations that add additional constraints to the mass of the components, yielding very precise masses from light-curve analysis even with few RV measurements or in the case of single-lined eclipsing systems.

With respect to very young, very low-mass stars, the number of EBs in young regions and open clusters is small. Most of them have been identified in Orion (Cargile et al. 2008; Gómez Maqueo Chew et al. 2012), 25 Ori (van Eyken et al. 2011), and in NGC 2264 with CoRoT (Gillen et al. 2014) (see Stassun et al. 2014 for a review). New low-mass EBs with M components have been announced in Upper Scorpius (Kraus et al. 2015; Lodieu et al. 2015; David et al. 2016), in the Pleiades (David et al. 2015), and in Praesepe (e.g., Kraus et al. 2017) thanks to the *Kepler* and *K2* missions. These are the first masses and radii determined independently from evolutionary models for M dwarfs with ages of 5–10 Myr, 125 Myr, and 600 Myr with uncertainties of 5% or less. These objects show that the sequence at 10 Myr and 120 Myr are well differentiated from the older field M dwarfs. These measurements also confirm that radii are larger at young ages and smaller for older stars, as they contract in their evolution towards the main-sequence. At the age of Praesepe (590–660 Myr; Mermilliod 1981; Fossati et al. 2008; Delorme et al. 2011; Gossage et al. 2018) and the Hyades (625±100 Myr; Lebreton et al. 2001; Martín et al. 2018; Lodieu et al. 2018), M dwarfs do not stand out from older (>1 Gyr) stars in the mass-radius diagram (e.g., Fig. 10 in Lodieu et al. 2015). The radius of 0.2–0.25 M_\odot low-mass M dwarfs at ages older than 600 Myr are approximately 0.25 R_\odot within 10%, while Pleiades-type M dwarfs (age of 125 Myr) reveal slightly larger radii (0.32–0.34 R_\odot for 0.28–0.30 M_\odot). The difference in radii increases at the age of 5–10 Myr, where the radii at $M \lesssim 0.25 M_\odot$ are about three times larger with values of 0.65–0.75 R_\odot for masses of 0.2–0.3 M_\odot .

The difference is even larger for M dwarfs younger than 5 Myr, with radii as large as $0.9\text{--}1.2 R_{\odot}$ having uncertainties below 15–20% for masses of $0.15\text{--}0.25 M_{\odot}$. There is a clear need to populate the mass-radius diagram for M dwarfs for ages younger than 125 Myr and to find more substellar EBs, as only one is known in Orion to date (Stassun et al. 2006, 2007).

M-dwarf companions in EB systems can be used to obtain precise mass-luminosity calibrations that enable the determination of the masses of single isolated M dwarfs from photometry (see, e.g., Delfosse et al. 2000; Benedict et al. 2016, and Sect. 4.4). Such calibrations are required to test the predictions of stellar structure and evolutionary models and improve them. Comparisons so far revealed a discrepancy between models and observations, possibly caused by stellar magnetic activity (see, e.g., Torres and Ribas 2002; López-Morales and Ribas 2005; Ribas et al. 2008). Many of the low-mass binaries analysed so far are short-period systems, in which the rotation of the components is synchronized with the orbital motion. These are, therefore, fast rotators and magnetically active stars. The presence of photospheric spots caused by magnetic fields produces both photometric and RV variability that must be accounted for when analysing the data because it may bias the results and/or increase the uncertainties. Indeed, the analysis of light curves of spotted stars has shown that the determination of the radius can vary by about 3% depending on the spot configuration (Morales et al. 2010; Windmiller et al. 2010; Wilson et al. 2017). On the other hand, spots can change the profiles of spectral lines, from which RVs are determined, causing variability of a few km s^{-1} (see e.g., Morales et al. 2009b). The effect on the derived masses is typically smaller than for the radii ($<1\%$). These uncertainties are still smaller than the 5–10% radius and effective temperature discrepancies found between models and observations of binary systems, thus proving that stellar activity may also have an impact on the structure of these lowest-mass stars (Chabrier et al. 2007; Mullan and MacDonald 2010; MacDonald and Mullan 2014; Feiden and Chaboyer 2014). Higl and Weiss (2017) demonstrated that EBs with low-mass components can be modelled correctly if the stellar models include stellar spots as introduced by Spruit and Weiss (1986).

In Table 4 we present a total of 28 benchmark EB systems with at least one late-K or M-dwarf component having $M \lesssim 0.7 M_{\odot}$ and fundamentally determined masses. We list 26 binary systems, one triple system, and a binary system with a transiting planet. Again, the table entries are compiled from Torres et al. (2010) and the DEBCat (Southworth 2015). Two more such binaries were already included in Table 2 and are not repeated in Table 4, which now contains the list of stars with absolute mass determinations having uncertainties below 3%. Table 4 is sorted according to the reported uncertainty level of the primary component. All the stars in Table 4 have been included in Fig. 2, where the cyan triangles indicate pre-MS stars. As can be seen in the insets in Fig. 2, the stars with mass below $\sim 0.5 M_{\odot}$, show a tight mass–radius correlation for stars older than ~ 400 Myr. The stars from the three pre-MS systems, with estimated ages $\lesssim 70$ Myr, clearly deviate from this correlation. More massive systems show larger dispersion, which may be a signature of the spread in age and/or metallicity.

Table 4 List of eclipsing binaries containing at least one low-mass star with $M < 0.7 M_{\odot}$ and relative errors $< 3\%$ in masses, sorted by the size of this error

Name	P (d)	M (M_{\odot})	Error (%)	R (R_{\odot})	Error (%)	T (K)	[Fe/H] (dex)	Ref.
<i>Eclipsing binaries</i>								
2MASS J20115132 + 0337194	0.63	0.557 ± 0.001	0.18	0.569 ± 0.023	4.04	3690 ± 80	...	Kra11
LP 661-13	4.70	0.535 ± 0.001	0.19	0.500 ± 0.014	2.80	3610 ± 80		
CU Cnc	2.77	0.30795 ± 0.00084	0.27	0.3226 ± 0.0033	1.02	...	-0.07 ± 0.10	Diti7
		0.19400 ± 0.00034	0.18	0.2174 ± 0.0023	1.06			
		0.4349 ± 0.0012	0.28	0.4323 ± 0.0055	1.27	3160 ± 150		Tor10
2MASS J07431157 + 0316220	1.55	0.3992 ± 0.0009	0.23	0.3916 ± 0.0094	2.40	3125 ± 150		Kra11
		0.584 ± 0.002	0.34	0.560 ± 0.005	0.89	3730 ± 90	-1.26 ± 0.05	
		0.544 ± 0.002	0.37	0.513 ± 0.008	1.56	3610 ± 90	-1.40 ± 0.05	Kra11
2MASS J04480963 + 0317480	0.83	0.567 ± 0.002	0.35	0.552 ± 0.013	2.36	3920 ± 80	-1.19 ± 0.04	Kra11
		0.532 ± 0.002	0.38	0.532 ± 0.008	1.50	3810 ± 80		
2MASS J03262072 + 0312362	1.59	0.527 ± 0.002	0.38	0.505 ± 0.008	1.58	3330 ± 60	-1.55 ± 0.05	Kra11
		0.491 ± 0.001	0.20	0.471 ± 0.007	1.49	3270 ± 60		
CM Dra	1.27	0.231 ± 0.001	0.43	0.253 ± 0.002	0.79	3133 ± 73	-0.3 ± 0.12	Mor09a
		0.214 ± 0.001	0.46	0.240 ± 0.002	0.83	3119 ± 98		
2MASS J10305521 + 0334265	1.64	0.499 ± 0.002	0.40	0.457 ± 0.006	1.31	3730 ± 20	-1.44 ± 0.03	Kra11
		0.443 ± 0.002	0.45	0.427 ± 0.006	1.41	3630 ± 20	-1.55 ± 0.03	
2MASS J23143816 + 0339493	1.72	0.469 ± 0.002	0.43	0.441 ± 0.002	0.45	3460 ± 180	-1.60 ± 0.09	Kra11
		0.382 ± 0.001	0.26	0.374 ± 0.002	0.53	3320 ± 180	-1.82 ± 0.09	
2MASS J08504984 + 1948364	6.02	0.3953 ± 0.0020	0.51	0.363 ± 0.008	2.20	3260 ± 60	0.14 ± 0.04	Kra17
		0.2098 ± 0.0014	0.67	0.272 ± 0.012	4.41	3120 ± 60		
LSPMJ1112 + 7626	41.03	0.3951 ± 0.0022	0.56	0.3815 ± 0.003	0.79	3130 ± 165	...	Irw11
		0.2749 ± 0.0011	0.40	0.2999 ± 0.0044	1.47	3015 ± 165		
2MASS J16502074 + 4639013	1.12	0.493 ± 0.003	0.61	0.453 ± 0.060	13.25	3500	...	Cre05
		0.489 ± 0.003	0.61	0.452 ± 0.050	11.06	3295 ± 150		

Table 4 continued

Name	P (d)	M (M_{\odot})	Error (%)	R (R_{\odot})	Error (%)	T (K)	[Fe/H] (dex)	Ref.
BD-15 2429	1.53	0.7029 ± 0.0045	0.64	0.694 ± 0.011	1.59	4230 ± 200	...	Hel11
V530 Ori	6.11	0.6872 ± 0.0049	0.71	0.699 ± 0.014	2.00	4080 ± 200	-0.12 ± 0.08	Tor14
		1.0038 ± 0.0066	0.66	0.980 ± 0.013	1.33	5890 ± 100		
NGC2204-S892	0.45	0.5955 ± 0.0022	0.37	0.5873 ± 0.0067	1.14	3880 ± 120	...	Roz09
		0.733 ± 0.005	0.68	0.719 ± 0.014	1.95	4200 ± 100		
UScoCTIO5 ^a	34.00	0.662 ± 0.005	0.76	0.680 ± 0.017	2.50	3940 ± 110	...	Kral5
		0.3287 ± 0.0024	0.73	0.834 ± 0.006	0.72	3200 ± 75		
KIC 6131659	17.53	0.3165 ± 0.0016	0.51	0.810 ± 0.006	0.74	3200 ± 75	-0.23 ± 0.20	Bas12
		0.922 ± 0.007	0.76	0.880 ± 0.0028	0.32	5789 ± 50		
GU Boo	0.49	0.685 ± 0.005	0.73	0.6395 ± 0.0061	0.95	4609 ± 32	...	Tor10
		0.6101 ± 0.0064	1.05	0.627 ± 0.016	2.55	3920 ± 130		
UCAC3 127-192903	2.29	0.5995 ± 0.0064	1.07	0.624 ± 0.016	2.56	3810 ± 130	-1.18 ... 0.02	Kal13
		0.8035 ± 0.0086	1.07	1.147 ± 0.010	0.87	6088 ± 108		
IM Vir	1.31	0.6050 ± 0.0044	0.73	0.6110 ± 0.0092	1.51	4812 ± 125	-0.28 ± 0.10	Mor09b
		0.981 ± 0.012	1.22	1.061 ± 0.016	1.51	5570 ± 100		
HAT551-027	4.08	0.6644 ± 0.0048	0.72	0.681 ± 0.013	1.91	4250 ± 130	0.0 ± 0.1	Zho15
		0.244 ± 0.003	1.23	0.261 ± 0.006	2.30	3190 ± 100		
RXJ0239.1-1028	2.07	0.179 ± 0.002	1.12	0.218 ± 0.011	5.05	2990 ± 110	...	Lop07
		0.730 ± 0.009	1.23	0.741 ± 0.004	0.54	4645 ± 20		
T-Lyr1-17236	8.43	0.693 ± 0.006	0.87	0.703 ± 0.002	0.28	4275 ± 15	...	Dev08
		0.680 ± 0.010	1.57	0.634 ± 0.043	6.78	4150		
NSVS 02502726 ^a	0.56	0.5226 ± 0.0061	1.17	0.525 ± 0.052	9.90	3700	...	Lee13
		0.689 ± 0.016	2.32	0.707 ± 0.007	0.99	4295 ± 200		
EPIC 203710387 ^a	2.81	0.341 ± 0.009	2.64	0.657 ± 0.008	1.22	3812 ± 200	...	Dav16
		0.1183 ± 0.0028	2.37	0.417 ± 0.010	2.40	2980 ± 75		

Table 4 continued

Name	P (d)	M (M_{\odot})	Error (%)	R (R_{\odot})	Error (%)	T (K)	[Fe/H] (dex)	Ref.
NSVS01031772	0.37	0.530 ± 0.014	2.64	0.559 ± 0.014	2.50	3750 ± 150	...	Lop07
<i>Eclipsing triple systems</i>								
KOI-126	33.92	1.347 ± 0.032	2.38	2.0254 ± 0.0098	0.48	5875 ± 100	0.15 ± 0.08	Car11
	1.77	0.2413 ± 0.003	1.24	0.2543 ± 0.0014	0.55	...		
<i>Binary system with transiting planets</i>								
Kepler 16	41.08	0.6897 ± 0.0035	0.51	0.6489 ± 0.0013	0.20	4450 ± 150	-0.3 ± 0.2	Doy11
		0.2026 ± 0.0007	0.33	0.2262 ± 0.0006	0.26	...		

The systems YY Gem and HAT-TR- 318-007 were already listed in Table 2 and are omitted here

Notes and References: ^(a)Pre main-sequence stars. Bas12: Bass et al. (2012); Car11: Carter et al. (2011); Cre05: Creevey et al. (2005); Dav16: David et al. (2016); Dit17: Dittmann et al. (2017); Doy11: Doyle et al. (2011); Hel11: Helminiak and Konacki (2011); Irw11: Irwin et al. (2011); Kal13: Kaluzny et al. (2013); Kra11: Kraus et al. (2011); Kra15: Kraus et al. (2015); Kra17: Kraus et al. (2017); Lee13: Lee et al. (2013); Lop07: López-Morales and Shaw (2007); Mor09a: Morales et al. (2009b); Mor09b: Morales et al. (2009a); Roz09: Rozycka et al. (2009); Tor10: Torres et al. (2010); Tor14: Torres et al. (2014); Zho15: Zhou et al. (2015)

2.5 Mass estimation of non-eclipsing spectroscopic binaries

Precise trigonometric distances (e.g., Gaia, Gaia Collaboration et al. 2016b; Gaia Collaboration et al. 2018) can be used to estimate the masses of double-lined spectroscopic binaries, even if they are not eclipsing, by using empirical mass-luminosity relationships (Baroch et al. 2018, Sect. 4.4). The radial-velocity analysis provides the mass ratio of the components, and the photometric observations and the distance yield the absolute magnitude M_A of the unresolved system. This system magnitude is related to the absolute magnitude of each component star and the flux ratio, α , between the components as follows:

$$\begin{aligned} M_{A,1} &= M_A + 2.5 \log_{10}(1 + \alpha), \\ M_{A,2} &= M_A + 2.5 \log_{10}(1 + 1/\alpha). \end{aligned} \quad (2)$$

Assuming an empirical mass–luminosity relation $f_{\text{MLR}}(M_A)$, it is possible to set a constraint on the mass ratio, q , of the system as

$$q = \frac{f_{\text{MLR}}(M_{A,1})}{f_{\text{MLR}}(M_{B,1})} = \frac{f_{\text{MLR}}[M_A + 2.5 \log_{10}(1 + \alpha)]}{f_{\text{MLR}}[M_A + 2.5 \log_{10}(1 + 1/\alpha)]}. \quad (3)$$

Therefore, combining this constraint with the mass ratio derived from the radial-velocity analysis, one obtains the individual masses of the system and also their flux ratio. While these masses are not fundamentally determined, they can be used to estimate the inclination of the systems and the probability of eclipses or for statistical studies of multiplicity fractions as a function of stellar mass.

The studies by Pourbaix and Jorissen (2000), Pourbaix and Boffin (2003), Jancart et al. (2005) and Escorza et al. (2019) combined spectroscopic orbital solutions with Hipparcos astrometric data to determine the mass of the unseen components in single-lined spectroscopic binary systems. To prepare the exploitation of *Gaia*, a long-term observational programme with the SOPHIE spectrograph at the Haute-Provence Observatory has been conducted by Halbwachs et al. (2014, 2016), Kiefer et al. (2016, 2018) and Halbwachs et al. (2020). About 70 double-lined spectroscopic binaries (some of them previously known only as single-line binaries) and also observed by *Gaia* (for most of them) were selected. The final objective is to determine masses at the level of 1% combining the RVs and *Gaia* astrometry once the third *Gaia* Data Release will be available. Up to now, the individual masses of 18 stars in nine systems have been derived precisely combining the RVs and long baseline or speckle interferometry. After the third *Gaia* data release, which will include binary astrometric solutions, this methodology will be applicable to many other non-eclipsing spectroscopic binaries.

2.6 Evolved stars

In Tables 2 and 4 the objects listed are mainly main-sequence or only moderately evolved stars, such as the primary of the V380 Cygni system indicated in red. Stars in later evolutionary stages, such as red giant and asymptotic branch giants are mostly missing. Exceptions are HD 187669 and TZ Fornacis listed in Table 2 and

also indicated in red in Fig. 2. An important class of objects are ζ Auriga systems, where the primary is a red giant, while the secondary is still on the main sequence. Schröder et al. (1997) and Higl and Weiss (2017) have used members of this class for testing stellar evolution theory, but the errors in the determined masses are typically larger than for the previously discussed systems. For example, the components of V2291 Oph have $3.86 \pm 0.15 M_{\odot}$ respectively, $2.95 \pm 0.09 M_{\odot}$, and these determinations are from the late 1990s (Griffin et al. 1995). An overview of 60 double-lined binaries of all types is given in Eggleton and Yakut (2017), but their list does not contain errors for the quoted masses (determined according to their prescription given in their Appendix A).

2.6.1 Intermediate-mass giants

Dynamical masses for evolved red giant stars are difficult to obtain. The dimensions of their binary systems are generally large and their periods are longer than 100 days. This means that the observational effort required to determine the orbital parameters is cumbersome. Additionally, the probability of observing eclipses becomes smaller. In the case of single-lined spectroscopic binaries, the primary component can be treated as a single star and its evolutionary mass can be determined as mentioned before. Afterwards, the dynamical properties can be used to obtain information about the secondary star. If the inclination of the orbit remains as an uncertainty because astrometric data are not available, deriving absolute masses will not be possible. In the case of double-lined spectroscopic binaries, spectral disentangling can also be used. Finally, independent constraints to the characteristic of the two components can be obtained if the binary can be spatially resolved via interferometric observations or direct imaging.

The All Sky Automated Survey (ASAS, Pojmanski 1997) has played an important role in the determination of accurate masses of evolved stars. Through the accurate determination of the distances to local galaxies, and in particular to the Large and Small Magellanic Clouds (LMC and SMC), the OGLE (Udalski et al. 1997) and ARAUCARIA (Pietrzyński and Gieren 2002) projects have provided very accurate masses of evolved stars as well. In particular, these projects targeted systems hosting two evolved stars of very similar masses. Results for double-lined EBs have mass uncertainties between 1 and 2% in most cases. Pietrzyński et al. (2013) presents 9 LMC systems of stars in the He-core burning phase. These results were updated and extended to 20 stars by Graczyk et al. (2018), while Graczyk et al. (2014) provides results for SMC systems. Both the LMC, and in particular the SMC, provide test cases for stellar evolution at intermediate masses and $[\text{Fe}/\text{H}]$ lower than typically found in the Milky Way for those masses.

In Table 5 we present the five systems with the longest periods and with mass uncertainties $< 1\%$ in the LMC (the complete list of stars is given in Graczyk et al. 2018) and four systems in the SMC. The same surveys have determined the masses of several Cepheids as well (see Pietrzyński et al. 2010, 2011 and Sect. 4.6). We list the results for those separately in Table 5. In the case of evolved systems, if dynamical masses are used to calibrate other mass determination methods (e.g. isochrone fitting, Sect. 5.1, or pulsational masses, Sect. 4.6), or as benchmark for

Table 5 Double-lined eclipsing systems of evolved stars

Name	P (d)	M (M_{\odot})	R (R_{\odot})	T (K)	[Fe/H] (dex)	Ref.
<i>LMC systems</i>						
OGLE LMC-ECL-05430	505.18	2.717 ± 0.017	28.99 ± 0.36	4710 ± 70	−0.37 ± 0.10	Gra18
		3.374 ± 0.018	34.64 ± 0.28	4760 ± 65		
OGLE LMC-ECL-13360	260.44	3.950 ± 0.024	30.46 ± 0.38	5495 ± 90	−0.30 ± 0.10	Gra18
		4.060 ± 0.024	39.46 ± 0.35	5085 ± 80		
OGLE LMC-ECL-01866	251.25	3.560 ± 0.020	26.79 ± 0.52	5300 ± 80	−0.49 ± 0.17	Gra18
		3.550 ± 0.031	47.11 ± 0.50	4495 ± 60		
OGLE LMC-ECL-09114	214.37	3.304 ± 0.023	26.33 ± 0.34	5230 ± 60	−0.38 ± 0.12	Gra18
		3.205 ± 0.025	18.79 ± 0.37	5425 ± 110		
OGLE LMC-ECL-06575	505.18	2.717 ± 0.017	28.99 ± 0.36	4710 ± 70	−0.37 ± 0.10	Gra18
		3.374 ± 0.018	34.64 ± 0.28	4760 ± 65		
<i>SMC systems</i>						
SMC101.8 14077	102.90	2.725 ± 0.034	17.90 ± 0.50	5580 ± 95	...	Gra14
		3.374 ± 0.018	34.64 ± 0.28	4760 ± 65	−1.01	
SMC108.1 14904	185.22	4.416 ± 0.041	46.95 ± 0.53	5675 ± 105	−0.95	Gra14
		4.429 ± 0.037	64.05 ± 0.50	4955 ± 90	−0.64	
SMC126.1 210	635.00	1.674 ± 0.037	43.52 ± 1.02	4480 ± 70	−0.94	Gra14
		1.669 ± 0.039	39.00 ± 0.98	4510 ± 70	−0.79	
SMC130.5 4296	120.47	1.854 ± 0.025	25.44 ± 0.25	4912 ± 80	−0.77	Gra14
		1.805 ± 0.027	46.00 ± 0.35	4515 ± 75	−0.99	
<i>Cepheids</i>						
OGLE-LMC-CEP0227	309.67	4.14 ± 0.05	32.4 ± 1.5	5900 ± 255	...	Pie10
		4.14 ± 0.07	44.9 ± 1.5	5080 ± 270	...	
OGLE-LMC-CEP1812	551.80	3.74 ± 0.06	17.4 ± 0.9	Pie11
		2.64 ± 0.04	12.1 ± 2.3	

References: Gra18: Graczyk et al. (2018), Gra14: Graczyk et al. (2014), Pie10: Pietrzyński et al. (2010), Pie11: Pietrzyński et al. (2011)

stellar evolution models, care needs to be taken to avoid systems in which binary effects might have played a role in the past evolution of the stars.

2.6.2 Red giant branch stars with oscillations

Interest in dynamical masses of evolved stars has also increased with the generalization of asteroseismology as a tool for stellar evolution and Galactic studies and the necessity to test its accuracy for mass determination (Sect. 6.1.2). Eclipsing red giant binaries have been discovered by *Kepler* and followed up spectroscopically, and so far 14 have been identified as double-lined EBs that also show solar-like oscillations. Stellar masses for these systems have been reported in several studies (Frandsen et al. 2013; Beck et al. 2014; Rawls et al. 2016; Gaulme et al. 2016; Themeßl et al. 2018; Beck et al. 2018a; Kallinger et al. 2018;

Table 6 Parameters of pulsating RGB stars in double-lined eclipsing systems

Name	P (d)	M (M_{\odot})	R (R_{\odot})	T (K)	[Fe/H] (dex)	Ref.
KIC 7037405	207.11	1.25 ± 0.04	14.1 ± 0.2	4516 ± 36	-0.34 ± 0.01	Gau16
		1.17 ± 0.02	14.0 ± 0.1	4500 ± 80	-0.27 ± 0.10	Bro18
KIC 8410637	408.32	1.557 ± 0.028	10.74 ± 0.11	4800 ± 80	0.10 ± 0.13	Fra13
		1.47 ± 0.02	10.60 ± 0.05	4605 ± 80	0.02 ± 0.08	The18
KIC 9970396	235.30	1.14 ± 0.03	8.0 ± 0.2	4916 ± 68	-0.23 ± 0.03	Gau16
		1.178 ± 0.015	8.035 ± 0.074	4860 ± 80	-0.35 ± 0.10	Bro18
KIC 9540226	175.44	1.33 ± 0.05	12.8 ± 0.1	4692 ± 65	-0.33 ± 0.04	Gau16
		1.378 ± 0.038	13.06 ± 0.16	4680 ± 80	-0.23 ± 0.10	Bro18
		1.39 ± 0.03	13.43 ± 0.17	4585 ± 75	-0.31 ± 0.09	The18

References: Gau16: Gaulme et al. (2016), Bro18: Brogaard et al. (2018), Fra13: Frandsen et al. (2013), The18: Themeßl et al. (2018)

Benbakoura et al. 2021), with typical uncertainties from 3 to 8%. Some systems have been the subject of more than one study with results not always in agreement. These results are summarized in Table 6. For all four cases results do not agree within 1σ . In particular the cases of KIC 7037405 and KIC 8410637 have at least 2σ discrepancies. While Brogaard et al. (2018) states that dynamical analyses in previous studies might be at the root of the problem, further studies of systems harbouring pulsating RGB stars are highly desirable for appropriate determination of the accuracy of seismic mass measurements (Sect. 6.1.2). Systematic differences in effective temperature determinations by different authors (see Beck et al. 2018b for a discussion) might also explain, albeit not completely, some of the differences.

Finally, we note the particularly interesting case is KIC9163976, an SB2 system with two oscillating components (Beck et al. 2018a). While from the radial-velocity amplitudes, a mass difference of $\sim 1\%$ was found, both stellar components of the binary system differ substantially. This system illustrates the impact of stellar mass on the pace of evolution and the importance of determining it correctly.

2.6.3 Interacting binaries

For AGB stars, the determination of dynamical masses is even more difficult due to the lack of double-lined eclipsing systems and of well-determined orbital parameters in general. A useful type of system is that of symbiotic binaries with a Mira type giant and a white dwarf or main-sequence star as a companion. But the dynamical data have to be supplemented usually with evolutionary tracks to determine the mass of the hot companion (Mikołajewska 2003). It is also difficult to determine whether the star is an AGB or a very luminous RGB star, close to the RGB-tip. There exist a number of well-studied systems, which are double-eclipsing and, therefore, have inclinations above 70° , and where the giant being an AGB star is highly probable. Examples are V1329 Cyg (Schild and Schmid 1997; Pribulla et al. 2003), with masses of $2.02 \pm 0.41 M_{\odot}$ and $0.71 \pm 0.09 M_{\odot}$ for the giant and

hot compact stars, respectively, FN Sgr (Brandi et al. 2005; Mikołajewska 2003) with $1.5 \pm 0.2 M_{\odot}$ and $0.7 \pm 0.08 M_{\odot}$, and AR Pav (Quiroga et al. 2002; Mikołajewska 2003) $2.5 \pm 0.6 M_{\odot}$ and $1 \pm 0.2 M_{\odot}$. Mass determinations for these systems have much larger uncertainties than dynamical masses for other types of systems discussed above.

2.6.4 CSPNe and hot subdwarfs

The situation improves in the case of binary Central Stars of Planetary Nebulae (CSPNe⁴). Some CSPNe are known to be part of close binary systems. Due to the small sizes of these systems several of them show eclipses, reflection effects or ellipsoidal modulations that can help to constrain the inclination of the systems through photometry and modelling of their light curve. The study of these systems is key for our understanding, and validation, of models of the common envelope stage which is thought to form them (e.g., Exter et al. 2005; Jones 2020). It also helps in our understanding of the possible double degenerate progenitors of Type Ia Supernovae (Santander-García et al. 2015).⁵ In Table 7 we list known double-lined binary CSPNe that have dynamically measured masses with different methods. The main uncertainties in these systems arise from the modelling of the light curve, and required irradiation effects, which are needed for an estimation of the inclination of the system. Also, as shown by Reindl et al. (2020), assessment of the contamination by diffuse interstellar absorption bands is required for a proper measurement of radial velocities of hot components. In addition to the double-lined systems listed in Table 7 there are other close binary CSPNe systems for which masses can be estimated with the help of different assumptions and models (see Jones 2020). The situation for wide CSPNe binaries is more complicated. Due to the large orbital semi-major axis and long orbital periods, spectroscopic determinations are more complicated and systems do not show light-curve variations, making the determination of the inclination of the system much less reliable, when possible. One of the best mass determinations in such systems is that of the central star of the PN NGC 1514, BD+30°623. This is a double-lined system with precise RV determinations, for which the orbital inclination has been deduced from the derived inclination of the surrounding PNe. This was done under the assumption that the axis of symmetry of the PNe lies orthogonal to the orbital plane (Jones et al. 2017).

Other evolved systems related to the common envelope phenomenon, for which dynamical masses can be estimated, are those composed by hot subdwarfs in close binary systems (see Heber 2016, for a detailed review of hot subdwarf properties). Dynamical mass determinations of hot subdwarfs are interesting because this family of objects is known to harbour at least two different families of pulsators for which masses can also be determined through asteroseismology (Fontaine et al. 2012). HW Vir systems composed of an sdB + cool low-mass companion are of special interest due to their photometric variability caused by eclipses, ellipsoidal

⁴ A regularly updated catalogue of binary CSPNe is maintained by David Jones and can be found at <http://www.drjdjones.net/bcspn/>.

⁵ See, however the recent redetermination of masses by Reindl et al. (2020).

Table 7 Double-lined eclipsing CSPNe with photometric variability

Name	Light-curve type	P (d)	i ($^\circ$)	M_{CSPN} (M_\odot)	Ref.
<i>Close binaries</i>					
Hen 2-428	Eclip., Ellip., Irr.	0.176	63.59 ± 0.54	0.66 ± 0.11 0.42 ± 0.07	Rei20
BE UMa (LTNF 1)	Eclip., Irr.	2.29	84 ± 1	0.70 ± 0.07 0.36 ± 0.07	Fer99
V477 Lyr (Abell 46)	Eclip., Irr.	0.472	80.33 ± 0.06	0.508 ± 0.046 0.145 ± 0.021	Afs08
UU Sge (Abell 63)	Eclip., Irr.	0.456	87.12 ± 0.19	0.628 ± 0.053 0.288 ± 0.031	Afs08
HaTr 1	Irr.	0.322	47.5 ± 2.5	0.53 ± 0.03 0.17 ± 0.03	Hil17
SP 1	Irr., Eclip.	2.91	9 ± 2	0.56 ± 0.04 0.71 ± 0.19	Hil16
KV Vel (DS 1)	Irr.	0.357	~ 62.5	~ 0.63 ~ 0.23	Hil96
<i>Wide binaries</i>					
BD+30 $^\circ$ 623 †	–	3306	$\sim 31^\dagger$	$\sim 0.9 \pm 0.7$ $\sim 2.3 \pm 0.8$	Jon17

Second, third, fourth and fifth columns indicate the cause of the photometric variability, the orbital period, the inclination, and the masses of the CSPNe and the companions, respectively

For each system, the first row corresponds to the CSPN

References: Rei20: Reindl et al. (2020), Fer99: Ferguson et al. (1999), Afs08: Afşar and Ibanoglu (2008), Hil17: Hillwig et al. (2017), Hil16: Hillwig et al. (2016), Hil96: Hilditch et al. (1996), Jon17: Jones et al. (2017)

Irr. Irradiation Effect on the companion, *Ellip.* Ellipsoidal Modulation of the light curve, *Eclip.* Eclipsing Binary

† BD+30 $^\circ$ 623 is a wide binary with no eclipses or irradiation effects, here the inclination is estimated from the inclination of the surrounding PNe

deformation and irradiation effects, which allows for an estimation of the inclination of the system (Schaffenroth et al. 2015, 2019). Unfortunately most of these systems are only single-lined spectroscopic variables, and either the mass of the primary has to be derived from light-curve modelling and assuming a mass–radius relation for the sdB star, or by relying on theoretical or observational arguments (e.g., Drechsel et al. 2001; Østensen et al. 2010). In many cases a canonical mass of $\sim 0.47M_\odot$ is assumed for the sdB star, a value based both on asteroseismological determinations (Fontaine et al. 2012) and on theoretical predictions (Dorman et al. 1993). These assumptions have been confirmed by detailed analysis of the AA Dor system by Vučković et al. (2016). AA Dor is a bona fide member of the HW Vir class, for which irradiated light from the super-heated face of the secondary has been measured. This allows for RV measurements from the irradiated face of the super-

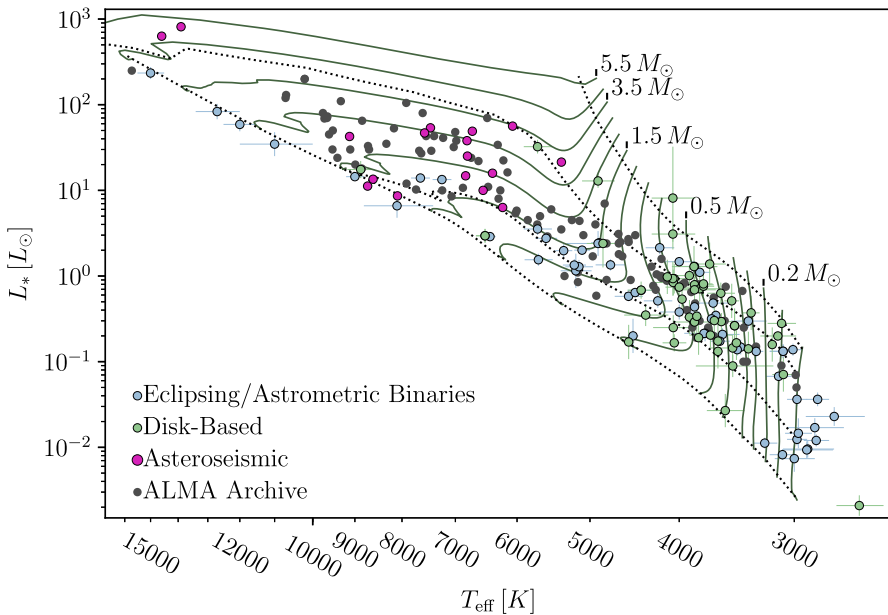


Fig. 3 The pre-MS HRD, with the MIST evolutionary tracks (Choi et al. 2016) spaced logarithmically in mass (adjacent tracks differ by 25% in M) and “benchmark” dynamical masses from eclipsing/astrometric binaries, protoplanetary disk-based measurements, and asteroseismology. Proposed ALMA dynamical mass surveys (black points) will more than double the total number of pre-MS sources with dynamical mass measurements. Isochrones (dotted lines) label 0.1, 1, 10, and 100 Myr. Only 0.1–10 Myr are shown for the highest masses

heated companion, making AA Dor the only system for which precise mass determinations can be made only on the basis of the RV measurements along with modelling of the light curve. With this approach, Vučković et al. (2016) determined the radial velocity of the secondary and derived the masses of the system components to $M_{\text{sdb}} = 0.46 \pm 0.01 M_{\odot}$ and $M_{\text{comp}} = 0.079 \pm 0.002 M_{\odot}$, in perfect agreement with the expectation for the canonical sdB mass.

2.7 Pre-main sequence stellar masses from protoplanetary disk rotation

The number of pre-MS EBs with accurate mass determination has grown in the past decade with *Kepler* and *K2* missions, but the sample is still small (see Fig. 3). Other traditional methods, e.g., comparison of surface temperature and spectral type against stellar models, have limitations due to the active nature of many of these objects, and also due to the inadequacy of stellar models.

While efforts to expand the eclipsing binary sample continue, the last few years have seen the development of a new technique relying on the dynamics of protoplanetary disks. The formation of such a disk, rich in dust and molecular gas, is an intrinsic part of the star formation process for low and intermediate mass stars. These disks, in Keplerian rotation around the star, last up to ~ 10 Myr. Radio interferometers like the Atacama Large Millimeter/submillimeter Array (ALMA)

deliver spatially and spectrally resolved mm-observations of optically thick molecular emission from these disks, which probe the velocity field of the disk with exquisite resolution ($0.02''$ beam at $<80 \text{ m s}^{-1}$). Forward modelling of this kinematic signature can yield a precise measurement of the central stellar mass, which is the dominant contribution to the gravitational field (Guilloteau and Dutrey 1998; Simon et al. 2000). Even for low S/N data (peak S/N per beam of 12), statistical uncertainties of M as low as 1% are consistently achieved. Analyses by Rosenfeld et al. (2012) and Czekala et al. (2015, 2016, 2017a) have validated the systematic precision of the technique ($<4\%$) by comparison to independently determined masses of spectroscopic binaries and extended the sample towards the lowest mass stars (Simon et al. 2017).

With the sensitivity of ALMA, this technique can now be readily applied to a large sample of stars. For many disks, sometimes only a single 30-minute interferometric observation is needed, in comparison to the many photometric and/or spectroscopic epochs needed for the traditional mass determination techniques. Because the requirements of the technique are fairly general, there are many ALMA observations already acquired for other scientific objectives, which are suitable for dynamical analysis and publicly available in the ALMA archive (see targets in Fig. 3). These observations can be used to create new pre-MS benchmarks to act as another “lever-arm” to constrain stellar models typically focused on the main sequence and calibrated using approaches outlined elsewhere in this document. In addition, because nearly all stars hosting a protoplanetary disk are pre-MS stars, this technique holds the largest reservoir of potential pre-MS benchmarks that can be used to test evolutionary models in novel ways. For example, one could design a survey focused around empirically measuring the scatter in photospheric properties for stars of the same mass and similar age. Because M-type stars should evolve along iso-temperature tracks, a measurement of the temperature scatter would indicate the degree to which unconsidered effects like star spots and rotation bias photospherically derived masses.

3 Direct method: gravitational lensing

The passage of a foreground star (the “lens”) in front of a background source leads to gravitational lensing effects (see the textbook by Schneider et al. (1992) for a general introduction). Among those is the apparent amplification of the background source’s brightness, which was used in several searches (EROS: Aubourg et al. 1993; MACHO: Bennett et al. 1993; OGLE: Udalski et al. 1993) for massive compact halo objects in the late 1990s to identify the nature of dark matter. Another effect is the apparent shift of the source position, which was used as the most prominent verification of General Relativity during the famous total solar eclipse of 1919 (Dyson et al. 1923). In this case, the mass of the lens, the Sun, was known, and the apparent shift of background star positions was used to verify Einstein’s revolutionary theory. Alternatively, one can use the apparent displacement of the source to determine the mass of the lens.

The decisive relation that sets the scale of the apparent position shift is the radius of the Einstein ring, Θ_E , for a perfect alignment of observer, lens, and source:

$$\Theta_E = \sqrt{4GM/c^2 D_r}. \quad (4)$$

In the case of a lens within the Galaxy, $1/D_r = 1/D_L - 1/D_S$ is the reduced distance between the distance to lens (D_L) and source (D_S); furthermore, G the gravitational constant and c the speed of light. For galactic lens events Θ_E ranges between a few to some ten milliarcseconds. If source and lens are moving relative to each other, the projected angular separation between source and lens would be $\Delta\theta$. Due to the lens effect, however, it deviates from this value by an amount $\delta\theta$, according to

$$\delta\theta = 0.5 \left[(\Delta\theta/\Theta_E) - \sqrt{(\Delta\theta/\Theta_E)^2 + 4} \right] \Theta_E. \quad (5)$$

It is, therefore, a matter of determining source and lens positions and proper motions long before and during a narrow approach as well as the distances D_S and D_L . In case a distant quasar is used as the source D_r simplifies to D_L , and no proper motion of the source has to be taken into account.

Close approaches of a potential lens to one or more background sources can thus be used to determine the mass of the lens. *Gaia* and HST have allowed one to perform such determinations. Sahu et al. (2017) used HST astrometry to determine the mass of the nearby white dwarf Stein 2051 B, the companion of an M4 main-sequence star, approaching closest (within ~ 0.1 arcsec) of an 18.3 mag star in March 2014. The measurement of a shift of 0.25 ± 0.1 mas resulted in $\Theta_E = 31.53 \pm 1.20$ mas, and together with the known distances in a mass of $0.675 \pm 0.051 M_\odot$ for Stein 2051 B, which agrees with the predicted mass of a CO-WD from the mass-radius relation, and implied a cooling age of 1.9 ± 0.4 Gyr.

In a similar manner, the mass of Proxima Centauri was determined by Zurlo et al. (2018) to be $0.150_{-0.051}^{+0.062} M_\odot$, using the HST/WFC3 and the VLT/SPHERE instruments. The campaign followed the apparent path of Proxima Cen from 2015 on for two years. The error on this measurement is still very large and dominated by the exact position of Proxima Centauri. Nevertheless this method is another direct mass determination method, even if its application depends on serendipitous approaches between foreground and background stars. It will be applied to additional cases in the future (e.g., Sahu et al. 2019).

4 Semi-empirical and analytic relations

4.1 Stellar granulation-based method

Traditional approaches to direct stellar masses rely on the orbit of another body about the star, i.e., a transiting planet or an eclipsing companion star. A new approach developed by Stassun et al. (2017a) provides a pathway to empirical masses of single stars. The approach makes use of the fact that an individual star's

surface gravity is accurately encoded in the amplitude of its granulation-driven brightness variations (e.g., Bastien et al. 2013; Corsaro et al. 2015; Kallinger et al. 2016; Bastien et al. 2016), which can be measured with precise light curves (e.g., *Kepler*, TESS, PLATO). Combined with an accurate stellar radius determined via the broadband spectral energy distribution (SED) and parallax (Stassun and Torres 2016a), the stellar mass follows directly. The method is applicable to stars that have surface convection, responsible for the granulation, and this defines the applicability limit to stars cooler than $T_{\text{eff}} \sim 7000$ K. The lower T_{eff} limit is about 4000 K and of instrumental nature. Below this T_{eff} granulation timescales become too short and convection cell sizes too small so the signal becomes very small and difficult to detect. At the present time the accuracy of this method is of order 25%.

A star's angular radius, θ , can be determined empirically through the stellar bolometric flux, F_{bol} , and effective temperature, T_{eff} , according to $\theta = (F_{\text{bol}}/\sigma T_{\text{eff}}^4)^{1/2}$, where σ is the Stefan–Boltzmann constant. F_{bol} is determined empirically by fitting stellar atmosphere models to the star's observed SED, assembled from archival broadband photometry over as large a span of wavelength as possible, preferably from the ultraviolet to the mid-infrared (i.e., GALEX to WISE). As demonstrated in Stassun et al. (2017b), with this wavelength coverage for the constructed SEDs, the resulting F_{bol} are generally determined with an accuracy of a few percent when T_{eff} is known spectroscopically. Stassun and Torres (2016a) showed that summing up the measured broadband fluxes and interpolating between them can recover $\sim 95\%$ of the bolometric flux. The use of atmosphere models is to provide a more physical interpolation between the measured fluxes than simple linear interpolation. It also allows to extrapolate to the UV for the hottest stars, where the measured broadband fluxes do not reach the same accuracy. *Gaia* parallaxes are then used to determine the physical stellar radius R_{\star} . In general, the interstellar extinction/reddening must also be included as a fitted parameter, unless an independent estimate is available from Galactic dust maps. In regions of high extinction (e.g., the Galactic plane), the extinction can introduce uncertainties in F_{bol} of a few percent or more, especially if the blue end of the SED is not well constrained (see, e.g., Stassun and Torres 2016a). However, the impact on the inferred stellar radius is still generally minor because $R_{\star} \propto F_{\text{bol}}^{1/2}$.

Finally, the bolometric luminosity can be calculated directly from the bolometric flux and the parallax, depending linearly on both, and, therefore, in most cases can be determined with an accuracy of a few per cent. This method is to be preferred over calculating the bolometric luminosity via the spectroscopic effective temperature and the Stefan–Boltzmann relation, as this would then introduce large uncertainties via the large dependence on T_{eff}^4 .

Figure 4 (top) shows that the SED+parallax-based stellar radius R_{\star} agree beautifully with the asteroseismic R_{\star} , and the scatter of $\sim 10\%$ is as expected for the typical parallax error in this sample of $\sim 10\%$. Figure 4 (bottom) demonstrates that the residuals between R_{\star} obtained from the two methods are normally distributed as expected. However, a small systematic offset is apparent. Applying the systematic correction to the *Gaia* DR1 parallaxes reported by Stassun and Torres (2016b) effectively removes this offset. The spread in the residuals is almost exactly

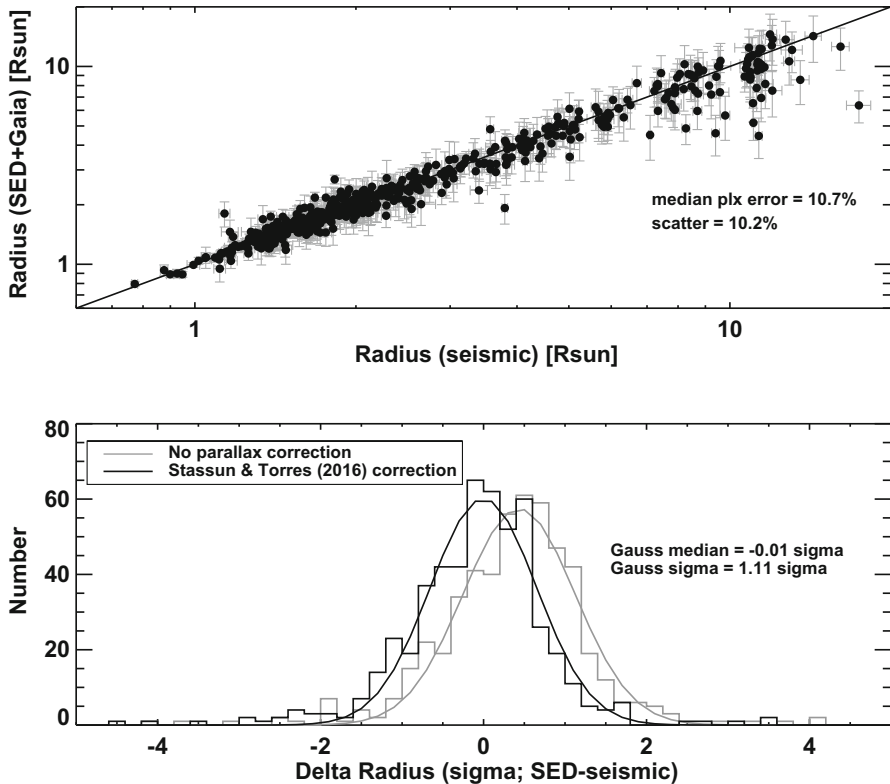


Fig. 4 Comparison of stellar radii obtained from SED+parallax versus stellar radii from asteroseismology. (Top) Direct comparison. (Bottom) Histogram of differences in units of measurement uncertainty; a small offset is explained by the systematic error in the *Gaia* DR1 parallaxes reported by Stassun and Torres (2016b). Image reproduced with permission from Stassun et al. (2018), copyright by AAS

that expected for the measurement errors (1.1σ , where σ represents the typical measurement error).

The granulation-based $\log g$ measurement is based on the “flicker” methodology of Bastien et al. (2013), which uses a simple measure of the r.m.s. variations of the light curve on an 8-hr timescale (F_8), representing the meso-granulation driven brightness fluctuations of the stellar photosphere. As described by Bastien et al. (2016), the stellar $\log g$ can be determined with a typical precision of ~ 0.1 dex.

Later on, Bugnet et al. (2018) developed a new metric, FLiPer, also relating the stellar variability to the surface gravity of the star, but based on the spectral power density rather than on the r.m.s. variations of the light. The technique infers the surface gravity and the frequency at maximum power of solar-like oscillations (see Sect. 6.1) for all solar-like pulsators, including main sequence stars, subgiants, red giants and clump stars, up to the AGB. It determines $\log g$ on a wider interval, from 0.1 to 4.6 dex, with a net improvement on the $\log g$ -precision which is in the range 0.04–0.1 dex (mean absolute deviation 0.046 dex; Bugnet et al. 2019). The

granulation properties can also be extracted from the so-called “background” signal in the stellar power spectrum (b_{meso} ; Kallinger et al. 2014; Corsaro and De Ridder 2014; Corsaro et al. 2015), which has been shown to reach about 4% precision in g using the full set of observations from *Kepler* (Kallinger et al. 2016; Corsaro et al. 2017).

Figure 5 (top) shows the direct comparison of stellar mass M_{\star} from the above method to the M_{\star} from the *Kepler* asteroseismic sample, which is the best available set of stellar masses for single stars (Sect. 6). The mass estimated from the SED+parallax-based R_{\star} (with parallax systematic correction applied; see Stassun and Torres 2016a) and F_8 -based $\log g$ compares beautifully with the seismic M_{\star} . The scatter of $\sim 25\%$ is as expected for the combination of 0.08 dex $\log g$ error from F_8 and the median parallax error of $\sim 10\%$ for the sample.

The M_{\star} residuals are normally distributed (Fig. 5, middle), and the spread in the residuals is as expected for the measurement errors. The M_{\star} uncertainty is dominated by the F_8 -based $\log g$ error for stars with small parallax errors, and follows the expected error floor (Fig. 5, bottom, black). The M_{\star} precision is significantly improved for bright stars if we instead assume the $\log g$ precision expected from the granulation background modeling method of Corsaro et al. (2017). For parallax errors of less than 5%, as will be the case for most of the TESS stars with *Gaia* DR3, we can expect M_{\star} errors of less than $\sim 10\%$.

As shown in Table 8, we estimate that accurate and empirical M_{\star} measurements should be obtainable for $\sim 300\text{k}$ TESS stars via F_8 -based gravities. These masses should be good to about 25% (see above). In addition, we estimate that a smaller but more accurate and precise set of M_{\star} measurements should be possible via the granulation background modelling method for $\sim 33\text{k}$ bright TESS stars.

4.2 Spectroscopic mass estimates for low- and intermediate-mass stars

Several methods allow the mass of a star to be determined from its electromagnetic spectrum. Most of these techniques are, in essence, of an empirical nature as they rely on a set of relationships between spectral features and independently measured stellar mass or age, e.g., by means of asteroseismology. As such, these relationships are calibrations that are relatively easy to use for large samples of stars. So far, the following methods have been explored: H_{α} fitting (Bergemann et al. 2016), C/N ratio (Ness et al. 2016; Martig et al. 2016), and Li abundances (Do Nascimento et al. 2009). Each of these methods will be described in detail below.

4.2.1 H_{α} fitting

The Balmer α line (hereafter, H_{α}) is the main diagnostic feature in the spectrum of an FGK type star. It has traditionally been used as a tracer of chromospheric activity, mass loss, and outflows (Dupree et al. 1984; Rutten and Uitenbroek 2012). The empirical study by Bergemann et al. (2016) suggests that the shape of the line—especially the slope of its unblended blue wing—is sensitive to the mass of an RGB star. The physical basis of this relationship has not been unambiguously identified yet, but it could be related to the chromospheric activity, which depends

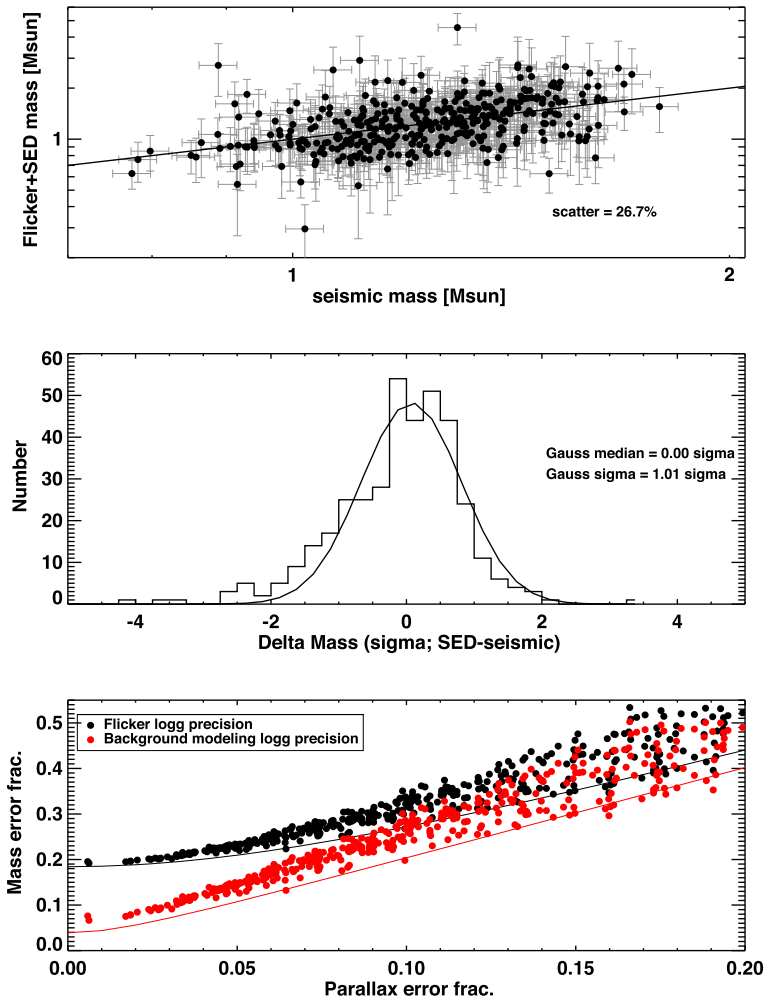


Fig. 5 (Top) Comparison of M_{\star} obtained from F_8 -based $\log g$ and SED+parallax based R_{\star} , versus M_{\star} from asteroseismology. (Middle) Histogram of the residuals from top panel. (Bottom) Actual M_{\star} precision versus parallax error for $\log g$ measured from F_8 (black) and the same but assuming improved $\log g$ precision achievable from granulation background modeling (Corsaro et al. 2017) applied to TESS data (red). Symbols represent actual stars used in this study; solid curves represent expected precision floor based on nominal $\log g$ precision (0.08 dex from F_8 , 0.02 dex from granulation background). (Figure credit: Stassun et al. 2018)

on the evolutionary stage of the star (Steiman-Cameron et al. 1985). The chromospheric back heating may influence line formation in the photospheric layers, leading to a characteristic brightening in the H_{α} line core. This phenomenon is well-known and has been applied, in particular, to Ca H & K lines (e.g., Lorenzo-Oliveira et al. 2018), as well as to the infra-red Ca triplet lines (Athay 1977; Martínez-Arnáiz et al. 2011; Lorenzo-Oliveira et al. 2016). The study by Bergemann et al. (2016) validated the method on high-resolution UVES spectra of RGB

Table 8 Approximate numbers of stars for which R_\star and M_\star can be obtained using the granulation flicker method, according to the data available with which to construct SEDs from visible (*Gaia*, SDSS, APASS, Tycho-2) and infrared (2MASS, WISE) photometry

	<i>Gaia</i> (visible)	2MASS (near-IR)	WISE (mid-IR)
R_\star for TESS stars in <i>Gaia</i> DR-2	97M	448M	311M
M_\star via F_8 for TESS stars with $T_{\text{mag}} < 10.5$	339k	339k	332k
M_\star via b_{meso} for TESS stars with $T_{\text{mag}} < 7$	34k	34k	33k

stars across a large range of metallicity, from $-2 \lesssim [\text{Fe}/\text{H}]$ to $+0.5$ and mass, from 0.7 to $1.8 M_\odot$. The main advantage of the method is that it allows direct tagging of stellar mass from the spectra of distant RGB stars, which are not accessible to asteroseismology. This method is also useful for extragalactic diagnostics of ages of stellar populations. The typical accuracy of masses derived by H_α fitting is 10–15%.

4.2.2 C/N fitting

The ratio of the stellar photospheric abundance of carbon and nitrogen has been proposed as a tracer of stellar mass (Masseron and Gilmore 2015; Martig et al. 2016; Ness et al. 2016) for evolved stars with masses below a few solar masses. This empirical relation is grounded in a globally understood property of stellar evolution, and we discuss here the theoretical background.

While a star is on the main sequence, the CNO cycle happening in its core increases locally the abundance in ^{14}N , decreases ^{12}C , and reduces the ratio of $^{12}\text{C}/^{13}\text{C}$. After leaving the main sequence, as the star starts to ascend the giant branch, it experiences the first dredge-up: the convective envelope reaches deep into the contracting core, into zones containing CNO-processed material (Icko 1965). This suddenly mixes the envelope with material from the core, which changes the surface abundances in carbon and nitrogen: after the first dredge-up, the surface $[\text{C}/\text{N}]$ ratio drops sharply. This post-dredge up $[\text{C}/\text{N}]$ ratio depends on stellar mass for two reasons. On the one hand, the more massive the star, the higher its core temperature so that a larger fraction of the core is involved in the CNO cycle. This implies that a larger fraction of the stellar core has a low $[\text{C}/\text{N}]$ ratio at the end of the main sequence. On the other hand, the higher the stellar mass, the deeper the convective envelope reaches into the core during the dredge-up. Those two effects combine to produce a smaller $[\text{C}/\text{N}]$ ratio at the surface of the more massive stars on the giant branch (e.g., Charbonnel 1994). In theory, it would then be possible to use stellar evolutionary models to determine the mass of a giant star as a function of its surface $[\text{C}/\text{N}]$ ratio (Salaris et al. 2015; Masseron and Gilmore 2015; Lagarde et al. 2017). However, uncertainties in the models, mainly concerning various kinds of mixing processes, make it difficult to predict the actual relation between $[\text{C}/\text{N}]$ and mass, and its dependence on metallicity (see also Sect. 4.3.2).

The ratio of $^{12}\text{C}/^{13}\text{C}$ and $^{12}\text{C}/^{14}\text{N}$ can be determined from medium- and high-resolution optical and infra-red stellar spectra. Qualitatively the observed abundance

measurements agree with the predictions of ab-initio stellar evolution models (e.g., Masseron and Gilmore 2015; Tautvaišienė et al. 2015; Drazdauskas et al. 2016; Smiljanic et al. 2018; Szigeti et al. 2018). Deriving stellar masses from comparing models and observations requires the measured chemical abundances to be accurate (and not just precise), which is a challenge. Casali et al. (2019) compare [C/N] ratios in the APOGEE and Gaia-ESO surveys, illustrating this difficulty, and Jofré et al. (2019) provide a general review of the difficulties in measuring abundances. Systematic differences between models and observations led a number of authors to try a data-driven approach instead, the results of which we will discuss in Sect. 4.3.

4.2.3 Li abundances

At the basis of the method is the relationship between the abundances of Li in stellar atmospheres and stellar ages (or masses). This method is supported by limited observational evidence available for metal-rich Galactic open clusters: M67, NGC 752, and Hyades (Castro et al. 2016; Carlos et al. 2020). As stars evolve away from the main sequence, the growing convective envelope touches the inner layers of a star, in which Li destruction takes place. The Li-poor material is then advected to the surface resulting into a strong, over two orders of magnitude, decline of photospheric Li abundances (Salaris and Weiss 2001; Charbonnel and Talon 2005; Do Nascimento et al. 2009; Xiong and Deng 2009). The decline of Li abundances has been well established from observations. Relating this to model predictions is not straightforward, because the depletion of Li in models depends not only on the initial mass and metallicity of a star, but also on the evolution of stellar angular momentum. However, modern stellar evolution codes, which take into account turbulent and rotational mixing (e.g., CESTAM models, Deal et al. 2018, 2020) satisfactorily describe the observed distribution of Li abundances in open clusters (Semenova et al. 2020). Present empirical investigations, based on metal-rich open clusters and solar-type stars, suggest that Li abundances yield model-dependent masses with the nominal precision of 5% (e.g., Do Nascimento et al. 2009; Carlos et al. 2019). The method has been applied to solar twins—stars with very similar surface parameters, T_{eff} , $\log g$, and [Fe/H] to the Sun—yielding a precision of $0.036M_{\odot}$, assuming a 36 K precision for the measured T_{eff} estimates. In addition, the method requires calibration of stellar models and it depends directly on the accuracy of stellar atmospheric parameters, such as T_{eff} , $\log g$, and [Fe/H]. Some studies suggest that the scatter of Li abundances in solar twins are related to different physical conditions during the pre-MS evolutionary stages (e.g., Thévenin et al. 2017). More precise mass estimates, to better than 3 %, can be obtained by combining Li abundance and rotation periods (e.g., Liu et al. 2014).

For brown dwarfs, Li abundances are also sensitive to the stellar mass. Lithium burns at temperatures higher than 2.5×10^6 K. Substellar objects with mass below $0.05M_{\odot}$ do not reach that temperature and Li is not burned. In the mass range between $0.05M_{\odot}$ and $0.06M_{\odot}$, there is partial Li depletion, with a strong dependence on stellar mass. According to Baraffe et al. (2015), at 1 Gyr Li depletion is 10% for a $0.05M_{\odot}$ but it is already complete for a $0.06M_{\odot}$ star. In this

mass range, it is a sensitive tool for mass determination. The minimum mass at which Li is depleted defines the Li depletion boundary. Lithium abundances can be combined with T_{eff} , luminosity determinations and stellar tracks to determine stellar masses and ages (see, e.g., work on the Pleiades Stauffer et al. 1998, Alpha Persei cluster Stauffer et al. 1999 and the Hyades Martín et al. 2018; Lodieu et al. 2018). It should be noted, however, that the Li depletion might be sensitive to strong, episodic, accretion phases in the very early stages of brown dwarf evolution, potentially changing the absolute of the mass at which Li depletion occurs (Baraffe and Chabrier 2010).

In all cases, mass determinations from lithium abundances rely heavily on stellar models and, in this regard, can also be considered to be strongly model-dependent, together with those methods discussed in Sect. 5.

4.2.4 Sphericity

The arguably most direct spectroscopic tag of the mass of a star is the extension of its atmosphere, to which spectral lines are, in principle, sensitive. It has been demonstrated that there are certain differences between model stellar spectra computed in plane-parallel and spherical geometry (Heiter and Eriksson 2006). The underlying physical connection is through the influence of geometry on the optical path of photons, that is on radiative transfer in the lines and in continua that causes changes in local heating and cooling, and thereby in the relationships of temperature and pressure with optical depth ($T(\tau)$ and $P(\tau)$) in model atmospheres. The characteristic signatures become stronger for more extended stellar atmospheres, which is the case for increasing stellar mass at given effective temperature and surface gravity. The main problem of this method is the weakness and degeneracy of the signal: the sensitivity of a spectral line to atmospheric geometry is typically much smaller than the effect of other stellar parameters, such as the chemical composition, T_{eff} , convective velocities. For instance, the effect of changing mass from 1 to 5 M_{\odot} can be mimicked by changing $\log g$ by 0.5 dex. Also, the effect on spectral lines is highly non-linear, and it makes some features weaker, whereas other lines become stronger. It has, therefore, not been possible yet to meaningfully employ this physical property for the determination of stellar masses.

4.2.5 Summary

Available spectroscopic methods rely on the determination of stellar masses using either empirical relations between stellar properties determined from observed data and stellar mass (H_{α} , C/N ratio) or by comparing these properties with stellar models, which depend on mass and metallicity (Li abundances) and on uncalibrated mixing properties. All these methods have a limited validity range: the H_{α} and C/N ratio methods work for red giant stars in the mass range from ~ 0.7 to $\sim 1.8 M_{\odot}$ and deliver precision of $\sim 15\%$. The method that relies on Li abundance measurements applies only to a very limited space of stellar parameters. It has only been validated on solar twins, that is stars with T_{eff} and $\log g$ very close to that of the Sun (~ 5780 K), and on stars with masses from $\sim 0.9 M_{\odot}$ to $1.7 M_{\odot}$ in several

Galactic open clusters at solar metallicity, $[\text{Fe}/\text{H}] \approx 0$. Some studies show that the method yields a precision of $\sim 5\%$ in mass for T_{eff} accurate to 40 K, but the error increases strongly with the uncertainty of T_{eff} .

The only quantity in a stellar spectrum that is directly dependent on the mass of a star is the sensitivity of spectral lines to the extension of the stellar atmosphere. Notwithstanding its simplicity, this diagnostic has not been utilized for the determination of stellar masses, owing to the very dependence of the lines and degeneracies with other atmospheric parameters.

4.3 Spectroscopic surface abundance method for low- and intermediate-mass stars

4.3.1 Data-driven methods

In Sect. 4.2.2 we have presented the arguments why the surface C/N-ratio of red giants can serve as a mass indicator, and why this method cannot be applied directly at the present stage. Currently, all studies that make use of this relation resort to an empirical calibration of the C/N ratio on mass and age determined by asteroseismology. As such, the accuracy of this technique depends on the quality of asteroseismic diagnostics. Moreover, it is limited by the assumption that the observed abundances are internally accurate (no intrinsic biases) and the C/N ratio at the time of formation of a star was close to solar ($[\text{C}/\text{N}] = 0$), that is, the effects of galactic chemical evolution are calibrated out. The idea behind such data-driven methods is to use a training set of stars with known masses and surface abundances and build a model relating those quantities. The model can then be applied to a large sample of stars for which abundances have been measured.

Martig et al. (2016) showed that this is a viable approach. Their training set consisted of stars from APOKASC, combining spectroscopic data from the APOGEE survey and *Kepler* asteroseismic masses. From this, they fitted a quadratic function to the relation between $[\text{M}/\text{H}]$ (“M” representing the global metallicity), $[\text{C}/\text{M}]$, $[\text{N}/\text{M}]$, $[(\text{C}+\text{N})/\text{M}]$, T_{eff} , and $\log g$ on the one hand, and stellar mass on the other hand. Applying this relation to stars in APOGEE, they were able to determine stellar masses for 52,000 giants. The dispersion for the masses obtained from this method, based on comparisons with masses determined by means of asteroseismology, is about 14 % for stars with masses from ~ 0.7 to $\sim 2.0 M_{\odot}$ (Martig et al. 2016). The same fitting function was used by Ho et al. (2017) to determine masses for stars observed by LAMOST. A similar approach was also adopted for LAMOST stars by Wu et al. (2018).

Sanders and Das (2018) and Das and Sanders (2019) have developed a Bayesian artificial neural network that also incorporates the C/N ratio as input data for stellar mass determination. While the training of the network relies on isochrones, once trained, the network can be used without further need of them. It is a highly efficient approach which has been used to provide masses for about 3 million stars across different surveys.

Another family of data-driven models bypasses the step where abundances of C and N are computed and relates directly the mass of a star to its spectrum. This was pioneered by Ness et al. (2016), using *The Cannon* to extract stellar mass from spectra by learning a mapping between wavelength and stellar parameters. They confirmed that mass information was contained in CN and CO molecular features and showed that both line strength and profile change visibly as a function of stellar mass. Finally, machine learning approaches have been recently developed to extract information directly from spectra, as in Mackereth et al. (2019) using a Bayesian Convolutional Neural Network (originally described in Leung and Bovy 2019) or in Wu et al. (2018, 2019) using Kernel Principal Component Analysis.

4.3.2 Performance and limitations

The various data-driven methods have led to a revolution in the field of Galactic archaeology, with masses (and thus ages) now determined for millions of giant stars across the Milky Way. The random mass uncertainties are typically of the order of 10% or slightly less (e.g., Martig et al. 2016; Ness et al. 2016; Das and Sanders 2019; Wu et al. 2019). Of course, because the methods rely on a training set, any systematic errors in the masses used during training are transferred to the predicted masses. In addition to this, masses can only be determined for stars in the same region of parameter space as the training set. This parameter space will be increased vastly when asteroseismic masses from K2, TESS, and PLATO are available and are combined with spectra. However, an additional complication comes from the mapping of [C/N] and the mass itself: the relation between [C/N] and mass flattens for $M > 1.5 M_{\odot}$ so that [C/N] is not a very precise mass indicator for intermediate-mass stars with $M > 1.5 M_{\odot}$.

Stars that are above the RGB bump present another challenge: it is now well established that they undergo some extra-mixing that further decreases their [C/N] ratio below what was established during the first dredge-up (e.g., Charbonnel 1994; Gratton et al. 2000; Martell et al. 2008; Angelou et al. 2012). This could be due to thermohaline mixing (Charbonnel and Zahn 2007), a double diffusive instability that develops at the RGB bump. There are other possible sources of extra-mixing, e.g., during the helium flash (Masseron et al. 2017). The extra mixing processes seem most efficient in low mass stars and at low metallicity (Charbonnel and Lagarde 2010; Lagarde et al. 2019; Shetrone et al. 2019). In any case, this means that any data-driven method should either avoid using low metallicity stars, or be flexible enough to learn that the mapping between [C/N] and mass varies with mass and metallicity (this is the case for many of the methods presented here).

Finally, an important limitation of [C/N]-based methods is that stars might exhibit abundance patterns that are not due to their internal evolution but to either galactic chemical evolution or external pollution. Overall, it seems that pre-dredge up [C/N] does not vary much as a function of location within the disk of the Milky Way (Martig et al. 2016; Hasselquist et al. 2019), but some regions like the Galactic center could have a more complex chemical evolution. Individual stars also can show surface abundances that do not follow Galactic chemical evolution: for instance the N-rich stars in Schiavon et al. (2017) were probably formed in globular

clusters. For these reasons, [C/N]-based methods should never be applied to derive masses for individual stars, but instead should only be used in a statistical sense to study the properties of large sample of stars.

A dataset that can be used to calibrate the relation between mass and [C/N] is the APOKASC catalogue (see Pinsonneault et al. 2018, for the second version). An earlier version of this dataset was published by Martig et al. (2016) and can be found at the CDS in Strasbourg.⁶

4.4 Analytical/empirical relations for estimating stellar masses

One of the most used techniques for estimating stellar masses relies on empirical relations, such as the mass-luminosity relation. These relations are, in general, data-driven relations for estimating a dependent variable (in our case the stellar mass) as a function of other independent observables, generally easier to obtain. The quality of the data used for inferring any data-driven relation is critical for a reliable result. In our case the stellar mass itself is the critical observable since other classical observables such as T_{eff} , $\log g$, [Fe/H], can be derived in a nominal way from observations. For the reference database, we need a group of stars with very precise masses since the real accuracy is harder to assess. Historically, the community has used DEBs (see Sect. 2) for constructing these reference datasets.

In the field of empirical relations for obtaining stellar masses (and also radii) there are two different and complementary working lines as follows:

- The classical $M - L$, $M - R$, and $M - T_{\text{eff}}$ relations based on data as shown in Fig. 2. These relations are derived following the original concepts by Hertzsprung (1923), Russell et al. (1923), and Eddington (1926). A recent revision of these relations has been treated by Eker et al. (2018).
- More complex functional forms where the stellar mass or radius are obtained as a function of a combination of different observables. This line was proposed by Andersen (1991), with many recent extensions or revisions (Gafeira et al. 2012; Eker et al. 2015; Benedict et al. 2016; Mann et al. 2019), with Torres et al. (2010) being a standard reference for DEBs.

Moya et al. (2018) boosted both lines gathering a large dataset to derive these relations. They combined mass and radius estimations coming from different techniques. The recent development of asteroseismology as a precise tool for stellar characterization and accurate interferometric radii make the extension of the observational sources used so far beyond DEBs possible. Moya et al. (2018) collected more than 750 main-sequence stars with spectral types from B down to M with precise masses, radii, T_{eff} , $\log g$, L , [Fe/H] and stellar density (ρ). With this database, they revised relations in the literature with a functional form M or $R = f(X)$ where X is any combination of independent variables [T_{eff} , $\log g$, L , [Fe/H], ρ], avoiding combinations containing highly correlated variables. The final result was a total of 38 new or revised empirical relations, one for almost every possible

⁶ <http://vizier.u-strasbg.fr/viz-bin/VizieR?-source=J/MNRAS/456/3655>.

combination of independent variables, and a mass range of applicability between 0.7 to $2.5 M_{\odot}$ approximately.

A summary of the statistical performance of these 38 relations is shown in Fig. 6. In the upper panel, we can see that all the relations have an $R^2 > 0.85$, meaning that they explain at least 85% of the variance found in mass or radius (depending on the

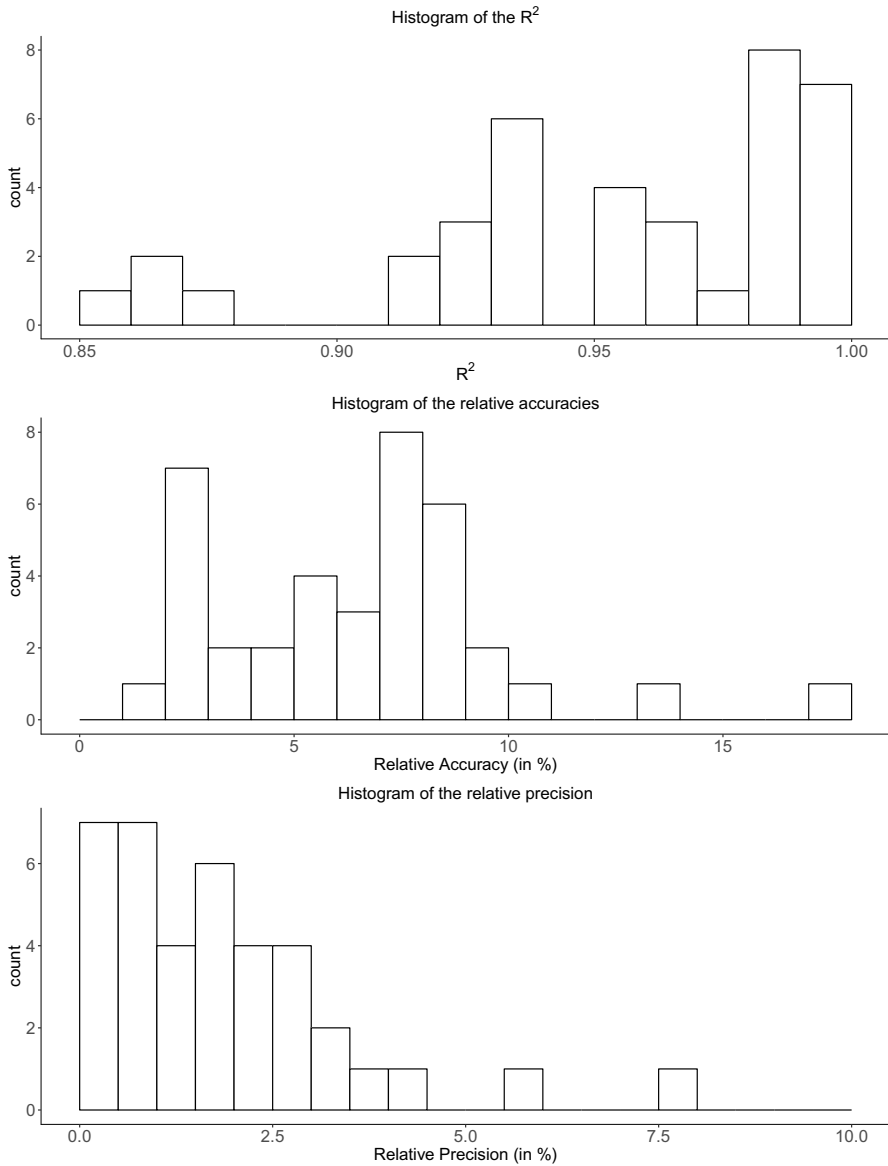


Fig. 6 Histogram showing the $adj-R^2$ (top panel), accuracy (central panel), and precision (bottom panel; both in terms of relative differences) of the 38 relations presented in Moya et al. (2018) (Figure credit: Moya et al. 2018)

Table 9 Comparison between different empirical mass relations in the literature and their fractional accuracy (Acc) and precision (Prec) (both in per cent), taking the ones in Moya et al. (2018) as a reference

Ref.	Relation	Acc/Prec	Ref.	Corresponding relation	Acc/Prec
T10	$M = f(X, X^2, X^3, \log^2 g, \log^3 g, [\text{Fe}/\text{H}])$	7.4/52.9	M18	$M = f(T_{\text{eff}}, \log g, [\text{Fe}/\text{H}])$	7.5/3.4
G12	$M = f(\log L, \log^2 L, \log^3 L)$	14.0/0.6	M18	$\log M = f(\log L)$	10.1/0.1
G12	$M = f(\log L, \log^2 L, \log^3 L, [\text{Fe}/\text{H}], [\text{Fe}/\text{H}]^2, [\text{Fe}/\text{H}]^3)$	8.9/0.8	M18	$\log M = f(\log L, [\text{Fe}/\text{H}])$	9.9/0.9
M07	$M = f(\log L, \log^2 L)$	11.2/—	M18	$\log M = f(\log L)$	10.08/0.13
E18	$\log L = f(\log M)$	33.3/6.9	M18	$\log L = f(\log M)$	31.9/0.6

References: T10 (Torres et al. 2010), G12 (Gafeira et al. 2012), M07 (Malkov 2007), E18 (Eker et al. 2018), M18 (Moya et al. 2018)

relation). In fact, all the relations except four of them (those with the lowest number of dimensions) have $R^2 > 0.9$. In the middle panel, we show the accuracy obtained by these relations. To obtain each relation, the authors used only a subset of their database, leaving the rest of the stars as the testing group. The accuracy displayed is a comparison of the estimations obtained with the empirical relations and the “real” values for the testing subset. Figure 6 reveals that, except in three cases (those with a lower number of dimensions), all the relations provide accuracies better than 10%. The lower panel reveals the internal precision of the 38 relations in terms of the uncertainties of their regression coefficients. In this case, all the relations except two (those with the largest number of dimensions) have precisions better than 5%. To obtain the final precision, the uncertainties of the observables must be included.

Table 9 shows the comparison between empirical relations in the literature and their counterparts in Moya et al. (2018). Torres et al. (2010) find a similar accuracy but a different precision due to the different number of independent variables adopted in the regressions. The precision based on the inclusion of the uncertainties of the observables, in addition to those of the regression coefficients, gets worse when the number of dimensions of the relations increases.

Gafeira et al. (2012) provided three relations for the stellar mass, but only two of them can be easily applied. The first one is a polynomial up to third order in $\log L$, and the second one adds different orders of $[\text{Fe}/\text{H}]$ to the first one. The main differences between the results by Gafeira et al. (2012) and Moya et al. (2018) come from the fact that the former study relied on only 26 stars. Malkov (2007) and Moya et al. (2018) found similar accuracy but the precisions cannot be compared since Malkov (2007) does not provide the coefficient uncertainties. Finally, Eker et al. (2018) provide a relation with the luminosity as the dependent variable to be estimated as a function of the stellar mass. There is no counterpart to this expression in Moya et al. (2018), but the authors compared this with relations stemming from the same polynomial. The results listed in Table 9 point to the worst accuracy (in

terms of L and not in $\log L$) due to the estimation of the luminosity from the stellar mass and the use of logarithms.

For very low mass dwarf stars, from spectral types K7 to M7 and mass in the range $0.1 < M/M_{\odot} < 0.6$, empirical relations are the primary way to determine the mass of field stars. In this mass range stars become fully convective and the relation between mass and luminosity changes, making the relations deviate from those for earlier spectral types. From a direct observational point of view, the most fundamental relations have been established using single photometric bands.

Following that approach, Delfosse et al. (2000) used a combination of visual, interferometric and eclipsing binaries to construct a sample of 32 stars with determined masses. They used this sample to calibrate empirical relations between stellar mass and absolute magnitudes in different photometry bands. Results showed tight relations between infrared luminosity and stellar mass, with a 10% dispersion when the K band is used, and less well-defined correlation in the visual band. Mann et al. (2015) reanalyzed the $M = f(M_{K_s})$ relation by Delfosse et al. (2000) on an enlarged binary sample and found it to be accurate to 5% in the mass range $0.1 < M/M_{\odot} < 0.6$. Benedict et al. (2016) and Mann et al. (2019) have derived updated relations with larger datasets. The latter provide an $M = f(M_{K_s})$ polynomial relation that provides a precision of $\approx 3\%$ in mass determination across the mass range $0.08 < M/M_{\odot} < 0.7$, with slightly worse precision close to the range limits. Caution should be taken that these relations are not applicable to young < 1 Gyr or active objects. Benedict et al. (2016) find a larger dispersion in their results, about 18% at $0.2 M_{\odot}$, and argue that heterogeneity in stellar ages, magnetic activity levels and metallicity hamper more precise mass estimates from one-parameter relations. A very recent application of the mass–radius relation including a complete discussion on the method can be found in Schweitzer et al. (2019), who determined radii and masses of 293 nearby, bright M dwarfs.

In summary, empirical relations are very useful and user-friendly tools for obtaining a reasonable first estimation of the stellar mass when no other technique is available or it is too time-consuming from a computational point of view. They can also be useful as a cross-check using other methods.

4.5 Spectroscopic masses of high-mass stars

Stellar parameters for hot stars of high mass (OB and Wolf–Rayet stars) are traditionally derived from the blue optical and H_{α} wavelength range ($\lambda 4000$ to 7000 \AA). Spectroscopic analyses are performed by fitting observed spectra with synthetic spectra computed with stellar atmosphere and radiative transfer codes. To obtain the spectroscopic mass, $M_{\text{spec}} = gL/(4\pi\sigma GT_{\text{eff}}^4)$ (with σ the Stefan-Boltzmann constant), the surface gravity ($\log g$), the bolometric luminosity (L) and the effective temperature (T_{eff}) of the star are required. The gravity is usually derived from the width of the Balmer lines, but the line broadening due to the projected rotational velocity ($v \sin i$) and other velocity fields at the surface often gathered in the so-called (v_{mac} Simón-Díaz and Herrero 2014; Aerts et al. 2014) must be known first to avoid overestimation of $\log g$. Moreover, in fast rotators $\log g$

should be corrected for the deformation of the star, resulting in a lower gravity due to the centrifugal acceleration.

High-mass stars can have strong stellar winds and these may add an emission line component to the absorption line profiles. Low-energy lines like H_α and H_β are more affected with filled emission than H_γ , H_δ and higher order Balmer lines. With increasing wind strength and mass-loss rate, eventually all Balmer lines turn into emission lines and the stellar wind becomes optically thick, as is the case for, e.g., Wolf–Rayet stars. For these, $\log g$ cannot be determined because the hydrostatic structure of the star is obscured by the dense stellar wind. Therefore, stellar masses of Wolf–Rayet stars are usually estimated using a $M - L$ relation. Under the assumption of chemical homogeneity, the $M - L$ relation from Gräfener et al. (2011) provides upper mass limits for hydrogen burning and lower limits for helium burning Wolf–Rayet stars.

With increasing stellar luminosity, the most massive stars approach the Eddington limit. The Eddington parameter is defined as the ratio of the radiative acceleration and surface gravity ($\Gamma = g_{\text{rad}}/g$). The proximity to the Eddington limit has implications for the $M - L$ relation, whose mass dependence changes from $L \propto M^3$ into $L \propto M$ as $\Gamma \rightarrow 1$ (Yusof et al. 2013). In addition, the measured $\log g$ is an effective value $g_{\text{eff}} = g(1 - \Gamma)$, with $\Gamma \propto L/M$ as well as $\propto T_{\text{eff}}^4/g$. This means that with increasing effective temperature, $\log g$ must increase as well to avoid surpassing the Eddington limit. This lies at the basis of the observed degeneracy between $\log g$ and T_{eff} in O-type stars as g_{eff} remains constant.

The effective temperature of the star is usually derived from the ionisation balance of He I and He II and N III, IV and V in O, Of/WN and Wolf-Rayet stars of type WN, Si II, III and IV in B stars and He I, He II, C III and IV in classical Wolf–Rayet stars of type WC and WO. To further obtain the stellar luminosity, the distance and the extinction towards the star are required. Based on the stellar parameters one can compute the bolometric correction of the star. For isolated field stars, the use of reddening maps is appropriate and allows one to derive the stellar luminosity. Recipes for the computation of the bolometric luminosities of field stars with parameters in the range $T_{\text{eff}} \in [10, 30] 10^3$ K and $\log g \in [2.5, 4.5]$ for a multitude of passbands and reddening maps are available in Pedersen et al. (2020). A more detailed estimate of the amount of extinction and type of reddening law is necessary for high-mass stars in OB associations. In this case, the reddening parameters R_V and $E(B - V)$ can be derived using a reddening law as in Cardelli et al. (1989), Fitzpatrick (1999) and Maíz Apellániz et al. (2014), in combination with multicolour photometry and the corresponding intrinsic colours inferred from the stellar parameters of the star. This can be done analytically (e.g. Bestenlehner et al. 2011, 2020) or by fitting the available photometry (Maíz 2007). Uncertainties for the three required stellar quantities that lie at the basis of spectroscopic masses for the best cases are $\Delta \log g \simeq 0.1$ dex, $\Delta \log L/L_\odot \simeq 0.1$ dex and $\Delta T_{\text{eff}} \simeq 5\% T_{\text{eff}}$.

In principle, spectroscopic and evolutionary masses (M_{evo} , Sect. 5.3) should agree, but about three decades ago a mass discrepancy was observed in Galactic O stars (Herrero et al. 1992). This discrepancy also occurs for B-type dwarfs (Tkachenko et al. 2020). Evolutionary masses are systematically larger than

spectroscopic masses (negative mass-discrepancy, $M_{\text{spec}} - M_{\text{evo}} < 0$). Improvements both in stellar atmosphere and evolutionary models over the past decades have reduced the discrepancy, but its existence and degree is an ongoing debate. Studies of stellar samples in the Milky Way and in the Magellanic Clouds have not given a definitive answer (e.g., Herrero et al. 2002; Massey et al. 2005; Trundle and Lennon 2005; Mokiem et al. 2007; Weidner and Vink 2010; Martins et al. 2012; Mahy et al. 2015; Markova and Puls 2015; McEvoy et al. 2015; Ramírez-Agudelo et al. 2017; Sabín-Sanjulián et al. 2017; Markova et al. 2018; Mahy et al. 2020).

Markova et al. (2018) suggested that the discrepancy might be caused by inaccurate stellar luminosities due to distance uncertainties, or uncertainties in the effective temperatures due to neglecting the turbulence pressure in the hydrostatic equation adopted in stellar atmosphere codes. By studying double-lined photometric binaries Mahy et al. (2020) reported that spectroscopic and dynamical masses (Sect. 2) agree well. However, in particular for semi-detached systems, evolutionary masses are systematically higher, which suggest that the mass discrepancy can be to some extent explained by previous or ongoing interactions between the stars. An alternative explanation for the mass-discrepancy problem has been proposed by Tkachenko et al. (2020) on the basis of a homogeneous data analysis treatment of a sample of intermediate- and high-mass eclipsing double-lined spectroscopic binaries. This study revealed that the mass discrepancy is largely solved for stars with masses between $4 M_{\odot}$ and $16 M_{\odot}$ when considering higher-than standard core masses (m_{cc}) due to the occurrence of extra near-core mixing not considered in standard evolutionary models. This is supported by gravity-mode asteroseismology of single stars in this mass range (cf. Sect. 6.3). Including asteroseismically calibrated near-core mixing, alongside with careful homogeneous treatment of the degeneracy between the effective temperature and the micro-turbulence to derive the atmospheric parameters, essentially solves the mass discrepancy for B-type stars. We come back to the asteroseismic inference on internal mixing and along with it m_{cc} along the evolution of stars born with a convective core in Sect. 6.3.

By studying O-type stars in the Milky Way (Mahy et al. 2015; Markova et al. 2018) and in the Large Magellanic Cloud (Bestenlehner et al. 2020) it was found that stars more massive than $\sim 35 M_{\odot}$ show a positive mass-discrepancy ($M_{\text{spec}} - M_{\text{evo}} > 0$), i.e., their spectroscopic masses are systematically larger than their evolutionary masses. Markova et al. (2018) proposed a possible explanation for the evolved and not too massive stars (up to $\sim 50 M_{\odot}$) in terms of overestimated mass-loss rates in evolutionary models based on the widely used prescriptions by Vink et al. (2000, 2001). If the mass-loss rates based on these prescriptions are too large, these stars have actually lost less mass than predicted by those evolutionary models. However, Higgins and Vink (2019) were only able to reproduce the dynamical masses and chemical composition of the eclipsing spectroscopic double-lined O supergiant system HD 166734 (Mahy et al. 2017) when considering similar mass-loss rates to Vink et al. (2000, 2001), increased convective core overshooting and rotational mixing. Bestenlehner et al. (2020) investigated in detail the systematics in the determination of spectroscopic and evolutionary masses which can only partially explain the observed discrepancy. Larger convective core

overshooting parameters, enhanced mixing due to rotation or binary mass transfer, would lead to even lower evolutionary masses and widen the divergence leaving the mass discrepancy for the most massive stars unsolved.

4.6 Pulsational mass of Cepheids

Already in the late 1960s and early 1970s of the past century it became evident that the mass of the radially pulsating Cepheids can be determined from their pulsation properties by various methods. To varying degree they are dependent on physical assumptions, additional measurements (such as distance, luminosity, or colour), and theoretical pulsation calculations. Cox (1980) summarized the methods and situation at that time. Here we concentrate on the most direct method (Christy 1968; Stobie 1969; Fricke et al. 1972) using the fact that theoretical models showed that the phase shift between the two maxima in light curves of bump Cepheids (e.g., Bono et al. 2002) depends on the ratio M/R (with a minor influence of metallicity). Similarly, the periods of the near-adiabatic radial pulsations are proportional to the average density M/R^3 . Together, this allows for the simultaneous determination of mass and radius.

Independent radius measurements, e.g., by interferometry, derived from spectroscopy, or by the Baade–Wesselink method can be used in addition. Both period and phase shift can be determined directly by observations. From the beginning it became evident that these so-called *pulsational masses* were definitely lower than the *evolutionary masses* (Caputo et al. 2005), obtained mainly from fitting evolutionary models to the luminosity of Cepheids (similar to the isochrone methods of Sect. 5.1).

Over the years a number of ideas and “solutions” to this *Cepheid mass discrepancy* were put forward, among them better distances, new opacities, and, of course, improved pulsational calculations. The quoted discrepancy ranged between about 10% and almost 50%. At the present time two solutions are favoured, and both concern corrections to the evolutionary mass. The first one concerns an enhanced, pulsation-driven mass loss (Neilson et al. 2011), which reduces the mass significantly. The second possibility is to increase the size of the convective, or more generally, the mixed core, leading to higher values of m_{cc} . This leads to higher luminosity for given initial stellar mass, and is achieved by either including overshooting in the models (Chiosi et al. 1992), or by additional mixing due to rapid core rotation (e.g., Anderson et al. 2016) or additional mixing phenomena in the near-core boundary layers. The latter effect solved the mass discrepancy problem in DEBs as discussed above (Tkachenko et al. 2020).

The fact that the stellar models have to be revised depends crucially on strong support for the correctness of the pulsational mass, which have repeatedly been confirmed by dynamical mass determinations. Recent detections of large numbers of Cepheids in DEBs made independent mass determinations (see also Sect. 2.6 and Table 5) possible. The most prominent example is OGLE-LMC-CEP-0227 (Pietrzyński et al. 2010), for which a dynamical mass of $4.14 \pm 0.05 M_{\odot}$ and a pulsational mass of $3.98 \pm 0.29 M_{\odot}$ was derived. Theoretical models employing the

above-mentioned changes to the input physics were able to model both components of the binary (Cassisi and Salaris 2011; Neilson and Langer 2012; Prada Moroni et al. 2012). A further example is OGLE-LMC-CEP-1812 (Pietrzyński et al. 2011), with a dynamical mass of $3.74 \pm 0.06 M_{\odot}$, which corresponds well with a pulsational mass of $3.27 \pm 0.64 M_{\odot}$, obtained, however, from a period-mass relation derived from theoretical models.

An overview of more recent results on the reliability of pulsational Cepheid masses is given by Pilecki et al. (2016). They conclude their summary with the words “...solve the famous Cepheid mass discrepancy problem with the pulsation theory as a winner.” This result from the radial pressure modes for Cepheids is completely in agreement with the findings from gravity-mode asteroseismology of B-type dwarfs, pointing out the need of higher convective core masses already in the earliest nuclear burning stages from asteroseismology of intermediate-mass stars (see Aerts 2021; Pedersen 2020, and also Sect. 6.3).

There are further indications that the period ratio between first overtone to fundamental mode as function of the fundamental mode (the Petersen-diagram) for classical RR Lyr stars depends on stellar mass, and computations of these classical pulsators may point to a slightly higher pulsational than evolutionary mass in the case of RR Lyr in the Carina dwarf galaxy (Coppola et al. 2015). However, pulsational masses for radial pulsators other than classical Cepheids are still in their infancy.

5 (Strongly) model-dependent methods

5.1 Isochrone fitting

Isochrone fitting is a technique as old as stellar evolutionary models. Since isochrones are made of a sequence of initial masses in the HRD, they naturally can provide mass estimates. Under the assumption that stars underwent a negligible amount of mass loss, constant mass tracks can be used to define the isochrone. Otherwise, the complete and mostly unknown mass loss history has to be taken into account. This adds another degree of complexity, and renders the isochrone method less accurate, in particular for massive stars. The method can be applied either to field stars, giving origin to a series of methods discussed elsewhere in this paper (see sections on spectroscopic masses, Sect. 4.2, and the asteroseismic grid-based methods, Sect. 6.1), or to eclipsing binaries (Sect. 2) and star clusters as a whole (Sect. 1.3). Cluster isochrone fitting is particularly valuable as it reveals the shortcomings of stellar models, which often reflect as systematic errors in the mass estimates of field stars. Among these shortcomings, three are especially worth mentioning, in the context of mass determinations.

First, there is the old problem of convective core overshooting, which affects all intermediate- and high-mass stars as of their birth. While there is wide consensus that overshooting takes place, there are still substantial uncertainties regarding both if and how it depends on stellar mass and about its maximum efficiency (see, e.g., Moravveji et al. 2015; Claret and Torres 2016; Deheuvels et al. 2016; Costa et al.

2019; Johnston et al. 2019b, c; Tkachenko et al. 2020, and references therein, see also Sect. 6.3). Mass estimates of unevolved dwarfs and of evolved giants can significantly change due to overshooting. The reason is that overshooting changes the relationship between the stellar mass and its post-main sequence core mass, which largely determines its luminosity (cf., Martins and Palacios 2013). As discussed above, this problem has been for long at the origin of the “Cepheid mass discrepancy” but is solved by including extra mixing deep inside the star, enhancing m_{cc} . Pulsation-driven mass loss can contribute to the solution as well for evolved stars, since it reduces the stellar mass while keeping the core unchanged (Neilson et al. 2011).

Second, there is the problem of rotation. Traditional stellar evolutionary models were calculated with low or no rotation and while modern models have begun including rotation, there are a number of different implementations which cause differences between the models (e.g., Georgy et al. 2013). Rotation can induce extra mixing within the stars, causing fresh H to be brought to the core and extending as such the main-sequence lifetime of a star (e.g., Eggenberger et al. 2010). Additionally, rotation can induce geometric effects on the star, affecting the effective temperature and luminosity. It is now clear that clusters host stars with a range of rotational velocities (e.g., Dupree et al. 2017; Kamann et al. 2018; Bastian et al. 2018; Marino et al. 2018), which can have a strong effect on the observed colour–magnitude diagram of the cluster. Moreover, as will be highlighted in Sect. 6.3, asteroseismology of intermediate-mass dwarfs has revealed extra mixing deep inside stars that may not only be related to rotation but to a whole variety of mixing phenomena. This means that there is no longer a one-to-one correspondence between luminosity and mass, even for stars on the main sequence. This problem resembles therefore that of the mass loss history, and is most pronounced for high-mass O and B-stars in clusters, although it is clearly observable in A and F-stars as well (e.g., Bastian and de Mink 2009; Johnston et al. 2019a), in agreement with asteroseismic results for field stars.

Third, stars of very low mass present their own problems with mass determinations that can be under-estimated by a factor of two at young ages (i.e., low gravities; Baraffe et al. 2002). Many surveys dedicated to open clusters and star-forming regions have been used for direct comparison with state-of-the-art evolutionary models to gauge their reliability in the low-mass and sub-stellar regimes below $0.6 M_{\odot}$ (see review by Bastian et al. 2010b and references therein). While most isochrones reproduce generally well the overall sequence of members in the oldest regions, discrepancies tend to increase with younger ages due to uncertainties on the molecular line lists, convection, and initial conditions. It is therefore important to identify multiple systems (preferentially eclipsing binaries; see Sect. 2) over a wide range of masses and ages to pin down the physical parameters responsible for the discrepancies between observations and model predictions.

Apart from the question how physically correct the stellar models from which the isochrones are deduced are, and which ingredients dominate the systematic uncertainties in the mass determination, the precision of the atmospheric parameters is important as well. This is in particular true for applications to ensembles of single

(field) stars. The fitting procedure is similar to isochrone fitting of populations of stars, but using only one data point. This has become widely used for medium to large samples of stars from spectroscopic surveys following the method of Jørgensen and Lindegren (2005) who present a Bayesian method to determine ages. The method is the same for determining mass. Bayesian methods relying on fitting isochrones or stellar evolution tracks become increasingly important at present, owing to their flexibility and capability to combine diverse observational information, such as photometry, parallaxes, and stellar models (Pont and Eyer 2004; Jørgensen and Lindegren 2005; Shkedy et al. 2007; Burnett and Binney 2010; Bailer-Jones 2011; Liu et al. 2012; Serenelli et al. 2013; Astraatmadja and Bailer-Jones 2016; Lebreton and Reese 2020). Schönrich and Bergemann (2014) combined the analysis of stellar spectra, photometric and astrometric data directly to perform isochrone fitting while correcting for survey selection functions. The codes based on these methods have found their application in various astronomical surveys, such as the Gaia-ESO survey, GALAH, and LAMOST.

The possible precision in mass or age determination using isochrone fitting is highly dependent on which parameters are available and the type of star in question. Typically spectroscopic samples have at least effective temperature (T_{eff}) and surface gravity ($\log g$) measurements. For low-mass stars, the highest precision can be obtained for subgiant stars where the atmospheric parameters of stars of different masses is the largest. To illustrate this, Fig. 7 shows solar metallicity PARSEC model isochrones (Bressan et al. 2012) coloured by the logarithm of mass. The larger mass separation of the subgiant stars in the covered mass range is clear.

For most spectroscopic samples, photometry is also available as well as *Gaia* DR2 distances. Serenelli et al. (2013) examined the accuracy and precision of stellar mass estimates using Bayesian methods based on evolutionary tracks. They showed that the absolute floor to mass accuracy is set by the accuracy of atmospheric stellar parameters: T_{eff} , $\log g$, and $[\text{Fe}/\text{H}]$, and that Non-local Thermodynamic Equilibrium (NLTE) models (Asplund 2005; Bergemann et al. 2012) are required to achieve the desired accuracy of stellar masses. Feuillet et al. (2016) and Sahlholdt et al. (2019) examine the achievable age precision using different observed atmospheric parameters. They both show that absolute magnitude or luminosity is a better constraint on age than $\log g$. As precision in age follows from precision in mass, their results show that $\log g$ is a poorer constraint for mass as well. Regardless of the other observed parameters used for isochrone matching, the stellar metallicity is always needed because of the mass-metallicity degeneracy in stellar evolution models. If the metallicity is not well-measured, then the mass cannot be precisely constrained, because metallicity is the other fundamental parameter needed for theoretical stellar tracks (Sect. 1.1).

5.2 HRD fitting of low- and intermediate-mass evolved stars

At later stages of stellar evolution, the observables that we normally trust to determine the mass of main-sequence stars are affected by physical processes that acquire more importance. For example, if one aims at obtaining the mass of single RGB, red clump or AGB stars by comparing their location on the HRD with

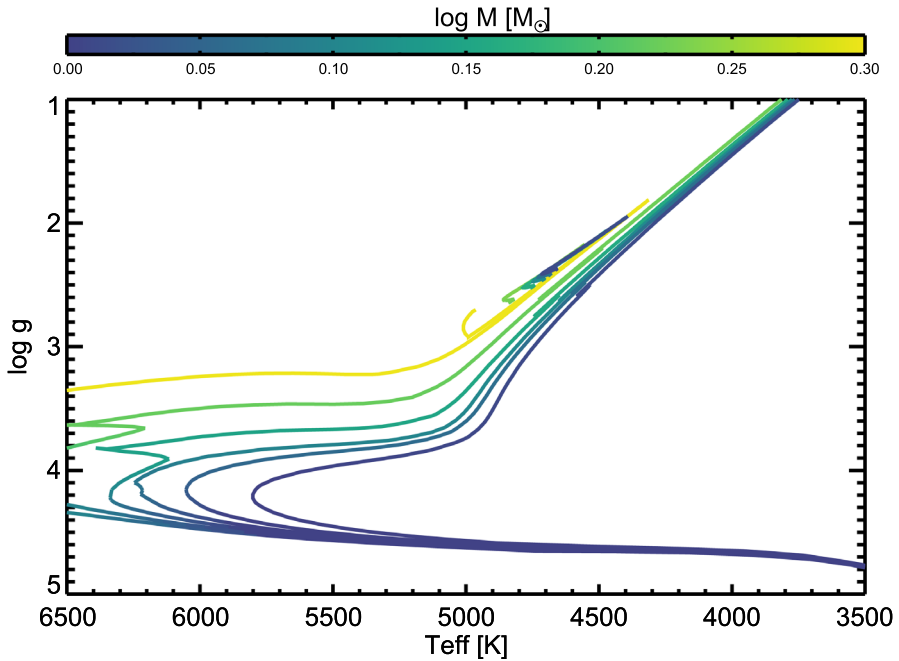


Fig. 7 The $\log g$ - T_{eff} diagram of PARSEC isochrones (Bressan et al. 2012) of different ages at solar metallicity. It is clear that mass (and age) can be determined with better precision on the subgiant branch than on the main sequence or giant branch

evolutionary models, additional obstacles must be considered and overcome. For these evolved stages, stellar tracks and isochrones get very close together as shown in Fig. 7. The dependence of T_{eff} , $\log g$ and $\log(L/L_{\odot})$ on mass along the RGB is approximately 40 K, 0.025 dex and 0.07 dex per $0.1 M_{\odot}$. Also, there is a degeneracy between mass and metallicity at the level of 0.1 dex per $0.1 M_{\odot}$ (see, e.g., Escorza et al. 2017). Therefore, very precise and accurate observations are required. Also, stellar evolutionary models need to predict the T_{eff} scale accurately. Stock et al. (2018) applied a Bayesian implementation of the method to a sample of 372 giant stars, including a subsample of 26 stars with asteroseismic masses to gauge the accuracy of the results in the mass range from 1 to $2.5 M_{\odot}$. The precision found, expressed here as the median mass error for the complete sample, was 8%.

For AGB stars there are further issues. Their very cool atmospheres are dominated by molecules, and in particular the C/O ratio enters as an additional dimension in the problem of determining the stellar parameters (Decin et al. 2012; Van Eck et al. 2017; Shetye et al. 2018) as well as in the stellar evolution models (Weiss and Ferguson 2009; Marigo et al. 2017; Wagstaff et al. 2020). The accurate determination of luminosities is also difficult because different physical effects can trick the observer towards the wrong measurement. For example, high-amplitude pulsations or huge convection cells in the photospheres of stars with extended

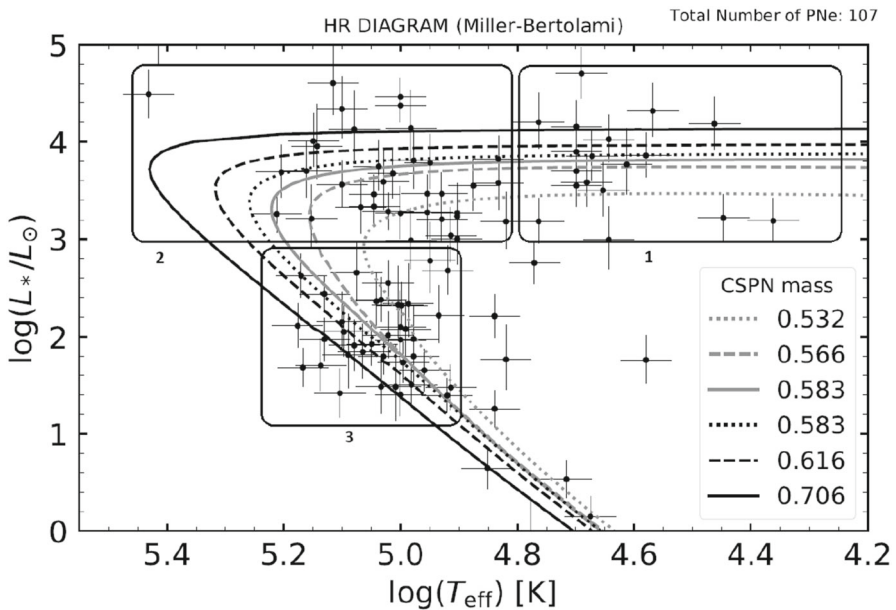


Fig. 8 Location of CSPNe in the HRD from González-Santamaría et al. (2020) overplotted with evolutionary tracks for $Z = 0.01$ models from (Miller Bertolami 2016). Regions indicate early, intermediate, and late evolutionary phases. Image reproduced with permission from González-Santamaría et al. (2020), copyright by the authors

convective envelopes cause big variations in their brightness (Chiavassa et al. 2011; Xu et al. 2019). Moreover, mass loss becomes more significant when stars evolve to lower effective temperatures and higher luminosities and the material that they expel can absorb stellar light making stars appear fainter. Last but not least, stars evolved to giants can be observed at far away distances, but then their parallaxes are small and comparable, in some cases, with the angular diameter of a typical AGB star (Mennesson et al. 2002). The surface brightness fluctuations mentioned before can also trigger photocenter fluctuations that complicate astrometric measurements.

The intrinsic difficulty of mass determination from HRD fitting can to a good extent be circumvented for RGB and early-AGB stars thanks to a combination of asteroseismology (Sect. 6.1.2) and spectroscopic and/or statistical methods trained on stars with asteroseismic measurements (Sects. 4.3 and 4.2). For stars higher on the AGB the situation is more difficult as recourse to asteroseismology is not possible.

HRD fitting for post-AGB and CSPNe stars is problematic both from the point of view of the models and the observations. One of the traditional bottlenecks has been the determination of the CSPNe luminosities, due to the lack of accurate distances. González-Santamaría et al. (2019) have published a catalogue of CSPNe based on *Gaia* DR2 (Gaia Collaboration et al. 2018), including the newly determined luminosities. Figure 8 shows the resulting HRD (González-Santamaría et al. 2020) and includes the evolutionary tracks from Miller Bertolami (2016) for a typical

subsolar metallicity ($Z = 0.01$). It is apparent from the plot that mass estimates can be achieved with precision of the order of 10 to 15% for CSPNe masses in the range $0.5 < M_{\text{CSPN}}/M_{\odot} < 0.8$. The situation worsens for more luminous CSPNe due to crowding of tracks next to the Eddington limit. The main uncertainty in the case of CSPNe masses comes from the debatable accuracy of the models. Many authors claim that binarity is key in the formation of PNe, and we know that at least some systems are formed after a common envelope event (Reindl et al. 2020). Tracks for a CSPN of a given mass greatly differ depending on whether the CSPN is assumed to come from the post-AGB evolution of a single star, or from the diversity of binary formation scenarios (e.g., wind mass transfer, Roche lobe overflow, common envelope evolution, etc.). See Reindl et al. (2020) for an example of this regarding the close binary CSPNe Hen-2 428. Consequently, the choice of the set of models/scenarios adopted for the derivation of the mass of a given CSPN is key for a correct determination of its mass. Other recent mass estimates based on good distance determinations come from CSPNe in open clusters, as presented by Fragkou et al. (2019a, 2019b). Interestingly, these two objects can also be used to constrain the IFMR (Sects. 1.1, 7.1).

5.3 Evolutionary masses for high-mass stars

As discussed in Sect. 5.1, stars are compared to stellar evolution models in the HRD or its cousin, the CMD. The positions of stars in these diagrams are often compared to models by eye and the closest stellar tracks and isochrones then provide the inferred masses and ages, respectively. Estimating best-fitting values and robust uncertainties of mass and age in this way is extremely difficult and subjective. In the following, we focus on high-mass stars.

5.3.1 Mass estimates for early stages

We mentioned above that the quality and quantity of observables influences the accuracy of masses determined by stellar track or isochrone fitting. With the advent of large stellar surveys, more is known about individual stars such that comparisons of observations with models need to be made in higher dimensional parameter spaces than just the HRD or CMD. Such comparisons require sophisticated statistical methods that can (i) match all observables simultaneously to models and (ii) properly propagate uncertainties from the observations to the inferred masses and ages. To this end, various methods have been developed, often within a Bayesian framework, which easily allows one to take prior knowledge into account (e.g., Pont and Eyer 2004; Jørgensen and Lindegren 2005; da Silva et al. 2006; Takeda et al. 2007; Shkedy et al. 2007; van Dyk et al. 2009; Burnett and Binney 2010; Serenelli et al. 2013; Schönrich and Bergemann 2014; Schneider et al. 2014; Valle et al. 2014; Maxted et al. 2015; Bellinger et al. 2016; Lin et al. 2018; Lebreton and Reese 2020). Prior knowledge can comprise information on the mass spectrum of stars (i.e., the stellar initial mass function; IMF) or on the age from, e.g., a host star cluster or a known star formation history. Besides such classical prior information, sophisticated statistical methods also take into account that stars spend

different amounts of time in different parts of the HRD (e.g., Pont and Eyer 2004; Johnston et al. 2019b). For example, observing a high-mass star just before it reaches the terminal-age main-sequence is much more likely than observing it shortly thereafter when it evolves quickly through the HRD on a thermal timescale towards the red (super-)giant branch. Such knowledge can be vital and is usually neglected when comparing stars to models by eye.

A goodness-of-fit test is a key aspect of any statistical method that attempts to determine parameters of a model using some observables. Most statistical methods will deliver best-fitting model parameters without checking them for consistency. The models might in fact not be able to reproduce the observables because they lack certain ingredients. For example in massive stars, the lacking ingredient could be binary star evolution. Binaries are common especially in massive stars and a significant fraction of all O-type stars ($\approx 25\%$) is thought to merge during their life (e.g., Sana et al. 2012). Merger products might have properties (e.g., surface gravity, effective temperature, luminosity, surface chemical abundances and rotational velocities) that cannot be simultaneously explained by any single star model. Attempting to infer the age or mass of a merger product using single star models should, therefore, fail and goodness-of-fit tests are vital to detect such cases. Standard χ^2 hypothesis testing and Bayesian posterior predictive checks have proven to be useful goodness-of-fit tests (Schneider et al. 2014). Such tests are also powerful tools to identify outliers and thereby improve stellar models by singling out stars that defy expectations. However, only few statistical tools (e.g., Bonnsai, Schneider et al. 2014) apply such tests by default to date.

In high-mass stars, one often determines the effective temperature (T_{eff}), surface gravity ($\log g$) and, if the distance to a star is known, also the luminosity ($\log L/L_{\odot}$) by modelling observed spectra with atmosphere codes (Sect. 4.5). Conservative 1σ uncertainties are of order $\Delta T_{\text{eff}} = 1000$ K, $\Delta \log g = 0.1$ and $\Delta \log L/L_{\odot} = 0.1$, and in many cases these quantities are known even better (e.g., Schneider et al. 2018). Assuming these uncertainties, we show in Fig. 9 the precision of the inferred initial masses by either fitting the luminosity and effective temperature or the surface gravity and effective temperature of stars to the single star models of Brott et al. (2011) using the Bayesian tool Bonnsai. Despite the quite large uncertainties, initial masses of stars in the range $5\text{--}40 M_{\odot}$ can be determined to a precision of $5\text{--}15\%$ in the HRD (from luminosity and effective temperature) and $8\text{--}40\%$ in the Kiel diagram (from surface gravity and effective temperature). The precision is better in the former case because the luminosity of a star is a very sensitive function of mass through the mass–luminosity relation and thus has a higher constraining power than gravity. Even when including the surface gravity in the fits alongside luminosity and effective temperature, the precision of the inferred mass does not improve (see, e.g., Fig. 7a in Schneider et al. 2017). The mass–luminosity relation flattens for higher masses and, consequently, the precision with which initial masses of higher mass stars can be determined gets worse. Halving the uncertainties also improves the precision of the inferred initial masses by roughly a factor of two.

Inferring masses is always closely connected to inferring ages of stars because models are degenerate to some extent in these two parameters. Different

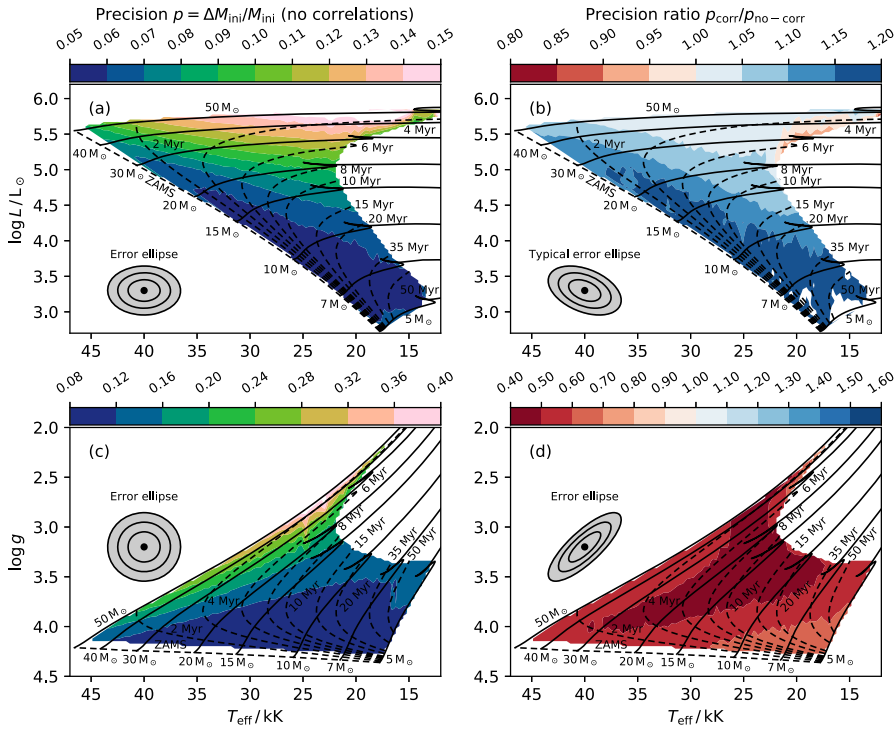


Fig. 9 Precision $p = \Delta M_{\text{ini}}/M_{\text{ini}}$ and precision ratio $p_{\text{corr}}/p_{\text{no-corr}}$ of inferred initial masses M_{ini} (1σ uncertainties ΔM_{ini}) of high-mass main-sequence stars from observations of luminosity and effective temperature (**a, b**) and surface gravity and effective temperature (**c, d**). In **a** and **c** it is assumed that the observables are uncorrelated while a typical correlation between the observables, as indicated by the error ellipses with 1σ , 2σ and 3σ contours, is assumed in **b** and **d**. The assumed uncertainties of luminosity, effective temperature and surface gravity are 0.1 dex, 1000 K and 0.1 dex, respectively. The precision scales almost linearly with the assumed uncertainties of the observables, i.e., for uncertainties of luminosity, effective temperature and surface gravity of 0.05 dex, 500 K and 0.05 dex, respectively, the precision halves. The stellar tracks and isochrones are from non-rotating, solar metallicity models of Brott et al. (2011). Image reproduced with permission from Schneider et al. (2017), copyright by ESO

combinations of mass and age can give similar observables: the initial mass can strongly co-vary with the stellar age. Usually, the correlation is such that larger masses co-vary with younger ages because more massive stars have shorter lifetimes. Braking this degeneracy with independent information, e.g., from other stars, has the potential to improve the precision with which masses can be determined.

Also the observables can be correlated and, in high-mass stars, luminosity and effective temperature, and also surface gravity and effective temperature usually co-vary. In principle, the former is because of the definition of effective temperature ($L = 4\pi R^2 \sigma T_{\text{eff}}^4$ with R the stellar radius and σ the Stefan–Boltzmann constant) and the latter is true when deriving gravity and effective temperature from fitting atmosphere models to observed spectra because both properties are degenerate and

affect many spectral lines in similar ways. In high-mass stars, a larger surface gravity requires a hotter effective temperature to fit a spectrum similarly well. Such correlations will affect the precision with which initial masses and other stellar parameters can be determined as illustrated in Fig. 9. In the HRD, the precision can worsen by up to 20% while it improves by 30–60% in the Kiel diagram. Also the most-likely initial mass is affected by correlations: in the HRD, the most likely mass might be lower by up to 0.18σ but does on average not change much; in the Kiel diagram, it is larger by up to 0.8σ and is underestimated by on average 0.5σ when neglecting correlations (Schneider et al. 2017). In conclusion, correlations are important when trying to infer precise initial masses and neglecting them can introduce biases.

So far, we have only considered the precision with which initial masses can be determined. Any statistical method is of course only as good as the underlying models and the quality of the observables. Such accuracies are currently not well constrained. They are given by the systematic uncertainties in the observables (Sect. 4.2), the statistical method (some of which has been discussed above) and the stellar models. For high-mass stars, the physical effects mentioned in Sect. 5.1, are particularly important. It is still not known with much confidence how much core overshooting is needed to explain high-mass main-sequence stars (e.g., Castro et al. 2014; Stancliffe et al. 2015), and neither is additional interior mixing by rotation or other phenomena understood (Johnston et al. 2019b; Pedersen 2020). TESS photometry of Galactic and LMC OB-type stars revealed the ubiquitous occurrence of internal gravity waves (Bowman et al. 2019a), the consequences of which in terms of chemical mixing (Rogers and McElwaine 2017) have not yet been included standardly in evolutionary models. Since such nonradial wave mixing occurs at the bottom of the radiative envelope, in the boundary layers of the convective core, it may affect the core masses m_{cc} appreciably (see Sect. 6.3). Apart from these, there are additional significant uncertainties in high-mass stellar models that influence the systematic uncertainties. Key effects are due to binary stars and binary mass exchange, stellar winds and magnetic fields. More information on recent advances on models of high-mass stars can be found in the reviews by Langer (2012) and Maeder and Meynet (2012).

For improved mass determinations of high-mass stars from atmospheric parameters as described here, the luminosity is key because it constrains masses the strongest for given theoretical models. More precise and more reliable distances from *Gaia* will greatly help to obtain better luminosities of massive stars in the Milky Way and thus lead to more precise mass estimates. Similarly, higher resolution and higher S/N spectra will help narrow down uncertainties of the atmospheric parameters of stars and thereby those of the inferred masses. While the properties of stars are known to ever increasing precision thanks to observational advances and new instruments, we have to better understand the systematic uncertainties of the whole mass-determination process, from the spectral to the stellar modelling to avoid a situation in which we are dominated by systematic uncertainties that hamper our ability to further understanding of stars.

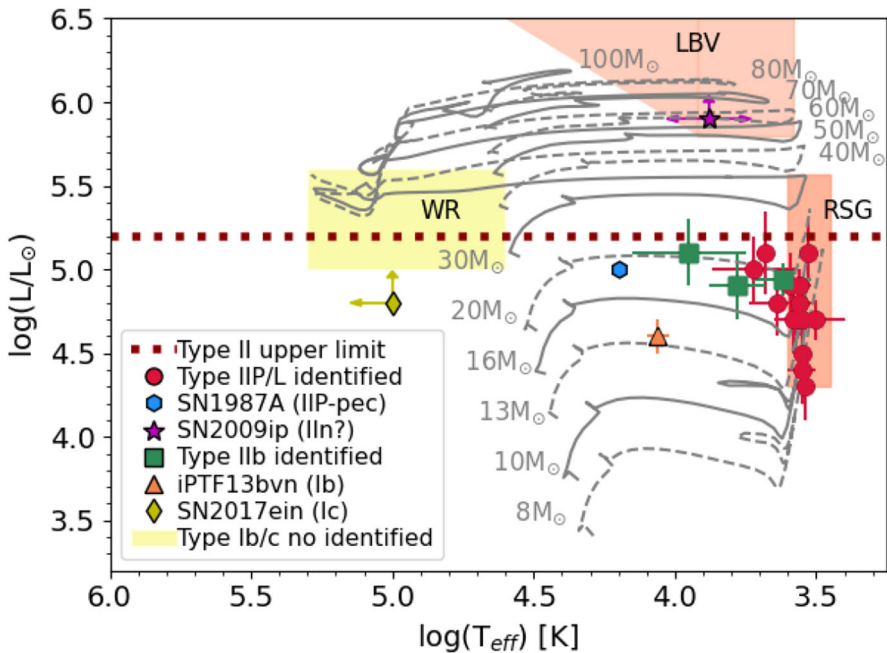


Fig. 10 HRD showing the temperature and luminosity of the identified progenitor stars and upper limits of the main type of SNe. For comparison, model stellar evolutionary tracks from Eldridge and Tout (2004) are also illustrated

5.3.2 Mass estimates for core-collapse supernovae progenitors

High-mass stars end their lives as core-collapse supernovae (CCSNe). These objects present a large observational heterogeneity. A key aspect of the study of CCSNe and their progenitors is to establish a link between the different classes of CCSNe and the underlying properties of the exploding star. In this context, the stellar mass at explosion, and the connection to the initial mass, is the most fundamental property that needs to be determined. Understanding this relation is necessary for constraining stellar evolution models of high-mass stars.

The determination of masses for CCSNe progenitors is also based on matching stellar models in an HRD. It has the added complication that the identification of progenitors has to be carried out in archival, pre-explosion images and it relies on the positional coincidence between the candidate precursor and the SN transient. This requires high spatial resolution and very accurate astrometry because, at the typical distance of the targets (> 30 Mpc), source confusion becomes an issue. Therefore, the chance of misidentification with foreground sources or associated companion stars is high. To date, about 20 CCSNe progenitors have been identified, the majority of them RSGs linked to type-IIP SNe. For CCSNe types other than type-IIP, there are just a handful of tentative detections. Identified progenitors are shown in a theoretical HRD in Fig. 10.

For RSGs progenitors in particular, once photometry from the archival data is consolidated, multiband photometry is used to determine physical parameters. It can be done by comparison with other observed and well studied RSGs, or by direct comparison with synthetic photometry from stellar evolution calculations (Van Dyk 2017). Either way this is done, the final step in the mass estimation is always by fitting the physical parameters to stellar evolutionary models. Figure 10 illustrates this. Typical uncertainties in mass are about 2 to 3 M_{\odot} . It has to be kept in mind, however, that uncertainties in stellar models (see Sect. 5.1) are particularly important for high-mass stars and this may have a strong impact on the estimated masses, not just the uncertainty. To complicate matters more, Farrell et al. (2020) has carried out a parametric study showing that the luminosity of RSGs is determined by the mass of their helium core, and that a strong degeneracy exists between the stellar luminosity and the hydrogen envelope mass. If confirmed, this would imply that estimating the mass of the progenitor would require an independent determination of the mass of the hydrogen envelope by modelling of the SN light curve. Adding the envelope mass to the helium core mass would yield the progenitor mass at the moment of explosion.

The degeneracy between hydrogen envelope mass and luminosity is avoided by nature if the integrated mass loss is small, as recently suggested by Beasor et al. (2020) based on observations in clusters NGC 2004 and RSGC1. If such is the case then, at least for single progenitors, HRD fitting is a promising avenue for determination of the progenitor mass at the moment of explosion and also for determination of the initial stellar mass.

Unfortunately, and despite a theoretical and observational effort, the overall number of identified SN progenitors is still too small to draw conclusions about the relation between initial stellar mass and the final explosion event. This includes the photometric and spectroscopic characteristics. Stellar models also need to be improved and also, crucially, empirical estimates of integrated mass loss are strongly needed.

Even for type-IIP, the SN type with best studied progenitors, stellar models predict a larger mass range of stars exploding in the red supergiant (RSG) phase than what is inferred from observations according to some studies (see, e.g., Smartt 2015; Van Dyk 2017, but also Davies and Beasor 2020). As a possible solution, it has been proposed that RSG stars above a certain mass threshold, about $18 M_{\odot}$, collapse directly to black holes (Sukhbold et al. 2016). Masses of CCSNe progenitors are then not only needed to understand the origin of the different CCSNe types, but also to be able to determine which remnant is formed by the collapse. This has very important consequences such as the formation of stellar mass black holes. Finally, this also has strong implications not just for stellar physics, but also for related fields such as chemical evolution of galaxies through its impact on the enrichment of the interstellar medium.

6 Asteroseismic masses

The space asteroseismology era implied a revolution for many topics in stellar astrophysics, notably for the study of stellar interiors. Indeed, the past CoRoT (Auvergne et al. 2009), *Kepler* (Koch et al. 2010), K2 (Howell et al. 2014), and currently operational TESS (Ricker et al. 2016) and BRITE (Weiss et al. 2014) space missions turned the topic of stellar interiors into an observational science. Tens of thousands of stars have meanwhile been observed and interpreted asteroseismically, the majority of which are low-mass stars.

Extensive reviews on asteroseismic observables derived from uninterrupted high-precision (at the level of parts-per-million or ppm) long-duration (from weeks to years) space photometry for low-mass stars of various evolutionary stages are available in Chaplin and Miglio (2013), Hekker and Christensen-Dalsgaard (2017) and García and Ballot (2019), to which we refer to details. Here, we limit to the aspect of asteroseismology that results in stellar masses with high precision. There is a notable dearth of asteroseismic mass estimation for high-mass stars because such targets were avoided in the *Kepler* field-of-view, while the time bases of the other space photometry time-series are too short to achieve high precision for this parameter. K2 and the still operational TESS missions have remedied this (Bursiens et al. 2019; Pedersen et al. 2019; Bowman et al. 2019a).

In contrast to some of the (quasi) model-independent derivations of the interior rotation of stars (cf. Aerts et al. 2019, for a summary), asteroseismic mass estimation is model dependent. The level of this model dependence is quite different for stars of various masses. Low-mass stars on the main sequence and sub-giant branch have a solar-like oscillation power spectrum dominated by pressure modes, or p-modes. Such solar-type stars have a convective envelope at birth, which implies they become slow rotators due to magnetic braking. For such slow rotators with solar-type structure, we can rely on the theory of nonradial oscillations for spherical stars and treat rotation as a small perturbation to the equilibrium structure, as done in helioseismology. In such circumstances, we use physical ingredients for the stellar interior similar to those occurring in the Sun when making asteroseismic inferences.

Intermediate- and high-mass stars, on the other hand, have essentially opposite structure during the core-hydrogen burning phase, i.e., a convective core and a radiative envelope, where the latter has a very thin outer convective envelope for $M < 2M_{\odot}$. Their interior physics is, therefore, prone to larger uncertainty, as physical ingredients that do not occur or are of less importance than in solar-type stars are prominent for their structure. Notably, such stars tend to rotate fast as they do not undergo magnetic braking in absence of a convective envelope. Moreover, they are subject to chemical mixing processes that have far more impact than in low-mass stars. Examples are convective (core) overshooting and element transport in the radiatively stratified envelope due to rotational mixing, wave mixing, microscopic atomic diffusion (including radiative levitation), etc. Without asteroseismic data, such phenomena can essentially only be evaluated from surface abundances, which have large uncertainties and hence limited probing power.

Chemical element transport in stellar interiors of intermediate- and high-mass stars thus remained largely uncalibrated prior to space asteroseismology. This implies quite large uncertainties on the stellar properties, among which mass, radius and age, particularly for high-mass stars (e.g., Martins and Palacios 2013, Fig. 7).

Space asteroseismology now allows us to make inferences about some of the critical element transport phenomena for stars of almost all masses. In this section, we discuss how such inferences can be achieved from asteroseismic modelling of detected and identified nonradial oscillation modes. An extensive review of how such inferences may lead to quantitative estimation of various properties of the stellar interior is available in Aerts (2021), to which we refer for more details that have to be omitted here.

6.1 Global asteroseismology of low-mass stars

6.1.1 Scaling relations

A large fraction of stars with asteroseismic measurements are solar-like oscillators, i.e., stars in which the mechanism responsible for stellar oscillations is the same as in the Sun. Near-surface turbulent convection excites stochastically, and also damps, stellar oscillations. The dominant restoring force for such oscillations is the pressure gradient; hence they are called pressure modes, or p modes in brief. The excited modes are characterized by the radial overtone n , the number of nodes of the eigenfunctions in the radial direction, and angular degree ℓ which is the number of surface nodal lines.⁷ Solar-like oscillators comprise main-sequence stars with $T_{\text{eff}} \lesssim 6500\text{K}$, subgiants and red giant stars, including first ascent RGBs, red clump and early AGB stars. Main-sequence K stars and cooler should also present solar-like oscillations, but amplitudes become too small so that at present no meaningful detections are available.

The global properties of the oscillation spectrum of solar-like pulsators are characterized by two quantities, the average large-frequency separation $\Delta\nu$ and the frequency of maximum power ν_{max} . The radial modes have $\ell = 0$ and correspond to pure acoustic waves. For these modes, the difference $\Delta\nu_n = \nu_{n,0} - \nu_{n-1,0}$ is to first-order constant, provided n is sufficiently large. This is expressed as the asymptotic relation of p-modes,

$$\nu_{n,0} = \Delta\nu(n + \varepsilon), \quad (6)$$

where $\Delta\nu$ is known as the large frequency separation and it is the inverse of the travel time it takes sound to cross the star (Duvall 1982; Aerts et al. 2010), i.e.,

⁷ In detail, (n, ℓ) determines a multiplet of $2\ell + 1$ modes that are degenerate in frequency for spherical stars. When the symmetry is broken, e.g., by rotation, the different components of the multiplet show up in the oscillation spectrum, with each component identified by the azimuthal number $m = -\ell, -\ell + 1, \dots, \ell - 1, \ell$.

$$\Delta\nu = \left[2 \int \frac{dr}{c} \right]^{-1}, \quad (7)$$

and ε slowly varies with the evolution of the star. This dynamical timescale, in turn, scales as the square root of the mean stellar density ρ , i.e., $\Delta\nu \propto \sqrt{\rho} \propto \sqrt{M/R^3}$ (Kjeldsen and Bedding 1995; Belkacem et al. 2013). Observationally, $\Delta\nu$ can be searched for as a periodic feature appearing in the power spectrum, and this makes it possible to measure it even if individual frequencies cannot be determined reliably. The second distinctive feature of solar-like oscillators relates to the amplitude of the modes, or distribution of power, as a function of frequency, which results from the balance between excitation and damping. For solar-like oscillators it has a well-defined maximum at the so-called frequency of maximum power, ν_{\max} , that scales with the surface gravity and T_{eff} of the star as $\nu_{\max} \propto g/\sqrt{T_{\text{eff}}} = GM/(R^2\sqrt{T_{\text{eff}}})$ (Christensen-Dalsgaard and Frandsen 1983; Kjeldsen and Bedding 1995; Belkacem et al. 2011).

The relations between $\Delta\nu$ and ν_{\max} and global stellar properties can be converted into the so-called scaling relations using the Sun as an anchor point as follows:

$$\nu_{\max} \simeq \nu_{\max,\odot} \frac{g}{g_{\odot}} \sqrt{\frac{T_{\text{eff},\odot}}{T_{\text{eff}}}} \quad (8)$$

$$\Delta\nu_{\text{scl}} \simeq \Delta\nu_{\odot} \sqrt{\frac{\rho}{\rho_{\odot}}}, \quad (9)$$

where $\Delta\nu_{\text{scl}}$ denotes that the large-frequency separation is computed directly from the mean stellar density. Other anchor points that define reference $\Delta\nu$ and ν_{\max} values are also possible. The stellar mass can be readily determined from global asteroseismic properties using the scaling relations, provided a T_{eff} measurement is also available as follows:

$$M/M_{\odot} \simeq \left(\frac{\nu_{\max}}{\nu_{\max,\odot}} \right)^3 \left(\frac{\Delta\nu_{\text{scl}}}{\Delta\nu_{\odot}} \right)^{-4} \left(\frac{T_{\text{eff}}}{T_{\text{eff},\odot}} \right)^{3/2}. \quad (10)$$

This relation provides a model independent mass determination. Its accuracy is determined by that of the scaling relations.

6.1.2 Grid-based modelling

A more powerful approach is possible using grids of stellar evolution models, a technique known as grid-based modelling (GBM). Equations 8 and 9 allow for adding global seismic quantities to stellar evolution tracks. This opens the possibility of using additional information, most importantly the metallicity $[\text{Fe}/\text{H}]$, to determine more refined stellar masses and also ages. It also has the important advantage of accounting for physical correlations between observable quantities that are the result of realistic stellar evolution models and which are absent in the pure scaling mass determination offered by Eq. 10. Finally, using stellar models allows

for the possibility of dropping Eq. 9 altogether. This is possible when the structure of each stellar model in the grid is used to compute the theoretical spectrum of radial oscillations. In this case, the set of radial frequencies is used to compute $\Delta\nu$ directly from stellar models (e.g., as described in White et al. 2011), without relying on the scaling relation (Eq. 9). The difference between $\Delta\nu$ computed from radial modes and $\Delta\nu_{\text{scl}}$ is a function of the stellar mass, T_{eff} and $[\text{Fe}/\text{H}]$ and the evolutionary stage, and it is always smaller than a few per cent. However, as the stellar mass depends approximately on the fourth power of the large-frequency separation, this choice has a relevant impact on the accuracy of mass determinations that is larger than typical uncertainties of the method.

The use of $\Delta\nu$ computed from stellar models should always be preferred to that of $\Delta\nu_{\text{scl}}$. The caveat in this case is that stellar models do not reliably reproduce the structure of the outermost layers of stars and give rise to the so-called surface effect that is related to the properties of turbulent pressure and the non-adiabaticity of the gas. In the Sun, this produces a 0.9% mismatch between $\Delta\nu$ computed from a solar model and the observed $\Delta\nu$. This is used to rescale $\Delta\nu$ in the grid of models by Serenelli et al. (2017a). Detailed asteroseismology (Sect. 6.2) for main sequence and subgiants suggests that the impact of surface corrections on $\Delta\nu$ for main sequence and subgiant stars is less than 2%, implying that a systematic uncertainty of $\lesssim 1\%$ in the calculation of $\Delta\nu$ remains after such a solar calibration. More work remains to be done, and progress in theoretical models of near-surface convection and non-adiabatic frequency calculations are paving the way towards a more detailed and physically based assessment of surface effects (Rosenthal et al. 1999; Ball and Gizon 2014; Sonoi et al. 2015; Jørgensen et al. 2019).

In analogy with the more traditional stellar modelling by isochrone fitting techniques (Sect. 5.3), several asteroseismic GBM pipelines have been developed relying on Monte Carlo (Stello et al. 2009; Basu et al. 2012; Hekker and Ball 2014) and/or Bayesian methods (Kallinger et al. 2010; Gruberbauer et al. 2012; Silva Aguirre et al. 2015; Serenelli et al. 2017a; Rodrigues et al. 2017; Lebreton and Reese 2020). The main difference with isochrone fitting techniques is that the likelihood function is computed using T_{eff} , $[\text{Fe}/\text{H}]$, $\Delta\nu$ and ν_{max} in this case. GBM methods have been applied to rather large samples of stars observed by CoRoT and *Kepler*, in combination with spectroscopic surveys (see, e.g., Rodrigues et al. 2014; Serenelli et al. 2017a; Pinsonneault et al. 2018; Valentini et al. 2019).

The precision in asteroseismic masses based on global asteroseismology of low-mass stars depends crucially on the quality of the $\Delta\nu$ and ν_{max} determinations. The *Kepler* mission has provided by far the best quality data, but even for this highest-quality space photometry the results depend mainly on the length of the light curves, which vary from 3 months (one quarter) up to 4 years (16 quarters). In view of this heterogeneity, we quote here median errors obtained in studies for large samples of stars and refer the reader to the papers for more detailed discussions.

The first large-scale GBM work on *Kepler* dwarfs and subgiants is that of Chaplin et al. (2014) and comprises more than 500 stars. At that time, no spectroscopy was available for most of them, so a fixed $[\text{Fe}/\text{H}] = -0.2$ dex value with a generous 0.3 dex error was adopted. Data only from the ten first months of *Kepler* observations were used to determine ν_{max} and $\Delta\nu$. The median mass

uncertainty reported was 10%. The update to this work is the APOKASC catalogue on *Kepler* dwarfs and subgiants (Serenelli et al. 2017a). It relies upon APOGEE spectroscopic results for the whole sample, and uses the full length of *Kepler* observations. The improved data lead to a median precision of 4% in mass determination for the whole sample. For giant stars, similar efforts by APOKASC, combining APOGEE spectroscopy and *Kepler* observations lead to a median precision of 4% for a sample of 3500 RGB stars and 5% for a sample of more than 2500 red clump and early AGB stars (Pinsonneault et al. 2018, Serenelli et al., in preparation). The precision depends almost completely on the errors of the input data and not on the numerical details of each GBM pipeline. Results from several GBM pipelines on the same data lead to very similar results regarding the precision of mass estimates (Serenelli et al. 2017a, Serenelli et al. in prep.)

GBM relies on stellar models and so mass determinations are prone to uncertainties in the models. Some attempts to capture systematic uncertainties from the physics adopted in the models have been done, but focused on age determinations which are more sensitive to choices for the internal physics than the inferred masses (Valle et al. 2015). The procedure that has been applied often is to take GBM masses determined with different GBM pipelines, which use different grids of stellar models and consider the dispersion in the results of these GBMs as a measure of systematic errors originating from stellar evolution. When considering this procedure, results from GBMs using $\Delta\nu$ computed from radial modes need to be considered. In this case, the median dispersion found for *Kepler* dwarfs and subgiants is 4% (see Serenelli et al. 2017a for a detailed discussion). For the APOKASC RGB stars, pipelines using $\Delta\nu$ computed from frequencies lead to median differences smaller than 2%, whereas for red clump and early AGB stars this is 5% (Pinsonneault et al. 2018, Serenelli et al. in prep.).

A second source of uncertainties related to stellar models originates from the use of different stellar evolution codes, which might lead to slightly different internal structures due to numerical differences even if the same physics is used. Silva Aguirre et al. (2020) and Christensen-Dalsgaard et al. (2020) have carried out a detailed study for RGB stars, where several stellar evolution codes were used to compute sets of calibrated RGB models. Results show that numerical details in the stellar evolution codes lead to differences in the theoretical oscillation frequencies that are larger than the typical observational uncertainties. However, the calculation of $\Delta\nu$ using radial modes is much more robust and, for all cases considered, fractional $\Delta\nu$ differences between codes are $\delta(\Delta\nu)/\Delta\nu < 0.002$. This leads to a fractional mass uncertainty $\delta M/M < 0.008$ in GBM studies.

6.1.3 Accuracy tests

Fundamental tests of the accuracy of mass determinations of low-mass stars with global asteroseismology can only be done through model independent mass determinations, i.e., dynamical masses. But in a more extended sense, techniques that allow us to determine stellar radii (interferometric or parallaxic) can also be used to test the accuracy of global asteroseismology. Although these are not direct

tests of mass determinations, the results can be used to gain understanding of the accuracy of global asteroseismology.

Several studies have discussed the accuracy of the scaling relations, both in terms of the validity of the Sun as a universal anchor point and in terms of the functional relation between stellar quantities and v_{\max} and $\Delta\nu$ (see Hekker 2020 for a recent review). However, the $\Delta\nu_{\text{sc1}}$ should not be used for mass determinations as described in the previous section. When relying on $\Delta\nu$ computed from models, the systematic uncertainty linked with surface effects is estimated to be around 1% after the solar correction is applied to models in the grid. For v_{\max} , the only possibility is to rely on the scaling relation as it cannot be computed from stellar models. Earlier, Coelho et al. (2015) established the validity of the v_{\max} scaling relation to about 1.5% for main-sequence and subgiant stars. More recently, Pinsonneault et al. (2018) used the open cluster NGC 6791 and NGC 6819 observed with *Kepler* to calibrate this relation. Eclipsing binaries close to the clusters turn-off were used to fix the mass scales of isochrones and subsequently used these to infer the masses of RGB stars from detailed asteroseismic studies (Handberg et al. 2017). From this, an ‘effective’ $v_{\max,\odot}$ is determined, not from the solar oscillation spectrum, but by calibrating GBM results to match the mass scales in these clusters. This calibration has a 0.6% uncertainty and a systematic difference from the true solar v_{\max} of only 0.5%.

Using *Gaia* DR2, Zinn et al. (2019) have determined the radii for about 300 dwarf and subgiant stars and about 3600 RGB stars observed with *Kepler* and having APOGEE spectroscopy. The authors compared the results with the asteroseismic radii determined in Pinsonneault et al. (2018). The results show that the asteroseismic radius scale is at the level of those from parallaxes at the -2.1% level for dwarfs and subgiants and $+1.7\%$ level for RGB stars with $R < 30 R_{\odot}$. While this is not a direct test of asteroseismic masses, the dependence of the radius on asteroseismic quantities is approximately $R \propto v_{\max}/\Delta\nu^2$. Linear propagation of errors leads to uncertainties for the radii that are typically a factor two to three lower than for the masses. Inverting the argument, a sensible estimate is that these sources of systematic uncertainties lead to a factor of about two to three larger systematic uncertainty for the asteroseismic mass scale determined from global asteroseismology. Analogous tests with *Gaia* DR2 data and results have been obtained for dwarfs (Sahlholdt and Silva Aguirre 2018) and red clump stars (Hall et al. 2019).

Several results are available on dynamical masses for RGB stars in double-lined EBs. Results presented in the most extensive work in which ten systems were analyzed Gaulme et al. (2016) showed a tendency of asteroseismic results to overestimate the dynamical mass with an average of 15%. However, Brogaard et al. (2018) reanalyzed three of these systems and found agreement of the two mass scales to the level of 4% with no systematic effect and highlighted that potential problems both in asteroseismic modelling and in the determination of dynamical masses might be affecting other stars in Gaulme et al. (2016). Moreover, a new analysis of the same stars and newly discovered *Kepler* red giants in EBs (Benbakoura et al. in prep.) has found that asteroseismic masses determined with GBM methods (Rodrigues et al. 2017) agree to within 5%, in line with the simulation study by Sekaran et al. (2019).

Taking into consideration all these results, it is estimated that the global asteroseismology mass scale for low-mass stars from solar-like oscillations is accurate to within 5%.

6.2 Detailed frequency modelling of solar-type stars

The grid-based modelling technique presented in Sect. 6.1.2 relies only on the two global asteroseismic quantities $\Delta\nu$ and ν_{\max} , allowing us to infer their masses. Much more information about the detailed structure of pulsating stars is contained in their individual oscillation-mode frequencies. Detailed modelling of the frequency spectrum thus allows us to further constrain their evolutionary stage, the relevant physical processes at play and ultimately the stellar properties (including mass, see, e.g., Christensen-Dalsgaard et al. 2011; Silva Aguirre et al. 2013; Lebreton and Goupil 2014).

Reproducing the individual frequencies of low-mass solar-type main-sequence stars and subgiants is one of the great achievements of space asteroseismology. The overall technique to fit the observations is similar for dwarfs and subgiants. However, the strategies to find the optimal solutions vary due to differences in the physical nature of the observed oscillations as these beautifully reveal the evolutionary stage of the targets. In the following sections we review the most common approaches employed to analyse these stars and the level of precision in mass that can be expected in each case.

6.2.1 Solar-type dwarfs

Low-mass stars of masses not too different from the one of the Sun present a rich frequency spectrum. Modes of angular degree $\ell = 0, 1, 2$ can now routinely be identified for such objects (and in the best cases also $\ell = 3$, see Metcalfe et al. (2012) for the case of 16 Cyg A and B). At present, two large compilations of observed frequencies and corresponding derived stellar properties exist for the current samples containing a total of almost 100 low-mass main-sequence oscillators. These are dubbed the Kages (Silva Aguirre et al. 2015; Davies et al. 2016) and the LEGACY (Lund et al. 2017; Silva Aguirre et al. 2017) samples and comprise the best asteroseismic data available for these type of stars until the advent of the future PLATO mission (Rauer et al. 2014).

The general strategy for fitting main-sequence oscillators is to use a stellar evolution code to produce a 1D stellar structure model in hydrostatic equilibrium at the appropriate evolutionary stage, calculate its theoretical oscillation frequencies using an adiabatic oscillation code and determine the goodness of the fit by comparing the observed frequencies (or a combination of them) to the predicted ones by means of a chosen merit function. There are a number of pipelines that have optimised this procedure in various manners, including χ^2 minimisation, MCMC, or Bayesian analyses based on pre-computed grids of models (e.g., Silva Aguirre et al. 2015; Rendle et al. 2019), as well as on-the-fly optimization using Levenberg–Marquardt, downhill simplex, or genetic algorithms (Miglio and Montalbán 2005;

Metcalfe et al. 2009; Lebreton and Goupil 2014; Appourchaux et al. 2015). A summary of some of the most employed pipelines for low-mass star asteroseismology can be found in Section 3 of Silva Aguirre et al. (2017).

Irrespective of the chosen minimisation method, each pipeline must also select the quantities involving individual frequencies that will be reproduced. The most straightforward case is direct comparison between the theoretically computed frequencies and the corresponding observed ones. However, as already highlighted above, the frequencies of the oscillation modes predicted by 1D stellar structure models carry the inadequacies of the descriptions for the outermost layers for all the stars where convection dominates the transport of energy in the outer envelope. The simplifications of this inherently hydrodynamical process, often represented by the mixing-length theory, produce a frequency-dependent shift that must be corrected for. The modelling pipelines choose one of several available prescriptions to correct the theoretical frequencies for surface effects prior to matching them to the observed ones.

A slightly different approach consists in matching combinations of individual p-mode frequencies, as it has been shown that some combinations can effectively suppress the influence of the poorly modelled outer stellar layers and allow for a direct comparison between observations and theoretical oscillations (see, e.g., Roxburgh and Vorontsov 2003; Cunha and Metcalfe 2007; Oti Floranes et al. 2005; Silva Aguirre et al. 2011). These combinations do introduce strong correlations that must be properly taken into account to avoid overfitting the data (Deheuvels et al. 2016; Roxburgh 2018).

For the Kages and LEGACY samples, individual pipelines fitting individual frequencies (or combinations thereof) together with spectroscopic effective temperatures and metallicities were able to determine stellar masses for these stars to a precision of $\sim 3\text{--}4\%$. This precision is slightly dependent on the chosen quantity to be reproduced (frequencies or frequency combinations), as well as the optimization algorithm and the sampling of the stellar evolution models.

6.2.2 Subgiant stars

Once solar-type stars finish central hydrogen burning and move towards the red giant branch, their interior structure results in the coupling of buoyancy-driven gravity-modes (g-modes) propagating in the stellar core to the p modes excited in the convective layers (Aizenman et al. 1977; Deheuvels and Michel 2011). The observational imprint of these modes of mixed character in subgiant stars leads to the existence of avoided crossing, which are deviations in the otherwise approximately regular spacing in frequency of the p modes. Non-radial modes displaying avoided crossings change their frequency rapidly during the stellar evolution. Correctly reproducing the oscillation spectrum of subgiants has tremendous diagnostic potential for their interior structure and physical properties (see, e.g., Bedding 2011; Beck et al. 2011, 2012; Christensen-Dalsgaard 2014; Deheuvels et al. 2014; Beck et al. 2011, and references therein).

The rapid evolution of mixed modes poses a challenge for fitting algorithms suited for low-mass main-sequence stars due to the much higher time resolution

Table 10 Benchmark stars with asteroseismic mass determination from detailed frequency modelling and interferometric data

Object	[Fe/H]	T_{eff} (K)	R (R_{\odot})	M (M_{\odot})	Based on	Ref.
<i>Solar-type</i>						
α Cen A	0.26 ± 0.08	5795 ± 19	1.2234 ± 0.0053	1.1055 ± 0.0039	Int+Dyn	1,2,3
α Cen B	0.22 ± 0.10	5231 ± 21	0.8632 ± 0.0037	0.9373 ± 0.0033	Int+Dyn	1,2,3
18 Sco	0.052 ± 0.005	5817 ± 4	1.010 ± 0.009	1.03 ± 0.03	Ast+Int	4
16 Cyg A	0.096 ± 0.026	5839 ± 42	1.22 ± 0.02	1.07 ± 0.02	Ast+Int	5,6,7
16 Cyg B	0.052 ± 0.021	5809 ± 39	1.12 ± 0.02	1.05 ± 0.02	Ast+Int	5,6,7
<i>F-type</i>						
θ Cyg	-0.02 ± 0.06	6749 ± 44	1.48 ± 0.02	1.346 ± 0.038	Ast+Int	6,8
<i>Subgiant</i>						
μ Her	0.280 ± 0.050	5562 ± 35	1.73 ± 0.02	1.11 ± 0.01	Ast+Int	9,10
HR 7322	-0.23 ± 0.04	6350 ± 90	2.00 ± 0.03	1.200 ± 0.006	Ast+Int	11

References: (1) Jofré et al. (2014); (2) Kervella et al. (2017); (3) Kervella et al. (2016); (4) Bazot et al. (2018); (5) Ramírez et al. (2009); (6) White et al. (2013); (7) Bazot (2020); (8) Guzik et al. (2016); (9) Jofré et al. (2015); (10) Grundahl et al. (2017); (11) Stokholm et al. (2019)

required when computing stellar models. Nevertheless, initial results in individual targets observed with ground-based telescopes and by the *Kepler* and TESS missions suggest that asteroseismic mass determinations in subgiant stars are feasible at the 5% level and below (Grundahl et al. 2017; Stokholm et al. 2019; Huber et al. 2019; Chaplin et al. 2020). This is particularly encouraging in light of the observations being collected by the TESS satellite, as subgiants comprise the bulk of its targets for which asteroseismic detections are expected (Schofield et al. 2019).

6.2.3 Accuracy of the obtained masses

Testing the accuracy of asteroseismically determined masses from individual frequency fitting in low-mass solar-type stars and subgiants has proven to be a difficult endeavour due to the lack of independent empirical measurements of stellar masses for pulsating stars. An alternative to partially circumvent this problem is to test the accuracy of other fundamental properties which have independent measurements (such as radius) and assume that stellar evolution models predict the correct mass–radius relation for stars of a given temperature, luminosity and composition. Examples of this approach are targets observed with interferometry, where the radius obtained from asteroseismic fitting is capable of reproducing the interferometric one (e.g., Grundahl et al. 2017; Bazot et al. 2018; Stokholm et al. 2019). Similarly, distances from the *Gaia* mission (Gaia Collaboration et al. 2016a) have been compared to distances predicted from asteroseismic radius, showing an excellent level of agreement (De Ridder et al. 2016; Silva Aguirre et al. 2017). Table 10 presents results for benchmark stars for which asteroseismic data can be

combined with interferometry, which provides independent constraint on radius, and thus leads to the most accurate asteroseismic mass determinations. α Cen is an additional benchmark for which the masses reported here are determined dynamically, and thus offers a further, independent benchmark for asteroseismic masses (Nsamba et al. 2018).

As already implied above, the accuracy of asteroseismically determined stellar properties will ultimately depend on the reliability of stellar evolution models. The following section gives an example of this for low-mass stars, focusing on the inclusion of microscopic atomic diffusion:

6.2.4 Uncertainties in seismic modelling due to atomic diffusion and initial helium abundance

Understanding the detailed physical processes that take place in stellar interiors is essential towards precise characterisation of stellar properties such as radius, mass and age. The inclusion of atomic diffusion when modelling the Sun has been shown to be a vital process if its mass and age are to be accurately reproduced (e.g., Bahcall et al. 2001). This implies that atomic diffusion is a vital chemical transport process in the radiative regions of solar-type stars. In general, element transport due to microscopic atomic diffusion is connected with various effects stemming from temperature and concentration gradients, gravitational settling and radiative levitation (Michaud et al. 2015). Modelling of low-mass stars often ignores radiative levitation, although it should be included for stars with a mass above $1.1 M_{\odot}$ (Deal et al. 2018).

The study of the impact of atomic diffusion cannot be seen disjoint from the choice of the chemical mixture inside the star. Indeed, various metal mixtures are used when modelling stars (e.g., Asplund et al. 2009; Grevesse and Sauval 1998). Differences in the absolute element abundances occur when different solar mixtures are compared. This is a potential source of systematic uncertainties on derived stellar masses in general, and particularly so when assessing the importance (or not) of atomic diffusion.

Nsamba et al. (2018) studied the effects of atomic diffusion (without radiative levitation) and of the chemical mixture on asteroseismic modelling of low-mass stars. The stellar sample they relied upon is part of *Kepler*'s LEGACY sample, where they took the observables and modelling results from the twin papers by Lund et al. (2017) and Silva Aguirre et al. (2017). The considered sample stars have masses in the range $0.7\text{--}1.2 M_{\odot}$. The upper panel of Fig. 11 shows that stellar masses derived from a grid with atomic diffusion (GS98sta) are higher than those computed from a grid without it (GS98nod). This in turn results in lower stellar ages obtained using GS98sta compared to GS98nod. This is consistent with the anti-correlation between mass and age expected from stellar evolution theory. The authors find a systematic uncertainty of 2.1% on the stellar mass arising from the inclusion of atomic diffusion. This systematic uncertainty is larger than the derived statistical uncertainty (see Fig. 2 of Nsamba et al. 2018).

The lower panel of Fig. 11 shows a comparison of stellar masses derived using grids varying the metal mixtures between those from Asplund et al. (2009) (denoted

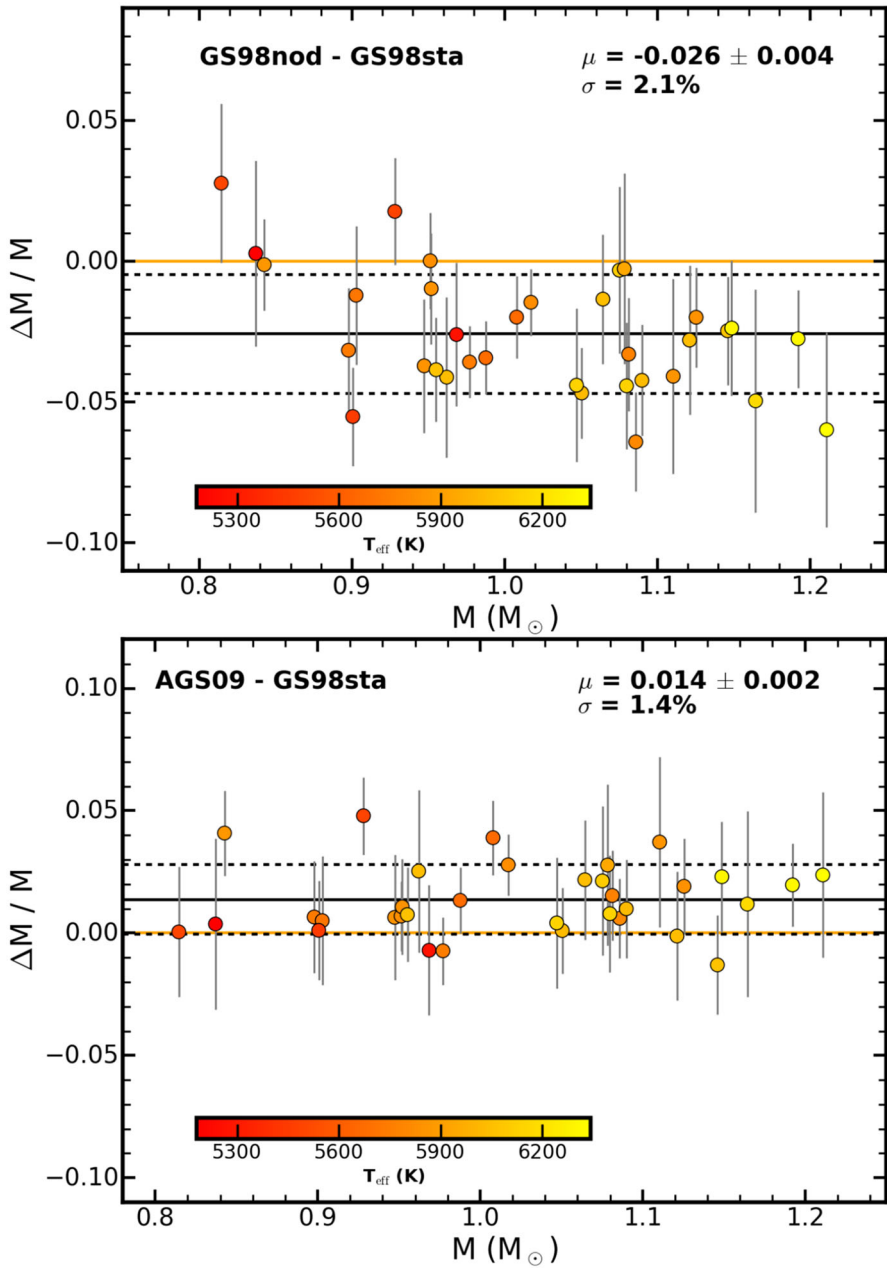


Fig. 11 Fractional differences in stellar mass resulting from the inclusion of atomic diffusion without radiative levitation (top) and from varying the metal mixtures (bottom) (abscissa values are from GS98sta). The orange line is the null offset, the black solid line represents the bias (μ) and the scatter (σ) is represented by the dashed lines. Image reproduced with permission from Nsamba et al. (2018), copyright by the authors

as AGS09) and from Grevesse and Sauval (1998) (denoted as GS98sta). This leads to a systematic uncertainty of 1.4%, which is comparable to statistical uncertainties (see Fig. 2 of Nsamba et al. 2018), in line with the earlier findings by Silva Aguirre et al. (2015). These results show that variations in the metal mixture adopted when modelling low-mass solar-type dwarfs has a limited impact on the derived stellar mass, notwithstanding its significant impact on the internal structure profile of the stellar models (Nsamba et al. 2019). On the other hand, atomic diffusion has a significant impact on the derived stellar mass and age. The case is worse for stars with a mass above $1.2 M_{\odot}$. For this mass range, Deal et al. (2020) found the effects of radiative levitation to be of similar importance as rotational mixing, leading to uncertainties up to 5% for the inferred masses of these late F-type stars. The radiative accelerations due to atomic diffusion have not been usually included in asteroseismic modelling of stars so far, given the computational demands it requires. However, for two slowly rotating A- and F-type pulsators Mombarg et al. (2020) found that the difference in inferred mass from models with and without atomic diffusion and radiative levitation can be as high as $\sim 13\%$.

The initial helium abundance Y is one major uncertainty stellar models have to face. Spectroscopy does not give access to Y because helium lines are not excited in the atmospheres of cool and tepid stars. In the mass estimate process, an anti correlation between the initial helium and mass is found (the so-called helium-mass degeneracy, see, e.g., Lebreton and Goupil 2014) which hampers the mass precision, even in the most favourable cases where individual oscillation frequencies are available. For instance, in the case of the CoRoT target HD 52265 ($M \approx 1.20 M_{\odot}$), Lebreton and Goupil (2014) evaluated that the scatter in mass due to unknown Y is of $\approx 0.1 M_{\odot}$. An indirect way to estimate the envelope helium content is to detect the signature of the acoustic glitch caused by the ionization of helium in precise oscillation frequency pattern (see, e.g., Verma et al. 2019, and references therein); notwithstanding the helium abundance in the envelope at current stellar age is different from the initial one due to the transport processes mentioned above.

6.3 Asteroseismic masses from gravity-mode pulsators

Gravito-inertial asteroseismology stands for the exploitation of nonradial gravity-mode oscillations (g modes in brief) in rotating stars. Here, the buoyancy force of Archimedes and the Coriolis force act together as restoring forces. In contrast to p modes probing stellar envelope physics, the g modes constitute a powerful tool to assess the properties of the deep stellar interiors of intermediate-mass dwarfs and of evolved high-mass stars. Given that such g modes have periodicities of the order of days, space photometry has initiated this recent subfield of asteroseismology. The first detection of g-mode period spacing patterns in CoRoT data of a slowly rotating B-type pulsator was only made a decade ago (Degroote et al. 2010). Meanwhile g-mode asteroseismology has become a mature topic, with major breakthroughs on the probing of near-core physics, notably rotation and element mixing.

In contrast to the large frequency separation $\Delta\nu$ occurring for high-order p modes in low-mass stars, the high-order g modes in intermediate-mass dwarfs reveal a characteristic g-mode asymptotic period spacing Π_0 . It can be derived from the individual periods, P_{nl} , of the g modes, which for the non-rotating case comply with the following:

$$P_{nl} = \frac{\Pi_0}{\sqrt{l(l+1)}} (|n| + \alpha), \quad (11)$$

with

$$\Pi_0 \equiv 2\pi^2 \left(\int_{r_1}^{r_2} N(r) \frac{dr}{r} \right)^{-1}, \quad (12)$$

where r_1 and r_2 denote the inner and outer positions of the g-mode cavity inside the star and $N(r)$ is its Brunt–Väisälä frequency. The phase term α is independent of the mode degree l for stars with a convective core (Aerts et al. 2010, Chapter 3). Thus, for such stars, the spacing in period between modes of the same degree l and of consecutive radial order is a constant. This Π_0 value gives direct information on the thermal and chemical structure in the deep stellar interior, since

$$N^2 \simeq \frac{g}{H_p} [\delta(\nabla_{\text{ad}} - \nabla) + \varphi \nabla_\mu] \quad (13)$$

has its highest value near the convective core of intermediate- and high-mass stars. In this approximate expression in Eq. (13), g is the local gravity, ∇_{ad} the adiabatic temperature gradient, ∇ the actual temperature gradient, ∇_μ the gradient of the molecular weight μ , and δ and φ are logarithmic derivatives depending on the equation-of-state (both are about equal to one in the case of a mono-atomic ideal gas). The measurement of Π_0 is tightly connected to the mass inside the convective core, which is heavily affected by mixing that takes place near the core and is also strongly correlated to the overall mass of the star (Kippenhahn et al. 2012). Deviations from a constant period spacing of g modes give additional direct observational information on the temperature and chemical structure in the region just above the convective core, which is subject to unknown mixing processes (Pedersen et al. 2018; Michielsen et al. 2019).

Intermediate- and high-mass stars tend to be much faster rotators than low-mass stars, as they do not experience magnetic braking due to the absence of a convective envelope. In the presence of rotation, the expression in Eq. (11) gets heavily affected by the Coriolis force and the modes with frequency below twice the rotation frequency are gravito-inertial modes rather than pure g modes (Aerts et al. 2019, for a detailed description). For such modes, the period spacing patterns reveal an upward or downward slope, depending on whether they are retrograde ($m < 0$) or prograde ($m > 0$). It was shown by Van Reeth et al. (2016) and by Ouazzani et al. (2017) that the measurement of this slope gives a direct estimate of the interior rotation frequency of the star in the zones where the g modes have probing power. This concerns the regions between the convective core, which recedes during the

evolution of the star, and the bottom of the radiative envelope. In this region $N(r)$ attains a high value and thus Π_0 probes the physical circumstances in that region.

Gravito-inertial asteroseismology gives access to a direct measurement of the interior rotation frequency of intermediate- and high-mass stars, provided that their gravity or gravito-inertial modes can be identified from period spacing patterns. In contrast to the p modes in low-mass stars, g-mode asteroseismology is not subject to complications due to envelope convection as such stars have radiative envelopes, i.e., there is no surface-effect to be dealt with. Even though stars do develop an outer convection zone as they evolve beyond the main sequence, the g-modes are not sensitive to this outer part of the star as their probing power is concentrated in the deep interior.

Kepler space photometry led to the discovery of period spacing patterns in hundreds of g-mode pulsators (Van Reeth et al. 2015; Pápics et al. 2017; Li et al. 2020; Pedersen et al. 2021), thanks to the 4-year-long data sets. These intermediate-mass dwarfs revealing g-mode pulsations are called γ Doradus (γ Dor) and Slowly Pulsating B (SPB) stars. The former have spectral types early-F to late-A and masses between $1.3M_{\odot} \lesssim M \lesssim 2.0M_{\odot}$, while the latter have spectral types between B3 to B9 and cover masses between $3M_{\odot} \lesssim M \lesssim 10M_{\odot}$. These types of pulsators are excellent laboratories for testing the theory of stellar rotation (Van Reeth et al. 2018; Ouazzani et al. 2017; Aerts et al. 2019) and element mixing (e.g., Moravveji et al. 2016; Szewczuk and Daszyńska-Daszkiewicz 2018; Pedersen et al. 2018; Michielsen et al. 2019; Pedersen et al. 2021). This includes the opportunity to infer both the overall stellar mass as well as the mass of the fully mixed convective core, m_{cc} , which gets heavily affected by the near-core physics during the evolution (see Sect. 1.1). The convective core mass influences crucially the method of isochrone fittings (Sect. 5.1).

As for the case of solar-like pulsators, g-mode asteroseismic modelling is based on the comparison between observed pulsation periods and theoretically predicted periods computed from stellar models. The dependencies of the theoretical predictions are, however, completely different for the p modes in low-mass stars than for the g modes in intermediate- and high-mass stars. Aerts et al. (2018) provides an extensive description of a forward modelling approach suitable for g modes, with focus on the correlation properties between the asteroseismic diagnostics and the free input parameters of the stellar models to be estimated, among which the mass and the amount of convective core overshooting affecting directly the mass of the convective core. An illustration is provided in Fig. 12, which shows how the global g-mode asteroseismic diagnostic Π_0 derived from the g-mode period spacing patterns, connects to the convective core mass m_{cc} of the star. Standard stellar models of intermediate-mass stars reveal a tight relation between the convective core mass and the overall mass of the stars during the core-hydrogen burning phase (Kippenhahn et al. 2012). An asteroseismic measurement of Π_0 thus gives a direct inference of the amount of extra mixing that occurs in the near-core region of the star at the particular phase in its evolution, as this mixing implies that more mass is brought into the core. This opportunity has been put into practise by Mombarg et al. (2019) and Pedersen et al. (2021) for γ Dor and SPB stars, respectively.

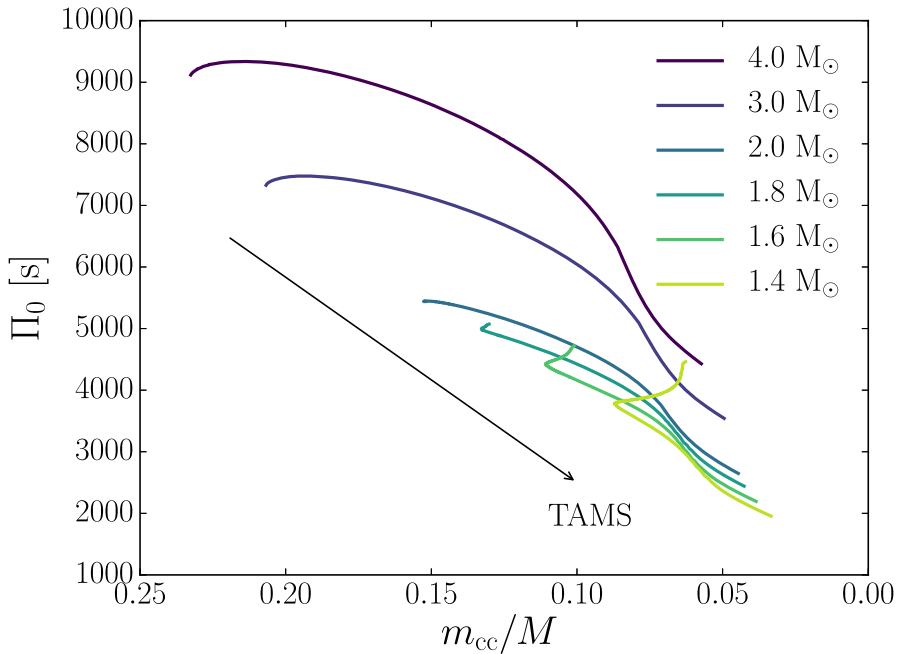


Fig. 12 Π_0 versus m_{cc} for models of various stellar masses, illustrating the asteroseismic potential of a measurement of this quantity to derive core properties

Just as with the solar-like p modes discussed above, there are two general approaches to asteroseismic modelling of g modes: fitting of the period spacing patterns (Degroote et al. 2010; Moravveji et al. 2015; Pedersen et al. 2021) or of the individual mode frequencies (Moravveji et al. 2016; Szweczuk and Daszyńska-Daszkiewicz 2018), each of which by taking into account additional classical observables. The best performance occurs when fitting the period spacings measured for modes of consecutive radial order, as they are less prone to systematic uncertainties in the equilibrium models than the individual mode frequencies or periods. Asteroseismic modelling of intermediate-mass pulsators has to rely on grids of equilibrium models spanning a wide variety of masses, rotation rates, metallicities and near-core mixing profiles. It takes into account measurement uncertainties as well as uncertainties due to the limitations of the input physics (see Aerts et al. 2018, for details). For this type of application, the inclusion of systematic uncertainties in the theoretical models follows naturally from the fact that phenomena not occurring in solar-like stars have to be estimated. The prime examples are convective core overshooting and moderate to fast rotation. For this reason, the use of scaling relations based on helioseismology as for p-mode asteroseismology of low-mass stars is not appropriate for g-mode asteroseismology of intermediate- and high-mass stars. Eclipsing binaries with intermediate- and high-mass components offer a good comparative calibration in this case. Excellent agreement on the levels of near-core mixing is found between inferences of m_{cc}

based on the estimation of core overshooting from g-mode asteroseismology and from eclipsing binary modelling (Tkachenko et al. 2020).

In the case of γ Dor stars, Mombarg et al. (2019) have investigated the combined modelling power of Π_0 and the spectroscopic (T_{eff} , $\log g$) to estimate stellar masses, ages and convective core masses. The fundamental parameters have been inferred by using the Π_0 values from Van Reeth et al. (2016) and the spectroscopic quantities from Van Reeth et al. (2015) for a sample of 37 stars. This leads to asteroseismic mass estimates with a relative precision of $\simeq 0.1M_{\odot}$, along with a precision of about 15% for the age, when the latter is defined in terms of the amount of central hydrogen still left normalised by the initial hydrogen mass fraction, X_c/X_{ini} .

Asteroseismic modelling of 26 SPB stars based on fitting of their dipole period spacings revealed relative precisions ranging from 2 to 20% for the masses and from ~ 10 to $\sim 50\%$ for the fractional main-sequence phases (Pedersen et al. 2021), where higher precision occurs for the slower rotators. It was found that the near-core mixing levels and envelope mixing character show large diversity, even for stars of the same mass, metallicity, surface rotation, and evolutionary stage. The current sample is too small to deduce general conclusions on the connection between the inferred mixing and other stellar parameters.

Finally, as for the solar-like p modes, it has also been assessed how important the inclusion of microscopic atomic diffusion, including radiative levitation, is for the asteroseismic modelling of g-mode pulsators. Radiative levitation shifts the g-mode periods appreciably (see Fig. 5 in Aerts 2021, for a quantitative assessment). For the time being, only the two slowest-rotating γ Dor stars observed with *Kepler* (Mombarg et al. 2020) have been modelled with atomic diffusion, revealing that models with levitation gave better fits in one case and less so in the other case. This study has yet to be generalised for a sample of g-mode pulsators representative in mass, age and rotation.

The mass and main-sequence phase estimates for all the g-mode pulsators that have been modelled asteroseismically so far have been assembled in Fig. 13, colour-coded with the near-core rotation frequency of the stars. It can be seen that the capacity of mass and age estimation is rather diverse, particularly for the SPB stars. This is connected with major variety in the number and radial orders of the modes revealed by these pulsators. Uncertain luminosities from *Gaia* DR2 occur for some of these γ Dor and SPB pulsators, propagating into uncertainty for their masses and evolutionary phases. In addition to the inferred masses, m_{cc} values were also deduced for all these 64 g-mode pulsators, revealing a range of $m_{\text{cc}}/M \in [7, 29]\%$ (Mombarg et al. 2019, 2020; Pedersen et al. 2021). This is observational proof that near-core boundary mixing, covering a wide range of levels, occurs in single intermediate-mass stars, in excellent agreement with the findings based on cluster extended MSTOs (Johnston et al. 2019b) and eclipsing binary modelling (Tkachenko et al. 2020). The large variety in the level of envelope mixing and interior rotation deduced from asteroseismology for the mass range $[1.1, 8.9] M_{\odot}$ has been assembled in Table 1 of Aerts (2021), to which we refer for more extensive discussions on the particular aspect of element transport in intermediate-mass stars.

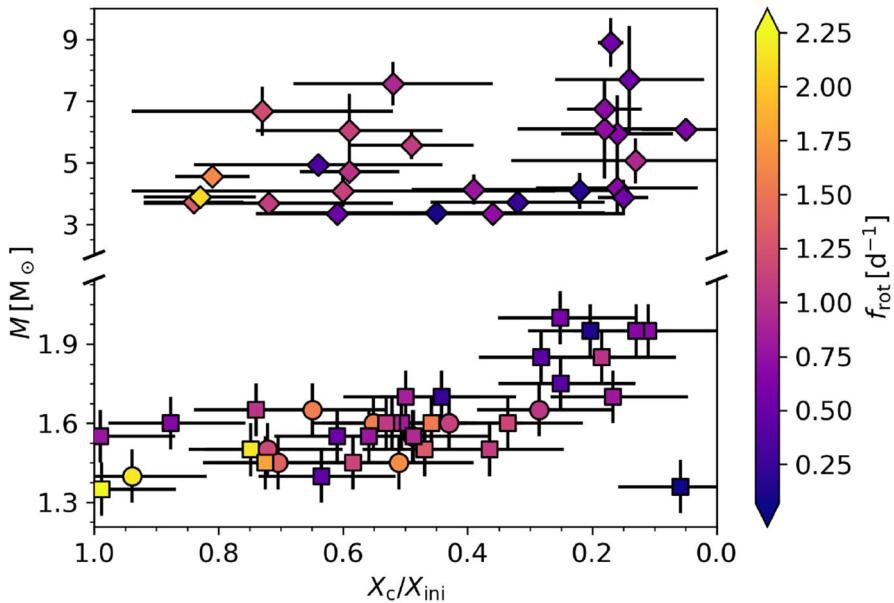


Fig. 13 Asteroseismically inferred stellar masses as a function of the main-sequence phase (X_c/X_{ini}) for 38 γ Dor stars (lower part) and 26 SPB stars (upper part), colour-coded by their near-core rotation rate. Stars with observed Rossby or Yanai modes in addition to gravito-inertial modes are plotted as circles. Figure produced from data in Van Reeth et al. (2016), Mombarg et al. (2019) and Pedersen et al. (2021)

6.4 Asteroseismic mass determination with inverse methods

The methods described in Sects. 6.1.2, 6.2 and 6.3, namely grid searches and detailed mode frequency/period matching, are examples of solving the forward modelling problem, and are strongly model-dependent. From an initial state, the equations of stellar structure (cause) are evolved forward in time to determine the observables (effect). The initial parameters that define the starting model, in particular its mass, and the current age properties that best fit the observed target, are then attributed to that star. An alternative to forward modelling is to solve the inverse problem. Rather than starting with an initial state and evolving it to find the best fitting time-dependent observables, inverse methods use various techniques to directly map the observable quantities (effect) to the stellar properties (cause). In so-called seismic inversions (Christensen-Dalsgaard et al. 1990; Basu 2003) the modes of oscillation are used to reconstruct the medium of propagation. Inversion methods in asteroseismology are extensively discussed in Basu and Chaplin (2017). These methods provide a ‘quasi-model independent’ measure of the stellar interior (Buldgen et al. 2015; Bellinger et al. 2017), but require a reference structure that is ‘close’ to the true underlying stellar stratification. For p-mode asteroseismology, the determined quantities are independent of the properties of the model (such as its mass) up to some limit. For stellar masses, inversions of the mean density combined with *Gaia* radii have shown great promise, resulting in uncertainties less than 10% (Reese et al. 2012; Buldgen et al. 2019). For g-mode asteroseismology, the interior

rotation frequency can be retrieved in a quasi-model independent way from inversion (Triana et al. 2015). However, g-mode structure inversion is yet to be developed.

One way to generalize the applicability of inversion methods is to increase the model dependency. Less reliance on accurate radii and wider inference can be achieved by identifying the mappings between the observables and fundamental stellar properties in detailed models. Due to the complexity and degeneracy of the stellar evolution parameter space the problem is well suited to machine learning, which can trivially devise the necessary non-linear, non-parametric relationships between parameters.

Machine learning algorithms (MLA) are applied widely in astrophysics. Data-driven regression models thus enable the interpretation of datasets that are large, complicated and multi-dimensional. They are typically applied when the underlying model is unknown such as in Sect. 4.3. In order for the MLA to determine the inverse relationships from asteroseismic observations, models take on the role of ‘data’ and the algorithms learn the underlying stellar evolution parameter space. The efficacy of this strategy has been demonstrated using random forest regression (see, for example Angelou et al. 2020, and references therein) as well as with neural networks for both p-mode and g-mode asteroseismic applications (Verma et al. 2016; Hendriks and Aerts 2019). Training on stellar models rather than the observations has several advantages. First, the number of training data, i.e., stellar models, can be increased as required. Second, there are known ground-truth values. The algorithms take the expected observables, as computed from the models, and find direct (non-linear) mappings to the stellar parameters. There is no need to calibrate the physics to benchmark systems such as the Sun or nearby clusters—doing so would inherently assume that their processes are representative of all stars and systems and bias the inferences on other stars, including on their mass. Finally, MLA are fast and scale well. After careful validation, real survey data are fed to the machine learning algorithms for rapid inferences on the stellar properties.

Initially it may seem convoluted to solve the forward equations to generate a grid of models, for the purpose of creating an inverse model but there are sound reasons for doing so. MLA require significantly less sampling density than traditional discrete searches through model libraries. Elaborate stellar models, varied widely in their processes and physical efficiencies, can be used to train the inverse model. By considering models varied in their complexity, the MLA improve the propagation of systematic uncertainty in the error analysis. Comparisons with grid-based searches show that this strategy can attain the same precision with an order of magnitude fewer models while exploring two extra physical processes in the case of p modes in low-mass stars (Bellinger et al. 2016). Additionally evaluating Monte Carlo realizations of the observables, the method is able to provide robust statistical uncertainties along with a systematic component. In Fig. 14 we plot cumulative distributions, showing the relative uncertainty of some estimated stellar parameter for 97 *Kepler* planet hosting stars. When input features are missing or unreliable, for example, if radius has not been measured for a particular star, new inverse models can easily be trained to make predictions. The new model makes use of the

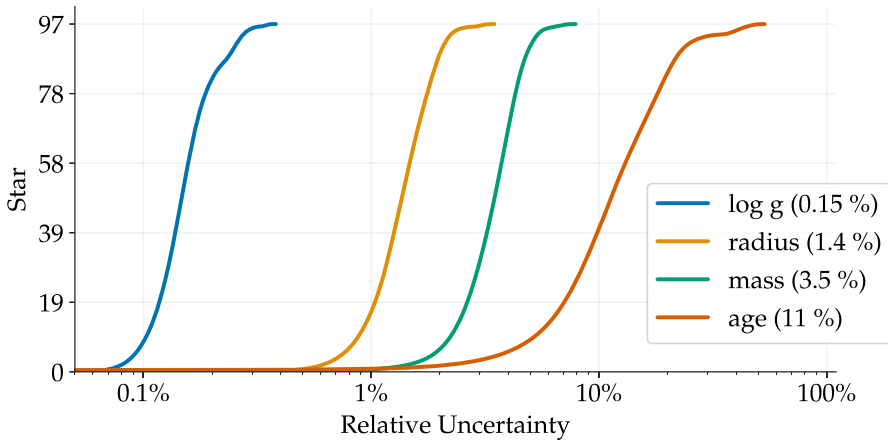


Fig. 14 Cumulative distributions showing the relative uncertainty of several estimated stellar parameters for each of the 97 Kepler Objects of Interest. Analyses were performed using the random-forest machine-learning algorithm

information redundancies in the other input features to predict the stellar properties, including the missing input feature.

In the machine learning approach, observables are used as input features to create a regression model for each individual stellar parameter of interest and the algorithms tend to be opaque in doing so. The inverse model needs to be carefully validated on systems with known truth values such as double-lined EBs and withheld models from the training data. If there is not enough training data the accuracy of the MLA will suffer. The amount of training data needed will depend on the complexity of the underlying parameter space, and this can only be ascertained via convergence testing. Equally important is the issue of overfitting. MLA can overfit the data, that is to say the algorithms fit the noise not the trends in the training data. If a model is overfit it will memorize the data rather than generalizing from it and thus perform poorly on real world data it has not seen. Statistical bagging methods, such as random forests, are designed to mitigate against overfitting. As the MLA devise regression models for individual parameters they do not deliver complete stellar models which might be needed for deeper asteroseismic analysis. However, they are efficient at locating regions of local minima which can be used as starting conditions for optimization or MCMC exploration.

Table 11 demonstrates the most important two and five parameter combinations for inferring various stellar parameters in the case of low-mass stars with p modes (Angelou et al. 2017). They essentially indicate which observable quantities carry the most information about the parameter of interest in this application to solar-like stars. Like other methods, MLA benefit from the seismic data, in particular the asteroseismic ratios ($\langle r_{02} \rangle$, $\langle r_{01} \rangle$, see Roxburgh and Vorontsov 2003). The reported errors indicate the average uncertainty across the entire main-sequence. For this type of methodology it is clear that asteroseismology provides very tight constraints for the ages and masses of stars on the main sequence (Angelou et al. 2017). For

Table 11 The best two and five parameter combinations for predicting stellar parameters of main-sequence stars

Parameter	Two parameters	Avg Err	Five parameters	Avg Err
R [R_{\odot}]	$\langle \Delta v_0 \rangle, v_{\max}$	0.027 R_{\odot}	$\langle \Delta v_0 \rangle, v_{\max}, T_{\text{eff}}, \log g, \langle r_{10} \rangle$	0.008 R_{\odot}
M [M_{\odot}]	$\langle \Delta v_0 \rangle, \log g$	0.072 M_{\odot}	$\langle \Delta v_0 \rangle, \log g, v_{\max}, T_{\text{eff}}, \langle r_{10} \rangle$	0.024 M_{\odot}
τ (Gyr)	$\langle r_{02} \rangle, v_{\max}$	0.642 Gyr	$\langle r_{02} \rangle, v_{\max}, \langle r_{01} \rangle, T_{\text{eff}}, [\text{Fe}/\text{H}]$	0.282 Gyr
R [R_{\odot}]	$\log g, [\text{Fe}/\text{H}]$	0.07 R_{\odot}		
M [M_{\odot}]	$\log g, T_{\text{eff}}$	0.11 M_{\odot}		
τ (Gyr)	$\log g, T_{\text{eff}}$	1.53 Gyr		

Below the horizontal line we use spectroscopic constraints only (Angelou et al. 2017)

comparison purposes, we indicate the accuracy when limited to spectroscopic constraints. MLA applications from g modes are so far limited to slowly rotating intermediate- and high-mass stars (Hendriks and Aerts 2019). Upgrades to realistic modelling for rotating stars with gravito-inertial modes are under way.

6.5 Onward to pre-main sequence asteroseismic masses

From our current knowledge of the physics of early stellar evolution, we expect the interior structures of pre-MS stars to be somewhat simpler than those of post-main-sequence stars. A major motivation to study the oscillations of pre-MS stars is to understand accretion phenomena, as the stars approach the onset of core-hydrogen burning, from their oscillation spectra. The latter tend to be less complex than those of main-sequence dwarfs, which should allow us to derive the young stars' interior structure and global parameters, among which the mass, relatively easily.

The first investigation of oscillations in pre-MS stars dates only to 1995, when the first seismic study of the young δ Sct type star HR 5999 was conducted (Kurtz and Marang 1995). Hence, asteroseismology of pre-MS stars is a rather young research field that is highly promising. To date, three types of pre-MS pulsators were identified observationally: (i) The heat-driven δ Sct type p-mode pre-MS pulsators are the largest group known with ~ 60 objects showing periods from ~ 20 minutes up to 6 hours (e.g., Zwintz et al. 2014). (ii) The few currently known g-mode pre-MS γ Dor-type objects (Zwintz et al. 2013) show pulsation periods between roughly 0.2 and 3 days. (iii) The most massive pre-MS objects of late B spectral types can display g modes as in the SPB stars (Zwintz et al. 2017). All these stars are in the crucial transition phase from gravitational contraction and accretion, to hydrogen-core burning. In this transition phase from partial to nuclear burning in full equilibrium, the star undergoes significant structural changes before arrival on the zero-age main-sequence.

For 13 pre-MS δ Sct, 2 γ Dor stars and 2 SPB stars in the temperature range from ~ 6200 K to $\sim 15\,000$ K, asteroseismic models provide individual masses between 1.5 and 5 M_{\odot} (see Fig. 3). Obviously, the inferred asteroseismic masses depend

strongly on the input physics adopted to compute the stellar evolution models. For these applications, the evolution code `YREC` (Demarque et al. 2008) was used to compute oscillation spectra following Guenther (1994), as well as the combination of MESA models (Paxton et al. 2019, and references therein) with the `GYRE` pulsation code (Townsend and Teitler 2013). A way to test the validity of the pre-MS models would be to compare masses derived for the same stars with independent methods, such as disk-based dynamical mass techniques (see Sect. 2.7) for a pulsating pre-MS star with a known asteroseismic mass, or to find a pulsating pre-MS binary for which a binary and an asteroseismic mass can be derived. Such comparative studies have not yet been done, given the very few pre-MS stars with space photometry and identified pulsation modes so far.

7 Remnants

The focus of this review is on how to determine the masses of “living” stars at various evolutionary stages. However, the masses of compact remnants of stars—white dwarfs (WDs), neutron stars (NSs) and black holes (BHs)—are of great interest, too, and hold crucial information on the evolution of stars. This is particularly true in an era of gravitational wave astronomy, where mergers of NS and BH binaries (e.g., Abbott et al. 2016, 2017, 2019b) are now detected and deliver new insights into massive stars and their compact remnants left behind at the end of their lives. In the following, we briefly review how individual masses of WDs (Sect. 7.1), NSs (Sect. 7.2) and BHs (Sect. 7.3) are determined. Finally we discuss methods to dynamically infer the masses of compact-remnant populations in globular clusters in Sect. 7.4.

When interpreting the determined masses of NSs and BHs in the context of stellar evolution, it is important to realise that most mass measurements are only possible in close binaries where the NSs and BHs are orbited by companions. This is true for (almost) all cases discussed below but also for many gravitational wave sources. These binaries are close in the sense that the progenitor stars that produced the compact remnants once had a radius that often (if not always) exceeded the current orbital separation of the binary system. This implies that there must have been some sort of mass exchange during the evolution of the stars (see, e.g., the reviews of Langer 2012; De Marco and Izzard 2017). These compact remnants are therefore from stars that did not evolve according to isolated single-star evolution but their evolutionary path could have been severely altered by mass transfer in the progenitor systems. This is important to keep in mind when interpreting masses determined in this way.

7.1 White dwarfs

All stars with initial masses below $\sim 8 M_{\odot}$ will end up their lives as white dwarfs. Although most stars in the Milky Way have masses low enough that they have not yet had time to evolve to their final fate, white dwarfs are the most abundant remnant in our Galaxy. Deprived of nuclear energy sources, these stellar remnants

are supported by electron degeneracy pressure which almost only depends on the mechanical properties of the object (total mass and resulting density profile). White dwarfs are therefore bound to cool down at near constant radii with characteristic timescales similar to the age of the Universe (see, e.g., Hansen 1999; Fontaine et al. 2001; Althaus et al. 2010; Salaris et al. 2013). The non-degenerate uppermost layers include less than 1% of the total mass. Nevertheless, they play an important role in increasing the radius by a small percentage compared to the fully degenerate approximation. This increase in radius depends on white dwarf age, but also on the total mass of light elements in the star (Romero et al. 2019). The mass-radius relation derived from white dwarf evolutionary calculations provides a direct link between surface gravity, radius, and mass that is unique to degenerate stars.

The mass-radius relation for white dwarfs is relatively well constrained from direct eclipsing binary measurements (Parsons et al. 2017), which yield 2.4% median uncertainty for the masses, and from determinations of dynamical masses in the Sirius, Procyon, and 40 Eri systems (Bond et al. 2015, 2017a, c). In the latter case, modelling the stellar flux is generally needed to constrain the white dwarf radius, although one exception is when a gravitational redshift is available (Joyce et al. 2018; Pasquini et al. 2019). The empirical mass-radius relation is generally in good agreement with evolutionary predictions, considering the allowed range for the total mass of hydrogen (Romero et al. 2019).

Most studies of white dwarf populations have been assuming a mass-radius relation to derive their masses. On the one hand, the spectroscopic technique which consists in fitting the Balmer or He I line profiles has historically been the most successful technique to obtain the atmospheric parameters T_{eff} and $\log g$ (Bergeron et al. 1992). The success of the technique resides in the fact that the line profiles are very sensitive to variations of the atmospheric parameters, resulting in a precision better than 0.04 dex in $\log g$ for high signal-to-noise observations (Liebert et al. 2005). Surface gravities can then be converted to masses with a precision within a few percent using the mass-radius relation. The accuracy of that technique depends critically on atomic physics and the predicted line profiles (Tremblay and Bergeron 2009). On the other hand, the photometric technique consists in using the parallax and absolute broadband fluxes to constrain the white dwarf T_{eff} and radius (Koester et al. 1979; Bergeron et al. 2001). The mass can then be recovered using the mass-radius relation. The advantage of this technique is that the broadband fluxes are much less sensitive to the details of the atomic physics and equation-of-state than the line profiles, and it can be applied to more complex spectral types (magnetic white dwarfs, metal polluted). The disadvantage of the method is that its accuracy is directly linked to the photometric calibration. The mass-radius relation implies that, unlike for main-sequence stars, the spectroscopic and photometric techniques provide independent mass determinations for white dwarfs.

Historically the photometric and spectroscopic methods have been in fairly good agreement, especially when using 3D model atmospheres for convective white dwarfs (Tremblay et al. 2013; Cukanovaite et al. 2018). The *Gaia* Data Release 2 (Gaia Collaboration et al. 2018) has recently been used to establish an all-sky sample of $\approx 260\,000$ white dwarfs that is homogeneous and nearly complete within the limiting magnitude of $G < 20$ (Gentile Fusillo et al. 2019), increasing by 2–3

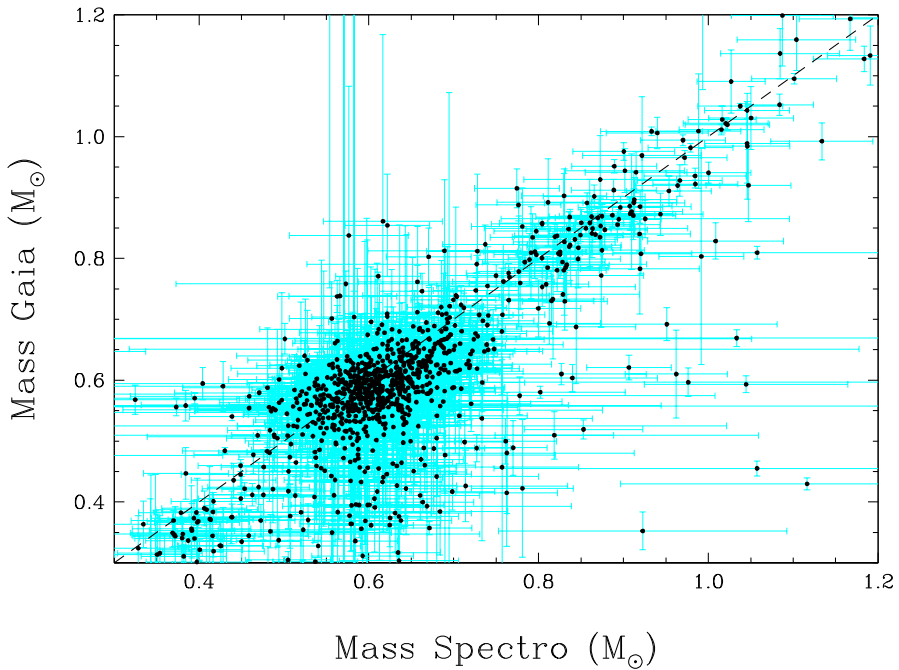


Fig. 15 Comparison of spectroscopic and photometric *Gaia* masses corrected for 3D effects (Tremblay et al. 2013) for a sample of pure-hydrogen atmosphere DA white dwarfs from Gianninas et al. (2011). The one-to-one agreement is illustrated by the dashed line. Many of the objects with a spectroscopic mass significantly larger than the photometric mass on the bottom right of the diagram are unresolved double white dwarfs. See also Tremblay et al. (2019)

orders of magnitude the number of white dwarfs with precise parallaxes. This has resulted in the determination of precise photometric masses for thousands of white dwarfs, characterising for the first time the trends as a function of mass, temperature and spectral types in the comparison between the photometric and spectroscopic masses. Figure 15 demonstrates that the two techniques are found to be in good agreement within a few percent for hydrogen-atmosphere (DA) white dwarfs (Tremblay et al. 2019; Genest-Beaulieu and Bergeron 2019). The advent of continuous observations from space (e.g., CoRoT, Kepler, and TESS missions) has also boosted the field of white dwarf asteroseismology (Córscico et al. 2019; Córscico 2020). Asteroseismology of pulsating white dwarfs has also been successful in deriving accurate masses that are generally in agreement with spectroscopy and photometry (Romero et al. 2012; Hermes et al. 2017; Giammichele et al. 2018). Of particular interest is the case of GW Vir pulsators for which a large number of pulsation frequencies can be determined (usually about 20 frequencies but up to 200 frequencies in the case of PG 1159-035). The large number of periods found in these WDs and pre-WDs allows masses to be determined to a precision of a few percent, exceeding what can be determined by spectroscopic means in this complicated regime (Werner and Herwig 2006; Althaus et al. 2009). It is clear that we can, now, know white dwarf masses within a few percent.

Pasquini et al. (2019) determined the mass of WDs in the Hyades cluster using the gravitational redshift of spectral lines. They showed that M/R can be measured with a precision of 5%. Various methods used to estimate R agreed within 5%, resulting in WD masses with an uncertainty between 5 and 10%. Interestingly, these masses were systematically smaller by $0.02 \dots 0.05 M_{\odot}$ than when determined by other methods, as those mentioned above. Although this discrepancy is within the errors, it may point to systematic problems in the method(s).

In contrast to main-sequence stars, white dwarfs have relatively well constrained cooling ages, making them precise cosmic clocks for the study of the evolution of the disk, halo, and clusters of our Galaxy (see, e.g., Winget et al. 1987; García-Berro et al. 2010). Degenerate stars also critically enlighten the mass-loss during the post-main-sequence evolution and constrain crucial aspects of AGB evolution models useful for galactic population synthesis (see, e.g., Kalirai et al. 2014; Hermes et al. 2017; Costa et al. 2019). However, white dwarf masses are generally not sufficient to perform these applications and the initial stellar mass is also needed. The initial mass of a white dwarf is recovered from the initial-to-final-mass relation (IFMR), which has been a key sub-field of white dwarf research since the pioneering work of Weidemann (1977) using white dwarfs in stellar clusters. Many studies have since described empirical IFMRs from clusters (Dobbie et al. 2006; Salaris et al. 2009; Williams et al. 2009; Cummings et al. 2019), wide binaries (Catalán et al. 2008), and field white dwarfs (El-Badry et al. 2018). The IFMR is routinely used to describe white dwarf progenitors (see, e.g., Tremblay et al. 2014).

7.2 Neutron stars

As for most fundamental mass measurements of stars, it is only possible to determine precise and accurate masses of NSs in binary systems. However, in NSs there is no spectrum that can be used to track the orbital motion from Doppler-shifted spectral lines as done in other binary systems. Luckily, some NSs emit pulsed radio waves that track the rotation of the NSs just like a lighthouse. These pulsars are extremely stable and are considered some of the most accurate clocks in the Universe. As with Doppler-shifted spectral lines, one can use the varying arrival times of the radio pulses to precisely track the orbital motion of the pulsar and thereby determine its mass.

Pulsars are extremely compact stars that bend spacetime around them such that their orbits cannot be explained by Newtonian gravity. Instead, post-Newtonian corrections are required that are valid in this strong-field regime. For Einstein's theory of gravity, five post-Newtonian parameters have been measured in the context of pulsar timing (e.g., Stairs 2003): (i) the rate of periastron advance which is analogous to the advance of the perihelion of Mercury; (ii) the Einstein delay due to variations in gravitational redshift and special relativistic time dilation in eccentric orbits; (iii) orbital period decay due to emission of gravitational waves; (iv) the range and (v) the shape of the Shapiro delay that is due to the propagation of the radio pulses through the gravitational potential of a binary companion. Only two of these need to be measured to be able to determine the two masses of the binary stars (for more information, see e.g., Stairs 2003). Because of this, observations of

pulsars allow for the most stringent tests of theories of gravity to date if more than two of the above post-Newtonian corrections can be measured. So far, all observations are in excellent agreement with General Relativity (e.g., Kramer et al. 2006; Wex 2014).

Recent reviews that include more detailed descriptions of how to determine the masses of NSs are those of Lattimer (2012) and Özel and Freire (2016), resulting in the somewhat up-to-date list of determined NS masses.⁸ Mostly, double neutron-star (DNS) or milli-second pulsar (MSP) and WD binaries are used to determine precise and accurate NSs masses but it is also possible to infer the masses of NSs in, e.g., X-ray binaries (see also Sect. 7.3). MSPs are so-called recycled pulsars, that is pulsars that have accreted mass from a binary companion that spun them up to milli-second rotational periods. They have particularly stable rotational properties and short rotational periods that make them ideal clocks for timing. In DNSs and MSP–WD binaries, the pulsar masses can be determined in some cases to up to 4–5 significant digits, i.e., to precisions better than 1.0–0.1% for a $1.4 M_{\odot}$ pulsar. One of the most massive pulsars known to date is MSP J0348+0432 with a mass of $2.01 \pm 0.04 M_{\odot}$ in a 2.46 h orbit with a $0.172 \pm 0.003 M_{\odot}$ WD (Antoniadis et al. 2013).

Because NSs are almost like macroscopic atomic nuclei, their gravitational mass M_g is not equal to their baryonic mass M_b . The baryonic mass directly links to the core of the progenitor star, while the gravitational mass is the one obtained from observations of NSs. The difference between the two masses is essentially the binding energy and depends on the equation of state of NS matter. A quadratic relation between gravitational and baryonic mass is often applied, $M_b = M_g + AM_g^2$ with A of the order of 0.080 (Lattimer and Yahil 1989; Lattimer and Prakash 2001).

7.3 Black holes

Mass determinations of stellar-mass BHs ($\sim 5\text{--}100 M_{\odot}$) and the corresponding BH mass function are of crucial importance for various topics in astrophysics, such as massive star evolution, the stellar IMF at high masses, the IFMR of massive stars, pair-instability supernovae and compact binary evolution.

For (non-accreting) BHs with a stellar companion, a lower limit on the BH mass can be found via the binary mass function (see Sect. 2), an example being the recent discovery of a BH with mass $\gtrsim 4 M_{\odot}$ in a detached binary in the Galactic globular cluster NGC 3201 (Giesers et al. 2018). To find the individual masses of the binary star, the mass ratio q and inclination i are also required, which is possible if the companion star fills its Roche lobe, via its light curve and spectrum (Wade and Horne 1988). A detailed discussion on dynamical mass determinations of BHs in X-ray binaries is presented in Casares and Jonker (2014), combined with results for 17 Galactic BH X-ray binaries.

For quiescently accreting BHs, a combined measurement of the X-ray and the radio luminosity can be used to infer BH masses (Gallo et al. 2006). At low accretion rates, BHs have compact jets which emit radio continuum via partially self-absorbed synchrotron emission (Blandford and Königl 1979). This makes them

⁸ <https://stellarcollapse.org/nsmasses>.

two orders of magnitudes more luminous in the radio than NSs with similar X-ray luminosity (Migliari and Fender 2006; Özel and Freire 2016). This has led to the discovery of several BHs with masses of $10\text{--}20M_{\odot}$ in Galactic globular clusters (e.g., Strader et al. 2012; Chomiuk et al. 2013). Unfortunately, no precise BH masses can be derived from this method.

The historic first detection of gravitational waves from merging binary BHs (Abbott et al. 2016) has opened a new window on our understanding of BHs and provides an extremely powerful new way to determine accurate BH masses up to large distances. In general relativity, the frequency of gravitational waves and its derivative can be used to derive the ‘chirp mass’ \mathcal{M} of the binary, which depends on the individual masses m_1 and m_2 of the BHs as $\mathcal{M} = (m_1 m_2)^{3/5} / (m_1 + m_2)^{1/5}$. Higher-order terms in the post-Newtonian expansion are needed to find m_1 and m_2 , which has been done for all 10 binary BH mergers detected in the second observing run (O2) of LIGO-Virgo (Abbott et al. 2019b), finding total masses in the range $19\text{--}85M_{\odot}$ (see also Abbott et al. 2019a, for the inferred BH population properties). Thanks to the improved sensitivity of the gravitational wave observatories we can expect hundreds of new detections in the near future. The same techniques are used to infer the masses of NSs in double NS mergers seen through their gravitational wave emission (Abbott et al. 2017).

7.4 Remnant populations

For a canonical stellar IMF, about 30–40% of the total mass of a stellar population resides in WDs, NSs and BHs at an age of 12 Gyr, implying that their presence has an effect on the motion of the visible stars. For old, baryon dominated stellar populations, such as globular clusters, an estimate of the dark remnant mass can thus be obtained, by deriving the dynamical mass (M_{dyn}) from the kinematics and surface brightness profile of the cluster, and comparing this to the luminosity. The (dynamical) mass-to-light ratio (Υ) of globular clusters provides, therefore, a zeroth order insight in the mass function of stars and remnants (e.g., Kimmig et al. 2015). Mass-to-light ratios of metal-rich ($[\text{Fe}/\text{H}] \gtrsim -1$) globular clusters in the Milky Way (e.g., Kimmig et al. 2015) and M31 (Strader et al. 2011) are lower than what is expected from stellar population models. This could point at an absence of remnants and therefore to a top-light IMF, which would be at odds with the recent finding of a top-heavy IMF in the 30 Doradus star-forming region (Schneider et al. 2018). Alternatively, the Υ variations are the result of systematic issues with the measurements as a result of equipartition and mass segregation (Sippel et al. 2012; Shanahan and Gieles 2015). Furthermore, Υ variations could result from both IMF variations at the low-mass end (i.e., more/less low-mass stars) or the high-mass end (i.e., more/less dark remnants).

Combining Υ values with measurements of the luminosity/mass function of visible stars, allows one to break the degeneracy between faint low-mass stars and dark remnants. By using dynamical models that include a prescription for the mass dependent (phase space) distribution of stars and remnants (e.g., Da Costa and

Freeman 1976; Gunn and Griffin 1979; Gieles and Zocchi 2015), or dynamical models of globular cluster evolution (e.g., Grabhorn et al. 1992; Giersz and Heggie 2011), the accuracy of the remnant mass determination can be improved. With the use of parameterised mass functions (e.g., Gieles et al. 2018), the shape of the WD mass function can be inferred from the data (e.g., Sollima et al. 2012). Combined with models for the IFMR of stars, these results can be turned into IMF inference (Hénault-Brunet et al. 2020). Finally, because of the strong effect of BHs on the phase space distribution of the visible stars (Breen and Heggie 2013; Zocchi et al. 2019), and their central location in globular clusters, it may be possible to infer the presence of stellar-mass BH populations from kinematic and photometric data of globular clusters (Peuten et al. 2016; Kremer et al. 2018; Askar et al. 2018; Hénault-Brunet et al. 2020).

8 Summary and conclusions: the mass ladder

Models of stellar structure and evolution form the basis of numerous inferences in modern astrophysics, from exoplanetary science to cosmology. These models rely on the conservation laws of physics applied to a gaseous sphere. Thanks to present-day computational power, stellar structure models become more and more sophisticated in terms of the physical ingredients. While the models rely on the current knowledge of atomic and nuclear physics at the microscopic scale, many of the macroscopic phenomena connected with the thermodynamics and radiation of the gas, as well as its rotation, magnetism, and binarity or multiplicity must be included by means of vastly simplified, often parametrised forms. As a result, the computation of the evolution of a star as it ages, given its birth mass and initial chemistry, depends on a myriad of choices of free parameters for all aspects of the input physics that remain uncalibrated. In order to make solid inferences from stellar models, it is of utmost importance to confront theoretical predictions with observational constraints in order to calibrate (some of) the physical processes upon which the models rely. Such calibrations are required throughout the entire life paths of the stars covering the entire range in possible initial conditions. As stressed at the beginning of this review, the mass of the star is by far the most important free parameter upon which the computation of stellar evolution and its chemical yields is based. As such, it is critical to obtain stellar masses with as high as possible accuracy throughout stellar evolution, in a model-independent way.

Following the considered methods to derive stellar masses discussed in this review, we arrive at the following “mass ladder”:

1. Double-lined spectroscopic eclipsing or visual binaries are the only astrophysical laboratories delivering model-independent stellar masses from their dynamical behaviour. For this reason, such binaries form the most solid possible first rung of the mass ladder. The derivation of the dynamical masses of the stars in a binary rely on light-curve modelling and spectral disentangling methods as critical data-analysis tools to arrive at proper solutions. For some of the brighter EBs, this leads to mass accuracies in the 0.5–3% range, depending on the mass regime and evolutionary stage. We have assembled more than one

hundred benchmark stars with such highly accurate dynamically derived masses in the tables throughout the text. Given the precision of recent and future space photometric light curves, numerous of these benchmark stars are being discovered to show oscillations and/or rotational modulation due to surface spots, with amplitudes at μmag level. This type of low-level intrinsic stellar variability went unnoticed in ground-based mmag-precision light curves and may have led to some systematic uncertainty in the derivation of the mass. Similarly, high-resolution high S/N échelle spectroscopy covering the orbital motion may reveal spectral line-profile variability due to intrinsic phenomena such as pulsations, rotation, or magnetism. Such line-profile variability is currently not yet taken into account in the spectral disentangling tools. The recent space photometry revolution implies that the binary modelling tools can no longer explain the modern data up to their level of precision. Upgrading the data analysis tools to fully exploit the high-precision time-series data requires tedious work but offers the potential to achieve the masses with even higher accuracy.

2. Asteroseismology based on space photometry delivers stellar masses whose model dependence increases with increasing mass. For low-mass stars with detected radial and nonradial oscillations as in the Sun, the oscillation spectra can be scaled with respect to those of the solar oscillation spectrum to deduce the mass (and radius) of the star to a very good approximation. Corrections that improve this approximation are on a good theoretical basis too. This method leads to masses with a precision of $\sim 2\%$ for the best cases. This has been achieved meanwhile for thousands of low-mass dwarfs, subgiants and red giants in the Milky Way. The oscillations of intermediate-mass and high-mass stars are of a different character than those of the Sun and low-mass stars. This implies somewhat larger model-dependence when applying forward asteroseismic modelling to deduce the mass, leading to mass precisions of $\sim 5\%$ for the best cases. This has been achieved for several tens of intermediate-mass stars in the Milky Way but not yet for high-mass stars. This lack will soon be remedied by TESS data for both the Milky Way and the LMC.
3. Semi-empirical mass determination from spectrum fitting or analytical mass–luminosity or mass–radius relations do rely on stellar structure models. Nevertheless, they are important as they are readily applicable to large samples of stars observed in spectroscopic surveys and with *Gaia* astrometry. Important points of attention for these methods are the proper statistical treatment of the analysis methods, including strong correlations among the observables as well as between the numerous stellar model parameters. Ideally, these methods are, therefore calibrated from model-independent dynamical and/or quasi model-independent asteroseismic masses. Moreover, inferences on the stellar masses is best done from a Bayesian statistical approach with proper precision derivation. Compact objects fulfilling a tight mass–radius relation, such as white dwarfs, are better off with semi-empirical mass determinations than yet evolving stars. Moreover, stellar remnants are not subject to mass loss. For this reason, their mass determinations are within reach of $\sim 5\%$ precision.

4. At the faint end of stellar brightness, high-resolution high-S/N spectroscopy is often not feasible to gather. In such cases one is, therefore, obliged to work with mass inferences from evolutionary model tracks in the HRD or CMD. Such evolutionary masses are subject to the largest uncertainties. However, for ensembles of stars belonging to the same populations, such as in a stellar cluster, relative precisions are somewhat better. Isochrone fitting of cluster turnoff masses also falls in this category of model-dependent mass determinations.

A major conclusion from various stellar modelling efforts for single and binary stars is that the models of stellar interiors lack element mixing. While the mixing of chemical elements is included in modern stellar evolution computations relying on phenomena such as rotational, pulsational or tidal mixing, these processes remained essentially uncalibrated until recently. Various methods described in this review point to the same and unambiguous conclusion that intermediate- and high-mass stellar models need extra mixing in the transition layers between the convective core and the radiative envelope as the star evolves. This conclusion was reached independently from binary, asteroseismic, evolutionary and cluster modelling, i.e., consistently throughout the rungs of the mass ladder defined in this work. This conclusion and the quantified levels and profiles of the mixing found from methods 1–4 above, will result in better calibrations of the mixing properties and their parameters used as input physics in stellar evolution models. Measurements of the ratio m_{cc}/M from binary (Tkachenko et al. 2020) or asteroseismic (Aerts 2021) modelling offer a suitable way to guide such improved calibrations.

Finally, an excellent outlook for better stellar masses comes from tidal asteroseismology. The *Kepler* and TESS data reveal many new discoveries of pulsating stars in close binaries whose oscillations are triggered and/or affected by the tide-generating potential of systems. This offers great potential to intertwine rungs 1 and 2 of the mass ladder in an iterative approach, where the model-independent dynamical masses can be imposed upon the asteroseismic modelling and as such take away part of the degeneracies among the stellar model parameters.

We provide a summary of all the methods to determine stellar masses covered in this review in Table 12. A simplified sketch of the capacities is shown in Fig. 16.

Table 12 Summary of main characteristics for mass determination methods

Direct and model independent methods	
	Dynamical
Objects	Visual binaries
Mass range (M_{\odot})	Detached eclipsing binaries No restriction $0.2 < M < 20$
Precision	$0.5\%(M > 8) - 0.05\%(M < 8)$ > 0.14%
Model dependent	No
Main dependencies	Phase coverage, S/N
No. of objects	Many
Prospects	Millimag photometry
Benchmarks	TZ For, V578Mon (Tables 2, 6)
Section	Sections 2.2, 2.6.1, 2.6.2
Dynamical	
Objects	Symbiotic binaries
Mass range (M_{\odot})	$1 < M < 4$ (giant) $0.5 < M < 0.8$ (hot comp./WD)
Precision	> 20%
Model dependent	Strong
Main dependencies	Inclination and radius
No. of objects	$\mathcal{O}(10)$
Prospects	-
Benchmarks	AR Pav, FN Sgr
Section	Section 2.6.3
Dynamical	
Objects	Visual binaries
Mass range (M_{\odot})	pre-MS T Tauri & Herbig Ae
Precision	$0.05 < M < 6$
Model dependent	4% (syst)-1% (stat)
Main dependencies	Spatially and spectrally resolved interferometry
No. of objects	35
Prospects	$\mathcal{O}(100)$ objects w/ALMA
Benchmarks	Circumbinary disks
Section	Section 2.7
Dynamical	
Objects	Gravitational lensing
Mass range (M_{\odot})	All stars
Precision	No restriction
Model dependent	3-8%
Main dependencies	Astrometric precision; single measurement
No. of objects	< 10
Prospects	Dedicated surveys
Benchmarks	None
Section	Section 3

Table 12 continued

Asteroseismic and pulsational		Asteros. (p- and mixed modes)	Asteros. (g-modes)	Global asteroseismology
Asteroseismic and pulsational		Asteros. (p- and mixed modes)	Asteros. (g-modes)	Global asteroseismology
Objects	Solar-like (surface convection)	MS (w/o surf. conv.)	MS (w/o surf. conv.)	Solar-like (MS to AGB)
Mass range (M_{\odot})	$0.7 < M < 1.5$ (MS) $0.7 < M < 2$ (subgiant)	$1.3 < M < 1.9$ (F0-F2) $3 < M < 10$ (B2-B9)	$1.3 < M < 1.9$ (F0-F2) $3 < M < 10$ (B2-B9)	$\lesssim 3M_{\odot}$ (RGB/Clump/AGB)
Precision	3–5%	2–20%	2–20%	≈ 5 –6%
Model dependent	Strong	Strong	Strong	Mild
Main dependencies	Long duration; high-precision light curves; T_{eff} and [Fe/H]			
No. of objects	$\mathcal{O}(100)$	$\mathcal{O}(100)$	$\mathcal{O}(100)$	$\mathcal{O}(10^4)$
Prospects	Up to $\sim 10^4$	$\mathcal{O}(1000)$	$\mathcal{O}(1000)$	$\mathcal{O}(10^4)$
Benchmarks	(\rightarrow Tables 6, 10)	–	–	Eclipsing binaries, stars w/interferometric radius
Section	Section 6.2	Section 6.3	Section 6.3	Section 6.1
Asteroseismic and pulsational		Asteros. inverse methods	Asteros. (g-modes)	Pulsational mass
Objects	Solar-like MS and subgiant		GW Vir stars	Classical radial pulsators
Mass range (M_{\odot})	$0.7 < M < 2$		$0.5 < M < 1$	$1 < M < 8$
Precision	1–20%		~ 5 –10%	$\sim 1\%$ (prec) $\sim 10\%$ (acc)
Model dependent	Weak to strong		Yes	Yes
Main dependencies	Seismic and spectroscopic data		Stellar tracks	Non-linear pulsation theory
No. of objects	Several hundreds		19	$\mathcal{O}(100) \dots \mathcal{O}(1000)$
Prospects	Up to $\sim 10^4$		–	Improved pulsation theory
Benchmarks	16 Cyg A, 16 Cyg B, Procyon		PG 1159-35	LMC binary Cepheids
Section	Section 6.4		Section 7.1	Section 4.6

Table 12 continued

HRD fitting, empirical and stellar granulation	
Isochrone (HRD) fitting/evolutionary masses	
Isochrone (HRD) fitting/evolutionary masses	
Objects	Isolated stars
Mass range (M_{\odot})	$0.1 < M < 10$
Precision	$> 10\%$
Model dependent	Strong
Main dependencies	Stellar models/isochrones, spectroscopic quantities, photometry, distances
No. of objects	$\mathcal{O}(10^6)$
Prospects	Large-scale surveys
Benchmarks	–
Section	Sections 5.1, 5.2
	Massive stars
	$10 < M$
	$\sim 10\%$ (MS)
	Strong
	–
	MW, LMC, SMC, other galaxies
	–
	Section 5.3
	Evolved stars
	$1 < M < 5$
	$> 10-30\%$
	Strong
	$\mathcal{O}(10^6)$
	Large-scale surveys
	–
	Section 5.2
HRD/Kiel diagram fitting	
Analytical/empirical relations	
Stellar granulation based	
Objects	CSPNe and post-AGB
Mass range (M_{\odot})	$0.4 < M < 0.9$
Precision	15%
Model dependent	Strong
Main dependencies	Stellar models
No. of objects	~ 200
Prospects	$\mathcal{O}(10^3)$; Gaia
Benchmarks	–
	MS stars (spect. type M to B)
	$0.1 < M < 0.6$ (low-mass) $0.6 < M < 3.4$ (classic)
	$0.2-20\%$ (prec) $1.5-20\%$ (acc)
	Weak
	Stellar models
	$\mathcal{O}(10^3)$
	Large-scale surveys
	–
	Solar-like (surface convection)
	$0.7 < M < 1.5$ (MS) $0.7 < M < 3$ (evolved)
	10%
	Weak
	Lightcurves, T_{eff} , [Fe/H], photometry, parallax
	3×10^4
	3×10^5
	Kepler stars w/seismic masses

Table 12 continued

	HRD/Kiel diagram fitting	Analytical/empirical relations	Stellar granulation based
Section	Section 5.2	Section 4.4	Section 4.1
Methods for white dwarfs			
	Asteros. (g-modes)		Photometry
Objects	DA and DB white dwarfs	All WD classes	All WD classes
Mass range (M_{\odot})	All white dwarf mass range		
Precision	$\sim 2\%$	$> 2\%$	$> 1\%$
Model dependent	Yes	Mild	Weak
Main dependencies	Stellar models, obs. modes	M-R relations, $\log g$, T_{eff}	M-R rel., colours, parallax
No. of objects	~ 300	$\sim 3 \times 10^4$	$\sim 2.5 \times 10^5$
Prospects	Space photometry	$\sim 3 \times 10^4$ (large-scale surveys)	$\mathcal{O}(10^7)$ (LSST, EUCLID)
Benchmarks	R548, G117-B15A, GD358	Nearby WDs	nearby WDs
Section	Section 7.1	Section 7.1	Section 7.1
	Eclipsing binaries		Astrometric binaries
Objects	All WD classes		
Mass range (M_{\odot})	All white dwarf mass range		
Precision	$\sim 1\%$	2–5%	1%
Model dependent	Very weak	Yes	No
Main dependencies	Photometric light curves, T_{eff}	Model atmospheres, $\log g$, v_r	Astrometry, observation time

Table 12 continued

	Eclipsing binaries	Gravitational redshift	Astrometric binaries
No. of objects	~50	~20 (Hyades)	Few
Prospects	~10 ³ (GAIA, LSST)	–	A few (long orbital period)
Benchmarks	Nearby systems	Sirius system	–
Section	Section 7.1	Section 7.1	Section 7.1
Spectroscopic-based			
	Surface abundances	H ₂ fitting	Lithium abundances
Objects	RGB (post 1st dredge-up)	Red giants	Solar-like stars
Mass range (M_{\odot})	0.7 < M < 2.0	0.7 < M < 1.8	0.95 < M < 1.05
Precision	10%(prec), 20%(acc)	10–15%	3–5%
Model dependent	Strong	No	Yes
Main dependencies	Stellar models, training sets	Spectroscopic data, training sets (asteroseismic masses)	Stellar models and atmospheres, spectroscopic parameters
No. of objects	> 10 ⁶	> 10 ⁸	$\mathcal{O}(10^3)$
Prospects	Training sets w/seismic masses	Large-scale spectroscopic surveys, extragalactic	Large-scale spectroscopic surveys
Benchmarks	–	–	–
Section	Section 4.2.2	Section 4.2.1	Section 4.2.3

When quoting precision or accuracy, the symbol > should be interpreted as ‘up to’ and the symbol < as ‘better than’

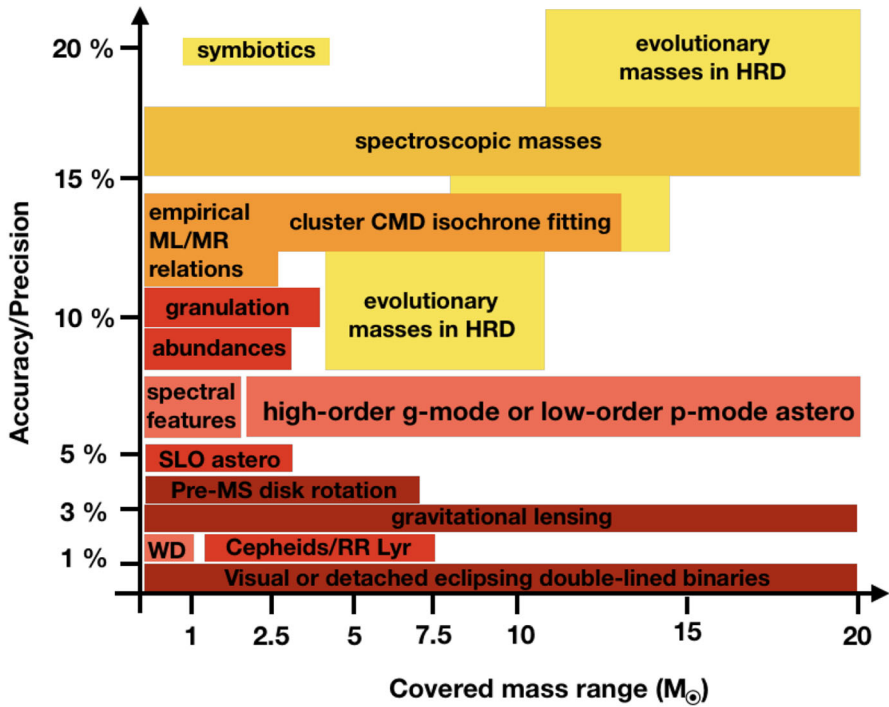


Fig. 16 A simplified sketch of the mass ladder, summarizing the capacity of the various methods listed in Table 12. We show typical precisions in such a way that the sketch remains well visible. WD stands for White Dwarfs, SLO for solar-like oscillations and ML/MR for mass-luminosity and mass-radius relations. Although the abscissa stops at $20 M_{\odot}$, the methods reaching that value continue up to higher masses as well. The darker the colour, the less model dependent the method is, where the darkest red regions deliver model-independent masses and hence provide not only precise but also accurate masses

Glossary

See Table 13.

Table 13 List of commonly used acronyms in the article

Acronym	
AGB	Asymptotic Giant Branch
ALMA	Atacama Large Millimeter/submillimeter Array
APOGEE	Apache Point Observatory Galactic Evolution Experiment
APOKASC	APOGEE/Kepler Asteroseismic Scientific Consortium Collaboration
ARAUCARIA	Survey of classical variables in the Local Group of galaxies
ARIEL	ESA's M4 mission: Atmospheric Remote-sensing Infrared Exoplanet Large-survey
ASAS	All Sky Automated Survey for SuperNovae
BH	Black Hole
BRITE	Bright (star) Target Explorer satellites

Table 13 continued

Acronym	
CCF	Cross correlation function
CCSN	Core-collapse supernova
CDS	Strasbourg astronomical Data Center
CMD	Color-magnitude diagram
CoRoT	Convection, Rotation and planetary Transits satellite
CSPN	Central star of planetary nebula
DEB	Detached eclipsing binary
DEBCat	Catalog of detached eclipsing binaries
DNS	Double neutron stars
DR	Data release
EB	Eclipsing binaries
E-ELT	European Extremely Large Telescope
EROS	Expérience de Recherche d'Objets Sombres collaboration
ESPRESSO	Echelle SPectrograph for Rocky Exoplanets and Stable Spectroscopic Observations
Flicker	Root mean square of stellar brightness fluctuations in 8-hour timescale
FliPer	Flicker in the spectral power density
Gaia	Global Astrometric Interferometer for Astrophysics
Gaia-ESO	ESO public spectroscopic survey to complement Gaia observations
GALAH	Galactic Archaeology with Hermes. Southern hemisphere spectroscopic survey
GBM	Grid based modelling
HARPS	High Accuracy Radial velocity Planet Searcher
HAT-Net	Hungarian-made Automated Telescope Network Exoplanet Survey
HIRES	High Resolution Spectrograph for E-ELT
HRD	Hertzsprung Russell diagram
HST	Hubble Space Telescope
IFMR	Initial-final mass relation
IMF	Initial mass function
JWST	James Webb Space Telescope
K2	Kepler's second life
Kepler	NASA planet hunting and asteroseismic mission
KIC	Kepler Input Catalogue
LAMOST	Large Sky Area Multi-Object Fiber Spectroscopic Telescope
LMC	Large Magellanic Cloud
LTE	Local thermodynamic equilibrium
MACHO	Massive Compact Halo Objects survey
MCMC	Monte Carlo Markov Chain
MEarth	Survey to detect planets around M dwarf stars
MIST	MESA isochrones & stellar tracks
MLA	Machine Learning Algorithm
MS	Main sequence
MSP	Milli-second pulsar
MSTO	Main sequence turn-off

Table 13 continued

Acronym	
NLTE	Non-Local Thermodynamic Equilibrium
NS	Neutron star
OGLE	Optical Gravitational Lensing Experiment
PARSEC	Padova and Trieste stellar evolution code tracks
PIONIER	Precision Integrated-Optics Near-infrared Imaging ExpeRiment
PLATO	ESA's M3 missions: PPlanetary Transits and Oscillations of stars
RGB	Red giant branch
RSG	Red supergiant star
RV	Radial velocity
SB2	Double-lined spectroscopic binaries
SED	Spectral energy distribution
SGB	Subgiant branch
SMC	Small Magellanic Cloud
SN	Supernova
SOPHIE	Spectrographe pour l'Observation des Phénomènes des Intérieurs stellaires et des Exoplanètes
SPB	Slowly pulsating B-type star
SPD	Spectral disentangling
SPHERE	Spectro-Polarimetric High-contrast Exoplanet REsearch
SuperWASP	Super Wide-Angle Search for Planets
TESS	NASA's Transiting Exoplanets Survey Satellite
TMT	Thirty Meter Telescope
TODCOR	Two Dimensional Correlation technique
VLT	Very Large Telescope
VLTI	Very Large Telescope Interferometer
WD	White dwarf star
WFC3	HST Wide Field Camera 3

Acknowledgements We thank the Lorentz Center and its staff for making it possible to organize a workshop in November 2018. This review resulted from the intense and pleasant onsite discussions during this meeting and follow-up collaborations. The contribution of the Lorentz Center staff in stimulating suggestions, giving feedback and taking care of all practicalities, helped us to focus on our research and to organize a meeting of high scientific quality. The authors are much indebted to all colleagues participating in the workshop, even though they were not involved in the textual contributions for this review paper. A.S. acknowledges support from Grants ESP2017-82674-R and PID2019-108709GB-I00 (MICINN) and 2017-SGR-1131 (AGAUR). C.A., J.S.G.M., and M.G.P. received funding from the European Research Council (ERC) under the European Union's Horizon 2020 research and innovation programme (Grant agreement no. 670519: MAMSIE) and from the KU Leuven Research Council (grant C16/18/005: PARADISE). M.B. is supported through the Lise Meitner grant from the Max Planck Society and acknowledges support by the Collaborative Research centre SFB 881 (projects A5, A10), Heidelberg University, of the Deutsche Forschungsgemeinschaft (DFG, German Research

Foundation). V.S.A. acknowledges support from the Independent Research Fund Denmark (Research grant 7027-00096B) and the Carlsberg foundation (Grant agreement CF19-0649). Funding for the Stellar Astrophysics Centre is provided by The Danish National Research Foundation (Grant agreement No. DNRF106). D.B., J.C.M., and I.R. acknowledge support from the Spanish Ministry of Science, Innovation and Universities (MICIU), and the Fondo Europeo de Desarrollo Regional (FEDER) through Grants ESP2016-80435-C2-1-R and PGC2018-098153-B-C33, as well as the support of the Generalitat de Catalunya (CERCA programme). N.B. gratefully acknowledge financial support from the Royal Society (University Research Fellowships) and from the European Research Council (ERC-CoG-646928, Multi-Pop). A.E. acknowledges support from the Research Foundation Flanders (FWO) under contract ZKD1501-00-W01 (Grant no. 792848). D.K.F. acknowledges funds from the Alexander von Humboldt Foundation in the framework of the Sofia Kovalevskaja Award endowed by the Federal Ministry of Education and Research and grant 2016-03412 from the Swedish Research Council. D.G. gratefully acknowledges financial support from the CRT foundation under Grant no. 2018.2323 “*Gaseous or rocky? Unveiling the nature of small worlds*”. L.G. acknowledges funding from LSST-Italy and from project MITic 2015. N.L. was financially supported by the Spanish Ministry of Economy and Competitiveness (MINECO) under Grant number AYA2015-69350-C3-2-P. A.M. acknowledges funding from the European Union’s Horizon 2020 research and innovation program under the Marie Skłodowska-Curie grant agreement No 749962 (project THOT). B.N. is supported by Fundação para a Ciência e a Tecnologia (FCT, Portugal) under Grant PD/BD/113744/2015 from PhD::SPACE, an FCT PhD program, and by the Alexander von Humboldt Foundation. Further support from FEDER – Fundo Europeu de Desenvolvimento Regional funds through the COMPETE 2020 – Operacional Programme for Competitiveness and Internationalisation (POCI), and by Portuguese funds through FCT – Fundação para a Ciência e a Tecnologia in the framework of the Project POCI-01-0145-FEDER-030389 is also acknowledged. K.P. acknowledges support from the Croatian Science Foundation (HRZZ research Grant IP-2014-09-8656). P.-E.T. has received funding from the European Research Council under the European Union’s Horizon 2020 research and innovation programme n. 677706 (WD3D). The authors thank our colleagues G. Bono, T.L. Campante, M.S. Cunha, P. Das, C. Johnston, F. Kiefer, P. Maxted, M.J.P.F.G. Monteiro, Th. Rodrigues, V. Schaffenroth, M. Vučković for helpful comments and useful discussions. This work presents results from the European Space Agency (ESA) space mission *Gaia* and from the American National Aeronautics and Space Administration (NASA) space missions *Kepler* and TESS.

References

- Abbott BP, et al [LIGO Scientific Collaboration, Virgo Collaboration] (2016) Observation of gravitational waves from a binary black hole merger. *Phys Rev Lett* 116(6):061102. <https://doi.org/10.1103/PhysRevLett.116.061102>. [arXiv:1602.03837](https://arxiv.org/abs/1602.03837) [gr-qc]
- Abbott BP, et al [LIGO Scientific Collaboration, Virgo Collaboration] (2017) GW170817: observation of gravitational waves from a binary neutron star inspiral. *Phys Rev Lett* 119(16):161101. <https://doi.org/10.1103/PhysRevLett.119.161101>. [arXiv:1710.05832](https://arxiv.org/abs/1710.05832) [gr-qc]
- Abbott BP, et al [LIGO Scientific Collaboration, Virgo Collaboration] (2019a) Binary black hole population properties inferred from the first and second observing runs of advanced LIGO and advanced Virgo. *ApJL* 882(2):L24. <https://doi.org/10.3847/2041-8213/ab3800>. [arXiv:1811.12940](https://arxiv.org/abs/1811.12940) [astro-ph.HE]
- Abbott BP, Abbott R, Abbott TD, [LIGO Scientific Collaboration, Virgo Collaboration] (2019b) GWTC-1: a gravitational-wave transient catalog of compact binary mergers observed by LIGO and Virgo during the first and second observing runs. *Phys Rev X* 9(3):031040. <https://doi.org/10.1103/PhysRevX.9.031040>. [arXiv:1811.12907](https://arxiv.org/abs/1811.12907) [astro-ph.HE]
- Aerts C (2021) Probing the interior physics of stars through asteroseismology. *Rev Mod Phys* 93(1):015001. <https://doi.org/10.1103/RevModPhys.93.015001>
- Aerts C, De Cat P (2003) β Cep stars from a spectroscopic point of view. *Space Sci Rev* 105(1):453–492. <https://doi.org/10.1023/A:1023983704925>
- Aerts C, Christensen-Dalsgaard J, Kurtz DW (2010) *Asteroseismology*. Springer, Dordrecht. <https://doi.org/10.1007/978-1-4020-5803-5>
- Aerts C, Simón-Díaz S, Groot PJ, Degroote P (2014) On the use of the Fourier transform to determine the projected rotational velocity of line-profile variable B stars. *A&A* 569:A118. <https://doi.org/10.1051/0004-6361/201424012>. [arXiv:1407.6611](https://arxiv.org/abs/1407.6611) [astro-ph.SR]

- Aerts C, Molenberghs G, Michielsen M, Pedersen MG, Björklund R, Johnston C, Mombarg JSG, Bowman DM, Buyschaert B, Pápics PI, Sekaran S, Sundqvist JO, Tkachenko A, Truyaert K, Van Reeth T, Vermeyen E (2018) Forward asteroseismic modeling of stars with a convective core from gravity-mode oscillations: parameter estimation and stellar model selection. *ApJS* 237:15. <https://doi.org/10.3847/1538-4365/aaccfb>. arXiv:1806.06869 [astro-ph.SR]
- Aerts C, Mathis S, Rogers TM (2019) Angular momentum transport in stellar interiors. *ARA&A* 57:35–78. <https://doi.org/10.1146/annurev-astro-091918-104359>. arXiv:1809.07779 [astro-ph.SR]
- Afşar M, Ibanoğlu C (2008) Two-colour photometry of the binary planetary nebula nuclei UU Sagitte and V477 Lyrae: oversized secondaries in post-common-envelope binaries. *MNRAS* 391(2):802–814. <https://doi.org/10.1111/j.1365-2966.2008.13927.x>. arXiv:0810.0949 [astro-ph]
- Aizenman M, Smeyers P, Weigert A (1977) Avoided crossing of modes of non-radial stellar oscillations. *A&A* 58:41
- Albrecht S, Winn JN, Torres G, Fabrycky DC, Setiawan J, Gillon M, Jehin E, Triaud A, Queloz D, Snellen I, Eggleton P (2014) The BANANA Project. V. Misaligned and precessing stellar rotation axes in CV Velorum. *ApJ* 785(2):83. <https://doi.org/10.1088/0004-637X/785/2/83>. arXiv:1403.0583 [astro-ph.SR]
- Althaus LG, Panei JA, Miller Bertolami MM, García-Berro E, Córscico AH, Romero AD, Kepler SO, Rohrmann RD (2009) New evolutionary sequences for hot H-deficient white dwarfs on the basis of a full account of progenitor evolution. *ApJ* 704(2):1605–1615. <https://doi.org/10.1088/0004-637X/704/2/1605>. arXiv:0909.2689 [astro-ph.SR]
- Althaus LG, Córscico AH, Isern J, García-Berro E (2010) Evolutionary and pulsational properties of white dwarf stars. *Astron Astrophys Rev* 18(4):471–566. <https://doi.org/10.1007/s00159-010-0033-1>. arXiv:1007.2659 [astro-ph.SR]
- Andersen J (1991) Accurate masses and radii of normal stars. *Astron Astrophys Rev* 3(2):91–126. <https://doi.org/10.1007/BF00873538>
- Anderson RI, Saio H, Ekström S, Georgy C, Meynet G (2016) On the effect of rotation on populations of classical Cepheids. II. Pulsation analysis for metallicities 0.014, 0.006, and 0.002. *A&A* 591:A8. <https://doi.org/10.1051/0004-6361/201528031>. arXiv:1604.05691 [astro-ph.SR]
- Andrews SM, Terrell M, Tripathi A, Ansdell M, Williams JP, Wilner DJ (2018) Scaling relations associated with millimeter continuum sizes in protoplanetary disks. *ApJ* 865:157. <https://doi.org/10.3847/1538-4357/aadd9f>. arXiv:1808.10510 [astro-ph.EP]
- Angelou GC, Stancliffe RJ, Church RP, Lattanzio JC, Smith GH (2012) The role of thermohaline mixing in intermediate- and low-metallicity globular clusters. *ApJ* 749(2):128. <https://doi.org/10.1088/0004-637X/749/2/128>. arXiv:1202.2859 [astro-ph.SR]
- Angelou GC, Bellinger EP, Hekker S, Basu S (2017) On the statistical properties of the lower main sequence. *ApJ* 839(2):116. <https://doi.org/10.3847/1538-4357/aa6a54>. arXiv:1703.10165 [astro-ph.SR]
- Angelou GC, Bellinger EP, Hekker S, Mints A, Elsworth Y, Basu S, Weiss A (2020) Convective boundary mixing in low- and intermediate-mass stars—I. Core properties from pressure-mode asteroseismology. *MNRAS* 493(4):4987–5004. <https://doi.org/10.1093/mnras/staa390>. arXiv:2002.02546 [astro-ph.SR]
- Antoniadis J, Freire PCC, Wex N, Tauris TM, Lynch RS, van Kerkwijk MH, Kramer M, Bassa C, Dhillion VS, Driebe T et al (2013) A massive pulsar in a compact relativistic binary. *Science* 340:448. <https://doi.org/10.1126/science.1233232>. arXiv:1304.6875 [astro-ph.HE]
- Appourchaux T, Antia HM, Ball W, Creevey O, Lebreton Y, Verma K, Vorontsov S, Campante TL, Davies GR, Gaulme P, Régulo C, Horch E, Howell S, Everett M, Ciardi D, Fossati L, Miglio A, Montalbán J, Chaplin WJ, García RA, Gizon L (2015) A seismic and gravitationally bound double star observed by Kepler. *A&A* 582:A25
- Askar A, Arca Sedda M, Giersz M (2018) MOCCA-SURVEY Database I: galactic globular clusters harbouring a black hole subsystem. *MNRAS* 478:1844–1854. <https://doi.org/10.1093/mnras/sty1186>. arXiv:1802.05284
- Asplund M (2005) New light on stellar abundance analyses: departures from LTE and homogeneity. *ARA&A* 43(1):481–530. <https://doi.org/10.1146/annurev.astro.42.053102.134001>
- Asplund M, Grevesse N, Sauval AJ, Scott P (2009) The chemical composition of the Sun. *Annu Rev Astron Astrophys* 47:481–522. <https://doi.org/10.1146/annurev.astro.46.060407.145222>. arXiv:0909.0948 [astro-ph.SR]

- Astraatmadja TL, Bailer-Jones CAL (2016) Estimating distances from parallaxes. II. Performance of Bayesian distance estimators on a Gaia-like catalogue. *ApJ* 832(2):137. <https://doi.org/10.3847/0004-637X/832/2/137>. [arXiv:1609.03424](https://arxiv.org/abs/1609.03424) [astro-ph.IM]
- Athay RG (1977) The solar chromosphere and corona: quiet Sun (book review). *ApJL* 19:29
- Aubourg E, Barette P, Brehin S, Gros M, Lachize-Rey M, Laurent B, Lesquoy E, Magneville C, Milsztajn A, Moscoso L, Queinac F, Rich J, Spiro M, Vigroux L, Zylberajch S, Ansari R, Cavalier F, Moniez M, Beaulieu JP, Ferlet R, Grison P, Vidal-Madjar A, Guibert J, Moreau O, Tajahmady F, Maurice E, Prevot L, Gry C (1993) The EROS search for dark halo objects. *Messenger* 72:20–27
- Ausseloos M, Aerts C, Lefever K, Davis J, Harmanec P (2006) High-precision elements of double-lined spectroscopic binaries from combined interferometry and spectroscopy. Application to the β Cephei star β Centauri. *A&A* 455(1):259–269. <https://doi.org/10.1051/0004-6361/20064829>. [arXiv:astro-ph/0605220](https://arxiv.org/abs/astro-ph/0605220)
- Auvergne M, Bodin P, Boisnard L et al (2009) The CoRoT satellite in flight: description and performance. *A&A* 506(1):411–424. <https://doi.org/10.1051/0004-6361/200810860>. [arXiv:0901.2206](https://arxiv.org/abs/0901.2206) [astro-ph.SR]
- Baglin A, Auvergne M, Boisnard L, Lam-Trong T, Barge P, Catala C, Deleuil M, Michel E, Weiss W (2006) CoRoT: a high precision photometer for stellar evolution and exoplanet finding. In: 36th COSPAR scientific assembly, p 3749
- Bagnuolo J, William G, Gies DR (1991) Tomographic separation of composite spectra: the components of the O-star spectroscopic binary AO Cassiopeiae. *ApJ* 376:266. <https://doi.org/10.1086/170276>
- Bahcall JN, Pinsonneault MH, Basu S (2001) Solar models: current epoch and time dependences, neutrinos, and helioseismological properties. *ApJ* 555:990–1012. <https://doi.org/10.1086/321493>. [arXiv:astro-ph/0010346](https://arxiv.org/abs/astro-ph/0010346)
- Bailer-Jones CAL (2011) Bayesian inference of stellar parameters and interstellar extinction using parallaxes and multiband photometry. *MNRAS* 411(1):435–452. <https://doi.org/10.1111/j.1365-2966.2010.17699.x>. [arXiv:1009.2766](https://arxiv.org/abs/1009.2766) [astro-ph.IM]
- Ball WH, Gizon L (2014) A new correction of stellar oscillation frequencies for near-surface effects. *A&A* 568:A123. <https://doi.org/10.1051/0004-6361/201424325>. [arXiv:1408.0986](https://arxiv.org/abs/1408.0986) [astro-ph.SR]
- Baraffe I, Chabrier G (2010) Effect of episodic accretion on the structure and the lithium depletion of low-mass stars and planet-hosting stars. *A&A* 521:A44. <https://doi.org/10.1051/0004-6361/201014979>. [arXiv:1008.4288](https://arxiv.org/abs/1008.4288) [astro-ph.EP]
- Baraffe I, Chabrier G, Allard F, Hauschildt PH (2002) Evolutionary models for low-mass stars and brown dwarfs: uncertainties and limits at very young ages. *A&A* 382:563–572. <https://doi.org/10.1051/0004-6361:20011638>. [arXiv:astro-ph/0111385](https://arxiv.org/abs/astro-ph/0111385)
- Baraffe I, Homeier D, Allard F, Chabrier G (2015) New evolutionary models for pre-main sequence and main sequence low-mass stars down to the hydrogen-burning limit. *A&A* 577:A42. <https://doi.org/10.1051/0004-6361/201425481>. [arXiv:1503.04107](https://arxiv.org/abs/1503.04107) [astro-ph.SR]
- Baroch D, Morales JC, Ribas I, Tal-Or L, Zechmeister M, Reiners A, Caballero JA, Quirrenbach A, Amado PJ, Dreizler S et al (2018) The CARMENES search for exoplanets around M dwarfs. Nine new double-line spectroscopic binary stars. *A&A* 619:A32. <https://doi.org/10.1051/0004-6361/201833440>. [arXiv:1808.06895](https://arxiv.org/abs/1808.06895) [astro-ph.SR]
- Bass G, Orosz JA, Welsh WF, Windmiller G, Ames Gregg T, Fetherolf T, Wade RA, Quinn SN (2012) Kepler studies of low-mass eclipsing binaries. I. Parameters of the long-period binary KIC 6131659. *ApJ* 761:157. <https://doi.org/10.1088/0004-637X/761/2/157>. [arXiv:1211.1068](https://arxiv.org/abs/1211.1068) [astro-ph.SR]
- Bastian N, de Mink SE (2009) The effect of stellar rotation on colour-magnitude diagrams: on the apparent presence of multiple populations in intermediate age stellar clusters. *MNRAS* 398(1):L11–L15. <https://doi.org/10.1111/j.1745-3933.2009.00696.x>. [arXiv:0906.1590](https://arxiv.org/abs/0906.1590) [astro-ph.GA]
- Bastian N, Covey KR, Meyer MR (2010a) A universal stellar initial mass function? A critical look at variations. *ARA&A* 48:339–389. <https://doi.org/10.1146/annurev-astro-082708-101642>. [arXiv:1001.2965](https://arxiv.org/abs/1001.2965) [astro-ph.GA]
- Bastian N, Covey KR, Meyer MR (2010b) A universal stellar initial mass function? A critical look at variations. *ARA&A* 48:339–389. <https://doi.org/10.1146/annurev-astro-082708-101642>. [arXiv:1001.2965](https://arxiv.org/abs/1001.2965) [astro-ph.GA]
- Bastian N, Kamann S, Cabrera-Ziri I, Georgy C, Ekström S, Charbonnel C, de Juan Ovelar M, Usher C (2018) Extended main sequence turnoffs in open clusters as seen by Gaia—I. NGC 2818 and the role of stellar rotation. *MNRAS* 480(3):3739–3746. <https://doi.org/10.1093/mnras/sty2100>. [arXiv:1807.10779](https://arxiv.org/abs/1807.10779) [astro-ph.SR]

- Bastien FA, Stassun KG, Basri G, Pepper J (2013) An observational correlation between stellar brightness variations and surface gravity. *Nature* 500:427–430. <https://doi.org/10.1038/nature12419>. arXiv:1308.4728 [astro-ph.SR]
- Bastien FA, Stassun KG, Basri G, Pepper J (2016) A granulation, “flicker”-based measure of stellar surface gravity. *ApJ* 818:43. <https://doi.org/10.3847/0004-637X/818/1/43>. arXiv:1512.03454 [astro-ph.SR]
- Basu S (2003) Stellar inversions. *Ap&SS* 284(1):153–164. <https://doi.org/10.1023/A:1023223115165>
- Basu S, Chaplin WJ (2017) Asteroseismic data analysis: foundations and techniques. Princeton University Press, Princeton
- Basu S, Verner GA, Chaplin WJ, Elsworth Y (2012) Effect of uncertainties in stellar model parameters on estimated masses and radii of single stars. *ApJ* 746(1):76. <https://doi.org/10.1088/0004-637X/746/1/76>. arXiv:1111.6976 [astro-ph.SR]
- Bazot M (2020) Uncertainties and biases in modelling 16 Cygni A and B. *A&A* 635:A26. <https://doi.org/10.1051/0004-6361/201935565>. arXiv:2002.11070 [astro-ph.SR]
- Bazot M, Creevey O, Christensen-Dalsgaard J, Meléndez J (2018) Modelling the solar twin 18 Scorpii. *A&A* 619:A172
- Beasor ER, Davies B, Smith N, van Loon JT, Gehrz RD, Figer DF (2020) A new mass-loss rate prescription for red supergiants. *MNRAS* 492(4):5994–6006. <https://doi.org/10.1093/mnras/staa255>. arXiv:2001.07222 [astro-ph.SR]
- Beck PG, Bedding TR, Mosser B, Stello D, García RA, Kallinger T, Hekker S, Elsworth Y, Frandsen S, Carrier F, De Ridder J, Aerts C, White TR, Huber D, Dupret MA, Montalbán J, Miglio A, Noels A, Chaplin WJ, Kjeldsen H, Christensen-Dalsgaard J, Gilliland RL, Brown TM, Kawaler SD, Mathur S, Jenkins JM (2011) Kepler detected gravity-mode period spacings in a red giant star. *Science* 332(6026):205. <https://doi.org/10.1126/science.1201939>
- Beck PG, Montalbán J, Kallinger T, De Ridder J, García RA, Hekker S, Dupret MA, Mosser B, Eggenberger P, Stello D, Elsworth Y, Frandsen S, Carrier F, Hillen M, Gruberbauer M, Christensen-Dalsgaard J, Miglio A, Valentini M, Bedding TR, Kjeldsen H, Girouard FR, Hall JR, Ibrahim KA (2012) Fast core rotation in red-giant stars as revealed by gravity-dominated mixed modes. *Nature* 481(7379):55–57. <https://doi.org/10.1038/nature10612>. arXiv:1112.2825 [astro-ph.SR]
- Beck PG, Hambleton K, Vos J, Kallinger T, Bloemen S, Tkachenko A, García RA, Østensen RH, Aerts C, Kurtz DW, De Ridder J, Hekker S, Pavlovski K, Mathur S, De Smedt K, Derekas A, Corsaro E, Mosser B, Van Winckel H, Huber D, Degroote P, Davies GR, Prša A, Debusscher J, Elsworth Y, Nemeth P, Siess L, Schmid VS, Pápics PI, de Vries BL, van Marle AJ, Marcos-Arenal P, Lobel A (2014) Pulsating red giant stars in eccentric binary systems discovered from Kepler space-based photometry. A sample study and the analysis of KIC 5006817. *A&A* 564:A36. <https://doi.org/10.1051/0004-6361/201322477>. arXiv:1312.4500 [astro-ph.SR]
- Beck PG, Kallinger T, Pavlovski K, Palacios A, Tkachenko A, Mathis S, García RA, Corsaro E, Johnston C, Mosser B, Ceillier T, do Nascimento JD, Raskin G (2018a) Seismic probing of the first dredge-up event through the eccentric red-giant and red-giant spectroscopic binary KIC 9163796. How different are red-giant stars with a mass ratio of 1.015? *A&A* 612:A22. <https://doi.org/10.1051/0004-6361/201731269>. arXiv:1712.05208 [astro-ph.SR]
- Beck PG, Mathis S, Gallet F, Charbonnel C, Benbakoura M, García RA, do Nascimento JD (2018b) Testing tidal theory for evolved stars by using red giant binaries observed by Kepler. *MNRAS* 479(1):L123–L128. <https://doi.org/10.1093/mnras/sly114>. arXiv:1806.07208 [astro-ph.SR]
- Bedding TR (2011) Solar-like oscillations: an observational perspective. In: Pallé PL (ed) Asteroseismology, Canary Islands Winter School of Astrophysics, vol XXII. Cambridge University Press, Cambridge. arXiv:11071723
- Belkacem K, Goupil MJ, Dupret MA, Samadi R, Baudin F, Noels A, Mosser B (2011) The underlying physical meaning of the $v_{\max}-v_c$ relation. *A&A* 530:A142. <https://doi.org/10.1051/0004-6361/201116490>. arXiv:1104.0630 [astro-ph.SR]
- Belkacem K, Samadi R, Mosser B, Goupil MJ, Ludwig HG (2013) On the seismic scaling relations $\Delta v-\rho$ and $v_{\max}-v_c$. In: Shibahashi H, Lynas-Gray AE (eds) Progress in physics of the Sun and stars: A new era in helio- and asteroseismology, ASP Conference Series, vol 479. Astronomical Society of the Pacific, San Francisco, p 61
- Bellinger EP, Angelou GC, Hekker S, Basu S, Ball WH, Guggenberger E (2016) Fundamental parameters of main-sequence stars in an instant with machine learning. *ApJ* 830:31. <https://doi.org/10.3847/0004-637X/830/1/31>. arXiv:1607.02137 [astro-ph.SR]

- Bellinger EP, Basu S, Hekker S, Ball WH (2017) Model-independent measurement of internal stellar structure in 16 Cygni A and B. *ApJ* 851(2):80. <https://doi.org/10.3847/1538-4357/aa9848>. [arXiv:1710.11487](https://arxiv.org/abs/1710.11487) [astro-ph.SR]
- Benbakoura M, Gaulme P, McKeever J, Sekaran S, Beck PG, Spada F, Jackiewicz J, Mathis S, Mathur S, Tkachenko A, García RA (2021) Spectroscopic and seismic analysis of red giants in eclipsing binaries discovered by Kepler. *A&A* 648:A113. <https://doi.org/10.1051/0004-6361/202037783> [arXiv:2101.05351](https://arxiv.org/abs/2101.05351) [astro-ph.SR]
- Benedict GF, Henry TJ, Franz OG, McArthur BE, Wasserman LH, Jao WC, Cargile PA, Dieterich SB, Bradley AJ, Nelan EP, Whipple AL (2016) The solar neighborhood. XXXVII: the mass-luminosity relation for main-sequence M dwarfs. *AJ* 152:141. <https://doi.org/10.3847/0004-6256/152/5/141>. [arXiv:1608.04775](https://arxiv.org/abs/1608.04775) [astro-ph.SR]
- Bennett DP, Akerlof C, Alcock C, Allsman R, Axelrod T, Cook KH, Freeman K, Griest K, Marshall S, Park HS, Perlmutter S, Peterson B, Quinn P, Rodgers A, Stubbs CW, Sutherland W (1993) The first data from the MACHO experiment. In: Akerlof CW, Srednicki MA (eds) *Texas/PASCOS '92: relativistic astrophysics and particle cosmology*, vol 688, p 612. <https://doi.org/10.1111/j.1749-6632.1993.tb43945.x>. [arXiv:astro-ph/9304014](https://arxiv.org/abs/astro-ph/9304014)
- Bergemann M, Lind K, Collet R, Magic Z, Asplund M (2012) Non-LTE line formation of Fe in late-type stars—I. Standard stars with 1D and (3D) model atmospheres. *MNRAS* 427(1):27–49. <https://doi.org/10.1111/j.1365-2966.2012.21687.x>. [arXiv:1207.2455](https://arxiv.org/abs/1207.2455) [astro-ph.SR]
- Bergemann M, Serenelli A, Schönrich R, Ruchti G, Korn A, Hekker S, Kovalev M, Mashonkina L, Gilmore G, Randich S, Asplund M, Rix HW, Casey AR, Jofré P, Pancino E, Recio-Blanco A, de Laverny P, Smiljanic R, Tautvaisiene G, Bayo A, Lewis J, Koposov S, Hourihane A, Worley C, Morbidelli L, Franciosini E, Sacco G, Magrini L, Damiani F, Bestenlehner JM (2016) The Gaia-ESO Survey: hydrogen lines in red giants directly trace stellar mass. *A&A* 594:A120. <https://doi.org/10.1051/0004-6361/201528010>. [arXiv:1606.05661](https://arxiv.org/abs/1606.05661) [astro-ph.SR]
- Bergeron P, Saffer RA, Liebert J (1992) A spectroscopic determination of the mass distribution of DA white dwarfs. *ApJ* 394:228. <https://doi.org/10.1086/171575>
- Bergeron P, Leggett SK, Ruiz MT (2001) Photometric and spectroscopic analysis of cool white dwarfs with trigonometric parallax measurements. *ApJS* 133(2):413–449. <https://doi.org/10.1086/320356>. [arXiv:astro-ph/0011286](https://arxiv.org/abs/astro-ph/0011286)
- Bestenlehner JM, Vink JS, Gräfenor G, Najarro F, Evans CJ, Bastian N, Bonanos AZ, Bressert E, Crowther PA, Doran E, Friedrich K, Hénault-Brunet V, Herrero A, de Koter A, Langer N, Lennon DJ, Maíz Apellániz J, Sana H, Soszynski I, Taylor WD (2011) The VLT-FLAMES Tarantula Survey. III. A very massive star in apparent isolation from the massive cluster R136. *A&A* 530:L14. <https://doi.org/10.1051/0004-6361/201117043>. [arXiv:1105.1775](https://arxiv.org/abs/1105.1775) [astro-ph.SR]
- Bestenlehner JM, Crowther PA, Caballero-Nieves SM, Schneider FRN, Simón-Díaz S, Brands SA, de Koter A, Gräfenor G, Herrero A, Langer N, Lennon DJ, Maíz Apellániz J, Puls J, Vink JS (2020) The R136 star cluster dissected with Hubble Space Telescope/STIS—II. Physical properties of the most massive stars in R136. *MNRAS* 499(2):1918–1936. <https://doi.org/10.1093/mnras/staa2801>. [arXiv:2009.05136](https://arxiv.org/abs/2009.05136) [astro-ph.SR]
- Blandford RD, Königl A (1979) Relativistic jets as compact radio sources. *ApJ* 232:34–48. <https://doi.org/10.1086/157262>
- Boden AF, Koresko CD, van Belle GT, Colavita MM, Dumont PJ, Gubler J, Kulkarni SR, Lane BF, Mobley D, Shao M, Wallace JK, [The PTI Collaboration], Henry GW (1999) The visual orbit of ι Pegasi. *ApJ* 515(1):356–364. <https://doi.org/10.1086/307030>. [arXiv:astro-ph/9811029](https://arxiv.org/abs/astro-ph/9811029)
- Boden AF, Torres G, Hummel CA (2005) Testing stellar models with an improved physical orbit for 12 Bootis. *ApJ* 627(1):464–476. <https://doi.org/10.1086/430058>. [arXiv:astro-ph/0502250](https://arxiv.org/abs/astro-ph/0502250)
- Bond HE, Gilliland RL, Schaefer GH, Demarque P, Girard TM, Holberg JB, Gudehus D, Mason BD, Kozhurina-Platais V, Burleigh MR, Barstow MA, Nelan EP (2015) Hubble Space Telescope astrometry of the Procyon system. *ApJ* 813(2):106. <https://doi.org/10.1088/0004-637X/813/2/106>. [arXiv:1510.00485](https://arxiv.org/abs/1510.00485) [astro-ph.SR]
- Bond HE, Bergeron P, Bédard A (2017a) Astrophysical implications of a new dynamical mass for the nearby white dwarf 40 Eridani B. *ApJ* 848(1):16. <https://doi.org/10.3847/1538-4357/aa8a63>. [arXiv:1709.00478](https://arxiv.org/abs/1709.00478) [astro-ph.SR]
- Bond HE, Schaefer GH, Gilliland RL, Holberg JB, Mason BD, Lindenblad IW, Seitz-McLeese M, Arnett WD, Demarque P, Spada F, Young PA, Barstow MA, Burleigh MR, Gudehus D (2017b) The Sirius system and its astrophysical puzzles: Hubble Space Telescope and ground-based astrometry. *ApJ* 840(2):70. <https://doi.org/10.3847/1538-4357/aa6af8>. [arXiv:1703.10625](https://arxiv.org/abs/1703.10625) [astro-ph.SR]

- Bond HE, Schaefer GH, Gilliland RL, Holberg JB, Mason BD, Lindenblad IW, Seitz-McLeese M, Arnett WD, Demarque P, Spada F, Young PA, Barstow MA, Burleigh MR, Gudehus D (2017c) The Sirius system and its astrophysical puzzles: Hubble Space Telescope and ground-based astrometry. *ApJ* 840(2):70. <https://doi.org/10.3847/1538-4357/aa6af8>. arXiv:1703.10625 [astro-ph.SR]
- Bond HE, Schaefer GH, Gilliland RL, VandenBerg DA (2020) Hubble Space Telescope astrometry of the metal-poor visual binary μ Cassiopeiae: dynamical masses, helium content, and age. *ApJ* 904(2):112. <https://doi.org/10.3847/1538-4357/abc172>. arXiv:2010.06609 [astro-ph.SR]
- Bono G, Castellani V, Marconi M (2002) Theoretical models for bump Cepheids. *ApJL* 565(2):L83–L86. <https://doi.org/10.1086/339420>. arXiv:astro-ph/0201106
- Borucki WJ, Koch D, Basri G, Batalha N, Brown T, Caldwell D, Caldwell J, Christensen-Dalsgaard J, Cochran WD, DeVore E et al (2010) Kepler planet-detection mission: introduction and first results. *Science* 327(5968):977. <https://doi.org/10.1126/science.1185402>
- Bouchy F, Deleuil M, Guillot T, Aigrain S, Carone L, Cochran WD, Almenara JM, Alonso R, Auvergne M, Baglin A et al (2011) Transiting exoplanets from the CoRoT space mission. XV. CoRoT-15b: a brown-dwarf transiting companion. *A&A* 525:A68. <https://doi.org/10.1051/0004-6361/201015276>. arXiv:1010.0179 [astro-ph.EP]
- Bowman DM, Burssens S, Pedersen MG, Johnston C, Aerts C, Buyschaert B, Michielsens M, Tkachenko A, Rogers TM, Edelmann PVF, Ratnasingham RP, Simón-Díaz S, Castro N, Moravveji E, Pope BJS, White TR, De Cat P (2019a) Low-frequency gravity waves in blue supergiants revealed by high-precision space photometry. *Nat Astron* 3:760–765. <https://doi.org/10.1038/s41550-019-0768-1>. arXiv:1905.02120 [astro-ph.SR]
- Bowman DM, Johnston C, Tkachenko A, Mkrtrichian DE, Gunsriwivat K, Aerts C (2019b) Discovery of tidally perturbed pulsations in the eclipsing binary U Gru: a crucial system for tidal asteroseismology. *ApJL* 883(1):L26. <https://doi.org/10.3847/2041-8213/ab3fb2>. arXiv:1908.08468 [astro-ph.SR]
- Brandt E, Mikołajewska J, Quiroga C, Belczyński K, Ferrer OE, García LG, Pereira CB (2005) The spectroscopic orbits and other parameters of the symbiotic binary FN Sgr. *A&A* 440(1):239–248. <https://doi.org/10.1051/0004-6361:20042552>
- Breen PG, Heggie DC (2013) Dynamical evolution of black hole subsystems in idealized star clusters. *MNRAS* 432:2779–2797. <https://doi.org/10.1093/mnras/stt628>. arXiv:1304.3401 [astro-ph.GA]
- Bressan A, Marigo P, Girardi L, Salasnich B, Dal Cero C, Rubele S, Nanni A (2012) PARSEC: stellar tracks and isochrones with the PAdova and TRieste Stellar Evolution Code. *MNRAS* 427(1):127–145. <https://doi.org/10.1111/j.1365-2966.2012.21948.x>. arXiv:1208.4498 [astro-ph.SR]
- Brogaard K, Bruntt H, Grundahl F, Clausen JV, Frandsen S, Vandenberg DA, Bedin LR (2011) Age and helium content of the open cluster NGC 6791 from multiple eclipsing binary members. I. Measurements, methods, and first results. *A&A* 525:A2. <https://doi.org/10.1051/0004-6361/201015503>. arXiv:1009.5537 [astro-ph.SR]
- Brogaard K, Vandenberg DA, Bedin LR, Milone AP, Thygesen A, Grundahl F (2017) The age of 47 Tuc from self-consistent isochrone fits to colour-magnitude diagrams and the eclipsing member V69. *MNRAS* 468(1):645–661. <https://doi.org/10.1093/mnras/stx378>. arXiv:1702.03421 [astro-ph.SR]
- Brogaard K, Hansen CJ, Miglio A, Slumstrup D, Frandsen S, Jessen-Hansen J, Lund MN, Bossini D, Thygesen A, Davies GR, Chaplin WJ, Arentoft T, Bruntt H, Grundahl F, Handberg R (2018) Establishing the accuracy of asteroseismic mass and radius estimates of giant stars—I. Three eclipsing systems at $[\text{Fe}/\text{H}] \sim -0.3$ and the need for a large high-precision sample. *MNRAS* 476(3):3729–3743. <https://doi.org/10.1093/mnras/sty268>. arXiv:1801.08167 [astro-ph.SR]
- Brott I, de Mink SE, Cantiello M, Langer N, de Koter A, Evans CJ, Hunter I, Trundle C, Vink JS (2011) Rotating massive main-sequence stars. I. Grids of evolutionary models and isochrones. *A&A* 530:A115. <https://doi.org/10.1051/0004-6361/201016113>. arXiv:1102.0530 [astro-ph.SR]
- Bugnet L, García RA, Davies GR, Mathur S, Corsaro E, Hall OJ, Rendle BM (2018) FliPer: a global measure of power density to estimate surface gravities of main-sequence solar-like stars and red giants. *A&A* 620:A38. <https://doi.org/10.1051/0004-6361/201833106>. arXiv:1809.05105 [astro-ph.SR]
- Bugnet L, García RA, Mathur S, Davies GR, Hall OJ, Lund MN, Rendle BM (2019) FliPer_{class}: in search of solar-like pulsators among TESS targets. *A&A* 624:A79. <https://doi.org/10.1051/0004-6361/201834780>. arXiv:1902.09854 [astro-ph.SR]
- Buldgen G, Reese DR, Dupret MA, Samadi R (2015) Stellar acoustic radii, mean densities, and ages from seismic inversion techniques. *A&A* 574:A42. <https://doi.org/10.1051/0004-6361/201424613>. arXiv:1411.2416 [astro-ph.SR]

- Buldgen G, Rendle B, Sonoi T, Davies GR, Miglio A, Salmon SJAJ, Reese DR, Bossini D, Eggenberger P, Noels A, Scuflaire R (2019) Mean density inversions for red giants and red clump stars. *MNRAS* 482(2):2305–2319. <https://doi.org/10.1093/mnras/sty2346>. arXiv:1808.08391 [astro-ph.SR]
- Burkert A, Ida S (2007) The separation/period gap in the distribution of extrasolar planets around stars with masses ($M \geq 1.2M_{\odot}$). *ApJ* 660(1):845–849. <https://doi.org/10.1086/512538>. arXiv:astro-ph/0608347
- Burkholder V, Massey P, Morrell N (1997) The “mass discrepancy” for massive stars: tests of models using spectroscopic binaries. *ApJ* 490(1):328–342. <https://doi.org/10.1086/304852>
- Burnett B, Binney J (2010) Stellar distances from spectroscopic observations: a new technique. *MNRAS* 407:339–354. <https://doi.org/10.1111/j.1365-2966.2010.16896.x>. arXiv:1004.4367 [astro-ph.IM]
- Bursens S, Bowman DM, Aerts C, Pedersen MG, Moravveji E, Buysschaert B (2019) New β Cep pulsators discovered with K2 space photometry. *MNRAS* 489(1):1304–1320. <https://doi.org/10.1093/mnras/stz2165>. arXiv:1908.02836 [astro-ph.SR]
- Campante TL, Veras D, North TSH, Miglio A, Morel T, Johnson JA, Chaplin WJ, Davies GR, Huber D, Kuszlewicz JS et al (2017) Weighing in on the masses of retired A stars with asteroseismology: K2 observations of the exoplanet-host star HD 212771. *MNRAS* 469(2):1360–1368. <https://doi.org/10.1093/mnras/stx876>. arXiv:1704.01794 [astro-ph.SR]
- Campbell B, Walker GAH (1979) Precision radial velocities with an absorption cell. *PASP* 91:540–545. <https://doi.org/10.1086/130535>
- Caputo F, Bono G, Fiorentino G, Marconi M, Musella I (2005) Pulsation and evolutionary masses of classical Cepheids. I. Milky Way variables. *ApJ* 629(2):1021–1033. <https://doi.org/10.1086/431641>. arXiv:astro-ph/0505149
- Cardelli JA, Clayton GC, Mathis JS (1989) The relationship between infrared, optical, and ultraviolet extinction. *ApJ* 345:245. <https://doi.org/10.1086/167900>
- Cargile PA, Stassun KG, Mathieu RD (2008) Discovery of Par 1802 as a low-mass, pre-main-sequence eclipsing binary in the Orion star-forming region. *ApJ* 674:329–335. <https://doi.org/10.1086/524346>. arXiv:0709.3356
- Carlos M, Meléndez J, Spina L, dos Santos LA, Bedell M, Ramirez I, Asplund M, Bean JL, Yong D, Yana Galarza J, Alves-Brito A (2019) The Li-age correlation: the Sun is unusually Li deficient for its age. *MNRAS* 485(3):4052–4059. <https://doi.org/10.1093/mnras/stz681>. arXiv:1903.02735 [astro-ph.SR]
- Carlos M, Meléndez J, do Nascimento JD, Castro M (2020) Li abundances for solar twins in the open cluster M67. *MNRAS* 492(1):245–249. <https://doi.org/10.1093/mnras/stz3504>. arXiv:2001.01850 [astro-ph.SR]
- Carretta E, Bragaglia A, Gratton RG, Lucatello S, Catanzaro G, Leone F, Bellazzini M, Claudi R, D’Orazi V, Momany Y, Ortolani S, Pancino E, Piotto G, Recio-Blanco A, Sabbi E (2009) Na-O anticorrelation and HB. VII. The chemical composition of first and second-generation stars in 15 globular clusters from GIRAFFE spectra. *A&A* 505:117–138. <https://doi.org/10.1051/0004-6361/200912096>. arXiv:0909.2938
- Carretta E, Bragaglia A, Gratton RG, Recio-Blanco A, Lucatello S, D’Orazi V, Cassisi S (2010) Properties of stellar generations in globular clusters and relations with global parameters. *A&A* 516:A55. <https://doi.org/10.1051/0004-6361/200913451>. arXiv:1003.1723
- Carter JA, Fabrycky DC, Ragozzine D, Holman MJ, Quinn SN, Latham DW, Buchhave LA, Van Cleve J, Cochran WD, Cote MT et al (2011) KOI-126: a triply eclipsing hierarchical triple with two low-mass stars. *Science* 331:562. <https://doi.org/10.1126/science.1201274>. arXiv:1102.0562 [astro-ph.SR]
- Casali G, Magrini L, Tognelli E, Jackson R, Jeffries RD, Lagarde N, Tautvaišienė G, Masseron T, Degl’Innocenti S, Prada Moroni PG, Kordopatis G, Pancino E, Randich S, Feltzing S, Sahlholdt C, Spina L, Friel E, Roccatagliata V, Sanna N, Bragaglia A, Drazdauskas A, Mikolaitis Š, Minkevičiūtė R, Stonkutė E, Chorniy Y, Bagdonas V, Jimenez-Esteban F, Martell S, Van der Swaelmen M, Gilmore G, Vallenari A, Bensby T, Koposov SE, Korn A, Worley C, Smiljanic R, Bergemann M, Carraro G, Damiani F, Prisinzano L, Bonito R, Franciosini E, Gonneau A, Hourihane A, Jofré P, Lewis J, Morbidelli L, Sacco G, Sousa SG, Zaggia S, Lanzafame AC, Heiter U, Frasca A, Bayo A, (2019) The Gaia-ESO survey: calibrating a relationship between age and the [C/N] abundance ratio with open clusters. *A&A* 629:A62. <https://doi.org/10.1051/0004-6361/201935282>. arXiv:1907.07350 [astro-ph.GA]
- Casares J, Jonker PG (2014) Mass measurements of stellar and intermediate-mass black holes. *Space Sci Rev* 183:223–252. <https://doi.org/10.1007/s11214-013-0030-6>. arXiv:1311.5118 [astro-ph.HE]

- Cassisi S, Salaris M (2011) A classical Cepheid in a large magellanic cloud eclipsing binary: evidence of shortcomings in current stellar evolutionary models? *ApJL* 728(2):L43. <https://doi.org/10.1088/2041-8205/728/2/L43>. arXiv:1101.0394 [astro-ph.SR]
- Castro N, Fossati L, Langer N, Simón-Díaz S, Schneider FRN, Izzard RG (2014) The spectroscopic Hertzsprung–Russell diagram of Galactic massive stars. *A&A* 570:L13. <https://doi.org/10.1051/0004-6361/201425028>. arXiv:1410.3499 [astro-ph.SR]
- Castro M, Duarte T, Pace G, do Nascimento JD (2016) Mass effect on the lithium abundance evolution of open clusters: Hyades, NGC 752, and M 67. *A&A* 590:A94. <https://doi.org/10.1051/0004-6361/201527583>. arXiv:1603.08809 [astro-ph.SR]
- Catalán S, Isern J, García-Berro E, Ribas I (2008) The initial-final mass relationship of white dwarfs revisited: effect on the luminosity function and mass distribution. *MNRAS* 387(4):1693–1706. <https://doi.org/10.1111/j.1365-2966.2008.13356.x>. arXiv:0804.3034 [astro-ph]
- Chabrier G, Gallardo J, Baraffe I (2007) Evolution of low-mass star and brown dwarf eclipsing binaries. *A&A* 472:L17–L20. <https://doi.org/10.1051/0004-6361:20077702>. arXiv:0707.1792
- Chaplin WJ, Miglio A (2013) Asteroseismology of solar-type and red-giant stars. *ARA&A* 51(1):353–392. <https://doi.org/10.1146/annurev-astro-082812-140938>. arXiv:1303.1957 [astro-ph.SR]
- Chaplin WJ, Basu S, Huber D, Serenelli A, Casagrande L, Silva Aguirre V, Ball WH, Creevey OL, Gizon L, Handberg R, Karoff C, Lutz R, Marques JP, Miglio A, Stello D, Suran MD, Pricopi D, Metcalfe TS, Monteiro MJPF, Molenda-Zakowicz J, Appourchaux T, Christensen-Dalsgaard J, Elsworth Y, García RA, Houdek G, Kjeldsen H, Bonanno A, Campante TL, Corsaro E, Gaulme P, Hekker S, Mathur S, Mosser B, Régulo C, Salabert D (2014) Asteroseismic fundamental properties of solar-type stars observed by the NASA Kepler mission. *ApJS* 210(1):1. <https://doi.org/10.1088/0067-0049/210/1/1>. arXiv:1310.4001 [astro-ph.SR]
- Chaplin WJ, Serenelli AM, Miglio A et al (2020) Age dating of an early Milky Way merger via asteroseismology of the naked-eye star ν Indi. *Nat Astron* 4:382–389. <https://doi.org/10.1038/s41550-019-0975-9>. arXiv:2001.04653 [astro-ph.GA]
- Charbonnel C (1994) Clues for non-standard mixing on the red giant branch from 12C/13C and 12C/14N ratios in evolved stars. *A&A* 282:811–820
- Charbonnel C, Lagarde N (2010) Thermohaline instability and rotation-induced mixing. I. Low- and intermediate-mass solar metallicity stars up to the end of the AGB. *A&A* 522:A10. <https://doi.org/10.1051/0004-6361/201014432>. arXiv:1006.5359 [astro-ph.SR]
- Charbonnel C, Talon S (2005) Influence of gravity waves on the internal rotation and Li abundance of solar-type stars. *Science* 309(5744):2189–2191. <https://doi.org/10.1126/science.1116849>. arXiv:astro-ph/0511265
- Charbonnel C, Zahn JP (2007) Thermohaline mixing: a physical mechanism governing the photospheric composition of low-mass giants. *A&A* 467(1):L15–L18. <https://doi.org/10.1051/0004-6361:20077274>. arXiv:astro-ph/0703302
- Chiavassa A, Pasquato E, Jorissen A, Sacuto S, Babusiaux C, Freytag B, Ludwig HG, Cruzalèbes P, Rabbia Y, Spang A, Chesneau O (2011) Radiative hydrodynamic simulations of red supergiant stars. III. Spectro-photocentric variability, photometric variability, and consequences on Gaia measurements. *A&A* 528:A120. <https://doi.org/10.1051/0004-6361/201015768>. arXiv:1012.5234 [astro-ph.SR]
- Chiosi C, Wood P, Bertelli G, Bressan A (1992) On the instability strip of the Cepheid stars. *ApJ* 387:320. <https://doi.org/10.1086/171084>
- Choi J, Dotter A, Conroy C, Cantiello M, Paxton B, Johnson BD (2016) Mesa isochrones and stellar tracks (MIST). I. Solar-scaled models. *ApJ* 823:102. <https://doi.org/10.3847/0004-637X/823/2/102>. arXiv:1604.08592 [astro-ph.SR]
- Chomiuk L, Strader J, Maccarone TJ, Miller-Jones JCA, Heinke C, Noyola E, Seth AC, Ransom S (2013) A radio-selected black hole X-ray binary candidate in the Milky Way globular cluster M62. *ApJ* 777:69. <https://doi.org/10.1088/0004-637X/777/1/69>. arXiv:1306.6624 [astro-ph.HE]
- Chontos A, Huber D, Latham DW, Bieryla A, Van Eylen V, Bedding TR, Berger T, Buchhave LA, Campante TL, Chaplin WJ et al (2019) The curious case of KOI 4: confirming Kepler’s first exoplanet detection. *AJ* 157(5):192. <https://doi.org/10.3847/1538-3881/ab0e8e>. arXiv:1903.01591 [astro-ph.EP]
- Christensen-Dalsgaard J (2014) Asteroseismology of red giants. In: Pallé PL, Esteban C (eds) *Asteroseismology, 22nd Canary Islands Winter School of Astrophysics*. Cambridge University Press, Cambridge, p 194

- Christensen-Dalsgaard J, Frandsen S (1983) Stellar 5 min oscillations. *Sol Phys* 82(1–2):469–486. <https://doi.org/10.1007/BF00145588>
- Christensen-Dalsgaard J, Schou J, Thompson MJ (1990) A comparison of methods for inverting helioseismic data. *MNRAS* 242:353–369. <https://doi.org/10.1093/mnras/242.3.353>
- Christensen-Dalsgaard J, Monteiro MJPGF, Rempel M, Thompson MJ (2011) A more realistic representation of overshoot at the base of the solar convective envelope as seen by helioseismology. *MNRAS* 414:1158–1174. <https://doi.org/10.1111/j.1365-2966.2011.18460.x>
- Christensen-Dalsgaard J, Silva Aguirre V, Cassisi S, Miller Bertolami M, Serenelli A, Stello D, Weiss A, Angelou G, Jiang C, Lebreton Y, Spada F, Bellinger EP, Deheuvels S, Ouazzani RM, Pietrinferni A, Mosumgaard JR, Townsend RHD, Battich T, Bossini D, Constantino T, Eggenberger P, Hekker S, Mazumdar A, Miglio A, Nielsen KB, Salaris M (2020) The Aarhus red giants challenge. II. Stellar oscillations in the red giant branch phase. *A&A* 635:A165. <https://doi.org/10.1051/0004-6361/201936766>. [arXiv:2002.02816](https://arxiv.org/abs/2002.02816) [astro-ph.SR]
- Christy RF (1968) The theory of Cepheid variability. *Q J R Astron Soc* 9:13
- Claret A, Torres G (2016) The dependence of convective core overshooting on stellar mass. *A&A* 592:A15. <https://doi.org/10.1051/0004-6361/201628779>
- Clausen JV, Torres G, Bruntt H, Andersen J, Nordström B, Stefanik RP, Latham DW, Southworth J (2008) Absolute dimensions of eclipsing binaries. XXVI. Setting a new standard: Masses, radii, and abundances for the F-type systems AD Bootis VZ Hydrae, and WZ Ophiuchi. *A&A* 487(3):1095–1117. <https://doi.org/10.1051/0004-6361/200809671>. [arXiv:0806.3218](https://arxiv.org/abs/0806.3218) [astro-ph]
- Clausen JV, Bruntt H, Claret A, Larsen A, Andersen J, Nordström B, Giménez A (2009) Absolute dimensions of solar-type eclipsing binaries. II. V636 Centauri: A 1.05 M_{\odot} primary with an active, cool, oversize 0.85 M_{\odot} secondary. *A&A* 502(1):253–265. <https://doi.org/10.1051/0004-6361/200912362>. [arXiv:0905.3077](https://arxiv.org/abs/0905.3077) [astro-ph.SR]
- Clausen JV, Frandsen S, Bruntt H, Olsen EH, Helt BE, Gregersen K, Juncher D, Krogstrup P (2010a) Absolute dimensions of eclipsing binaries. XXVIII. BK Pegasi and other F-type binaries: prospects for calibration of convective core overshoot. *A&A* 516:A42. <https://doi.org/10.1051/0004-6361/201014266>. [arXiv:1004.1903](https://arxiv.org/abs/1004.1903) [astro-ph.SR]
- Clausen JV, Olsen EH, Helt BE, Claret A (2010b) Absolute dimensions of eclipsing binaries. XXVII. V1130 Tauri: a metal-weak F-type system, perhaps with preference for $Y = 0.23$ – 0.24 . *A&A* 510:A91. <https://doi.org/10.1051/0004-6361/200913700>. [arXiv:0912.3108](https://arxiv.org/abs/0912.3108) [astro-ph.SR]
- Coelho HR, Chaplin WJ, Basu S, Serenelli A, Miglio A, Reese DR (2015) A test of the asteroseismic v_{max} scaling relation for solar-like oscillations in main-sequence and subgiant stars. *MNRAS* 451(3):3011–3020. <https://doi.org/10.1093/mnras/stv1175>. [arXiv:1505.06087](https://arxiv.org/abs/1505.06087) [astro-ph.SR]
- Coppola G, Marconi M, Stetson PB, Bono G, Braga VF, Ripepi V, Dall’Ora M, Musella I, Buonanno R, Fabrizio M, Ferraro I, Fiorentino G, Iannicola G, Monelli M, Nonino M, Thévenin F, Walker AR (2015) The Carina Project IX: on hydrogen and helium burning variables. *ApJ* 814(1):71. <https://doi.org/10.1088/0004-637X/814/1/71>. [arXiv:1509.02687](https://arxiv.org/abs/1509.02687) [astro-ph.SR]
- Corsaro E, De Ridder J (2014) DIAMONDS: a new Bayesian nested sampling tool. Application to peak bagging of solar-like oscillations. *A&A* 571:A71. <https://doi.org/10.1051/0004-6361/201424181>. [arXiv:1408.2515](https://arxiv.org/abs/1408.2515) [astro-ph.IM]
- Corsaro E, De Ridder J, García RA (2015) Bayesian peak bagging analysis of 19 low-mass low-luminosity red giants observed with Kepler. *A&A* 579:A83. <https://doi.org/10.1051/0004-6361/201525895>. [arXiv:1503.08821](https://arxiv.org/abs/1503.08821) [astro-ph.SR]
- Corsaro E, Mathur S, García RA, Gaulme P, Pinsonneault M, Stassun K, Stello D, Tayar J, Trampedach R, Jiang C, Nitschelm C, Salabert D (2017) Metallicity effect on stellar granulation detected from oscillating red giants in open clusters. *A&A* 605:A3. <https://doi.org/10.1051/0004-6361/201731094>. [arXiv:1707.07474](https://arxiv.org/abs/1707.07474) [astro-ph.SR]
- Córsico AH (2020) White-dwarf asteroseismology with the Kepler space telescope. *Front Astron Space Sci* 7:47. <https://doi.org/10.3389/fspas.2020.00047>. [arXiv:2006.04955](https://arxiv.org/abs/2006.04955) [astro-ph.SR]
- Córsico AH, Althaus LG, Miller Bertolami MM, Kepler SO (2019) Pulsating white dwarfs: new insights. *Astron Astrophys Rev* 27(1):7. <https://doi.org/10.1007/s00159-019-0118-4>. [arXiv:1907.00115](https://arxiv.org/abs/1907.00115) [astro-ph.SR]
- Costa G, Girardi L, Bressan A, Marigo P, Rodrigues TS, Chen Y, Lanza A, Goudfrooij P (2019) Mixing by overshooting and rotation in intermediate-mass stars. *MNRAS* 485(4):4641–4657. <https://doi.org/10.1093/mnras/stz728>. [arXiv:1903.04368](https://arxiv.org/abs/1903.04368) [astro-ph.SR]
- Cox AN (1980) The masses of Cepheids. *ARA&A* 18:15–41. <https://doi.org/10.1146/annurev.aa.18.090180.000311>

- Creevey OL, Benedict GF, Brown TM, Alonso R, Cargile P, Mandushev G, Charbonneau D, McArthur BE, Cochran W, O'Donovan FT et al (2005) A new detached M dwarf eclipsing binary. *ApJ* 625:L127–L130. <https://doi.org/10.1086/431278>. arXiv:astro-ph/0504490
- Cukanovaite E, Tremblay PE, Freytag B, Ludwig HG, Bergeron P (2018) Pure-helium 3D model atmospheres of white dwarfs. *MNRAS* 481(2):1522–1537. <https://doi.org/10.1093/mnras/sty2383>. arXiv:1809.00590 [astro-ph.SR]
- Cummings JD, Kalirai JS, Choi J, Georgy C, Tremblay PE, Ramirez-Ruiz E (2019) A novel approach to constrain rotational mixing and convective-core overshoot in stars using the initial-final mass relation. *ApJL* 871(1):L18. <https://doi.org/10.3847/2041-8213/aafc2d>. arXiv:1901.02904 [astro-ph.SR]
- Cunha MS, Metcalfe TS (2007) Asteroseismic signatures of small convective cores. *ApJ* 666:413
- Cunha MS, Aerts C, Christensen-Dalsgaard J, Baglin A, Bigot L, Brown TM, Catala C, Creevey OL, Domiciano de Souza A, Eggenberger P, Garcia PJV, Grundahl F, Kervella P, Kurtz DW, Mathias P, Miglio A, Monteiro MJPF, Perrin G, Pijpers FP, Pourbaix D, Quirrenbach A, Rousset-Perraud K, Teixeira TC, Thévenin F, Thompson MJ (2007) Asteroseismology and interferometry. *Astron Astrophys Rev* 14(3–4):217–360. <https://doi.org/10.1007/s00159-007-0007-0>. arXiv:0709.4613 [astro-ph]
- Czekala I, Andrews SM, Jensen ELN, Stassun KG, Torres G, Wilner DJ (2015) A disk-based dynamical mass estimate for the young binary AK Sco. *ApJ* 806:154. <https://doi.org/10.1088/0004-637X/806/2/154>. arXiv:1505.01850 [astro-ph.SR]
- Czekala I, Andrews SM, Torres G, Jensen ELN, Stassun KG, Wilner DJ, Latham DW (2016) A disk-based dynamical constraint on the mass of the young binary DQ Tau. *ApJ* 818:156. <https://doi.org/10.3847/0004-637X/818/2/156>. arXiv:1601.03806 [astro-ph.SR]
- Czekala I, Andrews SM, Torres G, Rodriguez JE, Jensen ELN, Stassun KG, Latham DW, Wilner DJ, Gully-Santiago MA, Grankin KN, Lund MB, Kuhn RB, Stevens DJ, Siverd RJ, James D, Gaudi BS, Shappee BJ, Hololo TWS (2017a) The architecture of the GW Ori young triple-star system and its disk: dynamical masses, mutual inclinations, and recurrent eclipses. *ApJ* 851:132. <https://doi.org/10.3847/1538-4357/aa9be7>. arXiv:1710.03153 [astro-ph.EP]
- Czekala I, Mandel KS, Andrews SM, Dittmann JA, Ghosh SK, Montet BT, Newton ER (2017b) Disentangling time-series spectra with Gaussian processes: applications to radial velocity analysis. *ApJ* 840(1):49. <https://doi.org/10.3847/1538-4357/aa6aab>. arXiv:1702.05652 [astro-ph.SR]
- Da Costa GS, Freeman KC (1976) The structure and mass function of the globular cluster M3. *ApJ* 206:128–137. <https://doi.org/10.1086/154363>
- da Silva L, Girardi L, Pasquini L, Setiawan J, von der Lüh O, de Medeiros JR, Hatzes A, Döllinger MP, Weiss A (2006) Basic physical parameters of a selected sample of evolved stars. *A&A* 458:609–623. <https://doi.org/10.1051/0004-6361/20065105>. arXiv:astro-ph/0608160
- Das P, Sanders JL (2019) MADE: a spectroscopic mass, age, and distance estimator for red giant stars with Bayesian machine learning. *MNRAS* 484(1):294–304. <https://doi.org/10.1093/mnras/sty2776>. arXiv:1804.09596 [astro-ph.GA]
- David TJ, Stauffer J, Hillenbrand LA, Cody AM, Conroy K, Stassun KG, Pope B, Aigrain S, Gillen E, Collier Cameron A et al (2015) HII 2407: an eclipsing binary revealed by K2 observations of the Pleiades. *ApJ* 814(1):62. <https://doi.org/10.1088/0004-637X/814/1/62>. arXiv:1510.06399 [astro-ph.SR]
- David TJ, Hillenbrand LA, Cody AM, Carpenter JM, Howard AW (2016) K2 discovery of young eclipsing binaries in Upper Scorpius: direct mass and radius determinations for the lowest mass stars and initial characterization of an eclipsing brown dwarf binary. *ApJ* 816:21. <https://doi.org/10.3847/0004-637X/816/1/21>. arXiv:1510.08087 [astro-ph.SR]
- Davies B, Beasor ER (2020) The ‘red supergiant problem’: the upper luminosity boundary of Type II supernova progenitors. *MNRAS* 493(1):468–476. <https://doi.org/10.1093/mnras/staa1174>. arXiv:2001.06020 [astro-ph.SR]
- Davies GR, Silva Aguirre V, Bedding TR, Handberg R, Lund MN, Chaplin WJ, Huber D, White TR, Benomar O, Hekker S, Basu S, Campante TL, Christensen-Dalsgaard J, Elsworth Y, Karoff C, Kjeldsen H, Lundkvist MS, Metcalfe TS, Stello D (2016) Oscillation frequencies for 35 Kepler solar-type planet-hosting stars using Bayesian techniques and machine learning. *MNRAS* 456(2):2183–2195. <https://doi.org/10.1093/mnras/stv2593>
- de Boer TJL, Tolstoy E, Saha A, Olsen K, Irwin MJ, Battaglia G, Hill V, Shetrone MD, Fiorentino G, Cole A (2011) Deep wide-field imaging down to the oldest main sequence turn-offs in the Sculptor

- dwarf spheroidal galaxy. *A&A* 528:A119. <https://doi.org/10.1051/0004-6361/201016398>. arXiv:1103.0015 [astro-ph.CO]
- de Boer TJL, Tolstoy E, Hill V, Saha A, Olsen K, Starkeburg E, Lemasle B, Irwin MJ, Battaglia G (2012) The star formation and chemical evolution history of the Sculptor dwarf spheroidal galaxy. *A&A* 539:A103. <https://doi.org/10.1051/0004-6361/201118378>. arXiv:1201.2408 [astro-ph.CO]
- De Marco O, Izzard RG (2017) Dawes review 6: the impact of companions on stellar evolution. *PASA* 34:e001. <https://doi.org/10.1017/pasa.2016.52>. arXiv:1611.03542 [astro-ph.SR]
- De Ridder J, Molenberghs G, Eyer L, Aerts C (2016) Asteroseismic versus Gaia distances: a first comparison. *A&A* 595:L3. <https://doi.org/10.1051/0004-6361/201629799>. arXiv:1609.08945 [astro-ph.SR]
- Deal M, Alecian G, Lebreton Y, Goupil MJ, Marques JP, LeBlanc F, Morel P, Pichon B (2018) Impacts of radiative accelerations on solar-like oscillating main-sequence stars. *A&A* 618:A10. <https://doi.org/10.1051/0004-6361/201833361>. arXiv:1806.10533 [astro-ph.SR]
- Deal M, Goupil MJ, Marques JP, Reese DR, Lebreton Y (2020) Chemical mixing in low mass stars. I. Rotation against atomic diffusion including radiative acceleration. *A&A* 633:A23. <https://doi.org/10.1051/0004-6361/201936666>. arXiv:1910.14335 [astro-ph.SR]
- Decin L, Cox NLJ, Royer P, Van Marle AJ, Vandenbussche B, Ladjal D, Kerschbaum F, Ottensamer R, Barlow MJ, Blommaert JADL, Gomez HL, Groenewegen MAT, Lim T, Swinyard BM, Waelkens C, Tielens AGGM (2012) The enigmatic nature of the circumstellar envelope and bow shock surrounding Betelgeuse as revealed by Herschel. I. Evidence of clumps, multiple arcs, and a linear bar-like structure. *A&A* 548:A113. <https://doi.org/10.1051/0004-6361/201219792>. arXiv:1212.4870 [astro-ph.SR]
- Degroote P, Aerts C, Baglin A, Miglio A, Briquet M, Noels A, Niemczura E, Montalbán J, Bloemen S, Oreiro R, Vučković M, Smolders K, Auvergne M, Baudin F, Catala C, Michel E (2010) Deviations from a uniform period spacing of gravity modes in a massive star. *Nature* 464(7286):259–261. <https://doi.org/10.1038/nature08864>
- Deheuvels S, Michel E (2011) Constraints on the structure of the core of subgiants via mixed modes: the case of HD 49385. *A&A*. <https://doi.org/10.1051/0004-6361/201117232>
- Deheuvels S, Doğan G, Goupil MJ, Appourchaux T, Benomar O, Bruntt H, Campante TL, Casagrande L, Ceillier T, Davies GR, De Cat P, Fu JN, García RA, Lobel A, Mosser B, Reese DR, Régulo C, Schou J, Stahn T, Thygesen AO, Yang XH, Chaplin WJ, Christensen-Dalsgaard J, Eggenberger P, Gizon L, Mathis S, Molenda-Zakowicz J, Pinsonneault M (2014) Seismic constraints on the radial dependence of the internal rotation profiles of six Kepler subgiants and young red giants. *A&A*. <https://doi.org/10.1051/0004-6361/201322779>
- Deheuvels S, Brandão I, Silva Aguirre V, Ballot J, Michel E, Cunha MS, Lebreton Y, Appourchaux T (2016) Measuring the extent of convective cores in low-mass stars using Kepler data: toward a calibration of core overshooting. *A&A*. <https://doi.org/10.1051/0004-6361/201527967>
- Deleuil M, Deeg HJ, Alonso R, Bouchy F, Rouan D, Auvergne M, Baglin A, Aigrain S, Almenara JM, Barbieri M et al (2008) Transiting exoplanets from the CoRoT space mission. VI. CoRoT-Exo-3b: the first secure inhabitant of the brown-dwarf desert. *A&A* 491:889–897. <https://doi.org/10.1051/0004-6361:200810625>. arXiv:0810.0919
- Delfosse X, Forveille T, Ségransan D, Beuzit JL, Udry S, Perrier C, Mayor M (2000) Accurate masses of very low mass stars. IV. Improved mass-luminosity relations. *A&A* 364:217–224 arXiv:astro-ph/0010586
- Delorme P, Collier Cameron A, Hebb L, Rostron J, Lister TA, Norton AJ, Pollacco D, West RG (2011) Stellar rotation in the Hyades and Praesepe: gyrochronology and braking time-scale. *MNRAS* 413:2218–2234. <https://doi.org/10.1111/j.1365-2966.2011.18299.x>. arXiv:1101.1222 [astro-ph.SR]
- Demarque P, Guenther DB, Li LH, Mazumdar A, Straka CW (2008) YREC: the Yale rotating stellar evolution code. Non-rotating version, seismology applications. *Ap&SS* 316:31–41. <https://doi.org/10.1007/s10509-007-9698-y>. arXiv:0710.4003
- Dittmann JA, Irwin JM, Charbonneau D, Berta-Thompson ZK, Newton ER, Latham DW, Latham CA, Esquerdo G, Berlind P, Calkins ML (2017) Discovery and precise characterization by the MEarth Project of LP 661–13, an eclipsing binary consisting of two fully convective low-mass stars. *ApJ* 836:124. <https://doi.org/10.3847/1538-4357/836/1/124>. arXiv:1609.03591 [astro-ph.SR]
- Do Nascimento JJD, Castro M, Meléndez J, Bazot M, Théado S, Porto de Mello GF, de Medeiros JR (2009) Age and mass of solar twins constrained by lithium abundance. *A&A* 501(2):687–694. <https://doi.org/10.1051/0004-6361/200911935>. arXiv:0904.3580 [astro-ph.SR]

- Dobbie PD, Napiwotzki R, Lodieu N, Burleigh MR, Barstow MA, Jameson RF (2006) On the origin of the ultramassive white dwarf GD50. *MNRAS* 373(1):L45–L49. <https://doi.org/10.1111/j.1745-3933.2006.00240.x>. arXiv:astro-ph/0608671
- Donati JF, Collier Cameron A (1997) Differential rotation and magnetic polarity patterns on AB Doradus. *MNRAS* 291(1):1–19. <https://doi.org/10.1093/mnras/291.1.1>
- Dorman B, Rood RT, O’Connell RW (1993) Ultraviolet radiation from evolved stellar populations. I. Models. *ApJ* 419:596. <https://doi.org/10.1086/173511>. arXiv:astro-ph/9311022
- Doyle LR, Carter JA, Fabrycky DC, Slawson RW, Howell SB, Winn JN, Orosz JA, Přsa A, Welsh WF, Quinn SN et al (2011) Kepler-16: a transiting circumbinary planet. *Science* 333:1602. <https://doi.org/10.1126/science.1210923>. arXiv:1109.3432 [astro-ph.EP]
- Drazdauskas A, Tautvaišienė G, Randich S, Bragaglia A, Mikolaitis Š, Janulis R (2016) The extent of mixing in stellar interiors: the open clusters Collinder 261 and Melotte 66. *A&A* 589:A50. <https://doi.org/10.1051/0004-6361/201628138>. arXiv:1603.09529 [astro-ph.SR]
- Drechsel H, Heber U, Napiwotzki R, Østensen R, Solheim JE, Johannessen F, Schuh SL, Deetjen J, Zola S (2001) HS 0705+6700: A new eclipsing sdB binary. *A&A* 379:893–904. <https://doi.org/10.1051/0004-6361:20011376>. arXiv:astro-ph/0110217
- Dupree AK, Hartmann L, Avrett EH (1984) Chromospheres and mass loss in metal-deficient giant stars. *ApJL* 281:L37–L39. <https://doi.org/10.1086/184280>
- Dupree AK, Dotter A, Johnson CI, Marino AF, Milone AP, Bailey IJI, Crane JD, Mateo M, Olszewski EW (2017) NGC 1866: first spectroscopic detection of fast-rotating stars in a young LMC cluster. *ApJL* 846(1):L1. <https://doi.org/10.3847/2041-8213/aa85dd>. arXiv:1708.03386 [astro-ph.GA]
- Duvall JTL (1982) A dispersion law for solar oscillations. *Nature* 300(5889):242–243. <https://doi.org/10.1038/300242a0>
- Dyson FW, Eddington AS, Davidson C (1923) A determination of the deflection of light by the Sun’s gravitational field, from observations made at the total eclipse of May 29, 1919. *Mem R Astron Soc* 62:A1
- Eddington AS (1926) *The internal constitution of the stars*. Cambridge University Press, Cambridge
- Eggenberger P, Miglio A, Montalbán J, Moreira O, Noels A, Meynet G, Maeder A (2010) Effects of rotation on the evolution and asteroseismic properties of red giants. *A&A* 509:A72. <https://doi.org/10.1051/0004-6361/200912897>. arXiv:0911.5307 [astro-ph.SR]
- Eggleton PP, Yakut K (2017) Models for 60 double-lined binaries containing giants. *MNRAS* 468(3):3533–3556. <https://doi.org/10.1093/mnras/stx598>. arXiv:1611.05041 [astro-ph.SR]
- Eker Z, Soyduğan F, Soyduğan E, Bilir S, Yaz Gökçe E, Steer I, Tüysüz M, Şenyüz T, Demircan O (2015) Main-sequence effective temperatures from a revised mass-luminosity relation based on accurate properties. *AJ* 149:131. <https://doi.org/10.1088/0004-6256/149/4/131>. arXiv:1501.06585 [astro-ph.SR]
- Eker Z, Bakış V, Bilir S, Soyduğan F, Steer I, Soyduğan E, Bakış H, Alıçavuş F, Aslan G, Alpsoy M (2018) Interrelated main-sequence mass-luminosity, mass-radius, and mass-effective temperature relations. *MNRAS* 479:5491–5511. <https://doi.org/10.1093/mnras/sty1834>. arXiv:1807.02568 [astro-ph.SR]
- El-Badry K, Rix HW, Weisz DR (2018) An empirical measurement of the initial-final mass relation with Gaia white dwarfs. *ApJL* 860(2):L17. <https://doi.org/10.3847/2041-8213/aaca9c>. arXiv:1805.05849 [astro-ph.SR]
- Eldridge JJ, Tout CA (2004) The progenitors of core-collapse supernovae. *MNRAS* 353(1):87–97. <https://doi.org/10.1111/j.1365-2966.2004.08041.x>. arXiv:astro-ph/0405408
- Escorza A, Boffin HJM, Jorissen A, Van Eck S, Siess L, Van Winckel H, Karinkuzhi D, Shetye S, Pourbaix D (2017) Hertzsprung–Russell diagram and mass distribution of barium stars. *A&A* 608:A100. <https://doi.org/10.1051/0004-6361/201731832>. arXiv:1710.02029 [astro-ph.SR]
- Escorza A, Karinkuzhi D, Jorissen A, Siess L, Van Winckel H, Pourbaix D, Johnston C, Miszalski B, Oomen GM, Abdul-Masih M, Boffin HJM, North P, Manick R, Shetye S, Mikołajewska J (2019) Barium and related stars, and their white-dwarf companions. II. Main-sequence and subgiant stars. *A&A* 626:A128. <https://doi.org/10.1051/0004-6361/201935390>. arXiv:1904.04095 [astro-ph.SR]
- Exter KM, Pollacco DL, Maxted PFL, Napiwotzki R, Bell SA (2005) A study of two post-common envelope binary systems. *MNRAS* 359(1):315–327. <https://doi.org/10.1111/j.1365-2966.2005.08898.x>
- Farrell EJ, Groh JH, Meynet G, Eldridge JJ (2020) The uncertain masses of progenitors of core-collapse supernovae and direct-collapse black holes. *MNRAS* 494(1):L53–L58. <https://doi.org/10.1093/mnras/llaa035>. arXiv:2001.08711 [astro-ph.SR]

- Feiden GA, Chaboyer B (2014) Magnetic inhibition of convection and the fundamental properties of low-mass stars. II. Fully convective main-sequence stars. *ApJ* 789:53. <https://doi.org/10.1088/0004-637X/789/1/53>. arXiv:1405.1767 [astro-ph.SR]
- Fekel FC, Scarfe CD, Barlow DJ, Hartkopf WI, Mason BD, McAlister HA (2002) The quadruple system μ Orionis: three-dimensional orbit and physical parameters. *AJ* 123(3):1723–1740. <https://doi.org/10.1086/339184>
- Fekel FC, Boden AF, Tomkin J, Torres G (2009) HR 8257: a three-dimensional orbit and basic properties. *ApJ* 695(2):1527–1536. <https://doi.org/10.1088/0004-637X/695/2/1527>
- Ferguson DH, Liebert J, Haas S, Napiwotzki R, James TA (1999) Masses and other parameters of the post-common envelope binary BE Ursae Majoris. *ApJ* 518(2):866–872. <https://doi.org/10.1086/307289>
- Feuillet DK, Bovy J, Holtzman J, Girardi L, MacDonald N, Majewski SR, Nidever DL (2016) Determining ages of APOGEE giants with known distances. *ApJ* 817(1):40. <https://doi.org/10.3847/0004-637X/817/1/40>. arXiv:1511.04088 [astro-ph.GA]
- Fitzpatrick EL (1999) Correcting for the effects of interstellar extinction. *PASP* 111(755):63–75. <https://doi.org/10.1086/316293>. arXiv:astro-ph/9809387
- Fontaine G, Brassard P, Bergeron P (2001) The potential of white dwarf cosmochronology. *PASP* 113(782):409–435. <https://doi.org/10.1086/319535>
- Fontaine G, Brassard P, Charpinet S, Green EM, Randall SK, Van Grootel V (2012) A preliminary look at the empirical mass distribution of hot B subdwarf stars. *A&A* 539:A12. <https://doi.org/10.1051/0004-6361/201118220>
- Foreman-Mackey D, Morton TD, Hogg DW, Agol E, Schölkopf B (2016) The population of long-period transiting exoplanets. *AJ* 152(6):206. <https://doi.org/10.3847/0004-6256/152/6/206>. arXiv:1607.08237 [astro-ph.EP]
- Fossati L, Bagnulo S, Landstreet J, Wade G, Kochukhov O, Monier R, Weiss W, Gebran M (2008) The effect of rotation on the abundances of the chemical elements of the A-type stars in the Praesepe cluster. *A&A* 483:891–902. <https://doi.org/10.1051/0004-6361/200809467>. arXiv:0803.3540
- Fragkou V, Parker QA, Zijlstra A, Shaw R, Lykou F (2019a) The central star of planetary nebula PHR 1315–6555 and its host Galactic open cluster AL 1. *MNRAS* 484(3):3078–3092. <https://doi.org/10.1093/mnras/stz108>. arXiv:1901.04174 [astro-ph.SR]
- Fragkou V, Parker QA, Zijlstra AA, Crause L, Barker H (2019b) A high-mass planetary nebula in a Galactic open cluster. *Nat Astron* 3:851–857. <https://doi.org/10.1038/s41550-019-0796-x>. arXiv:1906.10556 [astro-ph.SR]
- Frandsen S, Lehmann H, Hekker S, Southworth J, Debusscher J, Beck P, Hartmann M, Pigulski A, Kopacki G, Kołaczowski Z, Stęślicki M, Thygesen AO, Brogaard K, Elsworth Y (2013) KIC 8410637: a 408-day period eclipsing binary containing a pulsating giant star. *A&A* 556:A138. <https://doi.org/10.1051/0004-6361/201321817>. arXiv:1307.0314 [astro-ph.SR]
- Frebel A, Norris J (2015) Near-field cosmology with extremely metal-poor stars. *ARA&A* 53:631–688. <https://doi.org/10.1146/annurev-astro-082214-122423>. arXiv:1501.06921 [astro-ph.SR]
- Fricke K, Stobie RS, Strittmatter PA (1972) The masses of Cepheid variables. *ApJ* 171:593. <https://doi.org/10.1086/151313>
- Gaifeira R, Patacas C, Fernandes J (2012) Mass-luminosity relation for FGK main sequence stars: metallicity and age contributions. *Ap&SS* 341:405–410. <https://doi.org/10.1007/s10509-012-1125-3>. arXiv:1205.5484 [astro-ph.SR]
- Gaia Collaboration, Brown AGA, Vallenari A, Prusti T et al (2016a) Gaia Data Release 1. Summary of the astrometric, photometric, and survey properties. *A&A* 595:A2. <https://doi.org/10.1051/0004-6361/201629512>. arXiv:1609.04172 [astro-ph.IM]
- Gaia Collaboration, Prusti T, de Bruijne JHJ, Brown AGA, Vallenari A, Babusiaux C, Bailer-Jones CAL, Bastian U, Biermann M, Evans DW et al (2016b) The Gaia mission. *A&A* 595:A1. <https://doi.org/10.1051/0004-6361/201629272>. arXiv:1609.04153 [astro-ph.IM]
- Gaia Collaboration, Brown AGA, Vallenari A, Prusti T, de Bruijne JHJ, Babusiaux C, Bailer-Jones CAL, Biermann M, Evans DW, Eyer L et al (2018) Gaia Data Release 2. Summary of the contents and survey properties. *A&A* 616:A1. <https://doi.org/10.1051/0004-6361/201833051>. arXiv:1804.09365
- Gallenne A, Pietrzyński G, Graczyk D, Konorski P, Kervella P, Mérand A, Gieren W, Anderson RI, Villanova S (2016) The Araucaria project: high-precision orbital parallax and masses of the eclipsing binary TZ Fornacis. *A&A* 586:A35. <https://doi.org/10.1051/0004-6361/201526764>. arXiv:1511.07971 [astro-ph.SR]

- Gallenne A, Pietrzyński G, Graczyk D, Pilecki B, Storm J, Nardetto N, Taormina M, Gieren W, Tkachenko A, Kervella P, Mérand A, Weber M (2019) The Araucaria project: high-precision orbital parallax and masses of eclipsing binaries from infrared interferometry. *A&A* 632:A31. <https://doi.org/10.1051/0004-6361/201935837>. arXiv:1910.03393 [astro-ph.SR]
- Gallo E, Fender RP, Miller-Jones JCA, Merloni A, Jonker PG, Heinz S, Maccarone TJ, van der Klis M (2006) A radio-emitting outflow in the quiescent state of A0620-00: implications for modelling low-luminosity black hole binaries. *MNRAS* 370:1351–1360. <https://doi.org/10.1111/j.1365-2966.2006.10560.x>. arXiv:astro-ph/0605376
- Gandolfi D, Parviainen H, Fridlund M, Hatzes AP, Deeg HJ, Frasca A, Lanza AF, Prada Moroni PG, Tognelli E, McQuillan A, Aigrain S, Alonso R, Antoci V, Cabrera J, Carone L, Csizmadia S, Djupvik AA, Guenther EW, Jessen-Hansen J, Ofir A, Telting J (2013) Kepler-77b: a very low albedo, Saturn-mass transiting planet around a metal-rich solar-like star. *A&A* 557:A74. <https://doi.org/10.1051/0004-6361/201321901>. arXiv:1305.3891 [astro-ph.EP]
- Gandolfi D, Barragán O, Hatzes AP, Fridlund M, Fossati L, Donati P, Johnson MC, Nowak G, Prieto-Arranz J, Albrecht S et al (2017) The transiting multi-planet system HD 3167: a 5.7 M_{\oplus} super-Earth and an 8.3 M_{\oplus} mini-Neptune. *AJ* 154(3):123. <https://doi.org/10.3847/1538-3881/aa832a>. arXiv:1706.02532 [astro-ph.EP]
- Gandolfi D, Barragán O, Livingston JH, Fridlund M, Justesen AB, Redfield S, Fossati L, Mathur S, Grziwa S, Cabrera J et al (2018) TESS's first planet. A super-Earth transiting the naked-eye star π Mensae. *A&A* 619:L10. <https://doi.org/10.1051/0004-6361/201834289>. arXiv:1809.07573 [astro-ph.EP]
- García RA, Ballot J (2019) Asteroseismology of solar-type stars. *Living Rev Sol Phys* 16:4. <https://doi.org/10.1007/s41116-019-0020-1>. arXiv:1906.12262 [astro-ph.SR]
- García EV, Stassun KG, Pavlovski K, Hensberge H, Gómez Maqueo Chew Y, Claret A (2014) A strict test of stellar evolution models: the absolute dimensions of the massive benchmark eclipsing binary V578 Mon. *AJ* 148(3):39. <https://doi.org/10.1088/0004-6256/148/3/39>. arXiv:1405.0739 [astro-ph.SR]
- García-Berro E, Torres S, Althaus LG, Renedo I, Lorén-Aguilar P, Córscico AH, Rohrmann RD, Salaris M, Isern J (2010) A white dwarf cooling age of 8 Gyr for NGC 6791 from physical separation processes. *Nature* 465(7295):194–196. <https://doi.org/10.1038/nature09045>. arXiv:1005.2272 [astro-ph.SR]
- Gardner T, Monnier JD, Fekel FC, Williamson M, Duncan DK, White TR, Ireland M, Adams FC, Barman T, Baron F, ten Brummelaar T, Che X, Huber D, Kraus S, Roettenbacher RM, Schaefer G, Sturmann J, Sturmman L, Swihart SJ, Zhao M (2018) Precision orbit of δ Delphini and prospects for astrometric detection of exoplanets. *ApJ* 855(1):1. <https://doi.org/10.3847/1538-4357/aaac80>. arXiv:1802.00468 [astro-ph.SR]
- Gaulme P, McKeever J, Jackiewicz J, Rawls ML, Corsaro E, Mosser B, Southworth J, Mahadevan S, Bender C, Deshpande R (2016) Testing the asteroseismic scaling relations for red giants with eclipsing binaries observed by Kepler. *ApJ* 832(2):121. <https://doi.org/10.3847/0004-637X/832/2/121>. arXiv:1609.06645 [astro-ph.SR]
- Genest-Beaulieu C, Bergeron P (2019) A comprehensive spectroscopic and photometric analysis of DA and DB white dwarfs from SDSS and Gaia. *ApJ* 871(2):169. <https://doi.org/10.3847/1538-4357/aafac6>
- Gentile Fusillo NP, Tremblay PE, Gänsicke BT, Manser CJ, Cunningham T, Cukanovaite E, Hollands M, Marsh T, Raddi R, Jordan S, Toonen S, Geier S, Barstow M, Cummings JD (2019) A Gaia Data Release 2 catalogue of white dwarfs and a comparison with SDSS. *MNRAS* 482(4):4570–4591. <https://doi.org/10.1093/mnras/sty3016>. arXiv:1807.03315 [astro-ph.SR]
- Georgy C, Ekström S, Eggenberger P, Meynet G, Haemmerlé L, Maeder A, Granada A, Groh JH, Hirschi R, Mowlavi N et al (2013) Grids of stellar models with rotation. III. Models from 0.8 to 120 M_{\odot} at a metallicity $Z = 0.002$. *A&A* 558:A103. <https://doi.org/10.1051/0004-6361/201322178>. arXiv:1308.2914 [astro-ph.SR]
- Ghezzi L, Montet BT, Johnson JA (2018) Retired a stars revisited: an updated giant planet occurrence rate as a function of stellar metallicity and mass. *ApJ* 860(2):109. <https://doi.org/10.3847/1538-4357/aac37c>. arXiv:1804.09082 [astro-ph.SR]
- Giammichele N, Charpinet S, Fontaine G, Brassard P, Green EM, Van Grootel V, Bergeron P, Zong W, Dupret MA (2018) A large oxygen-dominated core from the seismic cartography of a pulsating white dwarf. *Nature* 554(7690):73–76. <https://doi.org/10.1038/nature25136>

- Gianninas A, Bergeron P, Ruiz MT (2011) A spectroscopic survey and analysis of bright, hydrogen-rich white dwarfs. *ApJ* 743(2):138. <https://doi.org/10.1088/0004-637X/743/2/138>. arXiv:1109.3171 [astro-ph.SR]
- Gieles M, Zocchi A (2015) A family of lowered isothermal models. *MNRAS* 454:576–592. <https://doi.org/10.1093/mnras/stv1848>. arXiv:1508.02120 [astro-ph.IM]
- Gieles M, Balbinot E, Yaaqib RISM, Hénault-Brunet V, Zocchi A, Peuten M, Jonker PG (2018) Mass models of NGC 6624 without an intermediate-mass black hole. *MNRAS* 473:4832–4839. <https://doi.org/10.1093/mnras/stx2694>. arXiv:1709.06874
- Giersz M, Heggie DC (2011) Monte Carlo simulations of star clusters—VII. The globular cluster 47 Tuc. *MNRAS* 410:2698–2713. <https://doi.org/10.1111/j.1365-2966.2010.17648.x>. arXiv:1008.3048 [astro-ph.GA]
- Giesers B, Dreizler S, Husser TO, Kamann S, Anglada Escudé G, Brinchmann J, Carollo CM, Roth MM, Weilbacher PM, Wisotzki L (2018) A detached stellar-mass black hole candidate in the globular cluster NGC 3201. *MNRAS* 475:L15–L19. <https://doi.org/10.1093/mnrasl/slx203>. arXiv:1801.05642 [astro-ph.SR]
- Gillen E, Aigrain S, McQuillan A, Bouvier J, Hodgkin S, Alencar SHP, Terquem C, Southworth J, Gibson NP, Cody A et al (2014) CoRoT 223992193: a new, low-mass, pre-main sequence eclipsing binary with evidence of a circumbinary disk. *A&A* 562:A50. <https://doi.org/10.1051/0004-6361/201322493>. arXiv:1311.3990 [astro-ph.SR]
- Gómez Maqueo Chew Y, Stassun KG, Prša A, Stempels E, Hebb L, Barnes R, Heller R, Mathieu RD (2012) Luminosity discrepancy in the equal-mass, pre-main-sequence eclipsing binary Par 1802: non-coevality or tidal heating? *ApJ* 745:58. <https://doi.org/10.1088/0004-637X/745/1/58>. arXiv:1111.2322 [astro-ph.SR]
- González-Santamaría I, Manteiga M, Manchado A, Ulla A, Dafonte C (2019) Properties of central stars of planetary nebulae with distances in Gaia DR2. *A&A* 630:A150. <https://doi.org/10.1051/0004-6361/201936162>. arXiv:1909.04601 [astro-ph.SR]
- González-Santamaría I, Manteiga M, Manchado A, Ulla A, Dafonte C (2020) Gaia DR2 distances to planetary Nebulae. *Galaxies* 8(2):29. <https://doi.org/10.3390/galaxies8020029>
- Gossage S, Conroy C, Dotter A, Choi J, Rosenfield P, Cargile P, Dolphin A (2018) Age determinations of the Hyades, Praesepe, and Pleiades via MESA models with rotation. *ApJ* 863:67. <https://doi.org/10.3847/1538-4357/aad0a0>. arXiv:1804.06441 [astro-ph.SR]
- Grabhorn RP, Cohn HN, Lugger PM, Murphy BW (1992) Evolving, dynamical models for collapsed-core globular clusters—M15 and NGC 6624. *ApJ* 392:86–98. <https://doi.org/10.1086/171408>
- Graczyk D, Pietrzyński G, Thompson IB, Gieren W, Pilecki B, Konorski P, Udalski A, Soszyński I, Villanova S, Górski M et al (2014) The Araucaria Project. The distance to the small magellanic cloud from late-type eclipsing binaries. *ApJ* 780(1):59. <https://doi.org/10.1088/0004-637X/780/1/59>. arXiv:1311.2340 [astro-ph.CO]
- Graczyk D, Smolec R, Pavlovski K, Southworth J, Pietrzyński G, Maxted PFL, Konorski P, Gieren W, Pilecki B, Taormina M et al (2016) A solar twin in the eclipsing binary LL Aquarii. *A&A* 594:A92. <https://doi.org/10.1051/0004-6361/201628918>. arXiv:1608.01000 [astro-ph.SR]
- Graczyk D, Pietrzyński G, Thompson IB, Gieren W, Pilecki B, Konorski P, Villanova S, Górski M, Suchomska K, Karczmarek P, Stepień K, Storm J, Taormina M, Kołaczowski Z, Wielgórski P, Narloch W, Zgirski B, Gallenne A, Ostrowski J, Smolec R, Udalski A, Soszyński I, Kervella P, Nardetto N, Szymański MK, Wyrzykowski Ł, Ulaczyk K, Poleski R, Pietrukowicz P, Kozłowski S, Skowron J, Mróz P (2018) The late-type eclipsing binaries in the Large Magellanic Cloud: catalog of fundamental physical parameters. *ApJ* 860(1):1. <https://doi.org/10.3847/1538-4357/aac2bf>. arXiv:1805.04952 [astro-ph.SR]
- Gräfenor G, Vink JS, de Koter A, Langer N (2011) The Eddington factor as the key to understand the winds of the most massive stars. Evidence for a Γ -dependence of Wolf–Rayet type mass loss. *A&A* 535:A56. <https://doi.org/10.1051/0004-6361/201116701>. arXiv:1106.5361 [astro-ph.SR]
- Gratton RG, Sneden C, Carretta E, Bragaglia A (2000) Mixing along the red giant branch in metal-poor field stars. *A&A* 354:169–187
- Grevesse N, Sauval AJ (1998) Standard solar composition. *Space Sci Rev* 85:161–174. <https://doi.org/10.1023/A:1005161325181>
- Griffin REM, Marshall KP, Griffin RF, Schroeder KP (1995) Optical spectra of ζ Aurigae binary systems. VII. The 1987 and 1989 eclipses of HR 6902. *A&A* 301:217
- Groenewegen MAT, Decin L, Salaris M, De Cat P (2007) The Pleiades eclipsing binary HD 23642 revisited. *A&A* 463(2):579–587. <https://doi.org/10.1051/0004-6361:20066303>

- Gruberbauer M, Guenther DB, Kallinger T (2012) Toward a new kind of asteroseismic grid fitting. *ApJ* 749(2):109. <https://doi.org/10.1088/0004-637X/749/2/109>. arXiv:1202.2330 [astro-ph.SR]
- Grundahl F, Fredslund Andersen M, Christensen-Dalsgaard J, Antoci V, Kjeldsen H, Handberg R, Houdek G, Bedding TR, Pallé PL, Jessen-Hansen J, Silva Aguirre V, White TR, Frandsen S, Albrecht S, Andersen MI, Arentoft T, Brogaard K, Chaplin WJ, Harpsøe K, Jørgensen UG, Karovicova I, Karoff C, Kjærgaard Rasmussen P, Lund MN, Sloth Lundkvist M, Skottfelt J, Norup Sørensen A, Tronsgaard R, Weiss E (2017) First results from the HERTzsprung SONG Telescope: asteroseismology of the G5 subgiant star μ Herculis. *ApJ* 836(1):142
- Guenther DB (1994) Nonadiabatic nonradial p-mode frequencies of the standard solar model, with and without helium diffusion. *ApJ* 422:400–411. <https://doi.org/10.1086/173735>
- Guilloteau S, Dutrey A (1998) Physical parameters of the Keplerian protoplanetary disk of DM Tauri. *A&A* 339:467–476
- Gunn JE, Griffin RF (1979) Dynamical studies of globular clusters based on photoelectric radial velocities of individual stars. I—M3. *AJ* 84:752–773. <https://doi.org/10.1086/112477>
- Guzik JA, Houdek G, Chaplin WJ, Smalley B, Kurtz DW, Gilliland RL, Mullally F, Rowe JF, Bryson ST, Still MD, Antoci V, Appourchaux T, Basu S, Bedding TR, Benomar O, García RA, Huber D, Kjeldsen H, Latham DW, Metcalfe TS, Pápics PI, White TR, Aerts C, Ballot J, Boyajian TS, Briquet M, Bruntt H, Buchhave LA, Campante TL, Catanzaro G, Christensen-Dalsgaard J, Davies GR, Doğan G, Dragomir D, Doyle AP, Elsworth Y, Frasca A, Gaulme P, Gruberbauer M, Handberg R, Hekker S, Karoff C, Lehmann H, Mathias P, Mathur S, Miglio A, Molenda-Zakowicz J, Mosser B, Murphy SJ, Régulo C, Ripepi V, Salabert D, Sousa SG, Stello D, Uytterhoeven K (2016) Detection of solar-like oscillations, observational constraints, and stellar models for θ Cyg, the brightest star observed by the Kepler mission. *ApJ* 831(1):17
- Hadrava P (1995) Orbital elements of multiple spectroscopic stars. *A&AS* 114:393
- Halbwachs JL, Arenou F, Pourbaix D, Famaey B, Lebreton Y, Salomon JB, Tal-Or L, Ibata R, Mazeh T (2014) Masses of the components of SB2 binaries observed with Gaia—I. Selection of the sample and mass ratios of 20 new SB2s discovered with Sophie. *MNRAS* 445(3):2371–2377. <https://doi.org/10.1093/mnras/stu1838>. arXiv:1409.1384 [astro-ph.SR]
- Halbwachs JL, Boffin HJM, Le Bouquin JB, Kiefer F, Famaey B, Salomon JB, Arenou F, Pourbaix D, Antonioz F, Grellmann R et al (2016) Masses of the components of SB2s observed with Gaia—II. Masses derived from PIONIER interferometric observations for Gaia validation. *MNRAS* 455(3):3303–3311. <https://doi.org/10.1093/mnras/stv2497>. arXiv:1510.07412 [astro-ph.SR]
- Halbwachs JL, Kiefer F, Lebreton Y, Boffin HJM, Arenou F, Le Bouquin JB, Famaey B, Pourbaix D, Guillout P, Salomon JB, Mazeh T (2020) Masses of the components of SB2 binaries observed with Gaia—V. Accurate SB2 orbits for 10 binaries and masses of the components of 5 binaries. *MNRAS* 496(2):1355–1368. <https://doi.org/10.1093/mnras/staa1571>. arXiv:2006.01467 [astro-ph.SR]
- Hall OJ, Davies GR, Elsworth YP, Miglio A, Bedding TR, Brown AGA, Khan S, Hawkins K, García RA, Chaplin WJ, North TSH (2019) Testing asteroseismology with Gaia DR2: hierarchical models of the Red Clump. *MNRAS* 486(3):3569–3585. <https://doi.org/10.1093/mnras/stz1092>. arXiv:1904.07919 [astro-ph.SR]
- Handberg R, Brogaard K, Miglio A, Bossini D, Elsworth Y, Slumstrup D, Davies GR, Chaplin WJ (2017) NGC 6819: testing the asteroseismic mass scale, mass loss and evidence for products of non-standard evolution. *MNRAS* 472(1):979–997. <https://doi.org/10.1093/mnras/stx1929>. arXiv:1707.08223 [astro-ph.SR]
- Handler G, Kurtz DW, Rappaport SA, Saio H, Fuller J, Jones D, Guo Z, Chowdhury S, Sowicka P, Kahraman Aliçavuş F, Streamer M, Murphy SJ, Gagliano R, Jacobs TL, Vandenberg A (2020) Tidally trapped pulsations in a close binary star system discovered by TESS. *Nat Astron* 4:684–689. <https://doi.org/10.1038/s41550-020-1035-1>. arXiv:2003.04071 [astro-ph.SR]
- Hansen BMS (1999) Cooling models for old white dwarfs. *ApJ* 520(2):680–695. <https://doi.org/10.1086/307476>. arXiv:astro-ph/9903025
- Hartman JD, Quinn SN, Bakos GÁ, Torres G, Kovács G, Latham DW, Noyes RW, Shporer A, Fulton BJ, Esquerdo GA et al (2018) HAT-TR-318-007: a double-lined M dwarf binary with total secondary eclipses discovered by HATNet and observed by K2. *AJ* 155:114. <https://doi.org/10.3847/1538-3881/aaa844>. arXiv:1801.03570 [astro-ph.SR]
- Hasselquist S, Holtzman JA, Shetrone M, Tayar J, Weinberg DH, Feuillet D, Cunha K, Pinsonneault MH, Johnson JA, Bird J, Beers TC, Schiavon R, Minchev I, Fernández-Trincado JG, García-Hernández DA, Nitschelm C, Zamora O (2019) APOGEE [C/N] abundances across the Galaxy: migration and

- infall from red giant ages. *ApJ* 871(2):181. <https://doi.org/10.3847/1538-4357/aaf859>. arXiv:1812.05092 [astro-ph.GA]
- Heber U (2016) Hot subluminal stars. *PASP* 128(966):082001. <https://doi.org/10.1088/1538-3873/128/966/082001>. arXiv:1604.07749 [astro-ph.SR]
- Heiter U, Eriksson K (2006) Geometry of giant star model atmospheres: a consistency test. *A&A* 452(3):1039–1048. <https://doi.org/10.1051/0004-6361/20064925>. arXiv:astro-ph/0603273
- Hekker S (2020) Scaling relations for solar-like oscillations: a review. *Front Astron Space Sci* 7:3. <https://doi.org/10.3389/fspas.2020.00003>. arXiv:1907.10457 [astro-ph.SR]
- Hekker S, Ball WH (2014) Grid-based seismic modelling at high and low signal-to-noise ratios. HD 181420 and HD 175272. *A&A* 564:A105. <https://doi.org/10.1051/0004-6361/201323121>. arXiv:1403.3529 [astro-ph.SR]
- Hekker S, Christensen-Dalsgaard J (2017) Giant star seismology. *Astron Astrophys Rev* 25:1. <https://doi.org/10.1007/s00159-017-0101-x>. arXiv:1609.07487 [astro-ph.SR]
- Helminiak KG, Konacki M (2011) Orbital and physical parameters of eclipsing binaries from the All-Sky Automated Survey catalogue. II. Two spotted $M < 1M_{\odot}$ systems at different evolutionary stages. *A&A* 526:A29. <https://doi.org/10.1051/0004-6361/200913336>. arXiv:1009.5610 [astro-ph.SR]
- Helminiak KG, Graczyk D, Konacki M, Pilecki B, Ratajczak M, Pietrzyński G, Sybilski P, Villanova S, Gieren W, Pojmański G et al (2015) Orbital and physical parameters of eclipsing binaries from the ASAS catalogue—VIII. The totally eclipsing double-giant system HD 187669. *MNRAS* 448(2):1945–1955. <https://doi.org/10.1093/mnras/stu2680>. arXiv:1412.4834 [astro-ph.SR]
- Helminiak KG, Konacki M, Maehara H, Kambe E, Ukita N, Ratajczak M, Pigulski A, Kozłowski SK (2019) HIDES spectroscopy of bright detached eclipsing binaries from the Kepler field—III. Spectral analysis, updated parameters and new systems. *MNRAS* 484(1):451–475. <https://doi.org/10.1093/mnras/sty3528>. arXiv:1901.00407 [astro-ph.SR]
- Hénault-Brunet V, Gieles M, Strader J, Peuten M, Balbinot E, Douglas KEK (2020) On the black hole content and initial mass function of 47 Tuc. *MNRAS* 491(1):113–128. <https://doi.org/10.1093/mnras/stz2995>. arXiv:1908.08538 [astro-ph.GA]
- Hendriks L, Aerts C (2019) Deep learning applied to the asteroseismic modeling of stars with coherent oscillation modes. *PASP* 131(1004):108001. <https://doi.org/10.1088/1538-3873/aaeeec>. arXiv:1811.03639 [astro-ph.SR]
- Hensberge H, Pavlovski K, Verschuere W (2000) The eclipsing binary V578 Mon in the Rosette nebula: age and distance to NGC 2244 using Fourier disentangled component spectra. *A&A* 358:553–571
- Hermes JJ, Gänsicke BT, Kawaler SD, Greiss S, Tremblay PE, Gentile Fusillo NP, Raddi R, Fanale SM, Bell KJ, Dennihy E, Fuchs JT, Dunlap BH, Clemens JC, Montgomery MH, Winget DE, Chote P, Marsh TR, Redfield S (2017) White dwarf rotation as a function of mass and a dichotomy of mode line widths: Kepler observations of 27 pulsating DA white dwarfs through K2 Campaign 8. *ApJS* 232(2):23. <https://doi.org/10.3847/1538-4365/aa8bb5>. arXiv:1709.07004 [astro-ph.SR]
- Herrero A, Kudritzki RP, Vilchez JM, Kunze D, Butler K, Haser S (1992) Intrinsic parameters of galactic luminous OB stars. *A&A* 261:209–234
- Herrero A, Puls J, Najarro F (2002) Fundamental parameters of Galactic luminous OB stars VI. Temperatures, masses and WLR of Cyg OB2 supergiants. *A&A* 396:949–966. <https://doi.org/10.1051/0004-6361:20021432>. arXiv:astro-ph/0210469
- Hertzsprung E (1923) On the relation between mass and absolute brightness of components of double stars. *Bull Astron Inst Neth* 2:15
- Higgins ER, Vink JS (2019) Massive star evolution: rotation, winds, and overshooting vectors in the mass-luminosity plane. I. A calibrated grid of rotating single star models. *A&A* 622:A50. <https://doi.org/10.1051/0004-6361/201834123>. arXiv:1811.12190 [astro-ph.SR]
- Higl J, Weiss A (2017) Testing stellar evolution models with detached eclipsing binaries. *A&A* 608:A62. <https://doi.org/10.1051/0004-6361/201731008>
- Hilditch RW (2001) An introduction to close binary stars. Cambridge University Press, Cambridge
- Hilditch RW, Harries TJ, Hill G (1996) On the reflection effect in three sdOB binary stars. *MNRAS* 279(4):1380–1392. <https://doi.org/10.1093/mnras/279.4.1380>
- Hillwig TC, Jones D, De Marco O, Bond HE, Margheim S, Frew D (2016) Observational confirmation of a link between common envelope binary interaction and planetary Nebula shaping. *ApJ* 832(2):125. <https://doi.org/10.3847/0004-637X/832/2/125>. arXiv:1609.02185 [astro-ph.SR]
- Hillwig TC, Frew DJ, Reindl N, Rotter H, Webb A, Margheim S (2017) Binary central stars of planetary Nebulae discovered through photometric variability. V. The central stars of HaTr 7 and ESO 330-9. *AJ* 153(1):24. <https://doi.org/10.3847/1538-3881/153/1/24>. arXiv:1612.01420 [astro-ph.SR]

- Ho AYQ, Rix HW, Ness MK, Hogg DW, Liu C, Ting YS (2017) Masses and ages for 230,000 LAMOST giants, via their carbon and nitrogen abundances. *ApJ* 841(1):40. <https://doi.org/10.3847/1538-4357/aa6db3>. arXiv:1609.03195 [astro-ph.SR]
- Howell SB, Sobeck C, Haas M, Still M, Barclay T, Mullally F, Troeltzsch J, Aigrain S, Bryson ST, Caldwell D, Chaplin WJ, Cochran WD, Huber D, Marcy GW, Miglio A, Najita JR, Smith M, Twicken JD, Fortney JJ (2014) The K2 mission: characterization and early results. *PASP* 126(938):398. <https://doi.org/10.1086/676406>. arXiv:1402.5163 [astro-ph.IM]
- Huber D, Chaplin WJ, Chontos A et al (2019) A hot Saturn orbiting an oscillating late subgiant discovered by TESS. *AJ* 157(6):245
- Hummel CA (2013) Recent advances in interferometry. In: Pavlovski K, Tkachenko A, Torres G (eds) Setting a new standard in the analysis of binary stars. EAS publications series, vol 64. EDP Sciences, pp 173–179. <https://doi.org/10.1051/eas/1364024>
- Hummel CA, Armstrong JT, Quirrenbach A, Buscher DF, Mozurkewich D, Elias INM, Wilson RE (1994) Very high precision orbit of Capella by long baseline interferometry. *AJ* 107:1859. <https://doi.org/10.1086/116995>
- Hummel CA, Armstrong JT, Buscher DF, Mozurkewich D, Quirrenbach A, Vivekanand M (1995) Orbits of small angular scale binaries resolved with the Mark III interferometer. *AJ* 110:376. <https://doi.org/10.1086/117528>
- Hummel CA, Mozurkewich D, Armstrong JT, Hajian AR, Elias INM, Hutter DJ (1998) Navy prototype optical interferometer observations of the double stars Mizar A and Matar. *AJ* 116(5):2536–2548. <https://doi.org/10.1086/300602>
- Hummel CA, Carquillat JM, Ginestet N, Griffin RF, Boden AF, Hajian AR, Mozurkewich D, Nordgren TE (2001) Orbital and stellar parameters of Omicron Leonis from spectroscopy and interferometry. *AJ* 121(3):1623–1635. <https://doi.org/10.1086/319391>
- Icko Iben J (1965) Stellar evolution. II. The evolution of a 3 M_{\odot} Star from the main sequence through core helium burning. *ApJ* 142:1447. <https://doi.org/10.1086/148429>
- Ilijić S, Hensberge H, Pavlovski K, Freyhammer LM (2004) Obtaining normalised component spectra with FDBinary. In: Hilditch RW, Hensberge H, Pavlovski K (eds) Spectroscopically and spatially resolving the components of close binary stars, ASP Conference Proceedings, vol 318. Astronomical Society of the Pacific, San Francisco, pp 111–113
- Irwin J, Buchhave L, Berta ZK, Charbonneau D, Latham DW, Burke CJ, Esquerdo GA, Everett ME, Holman MJ, Nutzman P et al (2010) NLTT 41135: a field M dwarf + brown dwarf eclipsing binary in a triple system, discovered by the MEarth observatory. *ApJ* 718:1353–1366. <https://doi.org/10.1088/0004-637X/718/2/1353>. arXiv:1006.1793 [astro-ph.SR]
- Irwin JM, Quinn SN, Berta ZK, Latham DW, Torres G, Burke CJ, Charbonneau D, Dittmann J, Esquerdo GA, Stefanik RP et al (2011) LSPM J1112+7626: detection of a 41 day M-dwarf eclipsing binary from the MEarth Transit Survey. *ApJ* 742:123. <https://doi.org/10.1088/0004-637X/742/2/123>. arXiv:1109.2055 [astro-ph.SR]
- Jancárt S, Jorissen A, Pourbaix D (2005) Hipparcos astrometric binaries in the ninth catalogue of spectroscopic binary orbits: a testbench for the detection of astrometric binaries with Gaia. In: Turon C, O’Flaherty KS, Perryman MAC (eds) The three-dimensional universe with Gaia. ESA Special Publication, vol 576. ESA, p 583. https://www.cosmos.esa.int/web/gaia/2004_proceedings
- Jofré P, Heiter U, Soubiran C, Blanco-Cuaresma S, Worley CC, Pancino E, Cantat-Gaudin T, Magrini L, Bergemann M, González Hernández JI, Hill V, Lardo C, de Laverny P, Lind K, Masseron T, Montes D, Mucciarelli A, Nordlander T, Recio-Blanco A, Sobeck J, Sordo R, Sousa SG, Tabernero H, Vallenari A, Van Eck S (2014) Gaia FGK benchmark stars: metallicity. *A&A* 564:A133
- Jofré E, Petrucci R, Saffe C, Saker L, Artur de la Villarmois E, Chavero C, Gómez M, Mauas PJD (2015) Stellar parameters and chemical abundances of 223 evolved stars with and without planets. *A&A* 574:A50
- Jofré P, Heiter U, Soubiran C (2019) Accuracy and precision of industrial stellar abundances. *ARA&A* 57:571–616. <https://doi.org/10.1146/annurev-astro-091918-104509>. arXiv:1811.08041 [astro-ph.SR]
- Johnson JA, Bowler BP, Howard AW, Henry GW, Marcy GW, Isaacson H, Brewer JM, Fischer DA, Morton TD, Crepp JR (2010) A hot Jupiter orbiting the 1.7 M_{\odot} subgiant HD 102956. *ApJL* 721(2):L153–L157. <https://doi.org/10.1088/2041-8205/721/2/L153>. arXiv:1007.4555 [astro-ph.EP]
- Johnston C, Aerts C, Pedersen MG, Bastian N (2019a) Isochrone-cloud fitting of the extended main-sequence turn-off of young clusters. *A&A* 632:A74. <https://doi.org/10.1051/0004-6361/201936549>. arXiv:1910.00591 [astro-ph.SR]

- Johnston C, Pavlovski K, Tkachenko A (2019b) Modelling of the B-type binaries CW Cephei and U Ophiuchi. A critical view on dynamical masses, core boundary mixing, and core mass. *A&A* 628:A25. <https://doi.org/10.1051/0004-6361/201935235>. arXiv:1905.12040 [astro-ph.SR]
- Johnston C, Tkachenko A, Aerts C, Molenberghs G, Bowman DM, Pedersen MG, Buyschaert B, Pápics PI (2019c) Binary asteroseismic modelling: isochrone-cloud methodology and application to Kepler gravity mode pulsators. *MNRAS* 482:1231–1246. <https://doi.org/10.1093/mnras/sty2671>. arXiv:1810.00780 [astro-ph.SR]
- Jones D (2020) Observational constraints on the common envelope phase. In: Kabáth P, Jones D, Skarka M (eds) *Reviews in frontiers of modern astrophysics: from space Debris to cosmology*. Springer, Cham, pp 123–153. https://doi.org/10.1007/978-3-030-38509-5_5
- Jones D, Van Winckel H, Aller A, Exter K, De Marco O (2017) The long-period binary central stars of the planetary nebulae NGC 1514 and LoTr 5. *A&A* 600:L9. <https://doi.org/10.1051/0004-6361/201730700>. arXiv:1703.05096 [astro-ph.SR]
- Jørgensen BR, Lindegren L (2005) Determination of stellar ages from isochrones: Bayesian estimation versus isochrone fitting. *A&A* 436:127–143. <https://doi.org/10.1051/0004-6361:20042185>
- Jørgensen ACS, Weiss A, Angelou G, Silva Aguirre V (2019) Mending the structural surface effect of 1D stellar structure models with non-solar metallicities based on interpolated 3D envelopes. *MNRAS* 484(4):5551–5567. <https://doi.org/10.1093/mnras/stz337>. arXiv:1902.04283 [astro-ph.SR]
- Joyce SRG, Barstow MA, Holberg JB, Bond HE, Casewell SL, Burleigh MR (2018) The gravitational redshift of Sirius B. *MNRAS* 481(2):2361–2370. <https://doi.org/10.1093/mnras/sty2404>. arXiv:1809.01240 [astro-ph.SR]
- Kalirai JS, Marigo P, Tremblay PE (2014) The core mass growth and stellar lifetime of thermally pulsing asymptotic giant branch stars. *ApJ* 782(1):17. <https://doi.org/10.1088/0004-637X/782/1/17>. arXiv:1312.4544 [astro-ph.SR]
- Kallinger T, Mosser B, Hekker S, Huber D, Stello D, Mathur S, Basu S, Bedding TR, Chaplin WJ, De Ridder J, Elsworth YP, Frand sen S, García RA, Gruberbauer M, Matthews JM, Borucki WJ, Bruntt H, Christensen-Dalsgaard J, Gilliland RL, Kjeldsen H, Koch DG (2010) Asteroseismology of red giants from the first four months of Kepler data: fundamental stellar parameters. *A&A* 522:A1. <https://doi.org/10.1051/0004-6361/201015263>. arXiv:1010.4589 [astro-ph.SR]
- Kallinger T, De Ridder J, Hekker S, Mathur S, Mosser B, Gruberbauer M, García RA, Karoff C, Ballot J (2014) The connection between stellar granulation and oscillation as seen by the Kepler mission. *A&A* 570:A41. <https://doi.org/10.1051/0004-6361/201424313>. arXiv:1408.0817 [astro-ph.SR]
- Kallinger T, Hekker S, García RA, Huber D, Matthews JM (2016) Precise stellar surface gravities from the time scales of convectively driven brightness variations. *Sci Adv* 2:1500654. <https://doi.org/10.1126/sciadv.1500654>
- Kallinger T, Beck PG, Stello D, García RA (2018) Non-linear seismic scaling relations. *A&A* 616:A104. <https://doi.org/10.1051/0004-6361/201832831>. arXiv:1805.06249 [astro-ph.SR]
- Kaluzny J, Thompson IB, Rozycka M, Dotter A, Krzeminski W, Pych W, Rucinski SM, Burley GS, Shectman SA (2013) The Cluster AgeS Experiment (CASE). V. Analysis of three eclipsing binaries in the globular cluster M4. *AJ* 145:43. <https://doi.org/10.1088/0004-6256/145/2/43>. arXiv:1301.2946 [astro-ph.SR]
- Kamann S, Bastian N, Husser TO, Martocchia S, Usher C, den Brok M, Dreizler S, Kelz A, Krajnović D, Richard J et al (2018) Cluster kinematics and stellar rotation in NGC 419 with MUSE and adaptive optics. *MNRAS* 480(2):1689–1695. <https://doi.org/10.1093/mnras/sty1958>. arXiv:1807.10612 [astro-ph.GA]
- Kervella P, Mignard F, Mérand A, Thévenin F (2016) Close stellar conjunctions of α Centauri A and B until 2050. An $mK = 7.8$ star may enter the Einstein ring of α Cen A in 2028. *A&A* 594:A107
- Kervella P, Bigot L, Gallenne A, Thévenin F (2017) The radii and limb darkenings of α Centauri A and B. Interferometric measurements with VLTI/PIONIER. *A&A* 597:A137. <https://doi.org/10.1051/0004-6361/201629505>. arXiv:1610.06185 [astro-ph.SR]
- Kiefer F, Halbwegs JL, Arenou F, Pourbaix D, Famaey B, Guillout P, Lebreton Y, Nebot Gómez-Morán A, Mazeh T, Salomon JB, Soubiran C, Tal-Or L (2016) Masses of the components of SB2 binaries observed with Gaia—III. Accurate SB2 orbits for 10 binaries and masses of HIP 87895. *MNRAS* 458(3):3272–3281. <https://doi.org/10.1093/mnras/stw545>. arXiv:1603.02861 [astro-ph.SR]
- Kiefer F, Halbwegs JL, Lebreton Y, Soubiran C, Arenou F, Pourbaix D, Famaey B, Guillout P, Ibata R, Mazeh T (2018) Masses of the components of SB2 binaries observed with Gaia—IV. Accurate SB2 orbits for 14 binaries and masses of three binaries. *MNRAS* 474(1):731–745. <https://doi.org/10.1093/mnras/stx2794>. arXiv:1710.09604 [astro-ph.SR]

- Kimmig B, Seth A, Ivans II, Strader J, Caldwell N, Anderton T, Gregersen D (2015) Measuring consistent masses for 25 Milky Way globular clusters. *AJ* 149:53. <https://doi.org/10.1088/0004-6256/149/2/53>. arXiv:1411.1763
- Kippenhahn R, Weigert A, Weiss A (2012) *Stellar structure and evolution*, 2nd edn. Springer, Heidelberg. <https://doi.org/10.1007/978-3-642-30304-3>
- Kirkby-Kent JA, Maxted PFL, Serenelli AM, Turner OD, Evans DF, Anderson DR, Hellier C, West RG (2016) Absolute parameters for AI Phoenicis using WASP photometry. *A&A* 591:A124. <https://doi.org/10.1051/0004-6361/201628581>. arXiv:1605.07059 [astro-ph.SR]
- Kirkby-Kent JA, Maxted PFL, Serenelli AM, Anderson DR, Hellier C, West RG (2018) WASP 0639-32: a new F-type subgiant/K-type main-sequence detached eclipsing binary from the WASP project. *A&A* 615:A135. <https://doi.org/10.1051/0004-6361/201731435>. arXiv:1804.06718 [astro-ph.SR]
- Kjeldsen H, Bedding TR (1995) Amplitudes of stellar oscillations: the implications for asteroseismology. *A&A* 293:87–106 arXiv:astro-ph/9403015
- Koch DG, Borucki WJ, Basri G et al (2010) Kepler mission design, realized photometric performance, and early science. *ApJL* 713(2):L79–L86. <https://doi.org/10.1088/2041-8205/713/2/L79>. arXiv:1001.0268 [astro-ph.EP]
- Koester D, Schulz H, Weidemann V (1979) Atmospheric parameters and mass distribution of DA white dwarfs. *A&A* 76:262–275
- Konacki M (2005) Precision radial velocities of double-lined spectroscopic binaries with an iodine absorption cell. *ApJ* 626(1):431–438. <https://doi.org/10.1086/429880>. arXiv:astro-ph/0410389
- Konacki M, Muterspaugh MW, Kulkarni SR, Helminiak KG (2009) The radial velocity Tatooine search for circumbinary planets: planet detection limits for a sample of double-lined binary stars—initial results from Keck I/Hires, Shane/CAT/Hamspec, and TNG/Sarg observations. *ApJ* 704(1):513–521. <https://doi.org/10.1088/0004-637X/704/1/513>. arXiv:0908.3775 [astro-ph.EP]
- Konacki M, Muterspaugh MW, Kulkarni SR, Helminiak KG (2010) High-precision orbital and physical parameters of double-lined spectroscopic binary stars—HD78418, HD123999, HD160922, HD200077, and HD210027. *ApJ* 719(2):1293–1314. <https://doi.org/10.1088/0004-637X/719/2/1293>. arXiv:0910.4482 [astro-ph.SR]
- Kramer M, Stairs IH, Manchester RN, McLaughlin MA, Lyne AG, Ferdman RD, Burgay M, Lorimer DR, Possenti A, D’Amico N et al (2006) Tests of general relativity from timing the double pulsar. *Science* 314:97–102. <https://doi.org/10.1126/science.1132305>. arXiv:astro-ph/0609417
- Kraus AL, Tucker RA, Thompson MI, Craine ER, Hillenbrand LA (2011) The mass-radius(–rotation?) relation for low-mass stars. *ApJ* 728:48. <https://doi.org/10.1088/0004-637X/728/1/48>. arXiv:1011.2757 [astro-ph.SR]
- Kraus AL, Cody AM, Covey KR, Rizzuto AC, Mann AW, Ireland MJ (2015) The mass-radius relation of young stars. I. USco 5, an M4.5 eclipsing binary in Upper Scorpius observed by K2. *ApJ* 807:3. <https://doi.org/10.1088/0004-637X/807/1/3>. arXiv:1505.02446 [astro-ph.SR]
- Kraus AL, Douglas ST, Mann AW, Agüeros MA, Law NM, Covey KR, Feiden GA, Rizzuto AC, Howard AW, Isaacson H et al (2017) The factory and the beehive. III. PTFEB132.707+19.810, a low-mass eclipsing binary in Praesepe observed by PTF and K2. *ApJ* 845:72. <https://doi.org/10.3847/1538-4357/aa7e75>. arXiv:1706.09390 [astro-ph.SR]
- Kremer K, Ye CS, Chatterjee S, Rodriguez CL, Rasio FA (2018) How black holes shape globular clusters: modeling NGC 3201. *ApJL* 855:L15. <https://doi.org/10.3847/2041-8213/aab26c>. arXiv:1802.09553 [astro-ph.HE]
- Kretke KA, Lin DNC, Garaud P, Turner NJ (2009) Assembling the building blocks of giant planets around intermediate-mass stars. *ApJ* 690(1):407–415. <https://doi.org/10.1088/0004-637X/690/1/407>. arXiv:0806.1521 [astro-ph]
- Kurtz DW, Marang F (1995) The discovery of delta Scuti pulsational variability in the pre-main-sequence Herbig AE star, HR 5999, and the discovery of rotational light variability in the remarkable He-weak BP star, HR 6000. *MNRAS* 276:191–198. <https://doi.org/10.1093/mnras/276.1.191>
- Kurtz DW, Handler G, Rappaport SA, Saio H, Fuller J, Jacobs T, Schmitt A, Jones D, Vanderburg A, LaCourse D, Nelson L, Kahraman Aliçavuş F, Giarrusso M (2020) The single-sided pulsator CO Camelopardalis. *MNRAS* 494(4):5118–5133. <https://doi.org/10.1093/mnras/staa989>. arXiv:2004.03471 [astro-ph.SR]
- Lacy CHS, Fekel FC, Pavlovski K, Torres G, Muterspaugh MW (2016) Absolute properties of the pre-main-sequence eclipsing binary star NP Persei. *AJ* 152(1):2. <https://doi.org/10.3847/0004-6256/152/1/2>

- Lagarde N, Robin AC, Reyl  C, Nasello G (2017) Population synthesis to constrain Galactic and stellar physics. I. Determining age and mass of thin-disc red-giant stars. *A&A* 601:A27. <https://doi.org/10.1051/0004-6361/201630253>. arXiv:1702.01769 [astro-ph.SR]
- Lagarde N, Reyl  C, Robin AC, Tautvai ien   G, Drazdauskas A, Mikolaitis  , Minkevi iut   R, Stonkut   E, Chorniy Y, Bagdonas V, Miglio A, Nasello G, Gilmore G, Randich S, Bensby T, Bragaglia A, Flaccomio E, Francois P, Korn AJ, Pancino E, Smiljanic R, Bayo A, Carraro G, Costado MT, Jim enez-Esteban F, Jofr  P, Martell SL, Masseron T, Monaco L, Morbidelli L, Sbordone L, Sousa SG, Zaggia S (2019) The Gaia-ESO Survey: impact of extra mixing on C and N abundances of giant stars. *A&A* 621:A24. <https://doi.org/10.1051/0004-6361/201732433>. arXiv:1806.01868 [astro-ph.SR]
- Lane BF, Muterspaugh MW, Griffin RF, Scarfe CD, Fekel FC, Williamson MH, Eaton JA, Shao M, Colavita MM, Konacki M (2014) The orbits of the triple-star system 1 Geminorum from phases differential astrometry and spectroscopy. *ApJ* 783(1):3. <https://doi.org/10.1088/0004-637X/783/1/3>
- Langer N (2012) Presupernova evolution of massive single and binary stars. *ARA&A* 50:107–164. <https://doi.org/10.1146/annurev-astro-081811-125534>. arXiv:1206.5443 [astro-ph.SR]
- Larsen SS, Baumgardt H, Bastian N, Brodie JP, Grundahl F, Strader J (2015) Radial distributions of sub-populations in the globular cluster M15: a more centrally concentrated primordial population. *ApJ* 804(1):71. <https://doi.org/10.1088/0004-637X/804/1/71>. arXiv:1503.00726 [astro-ph.GA]
- Larsen SS, Baumgardt H, Bastian N, Hernandez S, Brodie J (2019) Hubble Space Telescope photometry of multiple stellar populations in the inner parts of NGC 2419. *A&A* 624:A25. <https://doi.org/10.1051/0004-6361/201834494>. arXiv:1902.01416 [astro-ph.SR]
- Latham DW, Nordstrom B, Andersen J, Torres G, Stefanik RP, Thaller M, Bester MJ (1996) Accurate mass determination for double-lined spectroscopic binaries by digital cross-correlation spectroscopy: DM Virginis revisited. *A&A* 314:864–870
- Lattimer JM (2012) The nuclear equation of state and neutron star masses. *Annu Rev Nucl Part Sci* 62:485–515. <https://doi.org/10.1146/annurev-nucl-102711-095018>. arXiv:1305.3510 [nucl-th]
- Lattimer JM, Prakash M (2001) Neutron star structure and the equation of state. *ApJ* 550(1):426–442. <https://doi.org/10.1086/319702>. arXiv:astro-ph/0002232
- Lattimer JM, Yahil A (1989) Analysis of the neutrino events from supernova 1987A. *ApJ* 340:426. <https://doi.org/10.1086/167404>
- Lebreton Y, Goupil MJ (2014) Asteroseismology for “  la carte” stellar age-dating and weighing. *A&A*. <https://doi.org/10.1051/0004-6361/201423797>
- Lebreton Y, Reese DR (2020) SPInS, a pipeline for massive stellar parameter inference. A public Python tool to age-date, weigh, size up stars, and more. *A&A* 642:A88. <https://doi.org/10.1051/0004-6361/202038602>. arXiv:2009.00037 [astro-ph.SR]
- Lebreton Y, Fernandes J, Lejeune T (2001) The helium content and age of the Hyades: constraints from five binary systems and Hipparcos parallaxes. *A&A* 374:540–553. <https://doi.org/10.1051/0004-6361:20010757>. arXiv:astro-ph/0105497
- Lee JW, Youn JH, Kim SL, Lee CU (2013) Physical properties of the low-mass eclipsing binary NSVS 02502726. *AJ* 145:16. <https://doi.org/10.1088/0004-6256/145/1/16>. arXiv:1211.1105 [astro-ph.SR]
- Lester KV, Gies DR, Schaefer GH, Farrington CD, Guo Z, Matson RA, Monnier JD, ten Brummelaar T, Sturmman J, Vargas N, Weiss SA (2019a) Visual orbits of spectroscopic binaries with the CHARA Array. II. The eclipsing binary HD 185912. *AJ* 158(6):218. <https://doi.org/10.3847/1538-3881/ab449d>. arXiv:1909.09161 [astro-ph.SR]
- Lester KV, Gies DR, Schaefer GH, Farrington CD, Monnier JD, ten Brummelaar T, Sturmman J, Vargas N (2019b) Visual orbits of spectroscopic binaries with the CHARA Array. I. HD 224355. *AJ* 157(4):140. <https://doi.org/10.3847/1538-3881/ab064d>. arXiv:1902.05557 [astro-ph.SR]
- Lester KV, Fekel FC, Muterspaugh M, Gies DR, Schaefer GH, Farrington CD, Guo Z, Matson RA, Monnier JD, ten Brummelaar T, Sturmman J, Weiss SA (2020) Visual orbits of spectroscopic binaries with the CHARA Array. III. HD 8374 and HD 24546. *AJ* 160(2):58. <https://doi.org/10.3847/1538-3881/ab8f95>. arXiv:2005.00546 [astro-ph.SR]
- Leung HW, Bovy J (2019) Deep learning of multi-element abundances from high-resolution spectroscopic data. *MNRAS* 483(3):3255–3277. <https://doi.org/10.1093/mnras/sty3217>. arXiv:1808.04428 [astro-ph.GA]
- Li G, Van Reeth T, Bedding TR, Murphy SJ, Antoci V, Ouazzani RM, Barbara NH (2020) Gravity-mode period spacings and near-core rotation rates of 611 γ Doradus stars with Kepler. *MNRAS* 491(3):3586–3605. <https://doi.org/10.1093/mnras/stz2906>. arXiv:1910.06634 [astro-ph.SR]

- Liebert J, Bergeron P, Holberg JB (2005) The formation rate and mass and luminosity functions of DA white dwarfs from the Palomar Green Survey. *ApJS* 156(1):47–68. <https://doi.org/10.1086/425738>. arXiv:astro-ph/0406657
- Lin J, Dotter A, Ting YS, Asplund M (2018) Stellar ages and masses in the solar neighbourhood: Bayesian analysis using spectroscopy and Gaia DR1 parallaxes. *MNRAS* 477:2966–2975. <https://doi.org/10.1093/mnras/sty709>. arXiv:1803.10875 [astro-ph.SR]
- Liu C, Bailer-Jones CAL, Sordo R, Vallenari A, Borrachero R, Luri X, Sartoretti P (2012) The expected performance of stellar parametrization with Gaia spectrophotometry. *MNRAS* 426(3):2463–2482. <https://doi.org/10.1111/j.1365-2966.2012.21797.x>. arXiv:1207.6005 [astro-ph.IM]
- Liu K, Bi SL, Li TD, Tian ZJ, Ge ZS (2014) Fundamental stellar parameters of three Kepler stars accurately constrained by lithium abundance and rotation. *A&A* 563:A23. <https://doi.org/10.1051/0004-6361/201323277>
- Lodieu N, Alonso R, González Hernández RJI, Sanchis-Ojeda Narita N, Kawashima Y, Kawauchi K, Suárez Mascareño A, Deeg H et al (2015) An eclipsing double-line spectroscopic binary at the stellar/substellar boundary in the Upper Scorpius OB association. *A&A* 584:A128. <https://doi.org/10.1051/0004-6361/201527464>. arXiv:1511.03083 [astro-ph.SR]
- Lodieu N, Rebolo R, Perez-Garrido A (2018) Lithium in the Hyades L5 brown dwarf 2MASSJ04183483+2131275. *A&A* 615:L12. <https://doi.org/10.1051/0004-6361/201832748>. arXiv:1807.02794 [astro-ph.SR]
- López-Morales M, Ribas I (2005) GU Bootis: a new $0.6M_{\odot}$ detached eclipsing binary. *ApJ* 631:1120–1133. <https://doi.org/10.1086/432680>. arXiv:astro-ph/0505001
- López-Morales M, Shaw JS (2007) Testing low-mass stellar models: three new detached eclipsing binaries below $0.75M_{\odot}$. In: Kang YW, Lee HW, Leung KC, Cheng KS (eds) *The Seventh Pacific Rim Conference on Stellar Astrophysics*. ASP Conference Series, vol 362. Astronomical Society of the Pacific, San Francisco, p 26. arXiv:astro-ph/0603748
- Lorenzo-Oliveira D, de Porto Mello GF, Dutra-Ferreira L, Ribas I (2016) Fine structure of the age-chromospheric activity relation in solar-type stars. I. The Ca II infrared triplet: absolute flux calibration. *A&A* 595:A11. <https://doi.org/10.1051/0004-6361/201628825>. arXiv:1608.02288 [astro-ph.SR]
- Lorenzo-Oliveira D, Freitas FC, Meléndez J, Bedell M, Ramírez I, Bean JL, Asplund M, Spina L, Dreizler S, Alves-Brito A, Casagrande L (2018) The solar twin planet search. The age-chromospheric activity relation. *A&A* 619:A73. <https://doi.org/10.1051/0004-6361/201629294>. arXiv:1806.08014 [astro-ph.SR]
- Lund MN, Silva Aguirre V, Davies GR, Chaplin WJ, Christensen-Dalsgaard J, Houdek G, White TR, Bedding TR, Ball WH, Huber D, Antia HM, Lebreton Y, Latham DW, Handberg R, Verma K, Basu S, Casagrande L, Justesen AB, Kjeldsen H, Mosumgaard JR (2017) Standing on the shoulders of dwarfs: the Kepler asteroseismic LEGACY sample. I. Oscillation mode parameters. *ApJ* 835:172. <https://doi.org/10.3847/1538-4357/835/2/172>. arXiv:1612.00436 [astro-ph.SR]
- MacDonald J, Mullan DJ (2014) Surface magnetic field strengths: new tests of magnetoconvective models of M dwarfs. *ApJ* 787:70. <https://doi.org/10.1088/0004-637X/787/1/70>
- Macintosh B, Graham JR, Barman T et al (2015) Discovery and spectroscopy of the young Jovian planet 51 Eri b with the Gemini Planet Imager. *Science* 350:64–67. <https://doi.org/10.1126/science.aac5891>. arXiv:1508.03084 [astro-ph.EP]
- Mackereth JT, Bovy J, Leung HW, Schiavon RP, Trick WH, Chaplin WJ, Cunha K, Feuillet DK, Majewski SR, Martig M, Miglio A, Nidever D, Pinsonneault MH, Aguirre VS, Sobeck J, Tayar J, Zasowski G (2019) Dynamical heating across the Milky Way disc using APOGEE and Gaia. *MNRAS* 489(1):176–195. <https://doi.org/10.1093/mnras/stz1521>. arXiv:1901.04502 [astro-ph.GA]
- Maeder A, Meynet G (2012) Rotating massive stars: from first stars to gamma ray bursts. *Rev Mod Phys* 84:25–63. <https://doi.org/10.1103/RevModPhys.84.25>
- Mahy L, Rauw G, De Becker M, Eenens P, Flores CA (2015) A spectroscopic investigation of the O-type star population in four Cygnus OB associations. II. Determination of the fundamental parameters. *A&A* 577:A23. <https://doi.org/10.1051/0004-6361/201321985>. arXiv:1504.03107 [astro-ph.SR]
- Mahy L, Damerdjy Y, Gosset E, Nitschelm C, Eenens P, Sana H, Klotz A (2017) A modern study of HD 166734: a massive supergiant system. *A&A* 607:A96. <https://doi.org/10.1051/0004-6361/201730674>. arXiv:1707.02060 [astro-ph.SR]
- Mahy L, Almeida LA, Sana H, Clark JS, de Koter A, de Mink SE, Evans CJ, Grin NJ, Langer N, Moffat AFJ, Schneider FRN, Shenar T, Trammer F (2020) The Tarantula massive binary monitoring. IV.

- Double-lined photometric binaries. *A&A* 634:A119. <https://doi.org/10.1051/0004-6361/201936152>. [arXiv:1912.06853](https://arxiv.org/abs/1912.06853) [astro-ph.SR]
- Maíz Apellániz J (2007) A uniform set of optical/NIR photometric zero points to be used with CHORIZOS. In: Sterken C (ed) The future of photometric, spectrophotometric and polarimetric standardization. ASP Conference Series, vol 364. Astronomical Society of the Pacific, San Francisco, p 227. [arXiv:astro-ph/0609430](https://arxiv.org/abs/astro-ph/0609430)
- Maíz Apellániz J, Evans CJ, Barbá RH, Gräfenor G, Bestenlehner JM, Crowther PA, García M, Herrero A, Sana H, Simón-Díaz S, Taylor WD, van Loon JT, Vink JS, Walborn NR (2014) The VLT-FLAMES Tarantula Survey. XVI. The optical and NIR extinction laws in 30 Doradus and the photometric determination of the effective temperatures of OB stars. *A&A* 564:A63. <https://doi.org/10.1051/0004-6361/201423439>. [arXiv:1402.3062](https://arxiv.org/abs/1402.3062) [astro-ph.GA]
- Malkov OY (2007) Mass-luminosity relation of intermediate-mass stars. *MNRAS* 382:1073–1086. <https://doi.org/10.1111/j.1365-2966.2007.12086.x>
- Malla SP, Stello D, Huber D, Montet BT, Bedding TR, Fredslund Andersen M, Grundahl F, Jessen-Hansen J, Hey DR, Palle PL, Deng L, Zhang C, Chen X, Lloyd J, Antoci V (2020) Asteroseismic masses of four evolved planet-hosting stars using SONG and TESS: resolving the retired A-star mass controversy. *MNRAS* 496(4):5423–5435. <https://doi.org/10.1093/mnras/staa1793>. [arXiv:2006.07649](https://arxiv.org/abs/2006.07649) [astro-ph.SR]
- Mann AW, Feiden GA, Gaidos E, Boyajian T, von Braun K (2015) How to constrain your M dwarf: measuring effective temperature, bolometric luminosity, mass, and radius. *ApJ* 804(1):64. <https://doi.org/10.1088/0004-637X/804/1/64>. [arXiv:1501.01635](https://arxiv.org/abs/1501.01635) [astro-ph.SR]
- Mann AW, Dupuy T, Kraus AL, Gaidos E, Ansdell M, Ireland M, Rizzuto AC, Hung CL, Dittmann J, Factor S, Feiden G, Martinez RA, Ruiz-Rodríguez D, Thao PC (2019) How to constrain your M dwarf. II. The mass-luminosity-metallicity relation from 0.075 to 0.70 solar masses. *ApJ* 871(1):63. <https://doi.org/10.3847/1538-4357/aaf3bc>. [arXiv:1811.06938](https://arxiv.org/abs/1811.06938) [astro-ph.SR]
- Marcy GW, Butler RP (1992) Precision radial velocities with an iodine absorption cell. *PASP* 104:270. <https://doi.org/10.1086/132989>
- Marigo P, Girardi L, Bressan A, Rosenfield P, Aringer B, Chen Y, Dussin M, Nanni A, Pastorelli G, Rodrigues TS, Trabucchi M, Bladh S, Dalcanton J, Groenewegen MAT, Montalbán J, Wood PR (2017) A new generation of PARSEC-COLIBRI stellar isochrones including the TP-AGB phase. *ApJ* 835(1):77. <https://doi.org/10.3847/1538-4357/835/1/77>. [arXiv:1701.08510](https://arxiv.org/abs/1701.08510) [astro-ph.SR]
- Marino AF, Milone AP, Casagrande L, Przybilla N, Balaguer-Núñez L, Di Criscienzo M, Serenelli A, Vilardeff F (2018) Discovery of extended main sequence turnoffs in Galactic open clusters. *ApJL* 863(2):L33. <https://doi.org/10.3847/2041-8213/aad868>. [arXiv:1807.05888](https://arxiv.org/abs/1807.05888) [astro-ph.SR]
- Markova N, Puls J (2015) The mass discrepancy problem in O stars of solar metallicity. Does it still exist? In: Meynet G, Georgy C, Groh J, Stee P (eds) New windows on massive stars. IAU symposium, vol 307, Cambridge University Press, pp 117–118. <https://doi.org/10.1017/S1743921314006462>. [arXiv:1409.7784](https://arxiv.org/abs/1409.7784) [astro-ph.SR]
- Markova N, Puls J, Langer N (2018) Spectroscopic and physical parameters of Galactic O-type stars. III. Mass discrepancy and rotational mixing. *A&A* 613:A12. <https://doi.org/10.1051/0004-6361/201731361>. [arXiv:1803.03410](https://arxiv.org/abs/1803.03410) [astro-ph.SR]
- Marois C, Macintosh B, Barman T, Zuckerman B, Song I, Patience J, Lafrenière D, Doyon R (2008) Direct imaging of multiple planets orbiting the star HR 8799. *Science* 322:1348. <https://doi.org/10.1126/science.1166585>. [arXiv:0811.2606](https://arxiv.org/abs/0811.2606) [astro-ph]
- Martell SL, Smith GH, Briley MM (2008) Deep mixing and metallicity: carbon depletion in globular cluster giants. *AJ* 136(6):2522–2532. <https://doi.org/10.1088/0004-6256/136/6/2522>. [arXiv:0809.4470](https://arxiv.org/abs/0809.4470) [astro-ph]
- Martig M, Foesneau M, Rix HW, Ness M, Mészáros S, García-Hernández DA, Pinsonneault M, Serenelli A, Silva Aguirre V, Zamora O (2016) Red giant masses and ages derived from carbon and nitrogen abundances. *MNRAS* 456(4):3655–3670. <https://doi.org/10.1093/mnras/stv2830>. [arXiv:1511.08203](https://arxiv.org/abs/1511.08203) [astro-ph.SR]
- Martín EL, Lodieu N, Pavlenko Y, Béjar VJS (2018) The lithium depletion boundary and the age of the Hyades cluster. *ApJ* 856:40. <https://doi.org/10.3847/1538-4357/aaeb8>. [arXiv:1802.07155](https://arxiv.org/abs/1802.07155) [astro-ph.SR]
- Martínez-Arnáiz R, López-Santiago J, Crespo-Chacón I, Montes D (2011) Effect of magnetic activity saturation in chromospheric flux-flux relationships. *MNRAS* 414(3):2629–2641. <https://doi.org/10.1111/j.1365-2966.2011.18584.x>. [arXiv:1102.4506](https://arxiv.org/abs/1102.4506) [astro-ph.SR]

- Martins F, Palacios A (2013) A comparison of evolutionary tracks for single Galactic massive stars. *A&A* 560:A16. <https://doi.org/10.1051/0004-6361/201322480>. arXiv:1310.7218 [astro-ph.SR]
- Martins F, Mahy L, Hillier DJ, Rauw G (2012) A quantitative study of O stars in NGC 2244 and the Monoceros OB2 association. *A&A* 538:A39. <https://doi.org/10.1051/0004-6361/201117458>. arXiv:1110.4509 [astro-ph.SR]
- Masseron T, Gilmore G (2015) Carbon, nitrogen and α -element abundances determine the formation sequence of the Galactic thick and thin discs. *MNRAS* 453(2):1855–1866. <https://doi.org/10.1093/mnras/stv1731>. arXiv:1503.00537 [astro-ph.SR]
- Masseron T, Lagarde N, Miglio A, Elsworth Y, Gilmore G (2017) Nitrogen depletion in field red giants: mixing during the He flash? *MNRAS* 464(3):3021–3028. <https://doi.org/10.1093/mnras/stw2632>. arXiv:1610.03286 [astro-ph.SR]
- Massey P, Puls J, Pauldrach AWA, Bresolin F, Kudritzki RP, Simon T (2005) The physical properties and effective temperature scale of O-type stars as a function of metallicity. II. Analysis of 20 more Magellanic Cloud Stars and results from the complete sample. *ApJ* 627(1):477–519. <https://doi.org/10.1086/430417>. arXiv:astro-ph/0503464
- Maxted PFL, Serenelli AM, Southworth J (2015) Bayesian mass and age estimates for transiting exoplanet host stars. *A&A* 575:A36. <https://doi.org/10.1051/0004-6361/201425331>. arXiv:1412.7891 [astro-ph.IM]
- Maxted PFL, Gaulme P, Graczyk D, Helminiak KG, Johnston C, Orosz JA, Prša A, Southworth J, Torres G, Davies GR, Ball W, Chaplin WJ (2020) The TESS light curve of AI Phoenicis. *MNRAS* 498(1):332–343. <https://doi.org/10.1093/mnras/staa1662>. arXiv:2003.09295 [astro-ph.SR]
- Mayor M, Pepe F, Queloz D, Bouchy F, Rupprecht G, Lo Curto G, Avila G, Benz W, Bertaux JL, Bonfils X et al (2003) Setting new standards with HARPS. *Messenger* 114:20–24
- McEvoy CM, Dufton PL, Evans CJ, Kalari VM, Markova N, Simón-Díaz S, Vink JS, Walborn NR, Crowther PA, de Koter A, de Mink SE, Dunstall PR, Hénault-Brunet V, Herrero A, Langer N, Lennon DJ, Maíz Apellániz J, Najarro F, Puls J, Sana H, Schneider FRN, Taylor WD (2015) The VLT-FLAMES Tarantula Survey. XIX. B-type supergiants: atmospheric parameters and nitrogen abundances to investigate the role of binarity and the width of the main sequence. *A&A* 575:A70. <https://doi.org/10.1051/0004-6361/201425202>. arXiv:1412.2705 [astro-ph.SR]
- Mennesson B, Perrin G, Chagnon G, du Coudré Foresto V, Ridgway S, Merand A, Salome P, Borde P, Cotton W, Morel S, Kervella P, Traub W, Lacasse M (2002) Evidence for very extended Gaseous layers around O-rich Mira variables and M giants. *ApJ* 579(1):446–454. <https://doi.org/10.1086/342671>
- Mérand A, Kervella P, Pribulla T, Petr-Gotzens MG, Benisty M, Natta A, Duvert G, Schertl D, Vannier M (2011) The nearby eclipsing stellar system δ Velorum. III. Self-consistent fundamental parameters and distance. *A&A* 532:A50. <https://doi.org/10.1051/0004-6361/201116896>. arXiv:1106.2383 [astro-ph.SR]
- Mermilliod JC (1981) Comparative studies of young open clusters. III—Empirical isochronous curves and the zero age main sequence. *A&A* 97:235–244
- Metcalfe TS, Creevey OL, Christensen-Dalsgaard J (2009) A stellar model-fitting pipeline for asteroseismic data from the Kepler mission. *ApJ* 699:373
- Metcalfe TS, Chaplin WJ, Appourchaux T, García RA, Basu S, Brandão I, Creevey OL, Deheuvels S, Doğan G, Eggenberger P, Karoff C, Miglio A, Stello D, Yıldız M, Çelik Z, Antia HM, Benomar O, Howe R, Régulo C, Salabert D, Stahn T, Bedding TR, Davies GR, Elsworth Y, Gizon L, Hekker S, Mathur S, Mosser B, Bryson ST, Still MD, Christensen-Dalsgaard J, Gilliland RL, Kawaler SD, Kjeldsen H, Ibrahim KA, Klaus TC, Li J (2012) Asteroseismology of the solar analogs 16 Cyg A and B from Kepler observations. *ApJL*. <https://doi.org/10.1088/2041-8205/748/1/L10>
- Meylan G, Heggie DC (1997) Internal dynamics of globular clusters. *Astron Astrophys Rev* 8:1–143. arXiv:astro-ph/9610076
- Michaud G, Alecian G, Richer J (2015) Atomic diffusion in stars. Springer, Cham. <https://doi.org/10.1007/978-3-319-19854-5>
- Michielsen M, Pedersen MG, Augustson KC, Mathis S, Aerts C (2019) Probing the shape of the mixing profile and of the thermal structure at the convective core boundary through asteroseismology. *A&A* 628:A76. <https://doi.org/10.1051/0004-6361/201935754>. arXiv:1906.05304 [astro-ph.SR]
- Migliari S, Fender RP (2006) Jets in neutron star X-ray binaries: a comparison with black holes. *MNRAS* 366:79–91. <https://doi.org/10.1111/j.1365-2966.2005.09777.x>. arXiv:astro-ph/0510698
- Miglio A, Montalbán J (2005) Constraining fundamental stellar parameters using seismology. Application to α Centauri AB. *A&A* 441:615

- Mikołajewska J (2003) Orbital and stellar parameters of symbiotic stars. In: Corradi RLM, Mikołajewska R, Mahoney TJ (eds) *Symbiotic Stars Probing Stellar Evolution*, ASP Conference Proceedings, vol 303. Astronomical Society of the Pacific, San Francisco, pp 9–24
- Miller Bertolami MM (2016) New models for the evolution of post-asymptotic giant branch stars and central stars of planetary nebulae. *A&A* 588:A25. <https://doi.org/10.1051/0004-6361/201526577>. arXiv:1512.04129 [astro-ph.SR]
- Milone AP, Piotto G, Bedin LR, Cassisi S, Anderson J, Marino AF, Pietrinferni A, Aparicio A (2012) Luminosity and mass functions of the three main sequences of the globular cluster NGC 2808. *A&A* 537:A77. <https://doi.org/10.1051/0004-6361/201116539>. arXiv:1108.2391 [astro-ph.SR]
- Milone AP, Piotto G, Renzini A, Marino AF, Bedin LR, Vesperini E, D'Antona F, Nardiello D, Anderson J, King IR, Yong D, Bellini A, Aparicio A, Barbuy B, Brown TM, Cassisi S, Ortolani S, Salaris M, Sarajedini A, van der Marel RP (2017) The Hubble Space Telescope UV Legacy Survey of Galactic globular clusters—IX. The Atlas of multiple stellar populations. *MNRAS* 464:3636–3656. <https://doi.org/10.1093/mnras/stw2531>. arXiv:1610.00451 [astro-ph.SR]
- Mokiem MR, de Koter A, Evans CJ, Puls J, Smartt SJ, Crowther PA, Herrero A, Langer N, Lennon DJ, Najarro F, Villamariz MR, Vink JS (2007) The VLT-FLAMES survey of massive stars: wind properties and evolution of hot massive stars in the Large Magellanic Cloud. *A&A* 465(3):1003–1019. <https://doi.org/10.1051/0004-6361:20066489>. arXiv:0704.1113 [astro-ph]
- Mombarg JSG, Van Reeth T, Pedersen MG, Molenberghs G, Bowman DM, Johnston C, Tkachenko A, Aerts C (2019) Asteroseismic masses, ages, and core properties of γ Doradus stars using gravito-inertial dipole modes and spectroscopy. *MNRAS* 485(3):3248–3263. <https://doi.org/10.1093/mnras/stz501>. arXiv:1902.06746 [astro-ph.SR]
- Mombarg JSG, Dotter A, Van Reeth T, Tkachenko A, Gebruers S, Aerts C (2020) Asteroseismic modeling of gravity modes in slowly rotating A/F stars with radiative levitation. *ApJ* 895(1):51. <https://doi.org/10.3847/1538-4357/ab8d36>. arXiv:2004.13037 [astro-ph.SR]
- Morales JC, Ribas I, Jordi C, Torres G, Gallardo J, Guinan EF, Charbonneau D, Wolf M, Latham DW, Anglada-Escudé G et al (2009a) Absolute properties of the low-mass eclipsing binary CM Draconis. *ApJ* 691:1400–1411. <https://doi.org/10.1088/0004-637X/691/2/1400>. arXiv:0810.1541
- Morales JC, Torres G, Marschall LA, Brehm W (2009b) Absolute dimensions of the G7+K7 eclipsing binary star IM Virginis: discrepancies with stellar evolution models. *ApJ* 707:671–685. <https://doi.org/10.1088/0004-637X/707/1/671>. arXiv:0910.4458 [astro-ph.SR]
- Morales JC, Gallardo J, Ribas I, Jordi C, Baraffe I, Chabrier G (2010) The effect of magnetic activity on low-mass stars in eclipsing binaries. *ApJ* 718:502–512. <https://doi.org/10.1088/0004-637X/718/1/502>. arXiv:1005.5720 [astro-ph.SR]
- Moravveji E, Aerts C, Pápics PI, Triana SA, Vandoren B (2015) Tight asteroseismic constraints on core overshooting and diffusive mixing in the slowly rotating pulsating B8.3V star KIC 10526294. *A&A* 580:A27. <https://doi.org/10.1051/0004-6361/201425290>. arXiv:1505.06902 [astro-ph.SR]
- Moravveji E, Townsend RHD, Aerts C, Mathis S (2016) Sub-inertial gravity modes in the B8V Star KIC 7760680 reveal moderate core overshooting and low vertical diffusive mixing. *ApJ* 823:130. <https://doi.org/10.3847/0004-637X/823/2/130>. arXiv:1604.02680 [astro-ph.SR]
- Mortier A, Santos NC, Sousa SG, Fernandes JM, Adibekyan VZ, Delgado Mena E, Montalto M, Israelian G (2013) New and updated stellar parameters for 90 transit hosts. The effect of the surface gravity. *A&A* 558:A106. <https://doi.org/10.1051/0004-6361/201322240>. arXiv:1309.1998 [astro-ph.EP]
- Moya A, Zuccarino F, Chaplin WJ, Davies GR (2018) Empirical relations for the accurate estimation of stellar masses and radii. *Astrophys J Suppl Ser* 237:21. <https://doi.org/10.3847/1538-4365/aacdae>. arXiv:1806.06574 [astro-ph.SR]
- Mullan DJ, MacDonald J (2010) Magnetic models of the brown dwarfs HD 130948b and HD 130948c. *ApJ* 713:1249–1255. <https://doi.org/10.1088/0004-637X/713/2/1249>
- Muterspaugh MW, Lane BF, Fekel FC, Konacki M, Burke BF, Kulkarni SR, Colavita MM, Shao M, Wiktorowicz SJ (2008) Masses, luminosities, and orbital coplanarities of the μ Orionis quadruple-star system from phases differential astrometry. *AJ* 135(3):766–776. <https://doi.org/10.1088/0004-6256/135/3/766>. arXiv:0710.2126 [astro-ph]
- Muterspaugh MW, Fekel FC, Lane BF, Hartkopf WI, Kulkarni SR, Konacki M, Burke BF, Colavita MM, Shao M, Williamson M (2010) The phases differential astrometry data archive. IV. The Triple Star Systems 63 Gem A and HR 2896. *AJ* 140(6):1646–1656. <https://doi.org/10.1088/0004-6256/140/6/1646>. arXiv:1010.4045 [astro-ph.SR]
- Nardiello D, Milone AP, Piotto G, Anderson J, Bedin LR, Bellini A, Cassisi S, Libralato M, Marino AF (2018) The Hubble Space Telescope UV Legacy Survey of Galactic globular clusters— IV. Multiple

- stellar populations within M 15 and their radial distribution. *MNRAS* 477(2):2004–2019. <https://doi.org/10.1093/mnras/sty719>. arXiv:1803.05979 [astro-ph.SR]
- Neilson HR, Langer N (2012) Is there a mass discrepancy in the Cepheid binary OGLE-LMC-CEP0227? *A&A* 537:A26. <https://doi.org/10.1051/0004-6361/201117829>. arXiv:1110.6657 [astro-ph.SR]
- Neilson HR, Cantiello M, Langer N (2011) The Cepheid mass discrepancy and pulsation-driven mass loss. *A&A* 529:L9. <https://doi.org/10.1051/0004-6361/201116920>. arXiv:1104.1638 [astro-ph.SR]
- Ness M, Hogg DW, Rix HW, Martig M, Pinsonneault MH, Ho AYQ (2016) Spectroscopic determination of masses (and implied ages) for red giants. *ApJ* 823(2):114. <https://doi.org/10.3847/0004-637X/823/2/114>. arXiv:1511.08204 [astro-ph.SR]
- Niederhofer F, Bastian N, Kozhurina-Platais V, Larsen S, Hollyhead K, Lardo C, Cabrera-Ziri I, Kacharov N, Platais I, Salaris M, Cordero M, Dalessandro E, Geisler D, Hilker M, Li C, Mackey D, Mucciarelli A (2017) The search for multiple populations in Magellanic Cloud clusters—II. The detection of multiple populations in three intermediate-age SMC clusters. *MNRAS* 465:4159–4165. <https://doi.org/10.1093/mnras/stw3084>. arXiv:1612.00400 [astro-ph.SR]
- North TSH, Campante TL, Miglio A, Davies GR, Grunblatt SK, Huber D, Kuszlewicz JS, Lund MN, Cooke BF, Chaplin WJ (2017) The masses of retired A stars with asteroseismology: Kepler and K2 observations of exoplanet hosts. *MNRAS* 472(2):1866–1878. <https://doi.org/10.1093/mnras/stx2009>. arXiv:1708.00716 [astro-ph.SR]
- Nsamba B, Campante TL, Monteiro MJPF, Cunha MS, Rendle BM, Reese DR, Verma K (2018) Asteroseismic modelling of solar-type stars: internal systematics from input physics and surface correction methods. *MNRAS* 477:5052–5063. <https://doi.org/10.1093/mnras/sty948>. arXiv:1804.04935 [astro-ph.SR]
- Nsamba B, Campante TL, Monteiro MJPF, Cunha MS, Sousa SG (2019) On the nature of the core of Alpha Centauri A: the impact of the metallicity mixture. *Front Astron Space Sci* 6:25. <https://doi.org/10.3389/fspas.2019.00025>. arXiv:1904.01560 [astro-ph.SR]
- Ortiz M, Gandolfi D, Reffert S, Quirrenbach A, Deeg HJ, Karjalainen R, Montañés-Rodríguez P, Nespral D, Nowak G, Osorio Y, Palles E (2015) Kepler-432 b: a massive warm Jupiter in a 52-day eccentric orbit transiting a giant star. *A&A* 573:L6. <https://doi.org/10.1051/0004-6361/201425146>. arXiv:1410.3000 [astro-ph.EP]
- Osborn HP, Armstrong DJ, Brown DJA, McCormac J, Doyle AP, Loudon TM, Kirk J, Spake JJ, Lam KWF, Walker SR, Faedi F, Pollacco DL (2016) Single transit candidates from K2: detection and period estimation. *MNRAS* 457(3):2273–2286. <https://doi.org/10.1093/mnras/stw137>. arXiv:1512.03722 [astro-ph.EP]
- Østensen RH, Green EM, Bloemen S, Marsh TR, Laird JB, Morris M, Moriyama E, Oreiro R, Reed MD, Kawaler SD, Aerts C, Vučković M, Degroote P, Telting JH, Kjeldsen H, Gilliland RL, Christensen-Dalsgaard J, Borucki WJ, Koch D (2010) 2M1938+4603: a rich, multimode pulsating sdB star with an eclipsing dM companion observed with Kepler. *MNRAS* 408(1):L51–L55. <https://doi.org/10.1111/j.1745-3933.2010.00926.x>. arXiv:1006.4267 [astro-ph.SR]
- Oti Floranes H, Christensen-Dalsgaard J, Thompson MJ (2005) The use of frequency-separation ratios for asteroseismology. *MNRAS* 356:671
- Ouazzani RM, Salmon SJA, Antoci V, Bedding TR, Murphy SJ, Roxburgh IW (2017) A new asteroseismic diagnostic for internal rotation in γ Doradus stars. *MNRAS* 465:2294–2309. <https://doi.org/10.1093/mnras/stw2717>. arXiv:1610.06184 [astro-ph.SR]
- Özel F, Freire P (2016) Masses, radii, and the equation of state of neutron stars. *ARA&A* 54:401–440. <https://doi.org/10.1146/annurev-astro-081915-023322>. arXiv:1603.02698 [astro-ph.HE]
- Pápics PI, Tkachenko A, Van Reeth T, Aerts C, Moravveji E, Van de Sande M, De Smedt K, Bloemen S, Southworth J, Debosscher J, Niemczura E, Gameiro JF (2017) Signatures of internal rotation discovered in the Kepler data of five slowly pulsating B stars. *A&A* 598:A74. <https://doi.org/10.1051/0004-6361/201629814>. arXiv:1611.06955 [astro-ph.SR]
- Parsons SG, Gänsicke BT, Marsh TR, Ashley RP, Bours MCP, Breedt E, Burleigh MR, Copperwheat CM, Dhillon VS, Green M, Hardy LK, Hermes JJ, Irawati P, Kerry P, Littlefair SP, McAllister MJ, Rattanasoon S, Rebassa-Mansergas A, Sahman DI, Schreiber MR (2017) Testing the white dwarf mass-radius relationship with eclipsing binaries. *MNRAS* 470(4):4473–4492. <https://doi.org/10.1093/mnras/stx1522>. arXiv:1706.05016 [astro-ph.SR]
- Pasquini L, Pala AF, Ludwig HG, Leão IC, de Medeiros JR, Weiss A (2019) Masses of the Hyades white dwarfs. A gravitational redshift measurement. *A&A* 627:L8. <https://doi.org/10.1051/0004-6361/201935835>. arXiv:1907.01265 [astro-ph.SR]

- Paust NEQ, Reid IN, Piotto G, Aparicio A, Anderson J, Sarajedini A, Bedin LR, Chaboyer B, Dotter A, Hempel M, Majewski S, Marín-Franch A, Milone A, Rosenberg A, Siegel M (2010) The ACS Survey of Galactic globular clusters. VIII. Effects of environment on globular cluster global mass functions. *AJ* 139:476–491. <https://doi.org/10.1088/0004-6256/139/2/476>
- Pavlovski K, Hensberge H (2005) Abundances from disentangled component spectra: the eclipsing binary V578 Mon. *A&A* 439(1):309–315. <https://doi.org/10.1051/0004-6361:20052804>. [arXiv:astro-ph/0504433](https://arxiv.org/abs/astro-ph/0504433)
- Pavlovski K, Hensberge H (2010) Reconstruction and analysis of component spectra of binary and multiple stars. In: Prša A, Zejda M (eds) *Binaries – key to comprehension of the Universe*. ASP Conference Series, vol 435. Astronomical Society of the Pacific, San Francisco, p 207. [arXiv:0909.3246](https://arxiv.org/abs/0909.3246) [astro-ph.SR]
- Pavlovski K, Southworth J (2009) Chemical evolution of high-mass stars in close binaries— . The eclipsing binary V453 Cygni. *MNRAS* 394(3):1519–1528. <https://doi.org/10.1111/j.1365-2966.2009.14418.x>. [arXiv:0812.3769](https://arxiv.org/abs/0812.3769) [astro-ph]
- Pavlovski K, Southworth J, Kolbas V, Smalley B (2014) Absolute dimensions of detached eclipsing binaries—III. The metallic-lined system YZ Cassiopeiae. *MNRAS* 438(1):590–603. <https://doi.org/10.1093/mnras/stt2229>. [arXiv:1311.3482](https://arxiv.org/abs/1311.3482) [astro-ph.SR]
- Pavlovski K, Southworth J, Tamajo E (2018) Physical properties and CNO abundances for high-mass stars in four main-sequence detached eclipsing binaries: V478 Cyg, AH Cep, V453 Cyg, and V578 Mon. *MNRAS* 481(3):3129–3147. <https://doi.org/10.1093/mnras/sty2516>. [arXiv:1809.04061](https://arxiv.org/abs/1809.04061) [astro-ph.SR]
- Paxton B, Smolec R, Schwab J, Gautschy A, Bildsten L, Cantiello M, Dotter A, Farmer R, Goldberg JA, Jermyn AS, Kanbur SM, Marchant P, Thoul A, Townsend RHD, Wolf WM, Zhang M, Timmes FX (2019) Modules for experiments in stellar astrophysics (MESA): pulsating variable stars, rotation, convective boundaries, and energy conservation. *ApJS* 243(1):10. <https://doi.org/10.3847/1538-4365/ab2241>. [arXiv:1903.01426](https://arxiv.org/abs/1903.01426) [astro-ph.SR]
- Pecaut MJ, Mamajek EE (2016) The star formation history and accretion-disc fraction among the K-type members of the Scorpius–Centaurus OB association. *MNRAS* 461:794–815. <https://doi.org/10.1093/mnras/stw1300>. [arXiv:1605.08789](https://arxiv.org/abs/1605.08789) [astro-ph.SR]
- Pedersen MG (2020) Interior rotation, mixing, and ages of a sample of slowly pulsating b stars from gravity-mode asteroseismology. PhD thesis, KU Leuven, Belgium
- Pedersen MG, Aerts C, Pápics PI, Rogers TM (2018) The shape of convective core overshooting from gravity-mode period spacings. *A&A* 614:A128. <https://doi.org/10.1051/0004-6361/201732317>. [arXiv:1802.02051](https://arxiv.org/abs/1802.02051) [astro-ph.SR]
- Pedersen MG, Chowdhury S, Johnston C, Bowman DM, Aerts C, Handler G, De Cat P, Neiner C, David-Uraz A, Buzasi D, Tkachenko A, Simón-Díaz S, Moravveji E, Sikora J, Mirouh GM, Lovekin CC, Cantiello M, Daszyńska-Daszkiewicz J, Pigulski A, Vanderspek RK, Ricker GR (2019) Diverse variability of O and B stars revealed from 2-minute cadence light curves in sectors 1 and 2 of the TESS mission: selection of an asteroseismic sample. *ApJL* 872(1):L9. <https://doi.org/10.3847/2041-8213/ab01e1>. [arXiv:1901.07576](https://arxiv.org/abs/1901.07576) [astro-ph.SR]
- Pedersen MG, Escorza A, Pápics PI, Aerts C (2020) Recipes for bolometric corrections and Gaia luminosities of B-type stars: application to an asteroseismic sample. *MNRAS* 495(3):2738–2753. <https://doi.org/10.1093/mnras/staa1292>. [arXiv:2005.00881](https://arxiv.org/abs/2005.00881) [astro-ph.SR]
- Pedersen MG, Aerts C, Pápics PI, Michielsen M, Gebruers S, Rogers TM, Molenberghs G, Burssens S, Garcia S, Bowman DM (2021) Internal mixing of rotating stars inferred from dipole gravity modes. *Nat Astron* (in press)
- Pepe F, Cameron AC, Latham DW, Molinari E, Udry S, Bonomo AS, Buchhave LA, Charbonneau D, Cosentino R, Dressing CD et al (2013) An Earth-sized planet with an Earth-like density. *Nature* 503(7476):377–380. <https://doi.org/10.1038/nature12768>. [arXiv:1310.7987](https://arxiv.org/abs/1310.7987) [astro-ph.EP]
- Pepe F, Molaro P, Cristiani S et al (2014) ESPRESSO: The next European exoplanet hunter. *Astron Nachr* 335(1):8. <https://doi.org/10.1002/asna.201312004>
- Peuten M, Zocchi A, Gieles M, Gualandris A, Hénault-Brunet V (2016) A stellar-mass black hole population in the globular cluster NGC 6101? *MNRAS* 462:2333–2342. <https://doi.org/10.1093/mnras/stw1726>. [arXiv:1609.01720](https://arxiv.org/abs/1609.01720)
- Pietrzyński G, Gieren W (2002) The ARAUCARIA Project: deep near-infrared survey of nearby galaxies. I. The distance to the Large Magellanic Cloud from K-band photometry of red clump stars. *AJ* 124(5):2633–2638. <https://doi.org/10.1086/344075>. [arXiv:astro-ph/0208162](https://arxiv.org/abs/astro-ph/0208162)

- Pietrzyński G, Thompson IB, Gieren W, Graczyk D, Bono G, Udalski A, Soszyński I, Minniti D, Pilecki B (2010) The dynamical mass of a classical Cepheid variable star in an eclipsing binary system. *Nature* 468(7323):542–544. <https://doi.org/10.1038/nature09598>. arXiv:1012.0231 [astro-ph.GA]
- Pietrzyński G, Thompson IB, Graczyk D, Gieren W, Pilecki B, Udalski A, Soszynski I, Bono G, Konorski P, Nardetto N, Storm J (2011) The Araucaria Project: accurate determination of the dynamical mass of the classical cepheid in the eclipsing system OGLE-LMC-CEP-1812. *ApJL* 742(2):L20. <https://doi.org/10.1088/2041-8205/742/2/L20>. arXiv:1109.5414 [astro-ph.SR]
- Pietrzyński G, Graczyk D, Gieren W, Thompson IB, Pilecki B, Udalski A, Soszyński I, Kozłowski S, Konorski P, Suchomska K, Bono G, Moroni PGP, Villanova S, Nardetto N, Bresolin F, Kudritzki RP, Storm J, Gallenne A, Smolec R, Minniti D, Kubiak M, Szymański MK, Poleski R, Wyrzykowski Ł, Ulaczyk K, Pietrukowicz P, Górski M, Karczmarek P (2013) An eclipsing-binary distance to the Large Magellanic Cloud accurate to two per cent. *Nature* 495(7439):76–79. <https://doi.org/10.1038/nature11878>. arXiv:1303.2063 [astro-ph.GA]
- Pigulski A, Cugier H, Popowicz A, Kuschnig R, Moffat AFJ, Rucinski SM, Schwarzenberg-Czerny A, Weiss WW, Handler G, Wade GA, Koudelka O, Matthews JM, Mochnecki S, Orleañski P, Pablo H, Ramiaramanantsoa T, Whittaker G, Zocłońska E, Zwintz K (2016) Massive pulsating stars observed by BRITe-Constellation. I. The triple system β Centauri (Agena). *A&A* 588:A55. <https://doi.org/10.1051/0004-6361/201527872>. arXiv:1602.02806 [astro-ph.SR]
- Pilecki B, Pietrzyński G, Graczyk D, Gieren W (2016) Cepheids in eclipsing binary systems. In: Różańska A, Bejger M (eds) XXXVII Polish Astronomical Society Meeting, PTA Proceedings, vol 3. Warszawa, pp 31–34
- Pinsonneault MH, Elsworth YP, Tayar J, Serenelli A, Stello D, Zinn J, Mathur S, García RA, Johnson JA, Hekker S, Huber D, Kallinger T, Mészáros S, Mosser B, Stassun K, Girardi L, Rodrigues TS, Silva Aguirre V, An D, Basu S, Chaplin WJ, Corsaro E, Cunha K, García-Hernández DA, Holtzman J, Jönsson H, Shtrom H, Smith VV, Sobeck JS, Stringfellow GS, Zamora O, Beers TC, Fernández-Trincado JG, Frinchaboy PM, Hearty FR, Nitschelm C (2018) The second APOKASC catalog: the empirical approach. *ApJS* 239(2):32. <https://doi.org/10.3847/1538-4365/aabfd>. arXiv:1804.09983 [astro-ph.SR]
- Pojmanski G (1997) The all sky automated survey. *Acta Astron.* 47:467–481. arXiv:astro-ph/9712146
- Pont F, Eyer L (2004) Isochrone ages for field dwarfs: method and application to the age-metallicity relation. *MNRAS* 351:487–504. <https://doi.org/10.1111/j.1365-2966.2004.07780.x>. arXiv:astro-ph/0401418
- Popper DM, Hill G (1991) Rediscovery of eclipsing binaries. XVII. Spectroscopic orbits of OB systems with a cross-correlation procedure. *AJ* 101:600. <https://doi.org/10.1086/115709>
- Pourbaix D, Boffin HMJ (2003) Reprocessing the Hipparcos Intermediate Astrometric Data of spectroscopic binaries. II. Systems with a giant component. *A&A* 398:1163–1177. <https://doi.org/10.1051/0004-6361:20021736>. arXiv:astro-ph/0211483
- Pourbaix D, Jorissen A (2000) Re-processing the Hipparcos Transit Data and Intermediate Astrometric Data of spectroscopic binaries. I. Ba, CH and Tc-poor S stars. *A&AS* 145:161–183. <https://doi.org/10.1051/aas:2000346>. arXiv:astro-ph/0006175
- Prada Moroni PG, Gennaro M, Bono G, Pietrzyński G, Gieren W, Pilecki B, Graczyk D, Thompson IB (2012) On the evolutionary and pulsation mass of classical Cepheids. III. The case of the eclipsing binary Cepheid CEP0227 in the Large Magellanic Cloud. *ApJ* 749(2):108. <https://doi.org/10.1088/0004-637X/749/2/108>. arXiv:1202.2855 [astro-ph.SR]
- Pribulla T, Chochol D, Parimucha Š (2003) Photometric and spectroscopic study of the symbiotic Nova V1329 Cyg. In: Corradi RLM, Mikolajewska R, Mahoney TJ (eds) Symbiotic stars probing stellar evolution. ASP Conference Series, vol 303. Astronomical Society of the Pacific, San Francisco, p 245
- Prieto-Arranz J, Palle E, Gandolfi D, Barragán O, Guenther EW, Dai F, Fridlund M, Hirano T, Livingston J, Luque R et al (2018) Mass determination of the 1:3:5 near-resonant planets transiting GJ 9827 (K2-135). *A&A* 618:A116. <https://doi.org/10.1051/0004-6361/201832872>. arXiv:1802.09557 [astro-ph.EP]
- Quiroga C, Mikołajewska J, Brandi E, Ferrer O, García L (2002) The spectroscopic orbits and the geometrical configuration of the symbiotic binary AR Pavonis. *A&A* 387:139–150. <https://doi.org/10.1051/0004-6361:20020335>. arXiv:astro-ph/0203288
- Raffelt G, Weiss A (1995) Red giant bound on the axion–electron coupling reexamined. *Phys. Rev. D* 51(4):1495–1498. <https://doi.org/10.1103/PhysRevD.51.1495>. arXiv:hep-ph/9410205

- Raghavan D, McAlister HA, Torres G, Latham DW, Mason BD, Boyajian TS, Baines EK, Williams SJ, ten Brummelaar TA, Farrington CD, Ridgway ST, Sturmman L, Sturmman J, Turner NH (2009) The visual orbit of the 1.1 day spectroscopic binary σ^2 Coronae Borealis from interferometry at the Chara Array. *ApJ* 690(1):394–406. <https://doi.org/10.1088/0004-637X/690/1/394>. arXiv:0808.4015 [astro-ph]
- Ramírez I, Meléndez J, Asplund M (2009) Accurate abundance patterns of solar twins and analogs. Does the anomalous solar chemical composition come from planet formation? *A&A* 508:L17
- Ramírez-Agudelo OH, Sana H, de Koter A, Tramper F, Grin NJ, Schneider FRN, Langer N, Puls J, Markova N, Bestenlehner JM, Castro N, Crowther PA, Evans CJ, García M, Gräfener G, Herrero A, van Kempen B, Lennon DJ, Maíz Apellániz J, Najarro F, Sabín-Sanjulián C, Simón-Díaz S, Taylor WD, Vink JS (2017) The VLT-FLAMES Tarantula Survey . XXIV. Stellar properties of the O-type giants and supergiants in 30 Doradus. *A&A* 600:A81. <https://doi.org/10.1051/0004-6361/201628914>. arXiv:1701.04758 [astro-ph.SR]
- Rasio FA, Tout CA, Lubow SH, Livio M (1996) Tidal decay of close planetary orbits. *ApJ* 470:1187. <https://doi.org/10.1086/177941>. arXiv:astro-ph/9605059
- Rauer H, Catala C, Aerts C et al (2014) The PLATO 2.0 mission. *Exp Astro* 38:249. <https://doi.org/10.1007/s10686-014-9383-4>
- Rawls ML, Gaulme P, McKeever J, Jackiewicz J, Orosz JA, Corsaro E, Beck PG, Mosser B, Latham DW, Latham CA (2016) KIC 9246715: the double red giant eclipsing binary with odd oscillations. *ApJ* 818(2):108. <https://doi.org/10.3847/0004-637X/818/2/108>. arXiv:1601.00038 [astro-ph.SR]
- Reese DR, Marques JP, Goupil MJ, Thompson MJ, Deheuvels S (2012) Estimating stellar mean density through seismic inversions. *A&A* 539:A63. <https://doi.org/10.1051/0004-6361/201118156>. arXiv:1201.1844 [astro-ph.SR]
- Reffert S, Bergmann C, Quirrenbach A, Trifonov T, Künstler A (2015) Precise radial velocities of giant stars. VII. Occurrence rate of giant extrasolar planets as a function of mass and metallicity. *A&A* 574:A116. <https://doi.org/10.1051/0004-6361/201322360>. arXiv:1412.4634 [astro-ph.EP]
- Reindl N, Schaffenroth V, Miller Bertolami MM, Geier S, Finch NL, Barstow MA, Casewell SL, Taubenberger S (2020) An in-depth reanalysis of the alleged type Ia supernova progenitor Henize 2-428. *A&A* 638:A93. <https://doi.org/10.1051/0004-6361/202038117>. arXiv:2006.14688 [astro-ph.SR]
- Rendle BM, Buldgen G, Miglio A, Reese D, Noels A, Davies GR, Campante TL, Chaplin WJ, Lund MN, Kuszewicz JS, Scott LJA, Scuflaire R, Ball WH, Smetana J, Nsamba B (2019) AIMS—a new tool for stellar parameter determinations using asteroseismic constraints. *MNRAS* 484(1):771–786
- Ribas I, Morales JC, Jordi C, Baraffe I, Chabrier G, Gallardo J (2008) Fundamental properties of low-mass stars. *Mem Soc Astron Ital* 79:562 arXiv:0711.4451 [astro-ph]
- Ricker GR, Winn JN, Vanderspek R, Latham DW, Bakos GÁ, Bean JL, Berta-Thompson ZK, Brown TM, Buchhave L et al (2015) Transiting Exoplanet Survey Satellite (TESS). *J Astron Telesc Instrum Syst* 1:014003. <https://doi.org/10.1117/1.JATIS.1.1.014003>
- Ricker GR, Vanderspek R, Winn J, Seager S, Berta-Thompson Z, Levine A, Villaseñor J, Latham D, Charbonneau D, Holman M, Johnson J, Sasselov D, Szentgyorgyi A, Torres G, Bakos G, Brown T, Christensen-Dalsgaard J, Kjeldsen H, Clampin M, Rinehart S, Deming D, Doty J, Dunham E, Ida S, Kawai N, Sato B, Jenkins J, Lissauer J, Jernigan G, Kaltenecker L, Laughlin G, Lin D, McCullough P, Narita N, Pepper J, Stassun K, Udry S (2016) The Transiting Exoplanet Survey Satellite. In: MacEwen HA, Fazio GG, Lystrup M (eds) *Space Telescopes and Instrumentation 2016: Optical, Infrared, and Millimeter Wave*. Proceedings of SPIE, vol 9904. SPIE, p 99042B. <https://doi.org/10.1117/12.2232071>
- Rodrigues TS, Girardi L, Miglio A, Bossini D, Bovy J, Epstein C, Pinsonneault MH, Stello D, Zasowski G, Allende Prieto C, Chaplin WJ, Hekker S, Johnson JA, Mészáros S, Mosser B, Anders F, Basu S, Beers TC, Chiappini C, da Costa LAN, Elsworth Y, García RA, García Pérez AE, Hearty FR, Maia MAG, Majewski SR, Mathur S, Montalbán J, Nidever DL, Santiago B, Schultheis M, Serenelli A, Shetrone M (2014) Bayesian distances and extinctions for giants observed by Kepler and APOGEE. *MNRAS* 445(3):2758–2776. <https://doi.org/10.1093/mnras/stu1907>. arXiv:1410.1350 [astro-ph.SR]
- Rodrigues TS, Bossini D, Miglio A, Girardi L, Montalbán J, Noels A, Trabucchi M, Coelho HR, Marigo P (2017) Determining stellar parameters of asteroseismic targets: going beyond the use of scaling relations. *MNRAS* 467(2):1433–1448. <https://doi.org/10.1093/mnras/stx120>. arXiv:1701.04791 [astro-ph.SR]

- Rogers TM, McElwaine JN (2017) On the chemical mixing induced by internal gravity waves. *ApJL* 848:L1. <https://doi.org/10.3847/2041-8213/aa8d13>. arXiv:1709.04920 [astro-ph.SR]
- Romero AD, Córscico AH, Althaus LG, Kepler SO, Castanheira BG, Miller Bertolami MM (2012) Toward ensemble asteroseismology of ZZ Ceti stars with fully evolutionary models. *MNRAS* 420(2):1462–1480. <https://doi.org/10.1111/j.1365-2966.2011.20134.x>. arXiv:1109.6682 [astro-ph.SR]
- Romero AD, Kepler SO, Joyce SRG, Lauffer GR, Córscico AH (2019) The white dwarf mass-radius relation and its dependence on the hydrogen envelope. *MNRAS* 484(2):2711–2724. <https://doi.org/10.1093/mnras/stz160>. arXiv:1901.04644 [astro-ph.SR]
- Rosenfeld KA, Andrews SM, Wilner DJ, Stempels HC (2012) A disk-based dynamical mass estimate for the young binary V4046 Sgr. *ApJ* 759:119. <https://doi.org/10.1088/0004-637X/759/2/119>. arXiv:1209.4407 [astro-ph.SR]
- Rosenthal CS, Christensen-Dalsgaard J, Nordlund Å, Stein RF, Trampedach R (1999) Convective contributions to the frequencies of solar oscillations. *A&A* 351:689–700
- Roxburgh IW (2018) Overfitting and correlations in model fitting with separation ratios. arXiv e-prints arXiv:1808.07556
- Roxburgh IW, Vorontsov SV (2003) The ratio of small to large separations of acoustic oscillations as a diagnostic of the interior of solar-like stars. *A&A* 411:215–220. <https://doi.org/10.1051/0004-6361:20031318>
- Rozyczka M, Kaluzny J, Pietrukowicz P, Pych W, Mazur B, Catelan M, Thompson IB (2009) A new lower main sequence eclipsing binary with detached components. *Acta Astron* 59:385–401 arXiv:0910.2543 [astro-ph.SR]
- Rucinski SM (1992) Spectral-line broadening functions of WUMa-type binaries. I. AW UMa. *AJ* 104:1968. <https://doi.org/10.1086/116372>
- Russell HN, Adams WS, Joy AH (1923) A comparison of spectroscopic and dynamical parallaxes. *PASP* 35:189. <https://doi.org/10.1086/123303>
- Rutten RJ, Uitenbroek H (2012) Chromospheric backradiation in ultraviolet continua and H α . *A&A* 540:A86. <https://doi.org/10.1051/0004-6361/201118525>. arXiv:1203.0396 [astro-ph.SR]
- Sabín-Sanjulián C, Simón-Díaz S, Herrero A, Puls J, Schneider FRN, Evans CJ, García M, Najarro F, Brott I, Castro N, Crowther PA, de Koter A, de Mink SE, Gräfener G, Grin NJ, Holgado G, Langer N, Lennon DJ, Maíz Apellániz J, Ramírez-Agudelo OH, Sana H, Taylor WD, Vink JS, Walborn NR (2017) The VLT-FLAMES Tarantula Survey. XXVI. Properties of the O-dwarf population in 30 Doradus. *A&A* 601:A79. <https://doi.org/10.1051/0004-6361/201629210>. arXiv:1702.04773 [astro-ph.SR]
- Sahlholdt CL, Silva Aguirre V (2018) Asteroseismic radii of dwarfs: new accuracy constraints from Gaia DR2 parallaxes. *MNRAS* 481(1):L125–L129. <https://doi.org/10.1093/mnras/sly173>. arXiv:1809.05112 [astro-ph.SR]
- Sahlholdt CL, Feltzing S, Lindegren L, Church RP (2019) Benchmark ages for the Gaia benchmark stars. *MNRAS* 482(1):895–920. <https://doi.org/10.1093/mnras/sty2732>. arXiv:1810.02829 [astro-ph.SR]
- Sahu KC, Anderson J, Casertano S, Bond HE, Bergeron P, Nelan EP, Pueyo L, Brown TM, Bellini A, Levay ZG, Sokol J, Dominik M, Calamida A, Kains N, Livio M (2017) Relativistic deflection of background starlight measures the mass of a nearby white dwarf star. *Science* 356(6342):1046–1050. <https://doi.org/10.1126/science.aal2879>. arXiv:1706.02037 [astro-ph.SR]
- Sahu KC, Anderson J, Bellini A, Belokurov V, Bergeron P, Bond HE, Bramich D, Brown TM, Calamida A, Casertano S, Dominik M, Evans W, Kains N, Klueter J, McGill P, Nelan E, Nielsen MB, Smart R, Smith L, Wambsgans J (2019) Accurate mass determination of the nearby single white dwarf L145-141 (LAWD 37) through astrometric microlensing. HST Proposal. Cycle 26, #15705
- Salaris M, Weiss A (2001) Atomic diffusion in metal-poor stars. II. Predictions for the Spite plateau. *A&A* 376:955–965. <https://doi.org/10.1051/0004-6361:20010982>. arXiv:astro-ph/0104406
- Salaris M, Serenelli A, Weiss A, Miller Bertolami M (2009) Semi-empirical white dwarf initial-final mass relationships: a thorough analysis of systematic uncertainties due to stellar evolution models. *ApJ* 692(2):1013–1032. <https://doi.org/10.1088/0004-637X/692/2/1013>. arXiv:0807.3567 [astro-ph]
- Salaris M, Althaus LG, García-Berro E (2013) Comparison of theoretical white dwarf cooling timescales. *A&A* 555:A96. <https://doi.org/10.1051/0004-6361/201220622>. arXiv:1306.2575 [astro-ph.SR]
- Salaris M, Pietrinfermi A, Piersimoni AM, Cassisi S (2015) Post first dredge-up [C/N] ratio as age indicator. Theoretical calibration. *A&A* 583:A87. <https://doi.org/10.1051/0004-6361/201526951>. arXiv:1509.06904 [astro-ph.SR]

- Sana H, de Mink SE, de Koter A, Langer N, Evans CJ, Gieles M, Gosset E, Izzard RG, Le Bouquin JB, Schneider FRN (2012) Binary interaction dominates the evolution of massive stars. *Science* 337:444–446. <https://doi.org/10.1126/science.1223344>. arXiv:1207.6397 [astro-ph.SR]
- Sanders JL, Das P (2018) Isochrone ages for 3 million stars with the second Gaia data release. *MNRAS* 481(3):4093–4110. <https://doi.org/10.1093/mnras/sty2490>. arXiv:1806.02324 [astro-ph.GA]
- Santander-García M, Rodríguez-Gil P, Corradi RLM, Jones D, Miszalski B, Boffin HMJ, Rubio-Díez MM, Kotze MM (2015) The double-degenerate, super-Chandrasekhar nucleus of the planetary nebula Henize 2–428. *Nature* 519(7541):63–65. <https://doi.org/10.1038/nature14124>. arXiv:1609.00178 [astro-ph.SR]
- Schaefer GH, Hummel CA, Gies DR, Zavala RT, Monnier JD, Walter FM, Turner NH, Baron F, ten Brummelaar T, Che X, Farrington CD, Kraus S, Sturmman J, Sturmman L (2016) Orbits, distance, and stellar masses of the massive triple star σ Orionis. *AJ* 152(6):213. <https://doi.org/10.3847/0004-6256/152/6/213>. arXiv:1610.01984 [astro-ph.SR]
- Schafferoth V, Barlow BN, Drechsel H, Dunlap BH (2015) An eclipsing post common-envelope system consisting of a pulsating hot subdwarf B star and a brown dwarf companion. *A&A* 576:A123. <https://doi.org/10.1051/0004-6361/201525701>. arXiv:1502.04459 [astro-ph.SR]
- Schafferoth V, Barlow BN, Geier S, Vučković M, Kilkenny D, Wolz M, Kupfer T, Heber U, Drechsel H, Kimeswenger S, Marsh T, Wolf M, Pelisoli I, Freudenthal J, Dreizler S, Kreuzer S, Ziegerer E (2019) The EREBOS project: investigating the effect of substellar and low-mass stellar companions on late stellar evolution. Survey, target selection, and atmospheric parameters. *A&A* 630:A80. <https://doi.org/10.1051/0004-6361/201936019>. arXiv:1907.09892 [astro-ph.SR]
- Schiavon RP, Zamora O, Carrera R, Lucatello S, Robin AC, Ness M, Martell SL, Smith VV, García-Hernández DA, Manchado A, Schönrich R, Bastian N, Chiappini C, Shetrone M, Mackereth JT, Williams RA, Mészáros S, Allende Prieto C, Anders F, Bizyaev D, Beers TC, Chojnowski SD, Cunha K, Epstein C, Frinchaboy PM, García Pérez AE, Hearty FR, Holtzman JA, Johnson JA, Kinemuchi K, Majewski SR, Muna D, Nidever DL, Nguyen DC, O’Connell RW, Oravetz D, Pan K, Pinsonneault M, Schneider DP, Schultheis M, Simmons A, Skrutskie MF, Sobek J, Wilson JC, Zasowski G (2017) Chemical tagging with APOGEE: discovery of a large population of N-rich stars in the inner Galaxy. *MNRAS* 465(1):501–524. <https://doi.org/10.1093/mnras/stw2162>. arXiv:1606.05651 [astro-ph.GA]
- Schild H, Schmid HM (1997) Spectropolarimetry and nebular geometry of the symbiotic star HBV 475. *A&A* 324:606–616
- Schlaufman KC, Winn JN (2013) Evidence for the tidal destruction of hot Jupiters by subgiant stars. *ApJ* 772(2):143. <https://doi.org/10.1088/0004-637X/772/2/143>. arXiv:1306.0567 [astro-ph.EP]
- Schneider FRN, Langer N, de Koter A, Brott I, Izzard RG, Lau HHB (2014) BONNSAI: a Bayesian tool for comparing stars with stellar evolution models. *A&A* 570:A66. <https://doi.org/10.1051/0004-6361/201424286>. arXiv:1408.3409 [astro-ph.SR]
- Schneider FRN, Castro N, Fossati L, Langer N, de Koter A (2017) BONNSAI: correlated stellar observables in Bayesian methods. *A&A* 598:A60. <https://doi.org/10.1051/0004-6361/201628409>. arXiv:1610.08071 [astro-ph.SR]
- Schneider FRN, Sana H, Evans CJ, Bestenlehner JM, Castro N, Fossati L, Gräfenor G, Langer N, Ramírez-Agudelo OH, Sabín-Sanjulián C et al (2018) An excess of massive stars in the local 30 Doradus starburst. *Science* 359:69–71. <https://doi.org/10.1126/science.aan0106>. arXiv:1801.03107 [astro-ph.SR]
- Schneider P, Ehlers J, Falco EE (1992) Gravitational lenses. Springer, Berlin. <https://doi.org/10.1007/978-3-662-03758-4>
- Schofield M, Chaplin WJ, Huber D, Campante TL, Davies GR, Miglio A, Ball WH, Appourchoux T, Basu S, Bedding TR, Christensen-Dalsgaard J, Creevey O, García RA, Handberg R, Kawaler SD, Kjeldsen H, Latham DW, Lund MN, Metcalfe TS, Ricker GR, Serenelli A, Silva Aguirre V, Stello D, Vanderspek R (2019) The asteroseismic target list for solar-like oscillators observed in 2 minute Cadence with the Transiting Exoplanet Survey Satellite. *Astrophys J Suppl Ser* 241(1):12
- Schönrich R, Bergemann M (2014) Fundamental stellar parameters and metallicities from Bayesian spectroscopy: application to low- and high-resolution spectra. *MNRAS* 443:698–717. <https://doi.org/10.1093/mnras/stu1072>. arXiv:1311.5558 [astro-ph.SR]
- Schröder KP, Pols OR, Eggleton PP (1997) A critical test of stellar evolution and convective core ‘overshooting’ by means of zeta Aurigae systems. *MNRAS* 285(4):696–710. <https://doi.org/10.1093/mnras/285.4.696>

- Schweitzer A, Passegger VM, Cifuentes C, Béjar VJS, Cortés-Contreras M, Caballero JA, del Burgo C, Czesla S, Kürster M, Montes D, Zapatero Osorio MR, Ribas I, Reiners A, Quirenbach A, Amado PJ, Aceituno J, Anglada-Escudé G, Bauer FF, Dreizler S, Jeffers SV, Guenther EW, Henning T, Kaminski A, Lafarga M, Marfil E, Morales JC, Schmitt JHMM, Seifert W, Solano E, Tabernero HM, Zechmeister M (2019) The CARMENES search for exoplanets around M dwarfs. Different roads to radii and masses of the target stars. *A&A* 625:A68. <https://doi.org/10.1051/0004-6361/201834965>. arXiv:1904.03231 [astro-ph.SR]
- Seager S, Mallén-Ornelas G (2003) A unique solution of planet and star parameters from an extrasolar planet transit light curve. *ApJ* 585(2):1038–1055. <https://doi.org/10.1086/346105>. arXiv:astro-ph/0206228
- Sekaran S, Johnston C, Tkachenko A, Beck PG, Prša A, Hambleton KM (2019) Two's a crowd? Characterising the effect of photometric contamination on the extraction of the global asteroseismic parameter v_{max} in red-giant binaries. *A&A* 624:A140. <https://doi.org/10.1051/0004-6361/201834095>. arXiv:1903.09146 [astro-ph.SR]
- Semenova E, Bergemann M, Deal M, Serenelli A, Hansen CJ, Gallagher AJ, Bayo A, Bensby T, Bragaglia A, Carraro G, Morbidelli L, Pancino E, Smiljanic R (2020) The Gaia-ESO survey: 3D NLTE abundances in the open cluster NGC 2420 suggest atomic diffusion and turbulent mixing are at the origin of chemical abundance variations. *A&A* 643:A164. <https://doi.org/10.1051/0004-6361/202038833>. arXiv:2007.09153 [astro-ph.SR]
- Serenelli AM, Bergemann M, Ruchti G, Casagrande L (2013) Bayesian analysis of ages, masses and distances to cool stars with non-LTE spectroscopic parameters. *MNRAS* 429:3645–3657. <https://doi.org/10.1093/mnras/sts648>. arXiv:1212.4497 [astro-ph.SR]
- Serenelli A, Johnson J, Huber D, Pinsonneault M, Ball WH, Tayar J, Silva Aguirre V, Basu S, Troup N, Hekker S, Kallinger T, Stello D, Davies GR, Lund MN, Mathur S, Mosser B, Stassun KG, Chaplin WJ, Elsworth Y, García RA, Handberg R, Holtzman J, Hearty F, García-Hernández DA, Gaulme P, Zamora O (2017a) The first APOKASC catalog of Kepler dwarf and subgiant stars. *ApJS* 233(2):23. <https://doi.org/10.3847/1538-4365/aa97df>. arXiv:1710.06858 [astro-ph.SR]
- Serenelli A, Weiss A, Cassisi S, Salaris M, Pietrinferni A (2017b) The brightness of the red giant branch tip. Theoretical framework, a set of reference models, and predicted observables. *A&A* 606:A33. <https://doi.org/10.1051/0004-6361/201731004>. arXiv:1706.09910 [astro-ph.SR]
- Shanahan RL, Gieles M (2015) Biases in the inferred mass-to-light ratio of globular clusters: no need for variations in the stellar mass function. *MNRAS* 448:L94–L98. <https://doi.org/10.1093/mnras/flu205>. arXiv:1501.04971
- Shetrone M, Tayar J, Johnson JA, Somers G, Pinsonneault MH, Holtzman JA, Hasselquist S, Masseron T, Mészáros S, Jönsson H, Hawkins K, Sobek J, Zamora O, García-Hernández DA (2019) Constraining metallicity-dependent mixing and extra mixing using [C/N] in alpha-rich field giants. *ApJ* 872(2):137. <https://doi.org/10.3847/1538-4357/aaff66>. arXiv:1901.09592 [astro-ph.SR]
- Shetye S, Van Eck S, Jorissen A, Van Winckel H, Siess L, Goriely S, Escorça A, Karinkuzhi D, Plez B (2018) S stars and s-process in the Gaia era. I. Stellar parameters and chemical abundances in a subsample of S stars with new MARCS model atmospheres. *A&A* 620:A148. <https://doi.org/10.1051/0004-6361/201833298>. arXiv:1810.07105 [astro-ph.SR]
- Shkedy Z, Decin L, Molenberghs G, Aerts C (2007) Estimating stellar parameters from spectra using a hierarchical Bayesian approach. *MNRAS* 377:120–132. <https://doi.org/10.1111/j.1365-2966.2007.11508.x>. arXiv:astro-ph/0701449
- Silva Aguirre V, Ballot J, Serenelli AM, Weiss A (2011) Constraining mixing processes in stellar cores using asteroseismology. Impact of semiconvection in low-mass stars. *A&A* 529:63
- Silva Aguirre V, Basu S, Brandão IM, Christensen-Dalsgaard J, Deheuvels S, Doğan G, Metcalfe TS, Serenelli AM, Ballot J, Chaplin WJ, Cunha MS, Weiss A, Appourchaux T, Casagrande L, Cassisi S, Creevey OL, García RA, Lebreton Y, Noels A, Sousa SG, Stello D, White TR, Kawaler SD, Kjeldsen H (2013) Stellar ages and convective cores in field main-sequence stars: first asteroseismic application to two Kepler targets. *ApJ* 769(2):141
- Silva Aguirre V, Davies GR, Basu S, Christensen-Dalsgaard J, Creevey O, Metcalfe TS, Bedding TR, Casagrande L, Handberg R, Lund MN, Nissen PE, Chaplin WJ, Huber D, Serenelli AM, Stello D, Van Eylen V, Campante TL, Elsworth Y, Gilliland RL, Hekker S, Karoff C, Kawaler SD, Kjeldsen H, Lundkvist MS (2015) Ages and fundamental properties of Kepler exoplanet host stars from asteroseismology. *MNRAS* 452(2):2127–2148. <https://doi.org/10.1093/mnras/stv1388>. arXiv:1504.07992 [astro-ph.SR]

- Silva Aguirre V, Lund MN, Antia HM, Ball WH, Basu S, Christensen-Dalsgaard J, Lebreton Y, Reese DR, Verma K, Casagrande L, Justesen AB, Mosumgaard JR, Chaplin WJ, Bedding TR, Davies GR, Handberg R, Houdek G, Huber D, Kjeldsen H, Latham DW, White TR, Coelho HR, Miglio A, Rendle B (2017) Standing on the shoulders of dwarfs: the Kepler asteroseismic LEGACY sample. II. Radii, masses, and ages. *ApJ* 835:173. <https://doi.org/10.3847/1538-4357/835/2/173>. arXiv:1611.08776 [astro-ph.SR]
- Silva Aguirre V, Christensen-Dalsgaard J, Cassisi S, Miller Bertolami M, Serenelli A, Stello D, Weiss A, Angelou G, Jiang C, Lebreton Y, Spada F, Bellinger EP, Deheuvels S, Ouazzani RM, Pietrinferni A, Mosumgaard JR, Townsend RHD, Battich T, Bossini D, Constantino T, Eggenberger P, Hekker S, Mazumdar A, Miglio A, Nielsen KB, Salaris M (2020) The Aarhus red giants challenge. I. Stellar structures in the red giant branch phase. *A&A* 635:A164. <https://doi.org/10.1051/0004-6361/201935843>. arXiv:1912.04909 [astro-ph.SR]
- Simkin SM (1974) Measurements of velocity dispersions and Doppler shifts from digitized optical spectra. *A&A* 31:129
- Simon KP, Sturm E (1994) Disentangling of composite spectra. *A&A* 281:286–291
- Simon M, Dutrey A, Guilloreau S (2000) Dynamical masses of T Tauri stars and calibration of pre-main-sequence evolution. *ApJ* 545:1034–1043. <https://doi.org/10.1086/317838>. arXiv:astro-ph/0008370
- Simon M, Guilloreau S, Di Folco E, Dutrey A, Grosso N, Piétu V, Chapillon E, Prato L, Schaefer GH, Rice E, Boehler Y (2017) Dynamical masses of low-mass stars in the Taurus and Ophiuchus star-forming regions. *ApJ* 844:158. <https://doi.org/10.3847/1538-4357/aa78f1>. arXiv:1706.03505 [astro-ph.SR]
- Simón-Díaz S, Herrero A (2014) The IACOB project. I. Rotational velocities in northern Galactic O- and early B-type stars revisited. The impact of other sources of line-broadening. *A&A* 562:A135. <https://doi.org/10.1051/0004-6361/201322758>. arXiv:1311.3360 [astro-ph.SR]
- Sippel AC, Hurley JR, Madrid JP, Harris WE (2012) N-body models of globular clusters: metallicities, half-light radii and mass-to-light ratios. *MNRAS* 427:167–179. <https://doi.org/10.1111/j.1365-2966.2012.21969.x>. arXiv:1208.4851
- Sivervd RJ, Beatty TG, Pepper J, Eastman JD, Collins K, Bieryla A, Latham DW, Buchhave LA, Jensen ELN, Crepp JR et al (2012) KELT-1b: a strongly irradiated, highly inflated, short period, 27 Jupiter-mass companion transiting a mid-F star. *ApJ* 761:123. <https://doi.org/10.1088/0004-637X/761/2/123>. arXiv:1206.1635 [astro-ph.EP]
- Smartt SJ (2015) Observational constraints on the progenitors of core-collapse supernovae: the case for missing high-mass stars. *PASA* 32:e016. <https://doi.org/10.1017/pasa.2015.17>. arXiv:1504.02635 [astro-ph.SR]
- Smiljanic R, Donati P, Bragaglia A, Lemasle B, Romano D (2018) Deep secrets of intermediate-mass giants and supergiants. Models with rotation seem to overestimate mixing effects on the surface abundances of C, N, and Na. *A&A* 616:A112. <https://doi.org/10.1051/0004-6361/201832877>. arXiv:1805.03460 [astro-ph.SR]
- Sollima A, Baumgardt H (2017) The global mass functions of 35 Galactic globular clusters: I. Observational data and correlations with cluster parameters. *MNRAS* 471(3):3668–3679. <https://doi.org/10.1093/mnras/stx1856>. arXiv:1708.09529 [astro-ph.GA]
- Sollima A, Bellazzini M, Lee JW (2012) A comparison between the stellar and dynamical masses of six globular clusters. *ApJ* 755:156. <https://doi.org/10.1088/0004-637X/755/2/156>. arXiv:1206.4828 [astro-ph.GA]
- Sonoi T, Samadi R, Belkacem K, Ludwig HG, Caffau E, Mosser B (2015) Surface-effect corrections for solar-like oscillations using 3D hydrodynamical simulations. I. Adiabatic oscillations. *A&A* 583:A112. <https://doi.org/10.1051/0004-6361/201526838>. arXiv:1510.00300 [astro-ph.SR]
- Southworth J (2010) Homogeneous studies of transiting extrasolar planets—III. Additional planets and stellar models. *MNRAS* 408(3):1689–1713. <https://doi.org/10.1111/j.1365-2966.2010.17231.x>. arXiv:1006.4443 [astro-ph.EP]
- Southworth J (2012) Homogeneous studies of transiting extrasolar planets—V. New results for 38 planets. *MNRAS* 426(2):1291–1323. <https://doi.org/10.1111/j.1365-2966.2012.21756.x>. arXiv:1207.5796 [astro-ph.EP]
- Southworth J (2015) DEBCat: a catalog of detached eclipsing binary stars. In: Rucinski SM, Torres G, Zejda M (eds) Living together: planets, host stars and binaries. ASP Conference Series, vol 496. Astronomical Society of the Pacific, San Francisco, p 164. arXiv:1411.1219 [astro-ph.SR]

- Southworth J, Clausen JV (2007) Absolute dimensions of eclipsing binaries. XXIV. The Be star system DW Carinae, a member of the open cluster Collinder 228. *A&A* 461(3):1077–1093. <https://doi.org/10.1051/0004-6361:20065614>. arXiv:astro-ph/0610404
- Southworth J, Maxted PFL, Smalley B (2004) Eclipsing binaries in open clusters—II. V453 Cyg in NGC 6871. *MNRAS* 351(4):1277–1289. <https://doi.org/10.1111/j.1365-2966.2004.07871.x>. arXiv:astro-ph/0403572
- Southworth J, Smalley B, Maxted PFL, Claret A, Etzel PB (2005) Absolute dimensions of detached eclipsing binaries—I. The metallic-lined system WW Aurigae. *MNRAS* 363(2):529–542. <https://doi.org/10.1111/j.1365-2966.2005.09462.x>. arXiv:astro-ph/0507629
- Southworth J, Bruntt H, Buzasi DL (2007) Eclipsing binaries observed with the WIRE satellite. II. β Aurigae and non-linear limb darkening in light curves. *A&A* 467(3):1215–1226. <https://doi.org/10.1051/0004-6361:20077184>. arXiv:astro-ph/0703634
- Southworth J, Pavlovski K, Tamajo E, Smalley B, West RG, Anderson DR (2011) Absolute dimensions of detached eclipsing binaries—II. The metallic-lined system XY Ceti. *MNRAS* 414(4):3740–3750. <https://doi.org/10.1111/j.1365-2966.2011.18676.x>. arXiv:1103.1519 [astro-ph.SR]
- Southworth J, Bowman DM, Tkachenko A, Pavlovski K (2020) Discovery of β Cep pulsations in the eclipsing binary V453 Cygni. *MNRAS* 497(1):L19–L23. <https://doi.org/10.1093/mnras/slaa091>. arXiv:2005.07559 [astro-ph.SR]
- Southworth J, Bowman DM, Pavlovski K (2021) A β Cephei pulsator and a changing orbital inclination in the high-mass eclipsing binary system VV Orionis. *MNRAS* 501(1):L65–L70. <https://doi.org/10.1093/mnras/slaa197>. arXiv:2012.03947 [astro-ph.SR]
- Sozzetti A, Torres G, Charbonneau D, Latham DW, Holman MJ, Winn JN, Laird JB, O'Donovan FT (2007) Improving stellar and planetary parameters of transiting planet systems: the case of TrES-2. *ApJ* 664(2):1190–1198. <https://doi.org/10.1086/519214>. arXiv:0704.2938 [astro-ph]
- Spitzer LJ, Hart MH (1971) Random gravitational encounters and the evolution of spherical systems. I. Method. *ApJ* 164:399
- Spruit HC, Weiss A (1986) Colors and luminosities of stars with spots. *A&A* 166:167–176
- Stairs IH (2003) Testing general relativity with pulsar timing. *Living Rev Relativ* 6:5. <https://doi.org/10.12942/lrr-2003-5>. arXiv:astro-ph/0307536 [astro-ph]
- Stancliffe RJ, Fossati L, Passy JC, Schneider FRN (2015) Confronting uncertainties in stellar physics: calibrating convective overshooting with eclipsing binaries. *A&A* 575:A117. <https://doi.org/10.1051/0004-6361/201425126>. arXiv:1501.05322 [astro-ph.SR]
- Stassun KG, Torres G (2016a) Eclipsing binaries as benchmarks for trigonometric parallaxes in the Gaia Era. *AJ* 152:180. <https://doi.org/10.3847/0004-6256/152/6/180>
- Stassun KG, Torres G (2016b) Evidence for a systematic offset of -0.25 mas in the Gaia DR1 Parallaxes. *ApJL* 831:L6. <https://doi.org/10.3847/2041-8205/831/1/L6>
- Stassun KG, Mathieu RD, Valenti JA (2006) Discovery of two young brown dwarfs in an eclipsing binary system. *Nature* 440:311–314. <https://doi.org/10.1038/nature04570>
- Stassun KG, Mathieu RD, Valenti JA (2007) A surprising reversal of temperatures in the brown dwarf eclipsing binary 2MASS J05352184-0546085. *ApJ* 664:1154–1166. <https://doi.org/10.1086/519231>. arXiv:0704.3106
- Stassun KG, Feiden GA, Torres G (2014) Empirical tests of pre-main-sequence stellar evolution models with eclipsing binaries. *New Astron Rev* 60:1–28. <https://doi.org/10.1016/j.newar.2014.06.001>. arXiv:1406.3788 [astro-ph.SR]
- Stassun KG, Collins KA, Gaudi BS (2017a) Accurate empirical radii and masses of planets and their host stars with Gaia parallaxes. *AJ* 153(3):136. <https://doi.org/10.3847/1538-3881/aa5df3>. arXiv:1609.04389 [astro-ph.EP]
- Stassun KG, Collins KA, Gaudi BS (2017b) Accurate empirical radii and masses of planets and their host stars with Gaia parallaxes. *AJ* 153:136. <https://doi.org/10.3847/1538-3881/aa5df3>
- Stassun KG, Corsaro E, Pepper JA, Gaudi BS (2018) Empirical accurate masses and radii of single stars with TESS and Gaia. *AJ* 155(1):22. <https://doi.org/10.3847/1538-3881/aa998a>. arXiv:1710.01460 [astro-ph.SR]
- Stauffer JR, Schultz G, Kirkpatrick JD (1998) Keck spectra of Pleiades brown dwarf candidates and a precise determination of the lithium depletion edge in the Pleiades. *ApJL* 499(2):L199–L203. <https://doi.org/10.1086/311379>. arXiv:astro-ph/9804005
- Stauffer JR, Barrado y Navascués D, Bouvier J, Morrison HL, Harding P, Luhman KL, Stanke T, McCaughrean M, Terndrup DM, Allen L, Assouad P (1999) Keck spectra of brown dwarf

- candidates and a precise determination of the lithium depletion boundary in the α Persei open cluster. *ApJ* 527(1):219–229. <https://doi.org/10.1086/308069>. arXiv:astro-ph/9909207
- Steffen JH, Fabrycky DC, Ford EB, Carter JA, Désert JM, Fressin F, Holman MJ, Lissauer JJ, Moorhead AV, Rowe JF et al (2012) Transit timing observations from Kepler—III. Confirmation of four multiple planet systems by a Fourier-domain study of anticorrelated transit timing variations. *MNRAS* 421:2342–2354. <https://doi.org/10.1111/j.1365-2966.2012.20467.x>. arXiv:1201.5412 [astro-ph.EP]
- Steiman-Cameron TY, Johnson HR, Honeycutt RK (1985) Chromospheric activity and TiO bands in M giants. *ApJL* 291:L51–L54. <https://doi.org/10.1086/184457>
- Stello D, Chaplin WJ, Bruntt H, Creevey OL, García-Hernández A, Monteiro MJPG, Moya A, Quirion PO, Sousa SG, Suárez JC, Appourchaux T, Arentoft T, Ballot J, Bedding TR, Christensen-Dalsgaard J, Elsworth Y, Fletcher ST, García RA, Houdek G, Jiménez-Reyes SJ, Kjeldsen H, New R, Régulo C, Salabert D, Toutain T (2009) Radius determination of solar-type stars using asteroseismology: what to expect from the Kepler mission. *ApJ* 700(2):1589–1602. <https://doi.org/10.1088/0004-637X/700/2/1589>. arXiv:0906.0766 [astro-ph.SR]
- Stello D, Huber D, Grundahl F, Lloyd J, Ireland M, Casagrande L, Fredslund M, Bedding TR, Palle PL, Antoci V, Kjeldsen H, Christensen-Dalsgaard J (2017) Asteroseismic masses of retired planet-hosting A-stars using SONG. *MNRAS* 472(4):4110–4116. <https://doi.org/10.1093/mnras/stx2295>. arXiv:1708.09613 [astro-ph.EP]
- Stobie RS (1969) Cepheid pulsation—II. Models fitted to evolutionary tracks. *MNRAS* 144:485. <https://doi.org/10.1093/mnras/144.4.485>
- Stock S, Reffert S, Quirrenbach A (2018) Precise radial velocities of giant stars. X. Bayesian stellar parameters and evolutionary stages for 372 giant stars from the Lick planet search. *A&A* 616:A33. <https://doi.org/10.1051/0004-6361/201833111>. arXiv:1805.04094 [astro-ph.SR]
- Stokholm A, Nissen PE, Silva Aguirre V, White TR, Lund MN, Mosumgaard JR, Huber D, Jessen-Hansen J (2019) The subgiant HR 7322 as an asteroseismic benchmark star. *MNRAS* 489(1):928–940
- Strader J, Caldwell N, Seth AC (2011) Star clusters in M31. V. Internal dynamical trends: some troublesome, some reassuring. *AJ* 142:8. <https://doi.org/10.1088/0004-6256/142/1/8>. arXiv:1104.4649
- Strader J, Chomiuk L, Maccarone TJ, Miller-Jones JCA, Seth AC (2012) Two stellar-mass black holes in the globular cluster M22. *Nature* 490:71–73. <https://doi.org/10.1038/nature11490>. arXiv:1210.0901 [astro-ph.HE]
- Sukhbold T, Ertl T, Woosley SE, Brown JM, Janka HT (2016) Core-collapse supernovae from 9 to 120 solar masses based on neutrino-powered explosions. *ApJ* 821(1):38. <https://doi.org/10.3847/0004-637X/821/1/38>. arXiv:1510.04643 [astro-ph.HE]
- Szewczuk W, Daszyńska-Daszkiewicz J (2018) KIC 3240411—the hottest known SPB star with the asymptotic g-mode period spacing. *MNRAS* 478:2243–2256. <https://doi.org/10.1093/mnras/sty1126>. arXiv:1805.07100 [astro-ph.SR]
- Szigeti L, Mészáros S, Smith VV, Cunha K, Lagarde N, Charbonnel C, García-Hernández DA, Shetrone M, Pinsonneault M, Allende Prieto C, Fernández-Trincado JG, Kovács J, Villanova S (2018) $^{12}\text{C}/^{13}\text{C}$ isotopic ratios in red-giant stars of the open cluster NGC 6791. *MNRAS* 474(4):4810–4817. <https://doi.org/10.1093/mnras/stx3027>. arXiv:1711.08183 [astro-ph.SR]
- Takeda G, Ford EB, Sills A, Rasio FA, Fischer DA, Valenti JA (2007) Structure and evolution of nearby stars with planets. II. Physical properties of ~ 1000 cool stars from the SPOCS catalog. *ApJS* 168:297–318. <https://doi.org/10.1086/509763>. arXiv:astro-ph/0607235
- Tautvaišienė G, Drazdauskas A, Mikolaitis Š, Barisevičius G, Puzeras E, Stonkutė E, Chorniy Y, Magrini L, Romano D, Smiljanic R, Bragaglia A, Carraro G, Friel E, Morel T, Pancino E, Donati P, Jiménez-Esteban F, Gilmore G, Randich S, Jeffries RD, Vallenari A, Bensby T, Flaccomio E, Recio-Blanco A, Costado MT, Hill V, Jofré P, Lardo C, de Laverny P, Masseron T, Moribelli L, Sousa SG, Zaggia S (2015) The Gaia-ESO Survey: CNO abundances in the open clusters Trumpler 20, NGC 4815, and NGC 6705. *A&A* 573:A55. <https://doi.org/10.1051/0004-6361/201424989>. arXiv:1411.2831 [astro-ph.SR]
- Tayar J, Somers G, Pinsonneault MH, Stello D, Mints A, Johnson JA, Zamora O, García-Hernández DA, Maraston C, Serenelli A, Allende Prieto C, Bastien FA, Basu S, Bird JC, Cohen RE, Cunha K, Elsworth Y, García RA, Girardi L, Hekker S, Holtzman J, Huber D, Mathur S, Mészáros S, Mosser B, Shetrone M, Silva Aguirre V, Stassun K, Stringfellow GS, Zasowski G, Roman-Lopes A (2017)

- The correlation between mixing length and metallicity on the giant branch: implications for ages in the Gaia Era. *ApJ* 840(1):17. <https://doi.org/10.3847/1538-4357/aa6a1e>. arXiv:1704.01164 [astro-ph.SR]
- Themeßl N, Hekker S, Southworth J, Beck PG, Pavlovski K, Tkachenko A, Angelou GC, Ball WH, Barban C, Corsaro E, Elsworth Y, Handberg R, Kallinger T (2018) Oscillating red giants in eclipsing binary systems: empirical reference value for asteroseismic scaling relation. *MNRAS* 478(4):4669–4696. <https://doi.org/10.1093/mnras/sty1113>. arXiv:1804.11151 [astro-ph.SR]
- Thévenin F, Oreshina AV, Baturin VA, Gorshkov AB, Morel P, Provost J (2017) Evolution of lithium abundance in the Sun and solar twins. *A&A* 598:A64. <https://doi.org/10.1051/0004-6361/201629385>. arXiv:1612.01331 [astro-ph.SR]
- Tinetti G, Drossart P, Eccleston P et al (2018) A chemical survey of exoplanets with ARIEL. *Exp Astron* 46(1):135–209. <https://doi.org/10.1007/s10686-018-9598-x>
- Tkachenko A, Van Reeth T, Tsymbal V, Aerts C, Kochukhov O, Debosscher J (2013) Denoising spectroscopic data by means of the improved least-squares deconvolution method. *A&A* 560:A37. <https://doi.org/10.1051/0004-6361/201322532>. arXiv:1310.3198 [astro-ph.SR]
- Tkachenko A, Aerts C, Pavlovski K, Degroote P, Pápics PI, Moravveji E, Lehmann H, Kolbas V, Clémer K (2014a) Modelling of σ Scorpii, a high-mass binary with a β Cep variable primary component. *MNRAS* 442(1):616–628. <https://doi.org/10.1093/mnras/stu885>. arXiv:1405.0924 [astro-ph.SR]
- Tkachenko A, Degroote P, Aerts C, Pavlovski K, Southworth J, Pápics PI, Moravveji E, Kolbas V, Tsymbal V, Debosscher J, Clémer K (2014b) The eccentric massive binary V380 Cyg: revised orbital elements and interpretation of the intrinsic variability of the primary component. *MNRAS* 438(4):3093–3110. <https://doi.org/10.1093/mnras/stt2421>. arXiv:1312.3601 [astro-ph.SR]
- Tkachenko A, Matthews JM, Aerts C, Pavlovski K, Pápics PI, Zwintz K, Cameron C, Walker GAH, Kuschnig R, Degroote P, Debosscher J, Moravveji E, Kolbas V, Guenther DB, Moffat AFJ, Rowe JF, Rucinski SM, Sasselov D, Weiss WW (2016) Stellar modelling of Spica, a high-mass spectroscopic binary with a β Cep variable primary component. *MNRAS* 458(2):1964–1976. <https://doi.org/10.1093/mnras/stw255>. arXiv:1601.08069 [astro-ph.SR]
- Tkachenko A, Pavlovski K, Johnston C, Pedersen MG, Michielsen M, Bowman DM, Southworth J, Tsymbal V, Aerts C (2020) The mass discrepancy in intermediate- and high-mass eclipsing binaries: the need for higher convective core masses. *A&A* 637:A60. <https://doi.org/10.1051/0004-6361/202037452>. arXiv:2003.08982 [astro-ph.SR]
- Tolstoy E, Hill V, Tosi M (2009) Star-formation histories, abundances, and kinematics of dwarf galaxies in the local group. *ARA&A* 47(1):371–425. <https://doi.org/10.1146/annurev-astro-082708-101650>. arXiv:0904.4505 [astro-ph.CO]
- Tomkin J, Fekel FC (2006) New precision orbits of bright double-lined spectroscopic binaries. I. RR Lyncis, 12 Bootis, and HR 6169. *AJ* 131(5):2652–2663. <https://doi.org/10.1086/501349>. arXiv:astro-ph/0601716
- Tonry J, Davis M (1979) A survey of galaxy redshifts. I. Data reduction techniques. *AJ* 84:1511–1525. <https://doi.org/10.1086/112569>
- Torres G (2004) Combining astrometry and spectroscopy. In: Hilditch RW, Hensberge H, Pavlovski K (eds) Spectroscopically and spatially resolving the components of the close binary stars. ASP Conference Series, vol 318. Astronomical Society of the Pacific, San Francisco, pp 123–131. arXiv:astro-ph/0312147
- Torres G (2014) Interferometry and the fundamental properties of stars. In: Creech-Eakman MJ, Guzik JA, Stencel RE (eds) Resolving the future of astronomy with long-baseline interferometry. ASP Conference Series, vol 487. Astronomical Society of the Pacific, San Francisco, p 21
- Torres G, Ribas I (2002) Absolute dimensions of the M-type eclipsing binary YY Geminorum (Castor C): a challenge to evolutionary models in the lower main sequence. *ApJ* 567(2):1140–1165. <https://doi.org/10.1086/338587>. arXiv:astro-ph/0111167
- Torres G, Stefanik RP, Andersen J, Nordstrom B, Latham DW, Clausen JV (1997) The absolute dimensions of eclipsing binaries. XXII. The unevolved F-type system HS Hydrae. *AJ* 114:2764. <https://doi.org/10.1086/118685>
- Torres G, Andersen J, Giménez A (2010) Accurate masses and radii of normal stars: modern results and applications. *Astron Astrophys Rev* 18(1–2):67–126. <https://doi.org/10.1007/s00159-009-0025-1>. arXiv:0908.2624 [astro-ph.SR]
- Torres G, Clausen JV, Bruntt H, Claret A, Andersen J, Nordström B, Stefanik RP, Latham DW (2012a) Absolute dimensions of eclipsing binaries. XXIX. The Am-type systems SW Canis Majoris and HW


- Canis Majoris. *A&A* 537:A117. <https://doi.org/10.1051/0004-6361/201117795>. arXiv:1112.3974 [astro-ph.SR]
- Torres G, Fischer DA, Sozzetti A, Buchhave LA, Winn JN, Holman MJ, Carter JA (2012b) Improved spectroscopic parameters for transiting planet hosts. *ApJ* 757(2):161. <https://doi.org/10.1088/0004-637X/757/2/161>. arXiv:1208.1268 [astro-ph.SR]
- Torres G, Sandberg Lacy CH, Pavlovski K, Feiden GA, Sabby JA, Bruntt H, Viggo Clausen J (2014) The G+M eclipsing binary V530 Orionis: a stringent test of magnetic stellar evolution models for low-mass stars. *ApJ* 797(1):31. <https://doi.org/10.1088/0004-637X/797/1/31>. arXiv:1410.6170 [astro-ph.SR]
- Torres G, Claret A, Pavlovski K, Dotter A (2015a) Capella (α Aurigae) revisited: new binary orbit, physical properties, and evolutionary state. *ApJ* 807(1):26. <https://doi.org/10.1088/0004-637X/807/1/26>. arXiv:1505.07461 [astro-ph.SR]
- Torres G, Sandberg Lacy CH, Pavlovski K, Fekel FC, Muterspaugh MW (2015b) Absolute dimensions of the metallic-line eclipsing binary V501 monocerotis. *AJ* 150(5):154. <https://doi.org/10.1088/0004-6256/150/5/154>. arXiv:1509.07873 [astro-ph.SR]
- Torres G, Stefanik RP, Latham DW (2019) Dynamical masses for the triple system HD 28363 in the Hyades cluster. *ApJ* 885(1):9. <https://doi.org/10.3847/1538-4357/ab43e2>. arXiv:1909.04668 [astro-ph.SR]
- Townsend RHD, Teitler SA (2013) GYRE: an open-source stellar oscillation code based on a new Magnus Multiple Shooting scheme. *MNRAS* 435:3406–3418. <https://doi.org/10.1093/mnras/stt1533>. arXiv:1308.2965 [astro-ph.SR]
- Tremblay PE, Bergeron P (2009) Spectroscopic analysis of DA white dwarfs: stark broadening of hydrogen lines including nonideal effects. *ApJ* 696(2):1755–1770. <https://doi.org/10.1088/0004-637X/696/2/1755>. arXiv:0902.4182 [astro-ph.SR]
- Tremblay PE, Ludwig HG, Steffen M, Freytag B (2013) Spectroscopic analysis of DA white dwarfs with 3D model atmospheres. *A&A* 559:A104. <https://doi.org/10.1051/0004-6361/201322318>. arXiv:1309.0886 [astro-ph.SR]
- Tremblay PE, Kalirai JS, Soderblom DR, Cignoni M, Cummings J (2014) White dwarf cosmochronology in the solar neighborhood. *ApJ* 791(2):92. <https://doi.org/10.1088/0004-637X/791/2/92>. arXiv:1406.5173 [astro-ph.SR]
- Tremblay PE, Cukanovaite E, Gentile Fusillo NP, Cunningham T, Hollands MA (2019) Fundamental parameter accuracy of DA and DB white dwarfs in Gaia Data Release 2. *MNRAS* 482(4):5222–5232. <https://doi.org/10.1093/mnras/sty3067>. arXiv:1811.03084 [astro-ph.SR]
- Triana SA, Moravveji E, Pápics PI, Aerts C, Kawaler SD, Christensen-Dalsgaard J (2015) The internal rotation profile of the B-type star KIC 10526294 from frequency inversion of its dipole gravity modes. *ApJ* 810(1):16. <https://doi.org/10.1088/0004-637X/810/1/16>. arXiv:1507.04574 [astro-ph.SR]
- Trundle C, Lennon DJ (2005) Understanding B-type supergiants in the low metallicity environment of the SMC II. *A&A* 434(2):677–689. <https://doi.org/10.1051/0004-6361:20042061>. arXiv:astro-ph/0501228
- Udalski A, Szymanski M, Kaluzny J, Kubiak M, Krzemiński W, Mateo M, Preston GW, Paczyński B (1993) The optical gravitational lensing experiment. Discovery of the first candidate microlensing event in the direction of the Galactic Bulge. *Acta Astron* 43:289–294
- Udalski A, Kubiak M, Szymanski M (1997) Optical gravitational lensing experiment. OGLE-2—the second phase of the OGLE Project. *Acta Astron* 47:319–344. arXiv:astro-ph/9710091
- Valentini M, Chiappini C, Bossini D, Miglio A, Davies GR, Mosser B, Elsworth YP, Mathur S, García RA, Girardi L, Rodrigues TS, Steinmetz M, Vallenari A (2019) Masses and ages for metal-poor stars. A pilot programme combining asteroseismology and high-resolution spectroscopic follow-up of RAVE halo stars. *A&A* 627:A173. <https://doi.org/10.1051/0004-6361/201834081>. arXiv:1808.08569 [astro-ph.SR]
- Valle G, Dell’Omodarme M, Prada Moroni PG, Degl’Innocenti S (2014) Uncertainties in grid-based estimates of stellar mass and radius. SCEPter: Stellar Characteristics Pisa Estimation gRid. *A&A* 561:A125. <https://doi.org/10.1051/0004-6361/201322210>. arXiv:1311.7358 [astro-ph.SR]
- Valle G, Dell’Omodarme M, Prada Moroni PG, Degl’Innocenti S (2015) Uncertainties in asteroseismic grid-based estimates of stellar ages. SCEPter: Stellar Characteristics Pisa Estimation gRid. *A&A* 575:A12. <https://doi.org/10.1051/0004-6361/201424686>. arXiv:1412.5895 [astro-ph.SR]
- Van Dyk SD (2017) Supernova progenitors observed with HST. In: Alsabti A, Murdin P (eds) *Handbook of Supernovae*. Springer, Cham, p 693. https://doi.org/10.1007/978-3-319-21846-5_126

- van Dyk DA, Degennaro S, Stein N, Jefferys WH, von Hippel T (2009) Statistical analysis of stellar evolution. *Ann Appl Stat* 3:117–143. <https://doi.org/10.1214/08-AOAS219SUPP>. arXiv:0905.2547 [stat.AP]
- van Eck S, Neyskens P, Jorissen A, Plez B, Edvardsson B, Eriksson K, Gustafsson B, Jørgensen UG, Nordlund Å (2017) A grid of MARCS model atmospheres for late-type stars. II. S stars and their properties. *A&A* 601:A10. <https://doi.org/10.1051/0004-6361/201525886>
- van Eyken JC, Ciardi DR, Rebull LM, Stauffer JR, Akeson RL, Beichman CA, Boden AF, von Braun K, Gelino DM, Hoard DW et al (2011) The Palomar Transient Factory Orion project: eclipsing binaries and young stellar objects. *AJ* 142(2):60. <https://doi.org/10.1088/0004-6256/142/2/60>. arXiv:1106.3570 [astro-ph.SR]
- Van Eylen V, Albrecht S (2015) Eccentricity from transit photometry: small planets in Kepler multi-planet systems have low eccentricities. *ApJ* 808(2):126. <https://doi.org/10.1088/0004-637X/808/2/126>. arXiv:1505.02814 [astro-ph.EP]
- Van Eylen V, Albrecht S, Gandolfi D, Dai F, Winn JN, Hirano T, Narita N, Bruntt H, Prieto-Arranz J, Béjar VJS et al (2016) The K2-ESPRINT Project. V. A short-period giant planet orbiting a subgiant star. *AJ* 152(5):143. <https://doi.org/10.3847/0004-6256/152/5/143>. arXiv:1605.09180 [astro-ph.EP]
- Van Eylen V, Dai F, Mathur S, Gandolfi D, Albrecht S, Fridlund M, García RA, Guenther E, Hjorth M, Justesen AB et al (2018) HD 89345: a bright oscillating star hosting a transiting warm Saturn-sized planet observed by K2. *MNRAS* 478(4):4866–4880. <https://doi.org/10.1093/mnras/sty1390>. arXiv:1805.01860 [astro-ph.EP]
- Van Eylen V, Albrecht S, Huang X, MacDonald MG, Dawson RI, Cai MX, Foreman-Mackey D, Lundkvist MS, Silva Aguirre V, Snellen I, Winn JN (2019) The orbital eccentricity of small planet systems. *AJ* 157(2):61. <https://doi.org/10.3847/1538-3881/aaf22f>. arXiv:1807.00549 [astro-ph.EP]
- Van Reeth T, Tkachenko A, Aerts C, Pápics PI, Triana SA, Zwintz K, Degroote P, Debosscher J, Bloemen S, Schmid VS, De Smedt K, Fremat Y, Fuentes AS, Homan W, Hrudkova M, Karjalainen R, Lombaert R, Nemeth P, Østensen R, Van De Steene G, Vos J, Raskin G, Van Winckel H (2015) Gravity-mode period spacings as a seismic diagnostic for a sample of γ Doradus stars from Kepler space photometry and high-resolution ground-based spectroscopy. *ApJS* 218:27. <https://doi.org/10.1088/0067-0049/218/2/27>. arXiv:1504.02119 [astro-ph.SR]
- Van Reeth T, Tkachenko A, Aerts C (2016) Interior rotation of a sample of γ Doradus stars from ensemble modelling of their gravity-mode period spacings. *A&A* 593:A120. <https://doi.org/10.1051/0004-6361/201628616>. arXiv:1607.00820 [astro-ph.SR]
- Van Reeth T, Mombarg JSG, Mathis S, Tkachenko A, Fuller J, Bowman DM, Buyschaert B, Johnston C, García Hernández A, Goldstein J, Townsend RHD, Aerts C (2018) Sensitivity of gravito-inertial modes to differential rotation in intermediate-mass main-sequence stars. *A&A* 618:A24. <https://doi.org/10.1051/0004-6361/201832718>. arXiv:1806.03586 [astro-ph.SR]
- Verma K, Hanasoge S, Bhattacharya J, Antia HM, Krishnamurthi G (2016) Asteroseismic determination of fundamental parameters of Sun-like stars using multilayered neural networks. *MNRAS* 461(4):4206–4214. <https://doi.org/10.1093/mnras/stw1621>. arXiv:1602.00902 [astro-ph.SR]
- Verma K, Raodeo K, Basu S, Silva Aguirre V, Mazumdar A, Mosumgaard JR, Lund MN, Ranadive P (2019) Helium abundance in a sample of cool stars: measurements from asteroseismology. *MNRAS* 483(4):4678–4694. <https://doi.org/10.1093/mnras/sty3374>. arXiv:1812.02751 [astro-ph.SR]
- Villanova S, Piotto G, King IR, Anderson J, Bedin LR, Gratton RG, Cassisi S, Momany Y, Bellini A, Cool AM, Recio-Blanco A, Renzini A (2007) The multiplicity of the subgiant branch of ω Centauri: evidence for prolonged star formation. *ApJ* 663(1):296–314. <https://doi.org/10.1086/517905>. arXiv:astro-ph/0703208
- Vink JS, de Koter A, Lamers HJGLM (2000) New theoretical mass-loss rates of O and B stars. *A&A* 362:295–309. arXiv:astro-ph/0008183
- Vink JS, de Koter A, Lamers HJGLM (2001) Mass-loss predictions for O and B stars as a function of metallicity. *A&A* 369:574–588. <https://doi.org/10.1051/0004-6361:20010127>. arXiv:astro-ph/0101509
- Vogt SS, Allen SL, Bigelow BC, Bresee L, Brown B, Cantrall T, Conrad A, Couture M, Delaney C, Epps HW, et al (1994) HIRES: the high-resolution echelle spectrometer on the Keck 10-m Telescope. In: Crawford DL, Craine ER (eds) *Instrumentation in Astronomy VIII. Proceedings of SPIE*, vol 2198. SPIE, p 362. <https://doi.org/10.1117/12.176725>
- Vos J, Clausen JV, Jørgensen UG, Østensen RH, Claret A, Hillen M, Exter K (2012) Absolute dimensions of solar-type eclipsing binaries. EF Aquarii: a G0 test for stellar evolution models. *A&A* 540:A64. <https://doi.org/10.1051/0004-6361/201118606>. arXiv:1202.4851 [astro-ph.SR]

- Vučković M, Østensen RH, Németh P, Bloemen S, Pápics PI (2016) Looking on the bright side: the story of AA Doradus as revealed by its cool companion. *A&A* 586:A146. <https://doi.org/10.1051/0004-6361/201526552>. arXiv:1510.01790 [astro-ph.SR]
- Wade RA, Horne K (1988) The radial velocity curve and peculiar TiO distribution of the red secondary star in Z Chamaeleontis. *ApJ* 324:411–430. <https://doi.org/10.1086/165905>
- Wagstaff G, Miller Bertolami MM, Weiss A (2020) Impact of convective boundary mixing on the TP-AGB. *MNRAS* 493(4):4748–4762. <https://doi.org/10.1093/mnras/staa3362>. arXiv:2002.01860 [astro-ph.SR]
- Weidemann V (1977) Mass loss towards the white dwarf stage. *A&A* 59(3):411–418
- Weidner C, Vink JS (2010) The masses, and the mass discrepancy of O-type stars. *A&A* 524:A98. <https://doi.org/10.1051/0004-6361/201014491>. arXiv:1010.2204 [astro-ph.SR]
- Weisberg JM, Huang Y (2016) Relativistic measurements from timing the binary pulsar PSR B1913+16. *ApJ* 829(1):55. <https://doi.org/10.3847/0004-637X/829/1/55>. arXiv:1606.02744 [astro-ph.HE]
- Weiss A, Ferguson JW (2009) New asymptotic giant branch models for a range of metallicities. *A&A* 508(3):1343–1358. <https://doi.org/10.1051/0004-6361/200912043>. arXiv:0903.2155 [astro-ph.SR]
- Weiss WW, Rucinski SM, Moffat AFJ, Schwarzenberg-Czerny A, Koudelka OF, Grant CC, Zee RE, Kuschnig R, Mochnacki S, Matthews JM, Orleanski P, Pamyatnykh A, Pigulski A, Alves J, Guedel M, Handler G, Wade GA, Zwintz K (2014) BRITe-constellation: nanosatellites for precision photometry of bright stars. *PASP* 126(940):573. <https://doi.org/10.1086/677236>. arXiv:1406.3778 [astro-ph.IM]
- Welsh WF, Orosz JA, Carter JA, Fabrycky DC, Ford EB, Lissauer JJ, Prša A, Quinn SN, Ragozzine D, Short DR et al (2012) Transiting circumbinary planets Kepler-34 b and Kepler-35 b. *Nature* 481:475–479. <https://doi.org/10.1038/nature10768>. arXiv:1204.3955 [astro-ph.EP]
- Werner K, Herwig F (2006) The elemental abundances in bare planetary Nebula central stars and the shell burning in AGB stars. *PASP* 118(840):183–204. <https://doi.org/10.1086/500443>. arXiv:astro-ph/0512320
- Wex N (2014) Testing relativistic gravity with radio pulsars. In: Kopeikin SM (ed) *Frontiers in Relativistic Celestial Mechanics, Vol 2: Applications and Experiments*. De Gruyter, Berlin, pp 39–102. https://doi.org/10.1515/9783110345667_39
- White TR, Bedding TR, Stello D, Christensen-Dalsgaard J, Huber D, Kjeldsen H (2011) Calculating asteroseismic diagrams for solar-like oscillations. *ApJ* 743(2):161. <https://doi.org/10.1088/0004-637X/743/2/161>. arXiv:1109.3455 [astro-ph.SR]
- White TR, Huber D, Maestro V, Bedding TR, Ireland MJ, Baron F, Boyajian TS, Che X, Monnier JD, Pope BJS, Roettenbacher RM, Stello D, Tuthill PG, Farrington CD, Goldfinger PJ, Mcalister HA, Schaefer GH, Sturmman J, Sturmman L, Ten Brummelaar TA, Turner NH (2013) Interferometric radii of bright Kepler stars with the CHARA Array: Cygni and 16 Cygni A and B. *MNRAS* 433(2):1262–1270
- Williams KA, Bolte M, Koester D (2009) Probing the lower mass limit for supernova progenitors and the high-mass end of the initial-final mass relation from white dwarfs in the open cluster M35 (NGC 2168). *ApJ* 693(1):355–369. <https://doi.org/10.1088/0004-637X/693/1/355>. arXiv:0811.1577 [astro-ph]
- Wilson RE, Pilachowski CA, Terrell D (2017) The M dwarf eclipsing binary CU Cancri. *ApJ* 835:251. <https://doi.org/10.3847/1538-4357/835/2/251>
- Windmiller G, Orosz JA, Etzel PB (2010) The effect of starspots on accurate radius determination of the low-mass double-lined eclipsing binary Gu Boo. *ApJ* 712:1003–1009. <https://doi.org/10.1088/0004-637X/712/2/1003>. arXiv:1002.2003 [astro-ph.SR]
- Winget DE, Hansen CJ, Liebert J, van Horn HM, Fontaine G, Nather RE, Kepler SO, Lamb DQ (1987) An independent method for determining the age of the Universe. *ApJL* 315:L77. <https://doi.org/10.1086/184864>
- Winn JN (2010) *Exoplanet transits and occultations*. University of Arizona Press, pp 55–77
- Wu Y, Xiang M, Bi S, Liu X, Yu J, Hon M, Sharma S, Li T, Huang Y, Liu K, Zhang X, Li Y, Ge Z, Tian Z, Zhang J, Zhang J (2018) Mass and age of red giant branch stars observed with LAMOST and Kepler. *MNRAS* 475(3):3633–3643. <https://doi.org/10.1093/mnras/stx3296>. arXiv:1712.09779 [astro-ph.SR]
- Wu Y, Xiang M, Zhao G, Bi S, Liu X, Shi J, Huang Y, Yuan H, Wang C, Chen B, Huo Z, Ren J, Tian Z, Liu K, Zhang X, Li Y, Zhang J (2019) Ages and masses of 0.64 million red giant branch stars from the LAMOST Galactic Spectroscopic Survey. *MNRAS* 484(4):5315–5329. <https://doi.org/10.1093/mnras/stz256>. arXiv:1901.07233 [astro-ph.SR]

- Xie JW, Dong S, Zhu Z, Huber D, Zheng Z, De Cat P, Fu J, Liu HG, Luo A, Wu Y et al (2016) Exoplanet orbital eccentricities derived from LAMOST-Kepler analysis. *PNAS* 113(41):11431–11435. <https://doi.org/10.1073/pnas.1604692113>. arXiv:1609.08633 [astro-ph.EP]
- Xiong DR, Deng L (2009) Lithium depletion in late-type dwarfs. *MNRAS* 395(4):2013–2028. <https://doi.org/10.1111/j.1365-2966.2009.14581.x>
- Xu S, Zhang B, Reid MJ, Zheng X, Wang G (2019) Comparison of Gaia DR2 parallaxes of stars with VLBI astrometry. *ApJ* 875(2):114. <https://doi.org/10.3847/1538-4357/ab0e83>. arXiv:1903.04105 [astro-ph.SR]
- Yusof N, Hirschi R, Meynet G, Crowther PA, Ekström S, Frischknecht U, Georgy C, Abu Kassim H, Schnurr O (2013) Evolution and fate of very massive stars. *MNRAS* 433(2):1114–1132. <https://doi.org/10.1093/mnras/st794>. arXiv:1305.2099 [astro-ph.SR]
- Zhou G, Bayliss D, Hartman JD, Rabus M, Bakos GÁ, Jordán A, Brahm R, Penev K, Csubry Z, Mancini L et al (2015) A $0.24+0.18 M_{\odot}$ double-lined eclipsing binary from the HATSouth survey. *MNRAS* 451:2263–2277. <https://doi.org/10.1093/mnras/stv1070>. arXiv:1505.02860 [astro-ph.SR]
- Zinn JC, Pinsonneault MH, Huber D, Stello D, Stassun K, Serenelli A (2019) Testing the radius scaling relation with Gaia DR2 in the Kepler field. *ApJ* 885(2):166. <https://doi.org/10.3847/1538-4357/ab44a9>. arXiv:1910.00719 [astro-ph.SR]
- Zocchi A, Gieles M, Hénault-Brunet V (2019) The effect of stellar-mass black holes on the central kinematics of ω Cen: a cautionary tale for IMBH interpretations. *MNRAS* 482:4713–4725. <https://doi.org/10.1093/mnras/sty1508>. arXiv:1806.02157
- Zucker S, Mazeh T (1994) Study of spectroscopic binaries with TODCOR. I. A new two-dimensional correlation algorithm to derive the radial velocities of the two components. *ApJ* 420:806. <https://doi.org/10.1086/173605>
- Zurlo A, Gratton R, Mesa D, Desidera S, Enia A, Sahu K, Almenara JM, Kervella P, Avenhaus H, Girard J, Janson M, Lagadec E, Langlois M, Milli J, Perrot C, Schlieder JE, Thalmann C, Vigan A, Giro E, Gluck L, Ramos J, Roux A (2018) The gravitational mass of Proxima Centauri measured with SPHERE from a microlensing event. *MNRAS* 480(1):236–244. <https://doi.org/10.1093/mnras/sty1805>. arXiv:1807.01318 [astro-ph.SR]
- Zwintz K, Fossati L, Ryabchikova T, Kaiser A, Gruberbauer M, Barnes TG, Baglin A, Chaintreuil S (2013) γ Doradus pulsation in two pre-main sequence stars discovered by CoRoT. *A&A* 550:A121. <https://doi.org/10.1051/0004-6361/201220127>. arXiv:1301.0991 [astro-ph.SR]
- Zwintz K, Fossati L, Ryabchikova T, Guenther D, Aerts C, Barnes TG, Themeßl N, Lorenz D, Cameron C, Kuschnig R, Pollack-Drs S, Moravveji E, Baglin A, Matthews JM, Moffat AFJ, Poretti E, Rainer M, Rucinski SM, Sasselov D, Weiss WW (2014) Echography of young stars reveals their evolution. *Science* 345:550–553. <https://doi.org/10.1126/science.1253645>. arXiv:1407.4928 [astro-ph.SR]
- Zwintz K, Moravveji E, Pápics PI, Tkachenko A, Przybilla N, Nieva MF, Kuschnig R, Antoci V, Lorenz D, Themeßl N, Fossati L, Barnes TG (2017) A comprehensive study of young B stars in NGC 2264. I. Space photometry and asteroseismology. *A&A* 601:A101. <https://doi.org/10.1051/0004-6361/201630327>. arXiv:1703.06456 [astro-ph.SR]

Authors and Affiliations

Aldo Serenelli^{1,2,3}  · Achim Weiss⁴ · Conny Aerts^{5,6} · George C. Angelou⁴ · David Baroch^{1,2} · Nate Bastian⁷ · Paul G. Beck^{8,9} · Maria Bergemann³ · Joachim M. Bestenlehner¹⁰ · Ian Czekala¹¹ · Nancy Elias-Rosa^{1,12} · Ana Escorza^{5,13,14} · Vincent Van Eylen³⁶ · Diane K. Feuillet^{3,15} · Davide Gandolfi¹⁶ · Mark Gieles^{17,18} · Léo Girardi¹⁹ · Yveline Lebreton^{20,21} · Nicolas Lodieu^{9,22} · Marie Martig⁷ · Marcelo M. Miller Bertolami^{23,24} · Joey S. G. Mombarg⁵ · Juan Carlos Morales^{1,2} · Andrés Moya^{25,26} · Benard Nsamba^{4,27} · Krešimir Pavlovski²⁸ · May G. Pedersen^{5,29} · Ignasi Ribas^{1,2} · Fabian R. N. Schneider^{30,31} · Victor Silva Aguirre³² · Keivan G. Stassun³³ · Eline Tolstoy³⁴ · Pier-Emmanuel Tremblay³⁵ · Konstanze Zwintz³⁷

✉ Aldo Serenelli
aldos@ice.csic.es

- ¹ Institute of Space Sciences (ICE, CSIC), Campus UAB, Carrer de Can Magrans S/N, 08193 Cerdanyola del Valles, Spain
- ² Institut d'Estudis Espacials de Catalunya (IEEC), C/Gran Capità 2-4, 08034 Barcelona, Spain
- ³ Max Planck Institute for Astronomy, Königstuhl 17, 69117 Heidelberg, Germany
- ⁴ Max Planck Institute for Astrophysics, Karl-Schwarzschild-Str. 1, 85741 Garching bei München, Germany
- ⁵ Department of Physics and Astronomy, Institute of Astronomy, KU Leuven, Celestijnenlaan 200 D, 3001 Leuven, Belgium
- ⁶ Department of Astrophysics, IMAPP, Radboud University Nijmegen, Heyendaalseweg 135, 6525 AJ Nijmegen, The Netherlands
- ⁷ Astrophysics Research Institute, Liverpool John Moores University, 146 Brownlow Hill, Liverpool L3 5RF, UK
- ⁸ Institute of Physics, Karl-Franzens University of Graz, NAWI Graz, Universitätsplatz 5/II, 8010 Graz, Austria
- ⁹ Instituto de Astrofísica de Canarias (IAC), Calle Vía Láctea s/n, 38200 La Laguna, Tenerife, Spain
- ¹⁰ Department of Physics and Astronomy, University of Sheffield, Hounsfield Road, Sheffield S3 7RH, UK
- ¹¹ Department of Astronomy, University of California, 501 Campbell Hall, Berkeley, CA 94720-3411, USA
- ¹² INAF Osservatorio Astronomico di Padova, Vicolo dell'Osservatorio 5, 35122 Padua, Italy
- ¹³ Institut d'Astronomie et d'Astrophysique, Université Libre de Bruxelles (ULB), CP 226, 1050 Brussels, Belgium
- ¹⁴ European Southern Observatory, Alonso de Córdova 3107, Vitacura, Casilla, 190001 Santiago, Chile
- ¹⁵ Department of Astronomy and Theoretical Physics, Lund Observatory, Box 43, 221 00 Lund, Sweden
- ¹⁶ Dipartimento di Fisica, Università di Torino, via Pietro Giuria 1, 10125 Turin, Italy

- 17 Institut de Ciències del Cosmos (ICCUB), Universitat de Barcelona, Martí i Franquès 1, 08028 Barcelona, Spain
- 18 ICREA, Pg. Lluís Companys 23, 08010 Barcelona, Spain
- 19 INAF Osservatorio Astronomico di Padova, Vicolo dell'Osservatorio 5, 35122 Padua, Italy
- 20 LESIA, Observatoire de Paris, Université PSL, CNRS, Sorbonne Université, Université Paris, 5 Place Jules Janssen, 92195 Meudon, France
- 21 Univ Rennes, CNRS, IPR (Institut de Physique de Rennes)-UMR 6251, 35000 Rennes, France
- 22 Departamento de Astrofísica, Universidad de La Laguna (ULL), 38206 La Laguna, Tenerife, Spain
- 23 Instituto de Astrofísica de La Plata, UNLP-CONICET, Paseo del Bosque s/n, B1900FWA La Plata, Argentina
- 24 Facultad de Ciencias Astronómicas y Geofísicas, UNLP, Paseo del Bosque s/n, B1900FWA La Plata, Argentina
- 25 Electrical Engineering, Electronics, Automation and Applied Physics Department, E.T.S.I.D.I, Polytechnic University of Madrid (UPM), 28012 Madrid, Spain
- 26 School of Physics and Astronomy, University of Birmingham, Edgbaston, Birmingham B15 2TT, UK
- 27 Instituto de Astrofísica e Ciências do Espaço, Universidade do Porto, Rua das Estrelas, PT4150-762 Porto, Portugal
- 28 Department of Physics, Faculty of Science, University of Zagreb, 10 000 Zagreb, Croatia
- 29 Kavli Institute of Theoretical Physics, University of California at Santa Barbara, Santa Barbara, CA 93106, USA
- 30 Heidelberger Institut für Theoretische Studien, Schloss-Wolfsbrunnengasse 35, 69118 Heidelberg, Germany
- 31 Astronomisches Rechen-Institut, Zentrum für Astronomie der Universität Heidelberg, Mönchhofstr. 12-14, 69120 Heidelberg, Germany
- 32 Stellar Astrophysics Centre (SAC), Department of Physics and Astronomy, Aarhus University, Ny Munkegade 120, 8000 Aarhus C, Denmark
- 33 Department of Physics and Astronomy, Vanderbilt University, Nashville, TN 37235, USA
- 34 Kapteyn Astronomical Institute, University of Groningen, Postbus 800, 9700 AV Groningen, The Netherlands
- 35 Department of Physics, University of Warwick, Coventry CV4 7AL, UK
- 36 Mullard Space Science Laboratory, University College London, Holmbury St Mary, Dorking, Surrey RH5 6NT, UK
- 37 Institute for Astro- and Particle Physics, Universität Innsbruck, Technikerstrasse 25, 6020 Innsbruck, Austria